International Committee for Future Accelerators

Sponsored by the Particles and Fields Commission of IUPAP

Beam Dynamics Newsletter

No. 58

Issue Editor:
E. Métral

Editor in Chief:
W. Chou

August 2012

Contents

1 Foreword

1.1 From the Chair

Weiren Chou, Fermilab
Mail to: chou@fnal.gov

The 4th of July 2012 (coincidentally the US Independence Day) was a good day for science, especially for particle physics. On that day, I had the opportunity to sit in the ICHEP2012 Conference Hall in Melbourne, Australia and witness a historical moment with hundreds of physicists from all over the world. At 17:00 Melbourne time (09:00 in Geneva, Switzerland) CERN announced that both the ATLAS and CMS experiments had discovered a new boson consistent with the Standard Model (SM) Higgs particle. This news spread to the entire planet instantaneously via teleconferences and the Internet. Such enormous public interest and media coverage on Higgs had rarely been seen. The headlines on TV news (BBC, ABC, CNN, etc.), radio news and newspapers (including all major Australian newspapers) were all about the Higgs. CERN Director General Rolf Heuer and British physicist Peter Higgs became instant celebrities and received endless requests for interviews and press conferences. Jokes about the Higgs boson were everywhere – here is one: "*Higgs makes me heavy. What I really need is anti-Higgs to help me lose weight.*" On a more serious note, the discovery of the Higgs could be a game changer in high-energy physics. Thanks to nature, the light mass of the Higgs (~125 GeV) puts a Higgs Factory within reach. At the ICFA meeting on July 8 in Melbourne, it was decided to organize a Higgs Factory workshop *HF2012* from November 14 to 16, 2012 at Fermilab, USA. (http://conferences.fnal.gov/hf2012) This workshop will discuss the possibilities for a future Higgs Factory, in particular make a comparison between a linear 125 × 125 GeV e^+e^- collider and a circular 125 GeV e^+e^- collider. It will also discuss physics requirements for a Higgs Factory and other options for a Higgs Factory, including a muon collider and a $\gamma\gamma$ collider. The workshop announcement can be found in Section 7.3.

A major topic at the July 8 ICFA meeting was the post-2012 ILC plan. The ILC GDE and RD will produce a Technical Design Report (TDR) and a Detector Baseline Design (DBD) by the end of 2012. These reports will include costs. Subsequently the current ILC Steering Committee (ILCSC) will cease to exist and will be replaced by a Linear Collider Board (LCB). Under the LCB there will be a Linear Collider Directorate. The ICFA has appointed Lyn Evans (CERN) as the first Linear Collider Director (LCD). He will appoint three associate directors, one each for the ILC, CLIC and the associated detectors. Evans will lead the Linear Collider organization to bring two existing large-scale linear collider programs – ILC and CLIC – under one governance. He will represent the combined effort to the worldwide science community and funding agencies. Evans will be based at CERN.

The ICFA decided to form a new panel on a neutrino factory. A charge for the new panel will be produced.

It was also decided that the next ICFA Seminar will be in mid-October 2014 at the IHEP in Beijing, China.

The collaboration between the ICFA and ICUIL is going well. In section 2, we publish two articles from a recent ICUIL Newsletter, in which readers can get a taste of some of the major activities in the laser community.

Application to participate in The Seventh International Accelerator School for Linear Colliders was closed on July 20. This school will be held from 27 November to 8 December 2012 at the Radisson Blu Hotel in Indore, India. More than 300 applications were received, a 30% increase from last year, mainly due to the overwhelming number of applicants from India. The Curriculum Committee has selected 60 highly qualified students from around the world. A report on the school can be found in Section 3.1. The school web address is http://www.linearcollider.org/school/2012/.

The editor of this issue is Dr. Elias Metral, a panel member and an accelerator scientist at CERN, Switzerland. Elias selected the theme of "*Prospect for Future Electron-Hadron Colliders*" and collected fifteen well-written articles on this theme. These articles give a comprehensive overview of this important accelerator field. In this issue there are also one workshop report (HOMSC12), five workshop announcements (BB2013, IBIC2012, HF2012, P3 and ICUIL2012), two doctoral thesis abstracts (Nicolas Mounet, École Politechnique Fédérale de Lausanne, Switzerland and Christopher Behrens, U. of Hamburg, Germany) and two obituaries (Andrey N. Lebedev and Dieter Möhl). I thank Elias for editing and producing a newsletter of great value and high quality for the world accelerator community.

1.2 From the Editor

Elias Métral, CERN
Mail to: Elias.Metral@cern.ch

This newsletter is devoted to the prospect for future electron-hadron colliders. This subject is discussed in 15 articles, structured as follows. In the first article, Vladimir Shiltsev (Fermilab) reviews the current landscape of high energy physics colliders while, in article 2, Max Klein (University of Liverpool) explains the physics motivation. Then, in the next six articles, four projects are discussed: (i) ENC (Electron-Nucleon Collider) at FAIR by Andreas Lehrach (Jülich), (ii) MEIC (Medium Energy Electron-Ion Collider) at Jefferson Lab by Yuhong Zhang (JLab), (iii) eRHIC (electron-ion collider, EIC, based on RHIC) at BNL by Vladimir Litvinenko (BNL), and (iv) LHeC (Large Hadron electron Collider) at CERN by Oliver Brüning (CERN) for the overview, Helmut Burkhardt (CERN) for the Ring-Ring option and Frank Zimmermann (CERN) for the ERL/Linac-Ring option. Afterward, as ERLs (Energy Recovery Linacs) are discussed in some scenarios, an overview of the existing ERLs is presented in article 9 by Chris Tennant and David Douglas (JLab), to be able to assess the challenges which have to be tackled. The status of the Cornell ERL is discussed in article 10 by Christopher Mayes (Cornell University). B*ERL*inPro (Berlin ERL Project), addressing the challenges of modern ERLs, is discussed in article 11 by Jens Knobloch (Berlin). The status of the Japanese ERLs is reviewd in article 12 by Ryoichi Hajima (JAEA-KEK), while the status of the Mainz ERL-facility MESA (Mainz Energy-recovering Superconducting Accelerator) is reviewed in article 13 by Kurt Aulenbacher (Mainz), and the status of the BNL R&D ERL is discussed in some detail in article 14 by Ilan Ben-Zvi (BNL). Finally, as the electron guns for future electron-hadron colliders will

have to be able to produce high average current beams with low emittance, the status of the electron guns is reviewed by Triveni Rao (BNL) in article 15.

As usual, there are also sections on activity reports, workshop and conference reports, recent doctoral theses abstracts, forthcoming beam dynamics events and annoucements of the beam dynamics panel.

This time, and for the first time, there is also a section for obituaries, devoted to Andrey N. Lebedev and Dieter Mohl who recently passed away.

I really would like to warmly thank all the contributors for their excellent contributions and co-operation. It was a great pleasure for me to edit this ICFA Beam Dynamics NewsLetter no.58 and I do hope that you will find this issue informative and useful.

2 News from ICUIL

2.1 ICUIL-ICFA Joint Task Force: White Paper

Toshi Tajima, ICUIL Chair
Mail to: toshiki.tajima@physik.uni-muenchen.de

Particle accelerators and lasers have made fundamental contributions to science and society, and are poised to continue making great strides in the 21st century. Lasers are essential to modern high performance accelerator facilities that support fundamental science and applications, and to the development of advanced accelerators. The demand for high average laser power even in near-future accelerator applications is already outpacing the state of the art in lasers. A class of more-futuristic accelerators for particle physics, driven entirely by lasers, would require average laser power far exceeding today's state of the art.

In September 2009 the ICFA-ICUIL Joint Task Force (JTF) chaired by Wim Leemans was launched to explore lasers for future accelerators through a collaboration of the ICFA and ICUIL communities. In April 2010 a first and inaugurating JTF Workshop was held at Darmstadt, followed with a second one in Berkeley in September of 2011. About 40 experts were invited from both the accelerator and laser communities.

The collaboration between the two communities has resulted in the creation of a substantial White Paper, entitled "High power laser technology for accelerators" and published in December 2011 issue (no. 56) of this ICFA Beam Dynamics Newsletter (http://www-bd.fnal.gov/icfabd/Newsletter56.pdf), which was edited by W. Leemans, W. Chou (chair, ICFA Beam Dynamics Panel) and M. Uesaka (chair, ICFA Advanced and Novel Accelerators Panel).

Four general areas in future accelerator science and technology were considered that will either be driven by lasers or have a need for laser technology beyond today's state of the art: colliders for high-energy physics based on lasers; laser stripping for H- sources; light sources (such as X-ray free electron lasers), and medical ion therapy accelerators.

Requirements for laser performance in each of the four areas were established and a first look at laser technologies that could meet these requirements was reported. Further details can be found in the whitepaper.

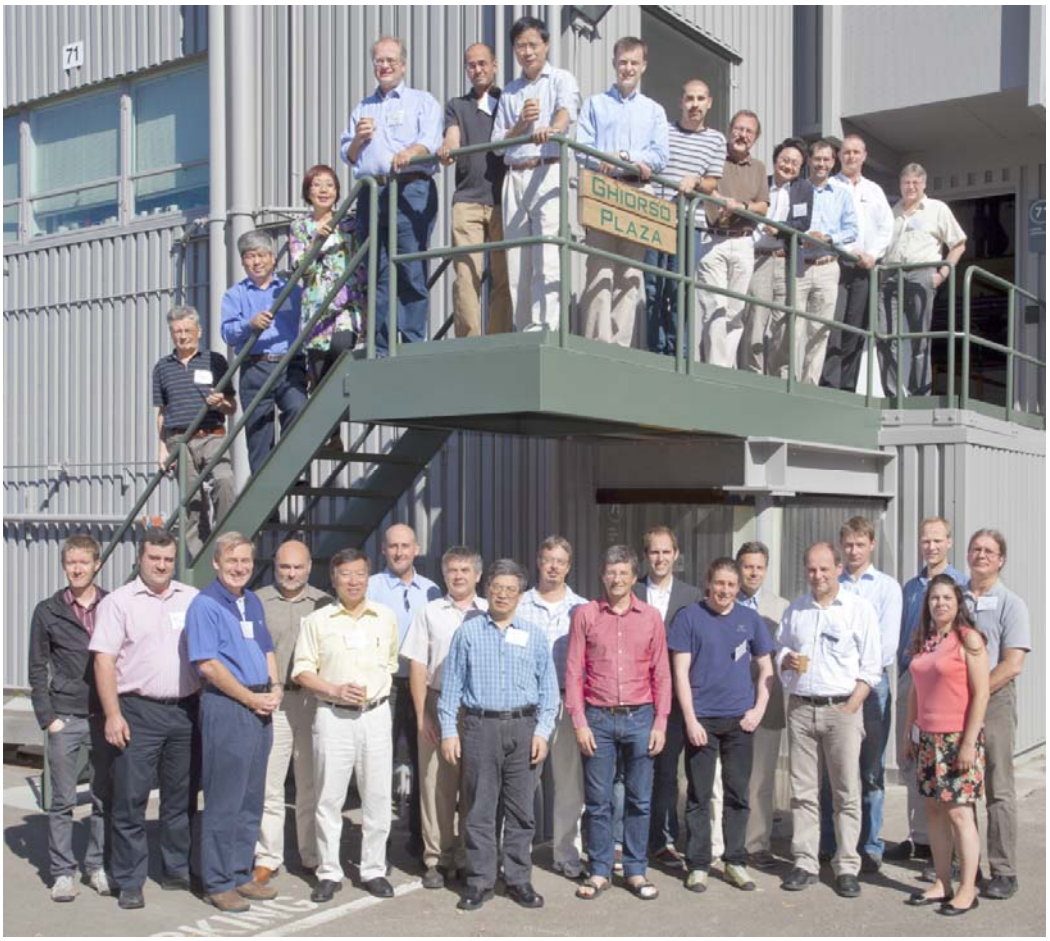

Figure 1: Group picture of the 2011 joint ICFA-ICUIL workshop on High Average Power Lasers for Future Accelerators, held at Lawrence Berkeley National Laboratory on September 20-22, 2011.

2.2 IZEST – International Zettawatt-Exawatt Science and Technology: Laser-based High Field Fundamental Physics

Gerard Mourou, ENSTA, France
Mail to: gerardmourou@gmail.com

IZEST aspires to play an important role in laser-Based High-Field Fundamental Physics. It intends to initiate a joint strategy, form coordination groups, and provide recommendations for the Exawatt facilities in the planning stage.

Fundamental High Energy Physics has been mainly driven by the high-energy fermionic colliding beam paradigm. Today the possibility to amplify laser to extreme energy and peak power offers, in addition to possibly more compact and cheaper ways to help HEP, a suit of complementary new alternatives underpinned by single shot, large field laser pulse, that together we could call Laser-based High Field Fundamental Physics.

The main mission of the International center on Zetta-Exawatt Science and Technology (IZEST) is to muster the scientific community behind this new concept. As an example, we project to use the laser field to probe the nonlinearity of vacuum due to nonlinearities and light-mass weak coupling fields such as Heisenberg-Euler QED, dark matter and dark energy. We envision that seeking the non-collider paradigm without large luminosity substantially shortens our time-line; we further accelerate the latter by adopting the existing large energy laser LIL. The accelerated research on the non-collider paradigm in TeV and beyond could, however stimulate innovation in collider thinking such as lower luminosity paths, novel radiation cooling, and gamma-gamma colliders. The advancement of intense short-pulsed laser energy by 2-3 orders of magnitude empowers us a tremendous potential of unprecedented discoveries. These include: TeV physics, physics beyond TeV, new light-mass weak-coupling field discovery potential, nonlinear QED and QCD fields, radiation physics in the vicinity of the Schwinger field, and zeptosecond dynamical spectroscopy of vacuum. In addition, we want to take advantage of the ultrashort particle or radiation pulses produced in the femto, atto, and zeptosecond timescale to perform a new type of particle/radiation precision metrology that would help to remove the uncertainty around the neutrino speed. Finally, the TeV particles that can be produced on demand could offer a new tool to TeV Astrophysics.

Today, a number of exawatt class facilities in Europe and in the world are already in the planning stage, like the ELI-Fourth Pillar and the Russian Mega Science Laser. IZEST should serve as a common platform opened to the international scientific community with a passion for this emerging opportuny and the desire to participate. IZEST headquarter will be located at the Ecole Polytechnique. The experimental program will be performed at the beginning on the most powerful European laser, the LIL and Petawatt laser at the CEA-CESTA in Bordeaux and on the Russian Exawatt once completed. It is expected that a large part of the work will also be carried out in the IZEST-associated laboratories around the world.

3 International Linear Collider (ILC)

3.1 Students Admitted to the Seventh International Accelerator School for Linear Colliders

Weiren Chou, Fermilab
Mail to: chou@fnal.gov

The student selection is complete for the Seventh International Accelerator School for Linear Colliders. This year's school will be held from 27 November to 8 December 2012 at the Radisson Blu Hotel, Indore, India, continuing the tradition of cycling the school between Europe, Asia and the Americas. The focus of the school will be on accelerator science and technology related to the next-generation TeV-scale colliders, including the International Linear Collider (ILC), the Compact Linear Collider (CLIC) and the Muon Collider.

This year we have again had a very large demand from many qualified applicants for the school. We selected 60 highly qualified students from a pool of 304 applicants

from 40 countries. 65% were from countries that have high-energy physics programs. The country distributions of the applicants as well as the accepted students are shown in the following figures. The admitted students include 30 from Asia and Oceania, 20 from Europe and 10 from North America. These students will be divided among two curricula: Class A for accelerator physics and Class B for radiofrequency (RF) technology.

The organisation of the Linear Collider accelerator school is done jointly by the Global Design Effort (GDE), the Compact Linear Collider (CLIC) Study and the International Committee for Future Accelerators (ICFA) Beam Dynamics Panel. The continuing popularity and success of the school clearly indicates the important need for providing advanced training in accelerator science for the high-energy physics community. Particle physics has been responsible for much of the development of particle accelerator science because of our own need for new accelerators for our research and therefore our investment in advanced accelerator R&D.

The attendees at the LC school are graduate students, postdoctoral fellows and junior researchers from around the world, including physicists who are considering a career change from experimental physics to accelerator physics. The subjects from accelerator dynamics to superconducting RF are forward-looking in the field with many possible applications beyond the next-generation Terascale lepton colliders. The curriculum will contain an overview of the different future collider options, a lecture on linac basics and a lecture on beam instrumentation, followed by a choice of two in-depth tracks: one on electron and positron sources, damping rings, linacs and beam delivery system; and one on superconducting and warm radiofrequency technology, low-level RF and high-power RF.

We have excellent lecturers, well-qualified students, an in-depth curriculum and a beautiful site for the school. We are set to have another successful LC accelerator school this year.

Lecturers of the 2012 LC Accelerator School

Lecture	Topic	Lecturer
I1	Introduction	Kaoru Yokoya (KEK)
I2	ILC	Barry Barish (Caltech)
I3	CLIC	Frank Tecker (CERN)
I4	Muon collider	Mark Palmer (Fermilab)
AB1	Linac basics	Daniel Schulte (CERN)
AB2	Beam instrumentation	Hermann Schmickler (CERN)
A1	Linac	Daniel Schulte (CERN)
A2	Sources	Masao Kuriki (Hiroshima Univ.)
A3	Damping rings & ring colliders	Susanna Guiducci (LNF-INFN)
A4	Beam delivery & beam-beam	Andrei Seryi (John Adams Inst.)
B1	Room temperature RF	Walter Wuensch (CERN)
B2	Superconducting RF	Jean Delayen (ODU/Jlab)
B3	LLRF & high power RF	Stefan Simrock (ITER)
	Hands-on training	P. R. Hannurkar (RRCAT)
	Site visit	Satish Joshi (RRCAT)

2012 LC Accelerator School – Applicants Distribution

304 applicants from 40 countries

- 65% from 16 HEP countries
- 21% from 24 other countries
- 14% unknown

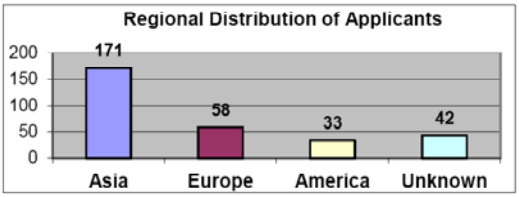

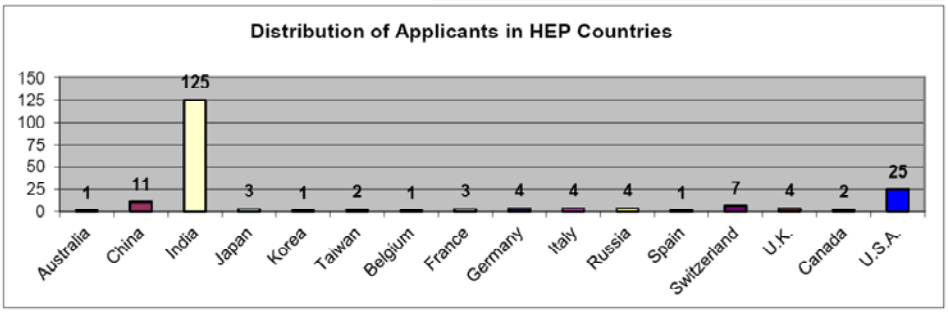

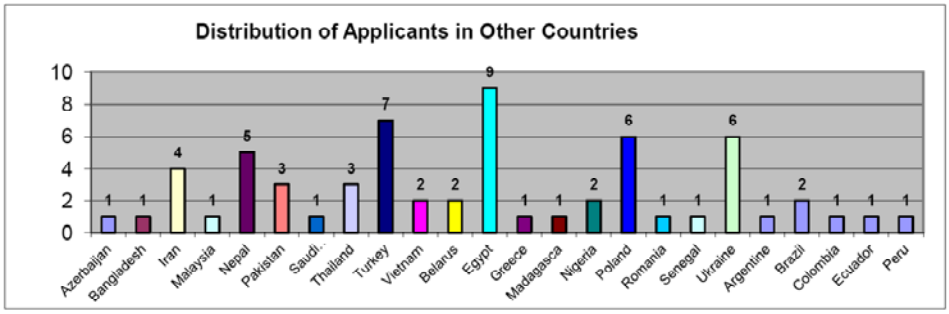

2012 LC Accelerator School – Students Distribution

- 60 students selected from 17 countries
- 92% from 13 HEP countries
- 8% from 4 other countries

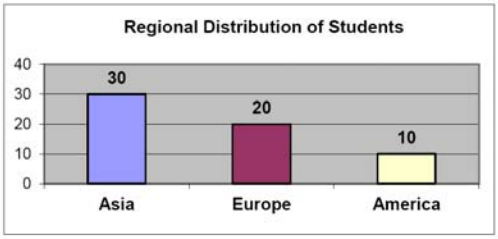

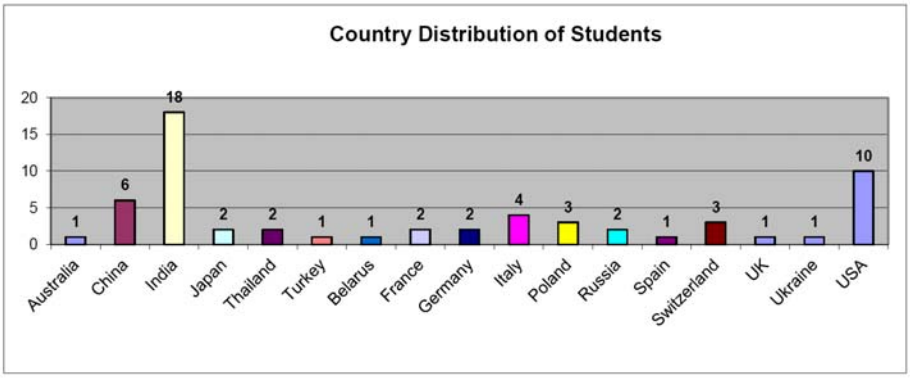

4 Prospect for Future Electron-Hadron Colliders

4.1 Current Landscape of High Energy Physics Colliders

Vladimir Shiltsev, Fermilab, PO Box 500, MS 221, Batavia, IL 60510, USA
Mail to: shiltsev@fnal.gov

4.1.1 Colliders of the Past and Present

Particle accelerators have been widely used for physics research since the early 20th century and have greatly progressed both scientifically and technologically since then. To gain an insight into the physics of elementary particles, one accelerates them to very high kinetic energy, let them impact on other particles, and detect products of the reactions that transform the particles into other particles. It is estimated that in the post-1938 era, accelerator science has influenced almost 1/3 of physicists and physics studies and on average contributed to physics Nobel Prize-winning research every 2.9 years [1]. Colliding beam facilities which produce high-energy collisions (interactions) between particles of approximately oppositely directed beams did pave the way for progress since the 1960's. Discussion below mainly follows recent publication [2].

Twenty nine colliders reached operational stage between the late 50's and now. The energy of colliders has been increasing over the years as demonstrated in Fig.1. There, the triangles represent maximum CM energy and the start of operation for lepton (usually, *e*+*e*-) colliders and full circles are for hadron (protons, antiprotons, ions, proton-electron) colliders. One can see that until the early 1990's, the CM energy on average increased by a factor of 10 every decade and, notably, the hadron colliders were 10-20 times more powerful. Since then, following the demands of high energy physics, the paths of the colliders diverged to reach record high energies in the particle reaction. The Large Hadron Colider (LHC) was built at CERN, while new *e*+*e*- colliders called "particle factories" were focused on detail exploration of phenomena at much lower energies.

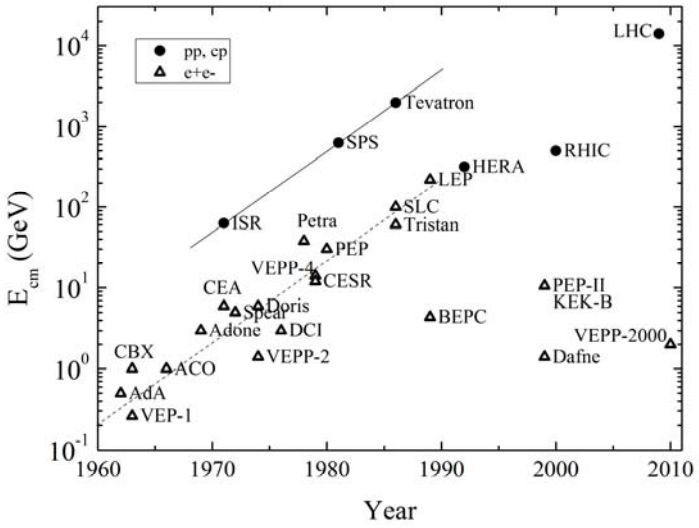

Figure 1: Colliders over the decades (from [2]).

Figure 2 demonstrates impressive progress of luminosities of colliding beam facilities since the invention of the method. Again, the triangles are lepton colliders and full circles are for hadron colliders. One can see that over the last 50 years, the performance of the colliders has improved by more than 6 orders of magnitude and reached record high values of over 10^{34}cm^{-2}s^{-1}. At such luminosity, one can expect to produce, e.g., 100 events over one year of operation (about 10^7 s) if the reaction cross section is 1 picobarn (pb) = 10^{-39} cm^2.

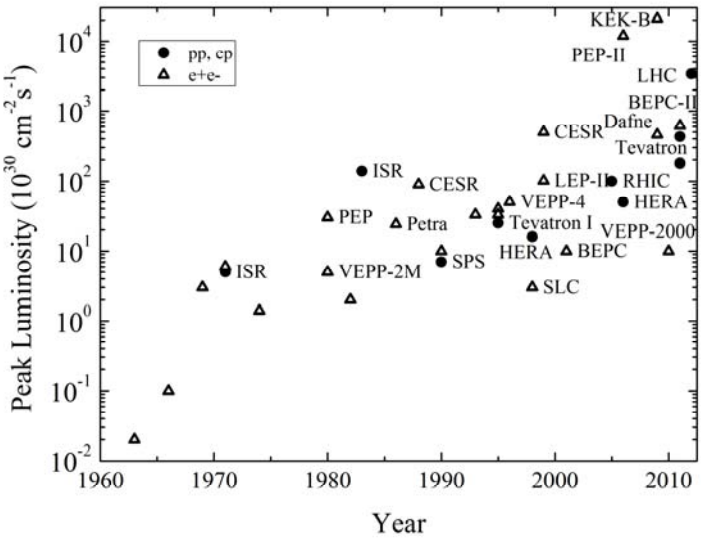

Figure 2: Peak luminosities of particle colliders.

Table 1: Past, present and possible future colliders; hadron colliders are in bold, lepton colliders in *Italic*, facilities under construction or in decisive design and planning stage are listed in parenthesis (…).

	early 1990's	early 2010's	2030's
Europe	**H*E*RA, (LHC)**	**LHC** (*Super-B,* **HL-LHC,**	**HE-LHC**
	LEP (Dafne)	**LH*e*C,** *E***NC**)	*CLIC?*
Russia	*VEPP-2, VEPP-4*	*VEPP-2000, VEPP-4M*	**NICA** ?
	(**UNK**, *VLEPP*)	(**NICA**, *Tau-Charm*)	*Higgs Factory* ?
United States	**Tevatron**, (**SSC**)	**RHIC**	*Muon Collider* ?
	SLC, CESR, (*PEP-II*)	(*e***RHIC**, *EL***IC**)	*PWLA/DLA* ?
Asia	*Tristan, BEPC*	*BEPC*	*ILC* ?
	(*KEK-B*)	(*Super-KEKB*)	*Higgs Factory* ?
Total	9 (7)	5 (9)	1 + ?

In general, one may say that colliders have had 50 glorious past years as not only many important particle discoveries were made at them, but they also initiated a wide range of innovation in accelerator physics and technology which resulted in 100-fold increase in energy (for each hadron and lepton colliding facilities) and 10^4-10^6 fold increase of the luminosity. At the same time, it is obvious that the progress in the maximum c.m. energy has drastically slowed down since the early 1990's and the lepton colliders even went backwards in energy to study rare processes – see Fig.1.

Moreover, the number of the facilities in operation has dropped from 9 to 5, as indicated in Table 1 which lists all operational colliders as of the early 1990's and now (early 2010's) and accounts for the projects under construction or under serious consideration at this time (in parenthesis). Our current landscape shows the end of the Tevatron era (the 26 years long ~2 TeV c.m. energy proton-antiproton Collider Run ended in September 2011) and is dominated by the LHC at CERN. The Tevatron, LEP and HERA established the Standard Model (SM) of particle physics. The next generation of colliders is expected to explore it at deeper levels and to eventually lead the exploration of the smallest dimensions beyond the current SM.

4.1.2 **Colliders of the Near Future (next 10 to 20 years)**

The future of the collider is ultimately driven by the demands of particle physics, but should stay within the limits of the available technologies and financial resources. All the projects currently under construction or at the design stage (see Table 1) satisfy those three requirements and, thus, have good prospects of becoming operational and deliver results in the next 20 years. Schematically they can be categorized by the area of the promising physics as follows:

Energy Frontier: the LHC luminosity upgrade project HL-LHC [3] will employ novel SC magnet technology based on the Nb_3Sn superconductors for tighter focusing at the interaction points and quintuple the performance of the energy frontier machine by mid-2020's to $5 \cdot 10^{34}$ $cm^{-2}s^{-1}$ with luminosity levelling at 14 TeV c.m. energy in proton-proton collisions and will enable to obtain about 250 fb^{-1} of the integrated luminosity per year with ultimate goal of 3000 fb^{-1} for both ATLAS and CMS experiments.

Low-energy hadron collisions: investigation of the mixed phase of quark–gluon matter and polarization phenomena at relatively low hadron energies has recently become of significant interest for the high energy physics community, and it is the main goal of the Nuclotron-based Ion Collider fAcility (NICA) currently under construction at JINR (Dubna, Russia) [4]. NICA will allow for the study of ion-ion (Au^{+79}) and ion-proton collisions in the energy range of 1-4.5 GeV/amu with average luminosity of 10^{27} cm^{-2} s^{-1} and also polarized proton-proton (5-12.6 GeV) and deuteron-deuteron (2-5.8 GeV/amu) collisions – in that regime luminosities up to 10^{31} cm^{-2} s^{-1} are foreseen. The plans indicate start of operation and first physics results later in this decade.

Electron-hadron collisions: deep inelastic electron-nucleon scattering is in the focus of a new electron-hadron collider project, the LHeC [5], in which polarized electrons of 60 GeV to possibly 140 GeV collide with LHC protons of 7000 GeV with design luminosity of about 10^{33} $cm^{-2}s^{-1}$. This would exceed the integrated luminosity collected at the previous *ep* collider HERA at DESY by two orders of magnitude in a 20 times wider kinematic range in the momentum transfer Q^2. Similar approach of reusing an existing beam facility and adding an accelerator for another species is taken in two collider projects in the US – eRHIC at BNL [6] and Electron-Ion Collider (ELIC) at JLab [7]. The eRHIC design is based on one of the existing RHIC(Relativistic Heavy Ion Collider) hadron rings which can accelerate polarized nuclear beam to 100 GeV/nucleon and polarized protons up to 250 GeV, and a new 20-30 GeV multi-pass energy-recovery linac (ERL) to accelerate polarized electrons; the luminosity varies

from 10^{33} $cm^{-2}s^{-1}$ to 10^{34} $cm^{-2}s^{-1}$ depending on the energy and species. The ELIC proposal re-uses the CEBAF 3-7 GeV polarized electron accelerator and requires the construction of a 30 to 150 GeV storage ring for ions (*p, d,* ^{3}*He* and *Li*, and unpolarized light to medium ion species). The attainment of very high luminosities in the ELIC, from $5 \cdot 10^{33}$ $cm^{-2}s^{-1}$ to 10^{35} $cm^{-2}s^{-1}$, an ERL-based continuous electron cooling facility is anticipated to provide low emittance and simultaneously very short ion bunches. Though with lower c.m. energy than LHeC, both of the projects in the US have the advantage of colliding both electron and ion species with polarized spins. It is believed that not more than one of the two can be supported and constructed.

Complementary physics programs can be realized at the proposed electron-nucleon collider ENC at the upcoming Facility for Antiproton and Ion Research FAIR at GSI Darmstadt (Germany) by utilizing the 15 GeV antiproton high-energy storage ring HESR for polarized proton and deuteron beams, with the addition of a 3.3 GeV storage ring for polarized electrons [8]. This will enable electron-nucleon collisions up to a center-of-mass energy up to 14 GeV with peak luminosities in the range of 10^{32} to 10^{33} $cm^{-2}s^{-1}$.

<u>*Electron-positron factories:*</u> In the late 1990's – early 2000's, two asymmetric-energy *e*+*e*− *B*-factories, the KEKB collider for the Belle experiment at KEK and the PEPII collider for the BaBar experiment at SLAC, had achieved tremendous success in confirmation of the Standard Model (SM) in the quark flavor sector and indicated that the Kobayashi-Maskawa mechanism is the dominant source of the observed *CP* violation in nature. Despite that, two fundamental questions remain unanswered in the flavor sector of quarks and leptons: a) it is not clear why the SM includes too many parameters and b) there is still a serious problem with the matter-antimatter asymmetry in the universe. To extend physics reach beyond two *B*-factories, much higher (by a factor of 40 or so) luminosity Super-*B* factories are either set up or considered for construction – one in Italy [9] and another in Japan [10]. Both are asymmetric-energy *e*+*e*− colliders with beam energies of about 4 GeV and 7 GeV and with a design luminosity approaching 10^{36} cm^{-2} s^{-1}, which is to be achieved via somewhat higher beam currents and very small beta-functions at the interaction points $\beta_y^* \sim 0.3$ mm made possible by employment of the above mentioned "crab waist" scheme. The physics run of the Super-KEKB in Japan is expected in 2015. Ultimately, Belle II detector should collect 40 times more *B*-meson samples per second than its predecessor – roughly 800 *BB* pairs per second and accumulate an integrated luminosity of 50 ab^{-1} = 50,000 fb^{-1} by 2021.

Many similar technical solutions, e.g. the "crab waist", will also be employed in the project of TauCharm factory in Novosibirsk (Russia) [11] which calls for c.m. collision energy variable from 3 GeV to 4.5 GeV (from *J/psi* resonances to charm barions), luminosity in excess of 10^{35} cm^{-2} s^{-1} and longitudinal polarization of at least one (electron) beam.

If one will project at the very end of the next 20 years, then the landscape of the collider physics is much less certain, there are several directions to advance and the choice between the options will be based upon the results from the LHC. The relevant results are expected to be available starting in 2012-13 (e.g., anticipated discovery of the Higgs boson) but they might easily slip well into the 2020's. Let us look into five possibilities for an after-LHC collider of 2030's.

Higher energy LHC: One of the most feasible opportunities is an energy upgrade of the LHC to 33 TeV c.m. proton-proton collisions [12]. The HE-LHC in the existing LHC tunnel will require 20T dipole magnets which are currently thought possible via combination of the NbTi, Nb_3Sn and HTS (high-temperature superconductor) SC magnet technology. Such a collider could follow the HL-LHC and start operation in the early 2030's. Despite the (presumed) feasibility of the machine, its energy reach is limited to ~2.5 times the LHC energy and it is not fully clear yet whether such a (relatively) small energy advance will justify its construction.

Higgs Factory: If the Higgs boson is discovered at the LHC in the presently anticipated range of its masses m_H=115-135 GeV range, the detailed studies and precise measurements of this unique spin-0 elementary particle might be of enough significant interest to justify construction of a $e+e-$ collider – a dedicated "Higgs factory". The maximum cross-section, and arguably the optimal centre-of-mass energy for studies of a number of Higgs boson properties, is at $E_{cm} \sim m_{\mathrm{H}} + (110\pm10)$ GeV ~250 GeV, and several opportunities for the facility are now under discussion, including one based on the ILC-type linear collider (see below) as well as several ring-ring versions [13]. The biggest challenge for the latter is the requirement to replenish energy loss of electrons and positrons due to the synchrotron radiation of the order of 10 GeV per turn even in 20-km or longer tunnels that with necessity means extensive use of high gradient SC RF accelerating cavities. Other challenges toward attainment of the required luminosity of $\sim 10^{34}$ cm^{-2} s^{-1} (equivalent to 20,000 events per year under assumption of the $e+e- \rightarrow HZ$ cross section of about 200 femtobarn (fb) = $2 \cdot 10^{-34}$ cm^2) will be significant electric power consumption on the order of 100 MW needed for continuous acceleration of ~10 mA of beam current and the need for very small beam emittances and very large momentum acceptance of the ring to accommodate the energy losses at the interaction points (see discussion on the *beamstrahlung* effect below). A cost saving option of the Higgs factory in an existing tunnel, e.g., 26.7 km long LHC tunnel or 21 km long UNK tunnel, looks particularly attractive.

Alternative way for production of the Higgs bosons is in the reaction $\mu+\mu- \rightarrow H$ (so called *s-channel* reaction) which has advantageously large cross section for muons, $(m_\mu / m_e)^2 \sim 40{,}000$ times higher than for electrons, and (another advantage) needs a $\mu+\mu-$ collider with factor of two lower c.m. energy $E_{cm} \sim m_{\mathrm{H}}$. The third advantage of that scheme is significantly smaller c.m. energy spread $\delta E_{cm} / E_{cm} \sim 0.01$-$0.003$ % (compared to ~ 0.2% for the $e+e-$ factories) that allows much better study of the outstandingly narrow width Higgs particle decays [14]. Production of ~4,000 events per year will require luminosity of at least 10^{31} cm^{-2} s^{-1} which seems to be very challenging because of the short muon lifetime and difficulties of the muon production (see discussion on high energy muon colliders below).

Energy Frontier Lepton Collider: It is presently widely believed that a multi-TeV lepton collider will be needed to follow the LHC discoveries. The most viable options currently under consideration are $e+e-$ linear colliders ILC (International Linear Collider) [15] and CLIC (Compact Linear Collider) [16] or $\mu+\mu-$ Muon Collider [17]. Each of these options has its own advantages, challenges and issues [18, 16].

Table 2: Comparison of Lepton Collider alternatives

	ILC	CLIC	MC
c.m energy, TeV	0.5	3	1.5-4
c.m. energy spread, rms	~2%	>5%	~0.1%
Luminosity , $cm^{-2}s^{-1}$	$2 \cdot 10^{34}$	$2 \cdot 10^{34}$ *	$(1\text{-}4) \cdot 10^{34}$
Feasibility report	2007	2012	2014-16
Technical design	2013	2016	~2020
Number of elements	38,000	260,000	10,000
Hi-Tech length, km	36	~60	14-20
Wall plug power, MW	230	580	~140

* peak luminosity within 1% c.m. energy spread.

The biggest challenge for the linear *e*+*e*- colliders is to accelerate the particles to the design energy within a reasonable facility footprint and with as high as possible power conversion from the "wall-plug" to the beams. The ILC employs pulsed 1.3 GHz SC RF cavities with average accelerating gradient of 33.5 MV/m, has the total length of the 0.5 TeV c.m. energy facility of about 31 km and has design power efficiency (beam power/total AC power) of about 8%. CLIC scheme is based on two-beam acceleration in 12 GHz normal conducting RF structures with average gradient of 100 MV/m, the total length of the main tunnel of 3 TeV c.m. collider is 48 km and overall beam power efficiency is ~ 5%. Both projects have in principle demonstrated technical feasibility of their key acceleration technologies. Both have very tight requirements on the beam emittance generated in several km long injection rings, emittance preservation in the main linacs where beam is subject of minuscule transverse kicks due to vibrations and other dynamic misalignments, and need for ultimate precision beam position monitors to stabilize beam trajectories on every shot using fast beam-based feedback systems. The stability tolerances are even tighter for the elements of several-km long "final focus" systems – accelerator beamlines to focus beams to unprecedented beam sizes of σ^*_y / σ^*_x = 6 nm / 640 nm in the ILC and 0.9 nm / 45 nm in CLIC. Another "not-so-easy" to get around challenge is the c.m. energy spread induced by beamstrahlung (the energy loss caused by radiation of gamma quanta by the incoming electron due to its interaction with the EM field electron (positron) bunch moving in the opposite direction) during the very moment of collision of short bunches with rms length of σ_z = 50-300 μm, that for parameters of interest can be approximated as

$$\frac{\delta E}{E} \propto \frac{\gamma N^2 r_e^3}{\sigma_x^2 \sigma_z}, \qquad (1)$$

and reach several % or even 10% (see Table 2). The induced radiation generates undesirable background in the detectors, makes handling of the beams after the collision more sophisticated and, most importantly, sets limitation on the energy resolution of the narrow resonances such as in the expected Higgs- and *Z'*-boson decay reactions.

Muons, which can be thought of as heavy electrons, are essentially free of all synchrotron radiation related effects, which are proportional to the fourth power of the Lorentz factor γ^4, and, thus, $(m_\mu / m_e)^4 = 207^4 = 2 \times 10^9$ times smaller. So, a multi-TeV $\mu^+\mu^-$ collider [18] can be circular and therefore have a compact geometry that will fit on existing accelerator sites, e.g., Fermilab's. The collider has a potentially higher energy

reach than linear *e*+*e*- colliders, its c.m. energy spread in a 1.5-4 TeV $\mu^+\mu^-$ collider can be as small as 0.1%, requires less AC power and operates with significantly smaller number of elements requiring high reliability and individual control for effective operation - see Table 2. Additional attraction of a Muon Collider (MC) is its possible synergy with the Neutrino Factory concept [19] as beam generation and injection complex of that facility and of a MC are similar (perhaps identical) [20]. As mentioned above, due to higher mass of the muon and superb energy resolution, a Higgs factory based on low(er) energy $\mu^+\mu^-$ collisions is very attractive, too.

The biggest challenges of a MC come from the very short lifetime of the muon - $\tau_0 = 2\mu s$ is just long enough to allow acceleration to high energy before the muon decays into an electron, a muon-type neutrino and an electron-type antineutrino ($\mu^- \to e^- \nu_\mu \bar{\nu}_e$) – and from the methods of the muon production as tertiary particles in the reactions $pN \to \pi + ... \to \mu + ...$, so, the beams of muons are generated with very large emittances. A high-energy, 1-5 TeV c.m., high- luminosity $O(10^{34})$ $cm^{-2}s^{-1}$ muon collider will require a factor of $O(10^6)$ reduction of the 6-dimensional muon beam phase space volume (muon cooling). Though there has been significant progress over the past decade in developing the concepts and technologies needed to produce, capture and accelerate muon beams with high intensities on the order of $O(10^{21})$ muons/year, the feasibility of the high luminosity multi-TeV muon collider can be claimed only after demonstration of the fast ionization cooling of muons and resolution of the related issue of normalconducting RF cavities breakdown in strong magnetic fields. The latter is expected to be addressed by 2014-16, while convincing demonstration of the 6D cooling might take another 4 to 6 years [18].

Possible options for ultra-high energy colliders for the time scale beyond 20 years from now are outlined in Ref. [2].

4.1.3 References

1. E. Haussecker, A.W.Chao, *Physics in Perspective* **13** 146 (2011).
2. V.Shiltsev, arXiv: 1205.3087, accepted for publication in *Physics Uspekhy* (2012).
3. L.Rossi, in Proc. 2011 Intl. Part. Accel. Conf. (Spain), p.908.
4. G.Trubnikov, et al., in Proc. 2010 Russian Part. Accel. Conf. (Protvino), p.14.
5. M.Klein, in Proc. 2011 Intl. Part. Accel. Conf. (Spain), p.908.
6. V.Ptitsyn, et al. in Proc. 2011 Intl. Part. Accel. Conf. (Spain), p.3726.
7. S.Ahmed, et al., in Proc. 2011 IEEE Part. Accel. Conf. (New York), p.2306.
8. A.Lehrach, et al., *J. Phys.: Conf. Ser.* **295** 012156 (2011).
9. M.Bagiani, P.Raimondi, J.Seeman, arxiv:1009.6178.
10. T.Abe, et al., arxiv:1011.0352.
11. E.Levichev, *Phys. Particles and Nuclei Lett.* **5** 554 (2008).
12. The High Energy Large Hadron Collider, Preprint CERN-2011-003 (2011).
13. A.Blondel, F.Zimmermann, arxiv:1112:2518.
14. C.Ankenbrandt, et al., *Phys. Rev. ST Accel Beams* **2** 081001 (1999).
15. *ILC Reference Design Report* ILC-Report-2007-001, http://www.linearcollider.org.
16. J.P.Delahaye, *Mod. Phys. Lett. A* **26** 2997 (2011).
17. S.Geer, Annu. Rev. Nucl. Part. Sci. **59**:347–65 (2009).
18. V.Shiltsev, *Mod. Phys. Lett. A* **25** 567 (2010).
19. *The Neutrino Factory Int'l Scoping Study Accelerator Working Group Report, JINST* **4** P07001 (2009).
20. A.Poklonskiy, D.Neufer, *Int.J.Mod.Phys.* **A24** 959 (2009).

4.2 Physics of ep Colliders

Max Klein, University of Liverpool, U.K.
Mail to: max.klein@cern.ch

4.2.1 Introduction

With leptons, as the electron, and hadrons, as the proton, one can build pure lepton, pure hadron and lepton-hadron scattering experiments, specifically, one can construct ee, pp and ep colliders. The elementary participants in the corresponding scattering process are electrons and partons, quarks or gluons. The principle difference between the interaction of leptons and of partons consists in the confinement of the latter, and the self-interaction of gluons. Leptons and quarks differ by their participation in the strong interactions, and are not (yet) embedded in a unified theory, which would comprise both the electroweak theory and Quantum Chromodynamics (QCD), for which the SU(5) theory had been an attractive but experimentally not confirmed example. They continue to be distinct of each other.

Pure lepton, mostly e^+e^-, experiments are free of the strong interaction effects in the initial state, while their energy, expressed as the center of mass energy for an energy symmetric collider of beam momentum E_e, $\sqrt{s} = 2\ E_e$, has been and likely will be inferior to that of a proton beam collider $2E_p$. Therefore, e^+e^- colliders have had their most significant successes in the precision spectroscopy of particles, especially of charmonium, bottonium and the investigation of the Z boson. Strong interaction effects appear in the final state, and the three-jet, qqg, events at PETRA could "visualize" the gluon for the first time. Proton-proton (or antiproton) experiments have been accessing the physics at the highest energies achievable with accelerators, with outstanding luminosity in pp. Consequently they are built primarily to search for new particles and symmetries, and have discovered the W and Z bosons, the top quark and very likely the Higgs boson as has been announced the day this article is submitted. There is no interpretation of pp collider results without an understanding of the dynamics of quarks and gluons in the initial state, as for example the Higgs boson is dominantly produced via gg fusion in pp scattering. The primary role of ep experiments consists in the exploration of proton's structure using the electron as a so far pointlike probe in deep inelastic scattering (DIS). As unique and rich the physics of quark-gluon dynamics, of perturbative and non-perturbative QCD is, it often poses a special challenge when one has to characterize briefly the purpose of ep colliders wishing to go beyond the obvious description of ep machines as "microscopes" of superior resolution.

In the comparison of the kinematics of the recent ee, ep and pp machines, LEP/SLC, HERA and the Tevatron, one observes a remarkable similarity of their energy range when one considers that the average Bjorken x of a quark participating in the generation of a final state is about 0.3. This brings the equivalent, fermionic $\sqrt{s}$ values of LEP, HERA and the Tevatron all close to O(100) GeV ~ $M_{Z,W}$. The "Fermi energy scale" could hence been jointly investigated with these accelerators over the past.

Besides the distinction of the initial states and the yet existing differences in kinematic reach, the dynamics of particle production and variation in its mechanisms is at the heart of the complementarity of ee, ep and pp initiated searches for new physics. The cross sections, for example, for singly produced eq resonant states, lepto-quarks, as are predicted in various extended symmetry theories, are much larger in ep than in pp.

The control of the initial state quantum numbers is particularly important, should such states exist in the kinematic range of an ep collider.

The first ep collider ever built was HERA at DESY, which was proposed in 1984 and started operation in 1992. This followed a whole series of not realized proposals, made between 1972 and 1981, for lower energy ep colliders as is described in [1]. HERA represents the continuation of the electron and muon fixed target DIS experiments, with its neutral current (NC) ep → eX measurements, and also of the former neutrino DIS experiments, with its inverse charged current (CC) ep → νX measurements. There are three principal advantages of an ep collider experiment over a fixed target DIS experiment: i) the cms energy squared is $4E_eE_p$ compared to only $2E_lM_p$ in lepton scattering off protons at rest, of mass M_p, according to which HERA was equivalent to a 52 TeV lp fixed target experiment; ii) the thus enlarged phase space and large acceptance of a DIS collider experiment and iii) a particularly reliable, precise kinematic reconstruction because Q^2 and x can be determined redundantly both with the scattered electron kinematics and from the hadronic final state X.

HERA covered a huge range of physics investigations [2], slowly converging to the final results [3]. There are possibly five most remarkable results of HERA: i) the observation that the neutral and weak charged current interactions approach similar strength at four-momentum transfer $\sqrt{Q^2}$ values of about the mass of the weak bosons, and quarks are pointlike down to ~ 10^{-19}m; ii) the discovery that the proton at low parton momentum fractions x is governed by the gluon density, and a related determination of parton, quark and gluon, distribution functions (PDF) in the proton, including initial measurements of the charm and beauty densities; iii) the provision of unique limits in the search for supersymmetry with R parity violation; iv) the foundation of deep inelastic diffractive scattering as a process free of spectator jet particle production through the process of mainly photon-Pomeron fusion in ep; v) the measurement of novel phenomena in deep inelastic scattering (DIS) namely of particle production in a large rapidity range and of deeply virtual Compton scattering, which have paved the way to the novel concepts of unintegrated and of generalized parton distributions, respectively, and therefore of more-dimensional views on PDFs and proton structure. HERA also served the HERMES polarization experiment but could not answer the question on the composition of the proton spin as is discussed below.

Besides its pioneering accelerator technology role and the above cited unique physics results, HERA has had two serious drawbacks: i) it was not given enough time: it did not pursue the hitherto standard, and also proposed, investigations of neutron and nuclear structure in DIS, i.e. no attempts were made for electron-deuteron nor electron-ion collisions, and the low energy operation period at the end of HERA was too short for high precision measurements of the longitudinal structure functions, in DIS and in diffractive DIS; ii) the luminosity, between 10^{31} $cm^{-2}s^{-1}$ in the first 8 years of operation (HERA I from 1992-2000) up to 4 10^{31} $cm^{-2}s^{-1}$ in the following years (HERA II from 2003-2007) was too small for precision electroweak and high Bjorken x measurements.

New ep colliders have two principal physics goals, to further develop Quantum Chromodynamics and to contribute to the exploration of physics beyond the Standard Model, including the Higgs particle. These two tasks are subsequently briefly described. For the general overview character of the present article no attempt has been made to provide complete references, one may inspect the LHeC design report [1] and the Seattle Workshop contributions on EIC physics [4] and references cited therein.

4.2.2 **Quantum Chromodynamics**

QCD predicts the evolution of **parton distribution functions** with Q^2. The x dependence, yet, is to be determined from experiment. Basic questions related to quark distributions are still not answered, despite a 40 year history of DIS and the spectacular results of HERA. For example, the d/u ratio is not known at low x and neither at $x \rightarrow 1$, which affects high mass predictions of new particle searches at the LHC. The strange quark density, an essential part of the light quark sea, has not been measured in any accurate way. Recent hints from ATLAS point to SU(3) flavour democracy in contrast to the conventional strangeness suppression results, which have been based on di-muon data in neutrino experiments. The beauty density is only measured to about 20% accuracy while it may become important as the main production mechanism, $bb \rightarrow A$, of a non-SM Higgs particle. The charm (and beauty) density needs to be determined much more accurately, across the charm-quark production threshold for pinning down the heavy quark treatment in the parton evolution, and at large $x \geq 0.05$ for finding a so-called intrinsic contribution of charm to nucleon structure long been predicted. At very high Q^2 values, accessible only at the LHeC, the top quark distribution will become a new field of PDF research. A general drawback of the current PDF determinations has been their reliance on QCD fits using parameterisations and symmetry assumptions. This poses principal difficulties and makes the quoted uncertainties depending on these assumptions arbitrary to a considerable extent.

HERA has discovered that **the gluon** is the dominating parton distribution at low x, where quark production in DIS proceeds dominantly in a photon-gluon fusion process. The exceptional rise of the gluon density towards low x is expected to lead to non-linear gg dynamics such that the linear, so called DGLAP parton distribution equations may not apply anymore. A region of phase space is to be explored which represents a novel phase of matter, where Q^2 is large for the strong coupling to be small but the gluon, and sea, density so high that non-perturbative methods may have to be applied. The dominant process for Higgs production at the LHC is gluon-gluon fusion. Understanding the gluon distribution is also crucial in the attempt to measure the strong coupling constant precisely as each gluon emission causes an order α_s to occur. Diffractive DIS proceeds via Pomeron exchange, which is a color singlet state phenomenologically treated as a two-gluon state. An interfering three gluon state, the Odderon, has been predicted but not yet observed. The chromodynamic theory of the gluon is rich of many facettes, with instantons or axions as further examples, and the understanding of the gluon of prime importance for QCD and particle physics in general. It is high energy ep scattering with which this is appropriately investigated.

There are many **new developments in QCD**, which are of high theoretical and also phenomenological importance and require much more stringent tests and more complex measurements in an extended phase space. Examples are: i) the generalised parton distribution approach, accessible with Deeply Virtual Compton Scattering. This leads to a set of new structure functions and is directed to develop a 3-dimensional view on proton structure; ii) the un-integrated parton distribution approach, in which the transverse momentum of the emitted parton is considered. This is important for understanding the chain of multiple parton emission, which may not universally follow the so-called k_t-ordering as is inherent in DGLAP; iii) in QCD parton distributions are considered to be universal in that general factorisation theorems apply. These are largely broken in diffractive DIS, and only a very high precision test relating LHC and

LHeC measurements will clarify whether factorisation indeed applies in inclusive, non-diffractive scattering as has always been assumed; iv) finally, the investigation of high-energy electron-proton scattering can be important for constructing a non-perturbative approach to QCD based on effective string theory in higher dimensions.

Of special importance is **electron-ion scattering** at new colliders. Because HERA has failed to study this, the experimental information on nuclear parton distributions is restricted to fixed target DIS measurements only. Thus even a medium energy eA collider, as for example eRHIC, has a novel programme to pursue. Extreme phenomena, however, as the observation of saturation of the gluon density, probably enhanced like $A^{1/3}$, require the largest possible cms energy, for accessing this regime at all and for being able to study it where perturbation theory in α_s applies. One expects to study two complex phenomena, saturation and hadronic effects, and disentangling these will be easier when the saturation phenomenon may appear already in ep at the machine which also does eA. In terms of modern AA physics, eA explores the initial conditions of the hot, dense medium. The physics of nuclear PDFs is still to be explored, it will be richer than the mere quantification of shadowing corrections, involve heavy quark production, and be pursued in a kinematic range which is extended by two (EIC) or even four (LHeC) orders of magnitude in Q^2 and 1/x. With the variation of the energy transfer, inherent in DIS, one is able to distinguish hadronisation in and outside the nulear medium and possibly gain information on the confinement and hadron production mechanism.

A special task is the investigation of **neutron structure**. It is only based on classic assumptions, such that the up-quark distribution in the proton should equal the down-quark distribution in the neutron, on which our understanding of neutron's structure rests. In ultra-high energy neutrino scattering, for example, one needs to know both the neutrino-proton and the neutrino-neutron cross sections. The evolution in QCD is separated in two different terms, so-called singlet and non-singlet distributions. With only the proton structure function F_2^p, one has not enough information available to stabilise it and the addition of F_2^D is important. Electron-deuteron scattering may lead to surprises for hidden color which may result in high multiplicity final states. Theoretically DIS diffraction and nuclear shadowing are related phenomena, which may be tested and also exploited in the determination of the nuclear PDFs for the first time. The experimental conditions for accessing the neutron structure are very favourable at ep colliders, because one should be able to tag the spectator proton in en scattering and thus reduce or eliminate the Fermi motion effects which have plagued the interpretation of e.g. the d/u measurements at high x since decades.

There has been no ep collider built, in which both the electron and the proton were polarised. This situation is unsatisfactory. The **proton spin** of ½ cannot be built with quarks, as is known since the EMC polarised muon experiment, and has been confirmed by HERMES at HERA and COMPASS at the SPS muon beam at CERN. The spin therefore must be generated with polarised gluons, ΔG, or/and result from angular momentum contributions. The present information on $\Delta G(x,Q^2)$ resembles in its poverty the early attempts by the BCDMS and CDHSW fixed target experiments to determine $xg(x,Q^2)$ with a very limited range in Q^2 in unpolarised DIS. The information on ΔG is extracted from a measurement of a polarisation asymmetry, $A_{\|}$, the size of which is governed by the size of the relative energy transfer, y. In order to obtain a suitable, two-dimensional measurement of the related structure function $g_1(x,Q^2)$ one therefore needs a collider of variable beam energy in a certain range, of high, switchable polarisation

and of large luminosity as the asymmetry vanishes with x. The measurement of scaling violation in $g_1 \sim \Delta G$ results from combinations of data at various energies. Such measurements, like in unpolarised ep, determine also the polarised quark distributions much better than hitherto. With the possibility of also transverse polarisation measurements, a plethora of new polarisation phenomena and structure functions can be accessed. Following Ji, there is a relation of two generalised structure functions, E and H, with the angular momentum of the proton. As there is no practical option to polarise the protons of the LHC, these questions are the unique domain of the EIC proposals. It may be worth noting, that lepton polarisation asymmetries have been considered to study with improved precision and extended range the energy scale dependence of the weak mixing angle, from very low Q^2 as at MESA and Jlab to beyond the Z resonance, with the LHeC.

4.2.3 **New Physics with ep Colliders**

There is certain room for physics beyond the SM at new ep colliders of lower energy, related to QCD developments and high precision. However, it is mainly the large energy of the LHeC giving ep its complementary position in the investigation of physics beyond the Standard Model (SM), which possibly dominates the field of particle physics of the coming decades. At the same time, with high pace, ee, pp and ep experiments followed their intrinsic logics.

The most spectacular piece of new physics, especially since today, has been the SM scalar boson, **the Higgs particle**. In ep the most copious elementary production mechanism is $e^-u \rightarrow W^-W^+d\nu \rightarrow H$ jet ν. The clear identification, with the missing energy in CC, of this production mode offers the unique possibility to study the charge and parity properties of that boson, which may be a CP even (SM) state, a CP odd (non-SM) state or a mixture. The Higgs branching at 126 GeV mass is dominantly into bb, which in ep (unlike in pp, with large pile-up complicating forward jet reconstruction) can be handled in a straightforward manner and allows the WW-H-bb vertex, as well as further decay modes, to be measured with high precision. The production cross section at the LHeC is of order $O(100)fb^{-1}$. It was too small for HERA. Higgs boson physics has been considered as a key process to optimise the LHeC detector [1]. It will be a prime motivation to achieve a very high luminosity at the LHeC, desirably in excess of 10^{33} $cm^{-2}s^{-1}$. From a first study with still a non-optimised detector simulation, one estimates to reconstruct O(500) WW → H → bb events from a clear signal with a polarised electron beam at 60 GeV energy, for 100 fb^{-1}.

The genuine new physics role of an ep collider at the energy frontier is the search for and possibly the investigation of **lepto-quarks**, LQs, (or lepto-gluons) which may be formed in the s channel of the e-q interaction. The cross section for singly produced LQs at the LHeC is about a hundred times higher than that at the LHC, which preferentially pair produces such states. The current limit is about 700 GeV of mass, depending on which state one considers. If indeed LQ states are found at the LHC, the whole design of the LHeC, and its operation mode, will be adjusted to such findings. Further singly produced states are excited electrons and neutrinos, for which an interesting region of particular sensitivity in the coupling-mass plane is observed in [1].

Key to the exploratory programme of the LHC has been the search for supersymmetric (**SUSY**) particles. By mid 2012, with slightly more than half the design energy and a total luminosity of about 10 fb^{-1}, there have been no new states observed

which would be commensurate with SUSY in the about 1 TeV mass region. The LHC by 2015 or 16 is expected to reach its design energy, and the search range for SUSY masses will be extended to high masses. In a calculation of gluino pair production, originating mainly from gg → g, one finds huge differences between the current PDF groups, which can be traced back to large differences of xg at larger x. The LHeC provides a high precision determination of xg, which in this context renders the otherwise huge PDF uncertainties not interesting.

According to **grand unified theories** (GUT), possibly with SUSY embedded, the three basic couplings, the fine structure constant, the Fermi constant and α_s approach a common value at the Planck energy scale. The uncertainty of this convergence is determined by the currently overriding uncertainty of the strong interaction constant. It has been shown that the LHeC has the potential to measure α_s with per mille precision, i.e. ten times better than hitherto. Realisation of this programme is a major task challenging theory much as it needs an N^3LO base. Experimentally it can be seen to become possible, with higher kinematic range and measurement accuracy, less dependence on PDF parameterisations or an LHeC determination of the charm mass parameter in heavy quark schemes to two per mille.

To end this brief overview, it is worthwhile reminding that every step into a new region of phase space and intensity can provide **new insight, surprises**, deviations from the conventional wisdom. Deep inelastic scattering was crucial to discover quarks, to pin down the left handed doublet structure of fermions in the Standard Model or to discover the striking role of the gluon, which by its self-interaction gives mass to the baryonic matter. It may lead to discovering unexpected substructure phenomena, for example along speculations of the W,Z and top to possess structure, or it may become crucial for disentangling contact interaction phenomena which could be observed, say at 30 TeV. Similarly, there may be no saturation of the gluon density despite common belief, or the application of PDFs to describe LHC phenomena becomes questionable when factorisation is observed to not hold. Nature keeps holding surprises. It is for the joint exploration of phenomena that ee, ep and pp colliders have their prime justification to be built. One can but should not reduce the understanding of nature to a too narrow circle of questions. Once there was an argument made about the “dualism” of ee and pp physics. This disregarded the unique role of ep physics. It would similarly be unfortunate if the future of ep colliders was narrowed to the energy frontier machine, the LHeC, for physics is richer and diversity a condition for insight and true understanding.

4.2.4 References

1. LHeC Study Group, *A Large Hadron Electron Collider at CERN*, J.Phys.G:Nucl.Part.Phys. **39** (2012) 075001, arXiv:1206.2913 [acc-ph].
2. M.Klein and R.Yoshida, *Collider Physics at HERA*, Prog.Part.Nucl.Phys. **61** (2008)343.
3. See, for example, the Proceedings of the 2011 and 2012 Workshops on Deep Inelastic Scattering, Newport News (USA) and Bonn (Germany).
4. D.Boer et al, *The EIC Science Case*, arXiv:1108.1713 [nucl-thy].

4.3 Polarized Electron-Nucleon Collider ENC at FAIR

Andreas Lehrach
Forschungszentrum Jülich, Institut für Kernphysik, Jülich, Germany
Mail to: a.lehrach@fz-juelich.de

4.3.1 Introduction

The ENC project attempts to realize an electron-nucleon collider at the upcoming Facility for Antiproton and Ion Research FAIR at GSI Darmstadt by utilizing the antiproton high-energy storage ring HESR for polarized proton and deuteron beams. The addition of a 3.3 GeV storage ring for polarized electrons will enable electron-nucleon collisions up to a center-of-mass energy of 14 GeV. In such a configuration peak luminosities in the range of $L = 10^{32}$ to 10^{33} $cm^{-2}s^{-1}$ are feasible. Beam-beam effects in a space-charge dominated regime in conjunction with high-energy electron cooling represents one of the main challenges for this project. Beside highest possible luminosity, the high-priority goal of the ENC project is to reach longitudinal polarized electron - nucleon collisions with high polarization of up to 80% in both beams.
In this paper beam- and spin-dynamics simulations are presented, together with the required modifications and extensions for a collision mode of the HESR storage ring and the conceptual design of this new collider complex.

4.3.2 Brief Status of HESR at FAIR

The FAIR Facility will provide antiproton and ion beams with unprecedented intensity and quality. In the final construction FAIR consists of up to eight accelerator rings, two linear accelerators and various beam transport lines [1]. The planned proton linac together with the existing GSI accelerators serves as injector for this new facility. Utilizing the new synchrotron ring SIS100 intense beams of secondary beams - unstable nuclei or antiprotons - can be produced. Several cooler storage rings substantially increase the quality of these secondary beams in terms of energy spread and emittance. The Modularized Start Version is a stepwise approach to the realization of FAIR [2].

The HESR [3] is an essential part of the antiproton physics program at FAIR. Primarily designed to provide antiprotons in the momentum range from 1.5 to 15 GeV/c for the internal target experiment PANDA [4], the HESR will serve as proton/deuteron storage ring. A consortium consisting of FZ Jülich (as leading institution), GSI Darmstadt, Universität Mainz and ICPE-CA Bucharest is in charge of HESR design and construction. An important feature of this new facility is the combination of phase space cooled beams and thick internal targets (e.g., pellet targets) which result in demanding beam parameter requirements for two operation modes: high luminosity mode with peak luminosities of up to 2 10^{32} $cm^{-2}s^{-1}$ and high resolution mode with a beam momentum spread down to 10^{-5} (rms).

Various beam dynamics studies have been performed to guarantee the required equilibrium beam parameters, beam lifetime and beam stability [5]. Powerful beam cooling is needed to reach demanding experimental requirements in terms of luminosity and beam quality. The construction phase of the FAIR including HESR already started.

4.3.3 General Layout of ENC

The proposed ENC concept integrates an appropriate 3.3 GeV electron ring in the HESR tunnel (Fig. 1). Center-of-mass energies of roughly 14 GeV for electron-proton and 9 GeV for electron-deuteron in head-on collisions can be provided [6,7]. Pre-acceleration of protons and deuterons would take place in the planned proton linac [8] and the heavy-ion linac UNILAC [9], respectively. The heavy-ion synchrotron SIS 18 [10] would be suitable to accelerate these beams to HESR injection momentum of 3.8 GeV/c. An additional beam line from SIS18 to HESR has already been proposed for HESR commissioning with protons. For polarized proton/deuteron beams, additional equipment has to be installed in the HESR and the pre-accelerators of its injection chain to measure and preserve the beam's polarization. A corresponding scheme to accelerate and store longitudinal polarized electrons is under investigation [11].

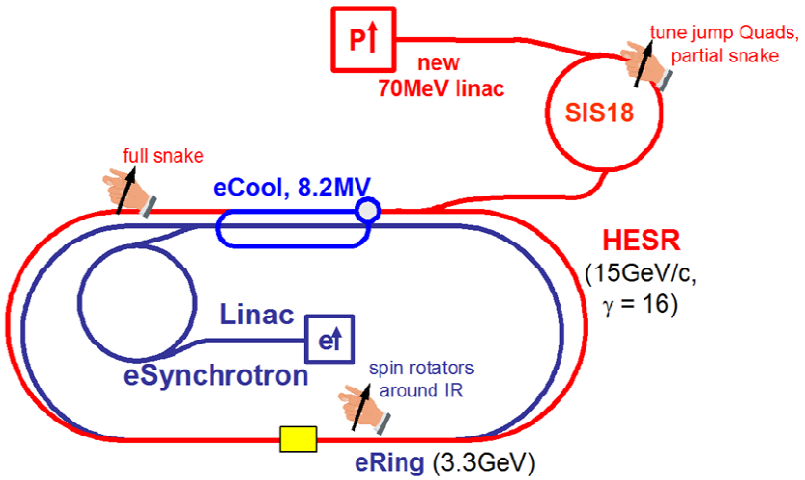

Figure 1: Scheme of ENC at FAIR for electron-proton collisions (not to scale).

4.3.4 Beam Dynamics Simulations

Calculations of cooled beam equilibria including intra-beam scattering and beam-beam interaction have been performed using the *BetaCool* code [12]. The model calculations assume a Gaussian beam distribution in phase space over all degrees of freedom. For electron cooling the *Parkhomchuk* model [13] of the friction force was chosen and for intra-beam scattering the *Martini* model [14] using ring lattice functions imported from the MAD program.

4.3.4.1 *Equilibrium Beam Parameter and Luminosity Estimates*

Different scenarios for electron-proton and electron-deuteron collisions have been investigated to estimate maximum luminosities. In tables 1 and 2 relevant equilibrium beam parameters and luminosity estimates are summarized. The numbers in brackets are based on a scenario with an advanced interaction-region design [15,16] that would allow for collisions with $\beta^{IP}_{x;y}$ = 0.1 m. Beam simulations indicate, that the electron cooler would need a major upgrade to an electron current of 3 A at 8.2 MeV electron energy to sufficiently cool proton beams during collisions. The deuteron beams would

only require the design parameter of the HESR electron cooler with a 1 A electron beam accelerated to 4.1 MeV [17]. Dedicated high-voltage storage RF systems in the frequency range from 52 to 104 MHz have to be incorporated into HESR to allow for multi-bunch operation of 100 to 200 bunches. During beam collisions an RF voltage of roughly 300 kV is sufficient to keep the beam particles inside the RF buckets.
The performed beam studies have clearly shown that peak luminosities are mainly limited by space charge and beam-beam parameter in the nucleon ring. Estimates indicate that maximum luminosities above $6 \cdot 10^{32}$ $cm^{-2}s^{-1}$ are challenging but can in principle be reached with present day technology.

More detailed studies and an advanced interaction region design are required to squeeze the beta function at the interaction point from $\beta^{IP}_{x;y} = 0.3$ m to 0.1 m; especially beam separation, beam-beam parameter and chromaticity correction are main objectives to be studied in detail.

Table 1: Equilibrium beam parameter and luminosity estimates for electron-proton collisions for baseline **(advanced)** design.

Parameter	***15 GeV/c protons***	**3.3 GeV electrons**
ε_{geo} [mm·mrad] (rms)	0.14	
$\Delta p/p$ (rms)	$4 \cdot 10^{-4}$	
$\beta^{IP}_{x;y}$ [m]	0.3 **(0.1)**	
r^{IP} [mm] (rms)	0.2**(0.1)**	
l (bunch length) [m]	0.27-0.35 **(0.19-0.25)**	0.1
n (particle / bunch)	5.4 **(3.6)**$\cdot 10^{10}$	$23 \cdot 10^{10}$
h (number of bunches)	100 **(200)**	
f_{coll} (collision freq) [MHz]	52 **(104)**	
l_{coll} (bunch distance) [m]	5.76 **(2.88)**	
ΔQ_{sc} (space-charge tune shift)	0.05 **(0.1)**	
ξ (beam-beam parameter)	0.014 **(0.014)**	0.015 **(0.01)**
L (luminosity) [$cm^{-2}s^{-1}$]	2 **(6)**$\cdot 10^{32}$	

Table 2: Equilibrium beam parameter and luminosity estimates for electron-deuteron collisions for baseline **(advanced)** design.

Parameter	***15 GeV/c deuterons***	**3.3 GeV electrons**
ε_{geo} [mm·mrad] (rms)	0.15	
$\Delta p/p$ (rms)	$2.4 \cdot 10^{-4}$	
$\beta^{IP}_{x;y}$ [m]	0.3 **(0.1)**	
r^{IP} [mm] (rms)	0.2**(0.1)**	
l (bunch length) [m]	0.17-0.19	0.1
n (particle / bunch)	$1.1 \cdot 10^{10}$	$23 \cdot 10^{10}$
h (number of bunches)	173	172
f_{coll} (collision freq) [MHz]	89.3	
l_{coll} (bunch distance) [m]	3.3	
Q_{sc} (space-charge tune shift)	0.1	
ξ (beam-beam parameter)	0.013 **(0.014)**	0.025 **(0.03)**
L (luminosity) [$cm^{-2}s^{-1}$]	0.6 **(1.8)**$\cdot 10^{32}$	

Crab crossing could further increase the performance of the proposed collider concept [18], by allowing for a crossing angle without loss of luminosity. Crab crossing has never been employed for hadron collisions, but it can be applied for electron-hadron collisions if only the electron bunches are tilted by the full crossing angle.

4.3.4.2 *Beam Bunching*

To get the anticipated number of bunches, a complicated re-bunching process in combination with phase-space cooling has to be performed to minimize cooling time and beam losses. The beam would first be accelerated in one or two bunches to collision energy, using the regular HESR accelerating cavity. Since the cooling time to equilibrium parameters with 200 bunches at 15 GeV/c would take many hours, the proposed scheme is to debunch the beam after acceleration and cool the unbunched beam to the required beam equilibrium before rebunching. That would reduce the cooling time to roughly 20 minutes. During the rebunch procedure the storage RF systems have to be adiabatically turned on while the beam is still cooled, to minimize beam losses. The required RF voltage for rebunching depends on details of the rebunch procedure and available cooling force. If the initial beam emittance before cooling is too large, one could in addition apply beam pre-cooling at injection energy up to the space-charge limit.

4.3.5 **Polarized Beams**

Polarized proton/deuteron beams have to be produced in a dedicated polarized ion source, pre-accelerated in the planned proton linac or UNILAC, and accelerated to HESR injection energy in SIS18. Acceleration and storage of polarized proton in medium and high energy circular accelerators is complicated since numerous spin resonances have to be crossed. In strong-focusing synchrotron and storage rings like SIS18 and HESR imperfection and intrinsic resonances can significantly depolarize the beam. Spin resonances and preservation of polarization for protons in SIS18 and HESR has already been discussed [19,20]. For a single Siberian snake longitudinal polarized proton beams can be prepared at the interaction point. Due to the much smaller gyromagnetic anomaly of deuterons this is not possible with reasonable technical effort for deuteron beams.

The scheme to accelerate and store longitudinal polarized electrons comprises polarized electron sources, a full energy electron injector (synchrotron or pulsed linac) and an electron storage ring. Spin lifetime under the influence of synchrotron radiation and providing longitudinal beam polarization at the interaction point are currently under investigation [11]. Spin dynamics simulations with a single Siberian snake scheme showed unacceptably short spin lifetimes in the range of few minutes. A scenario with multiple Siberian snakes has been proposed for the Novosibirsk c-tau factory project to increase spin lifetime of polarized electrons significantly [21].

4.3.5.1 *Spin Resonances in SIS 18*

In the momentum (energy) range from 369 MeV/c (70 MeV) to 3.8 GeV/c (3.0 GeV) six imperfection resonances for protons (γG = 2, 3, 4,..., 7) have to be crossed. For an acceleration rate of 1 GeV/c per 0.05 s a 3% partial snake (0.5 Tm solenoid) is sufficient to overcome these spin resonances by exciting adiabatic spin

flips. Due to high super-periodicity of the SIS18 lattice (P = 12) only one intrinsic resonance ($\gamma G = 0 + Q_y$) occurs, where Q_y is the vertical betatron tune. The preferred correction method for intrinsic resonance depends on the vertical beam emittance. For the expected normalized beam emittance in the range of few mm·mrad a tune-jump quadrupole is an adequate method to overcome intrinsic resonances [22]. A small beam emittance for efficient tune jumps and a lower acceleration rate to reduce the snake strength would be beneficial for polarized proton beam acceleration in SIS18.

For deuterons no first-order spin resonances have to be crossed up to HESR injection energy. Only one weak gradient-error spin resonance ($\gamma G = 3 - Q_y$) could lead to small polarization losses, but it could easily be crossed by tune jumping.

4.3.5.2 *Spin Resonances in HESR*

In total 25 imperfection resonances, 50 intrinsic resonances and 50 coupling spin resonances must be overcome during acceleration in HESR. The large number of resonances in the HESR makes it very hard to apply techniques of individual manipulation of single spin resonances [23]. The application of Siberian snakes is the only option to guarantee a setup with low polarization losses during acceleration. Therefore a magnet system with combined field types has been investigated [20]. It consists of four RHIC-type helical dipole magnets with a maximum field of 2.5 T and a 15 Tm solenoidal field. Space for the helical dipole snake has been reserved in the straight section where the electron cooler is located. To reach the required 15 Tm solenoidal field a DC electron cooler in combination with its rampable correction solenoid can be used.

For deuterons only one imperfection resonance ($\gamma G = -1$) and two intrinsic resonances ($\gamma G = -8 + Q_y$, $7 - Q_y$) have to be crossed. The proposed Siberian snake can only be operated as a partial snake and additional tune-jump quads have to be installed in the HESR. If the vertical betatron tune is placed close to in integer, a partial snake is in principle also suitable to overcome intrinsic resonances [24]. The challenge is to run a circular accelerator with a betatron tune close to an integer [25].

4.3.6 **Conclusion and Outlook**

The ENC study group aims to realize a polarized electron-nucleon collider at the upcoming FAIR facility within the next decade. Experiments with polarized beams would become available with maximum luminosities of roughly 2 to $6 \cdot 10^{32}$ $cm^{-2}s^{-1}$. The design of an adequate lattice for the electron ring including simulations to optimization of spin lifetime is of major importance for this project. Further studies of modifications and extensions to the HESR storage ring have to be performed. Especially electron cooling of relativistic ion beams, collective effects and extensive RF bunching require detailed beam studies. Operating a collider with large beam-beam tune shift in a space-charge dominated regime is certainly the main luminosity limitation for ENC. The integration of PANDA detector, taking into account the required detector acceptance angles and the given detector geometry, further restricts beam separation and focusing in the interaction region. A crossing angle at the collision point in combination with crab crossing could increase the performance of the ENC collider in terms of detector acceptance and peak luminosity.

4.3.7 **Acknowledgement**

The author wishes to acknowledge the encouragement from colleagues of the ENC accelerator study group: K. Aulenbacher, O. Boldt, R. Heine, W. Hillert, A. Jankowiak, C. Montag, P. Schnizer, and T. Weis. I'm also very grateful to the members of the HESR consortium, especially to the project leader R. Maier.

4.3.8 **References**

1. "An International Accelerator Facility for Beams of Ions and Antiprotons", FAIR Baseline Technical Report, GSI Darmstadt, ISBN 3-9811298-0-6 (2006).
2. "FAIR - Facility for Antiproton and Ion Research", Green Paper - The Modularized Start Version, Green Paper, October 2009, http://www.fair-center.de/.
3. A. Lehrach et al., "The high-energy storage ring (HESR) for FAIR", International Journal of Modern Physics (IJMPE) E 18 Issue 2, 420 (2009).
4. PANDA Collaboration, "Physics performance report for PANDA: strong interaction studies with antiprotons", arXiv:0903.3905v1 [hep-ex] (2009) http://arxiv.org/abs/0903.3905.
5. O. Boine-Frankenheim et al., Nucl. Instr. Meth. A 560, 245 (2006); A. Lehrach et al., Nucl. Instr. Meth. A 561, 289 (2006); F. Hinterberger, Beam-Target Interaction and Intrabeam Scattering in the HESR Ring, Report of the Forschungszentrum Jülich, Jül-4206, ISSN 0944-2952 (2006); H. Stockhorst et al., "Stochastic Momentum Cooling Experiments with a Barrier Bucket Cavity and Internal Targets at FAIR", Proc. of IPAC'10, Kyoto, Japan, MOPD068, 846 (2010).
6. A. Jankowiak et al., "A Concept for a Polarized Electron-Nucleon Collider at the HESR of the FAIR Project", Proceedings of the Particle Accelerator Conference (PAC'09), Vancouver, Canada, http://accelconf.web.cern.ch/AccelConf/PAC2009/papers/we6pfp063.pdf.
7. A. Lehrach et al., "The polarized electron-nucleon collider project ENC at GSI/FAIR", J. *Phys.: Conf. Ser.* 295, 012156 (2011).
8. L. Greoning et al., "The 70-MeV proton linac for the facility for antiproton and ion research FAIR", Proc. of LINAC 2006, Knoxville (TN) USA, http://accelconf.web.cern.ch/AccelConf/l06/PAPERS/MOP061.PDF.
9. W. Barth et al., "Long term perspective for the UNILAC as a high-current heavy ion injector for the FAIR-accelerator complex", Proc. of LINAC2006, Knoxville (TN) USA, http://accelconf.web.cern.ch/AccelConf/l06/PAPERS/MOP059.PDF.
10. K. Blasche et al., "The SIS heavy ion synchrotron project", Proc. of PAC1985, IEEE Transactions on Nuclear Science NS-32 No. 5, 2687 (1985).
11. O. Boldt et al., "Investigation of various electron ring concepts for the ENC with regard to depolarizing effects", *J. Phys.: Conf. Ser.* 295, 012157 (2011).
12. A.O. Sidorin et al., Nucl. Inst. Meth. A 558, 325 (2006).
13. V.V. Parkhomchuk, Nucl. Inst. Meth. A 441, 9 (2000).
14. M. Martini, CERN AA Report PS/84-9 (1994), Geneva Switzerland.
15. C. Montag et al., "Interaction region design for the electron-nucleon collider ENC at FAIR", Proc. of IPAC2010, Kyoto Japan, http://accelconf.web.cern.ch/AccelConf/IPAC10/papers/tupeb051.pdf.
16. P. Schnizer et al., "Magnet design of the ENC@FAIR interaction region", Proc. of IPAC2010, Kyoto Japan, http://accelconf.web.cern.ch/AccelConf/IPAC10/papers/mopeb026.pdf.
17. B. Gålnander et al., "Status of design work towards an electron cooler for HESR", Proc. of the Workshop on Beam Cooling and Related Topics COOL2007, Bad Kreuznach Germany.

18. R.B. Palmer, “Energy scaling, crab crossing and the pair problem”, SLAC-PUB-4707 (1988), Stanford (CA) USA.
19. A. Lehrach et al., “Modifications of the HESR layout for polarized antiproton-proton physics” Proc. of the 17th International Spin Physics Symposium SPIN2006, Kyoto Japan, AIP Conf. Proc. 915, 147 (2007).
20. A. Lehrach et al., “Polarized beams in the high-energy storage ring of the future GSI project”, Proc. of the 16th International Spin Physics Symposium SPIN2004, Trieste, Italy.
21. I. Koop et al.,”Longitudinally polarized electrons in Novosibirsk c-tau factory”, *J. Phys.: Conf. Ser.* 295, 012160 (2011).
22. A. Lehrach et al., “Overcoming depolarizing resonances at COSY”, AIP Conf. Proc. 667, 30 (2003).
23. K.Z. Khiari et al., Phys. Rev. 39, 45 (1989); H. Huang et al., Phys. Rev. Lett. 73, 2982 (1994); M. Bai et al., Phys. Rev. Lett. 80, 4673 (1998).
24. T. Roser et al., “Acceleration of polarized beams using multiple strong partial Siberian snakes”, Proc. of EPAC2004, Lucerne Switzerland, http://accelconf.web.cern.ch/AccelConf/e04/PAPERS/TUPLT190.pdf.
25. H. Huang et al., Phys. Rev. Lett. 99, 154801 (2007).

4.4 MEIC – A Polarized Medium Energy Electron Ion Collider at Jefferson Lab

Yuhong Zhang for the MEIC Study Group
Thomas Jefferson National Accelerator Facility, Newport News, VA 23606 USA
Mail to: yzhang@jlab.org

4.4.1 Introduction

Jefferson Lab’s response to U.S. scientific user demand for a future gluon microscope is to propose a high luminosity polarized medium energy electron-ion collider (MEIC). It is a natural expansion of the precision measurement based nuclear science program at Jefferson Lab, and opens new QCD research frontiers [1] with more than an order of magnitude increase in the center of mass (CM) energy coverage over the recent successfully completed 6 GeV CEBAF fixed target program, and the future 12 GeV CEBAF program after completion of the energy upgrade in 2015.

After over a decade of science and machine feasibility studies, the envisioned science program and accelerator technology developments have been driving this future electron-ion collider toward a medium CM energy range [2]. Currently, Jefferson Lab takes a two-step staging approach for this facility based on different CM energy coverage, namely, a low medium energy range and an upper medium energy range respectively, allowing a maximum science reach over the entire life of the proposed collider under the foreseen fiscal and technical constraints. During the last two years, the Jefferson Lab design effort has been focused primarily on the first stage, MEIC, with CM energy up to 66 GeV [3,4]. As a result of this effort, a conceptual machine design has been completed [5].

MEIC is currently designed as a ring-ring collider with up to three interaction points (IPs), enabling collisions of polarized electrons (and positrons) with polarized light ions (p, d, ^{3}He and possibly Li and Be) and non-polarized light to heavy ions (up to lead). It covers beam energy up to 11 GeV for electrons, 100 GeV for protons and 40 GeV/u for

heavy ions. It utilizes the CEBAF linac for injection of a full-energy electron beam into a new storage ring. To complete the facility, a new ion injector and storage ring complex will be added to the Jefferson Lab site. For meeting one project goal, the option of a future upgrade is preserved for reaching 140 GeV CM energy and 10^{35} $cm^{-2}s^{-1}$ luminosity. Figure 1 shows the MEIC and its future upgrade in the Jefferson Lab site map.

Since the beginning of this study, the machine design effort has been focused on achieving the highest collider performance [6] in terms of high luminosities simultaneous over multiple IPs, full or very large detector acceptance capability, and high beam polarizations for leptons and several light ions. MEIC has adopted several unique design features to ensure the high performance. They include high bunch repetition rates and ultra small bunch charge ion beams; multi-staged electron cooling of ion beams; a figure-8 shape for all ion booster synchrotrons and both collider rings; and crab crossing of colliding beams at IPs. With these design features and other advanced accelerator technologies MEIC should be able to reach high luminosity above 10^{34} $cm^{-2}s^{-1}$ and also maintain 70% or above polarization for both beams.

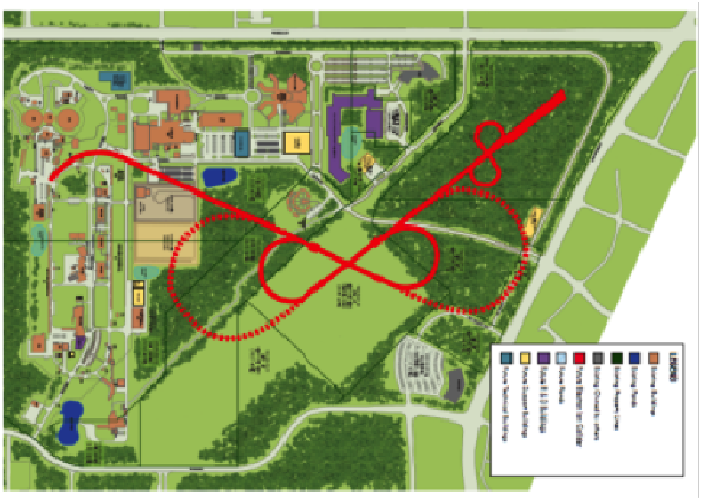

Figure 1: MEIC (solid red line) and its future upgrade (dashed red line) on the Jefferson Lab site. The ion injector (sources, linac and pre-booster) is in the upper right corner. CEBAF is on the left with a transfer line to the electron storage ring.

4.4.2 **Baseline Design**

The central part of the MEIC facility is two collider rings stacked vertically as shown in Figure 2. The electron ring stores 3 to 11 GeV electrons injected at full energy from CEBAF, while the superconducting ion ring stores 20 to 100 GeV protons or up to 40 GeV/u fully stripped ions. The two long straights of the figure-8 rings accommodate three IPs (the fourth symmetric location is reserved for a spin polarimetry); however, only two detectors are under consideration in the MEIC phase. As shown in Figure 2, the ion beams execute a vertical excursion to the plane of the electron ring for horizontal crab crossing at IPs. Such a design avoids the vertical motion of the electron beam for the purpose of preserving its low vertical emittance and spin polarization. An optional third detector may be placed at another IP for collisions of electrons with low energy (below 20 GeV/u) ions stored possibly in a dedicated compact storage ring.

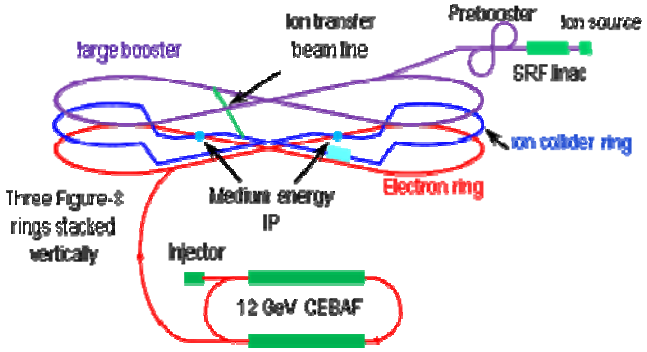

Figure 2: A schematic layout of MEIC at Jefferson Lab.

The MEIC machine parameters are summarized in Table 1 for *e-p* collisions at a 60×5 GeV^2 design point for both a full acceptance detector and a high luminosity detector (the values are in parentheses). Luminosities for *e-p* collisions with different CM energies are shown in Figure 3. Table 2 shows luminosity for *e-A* collisions for several representative ion species. To reach full detector acceptance, the magnet free detector space (the distance from an IP to the front face of the first focusing quad) must be at least 7 m for ions; however, it can be shortened to 3.5 m for electrons. For the second detector optimized for higher luminosities while still retaining a very large detector acceptance, the detector space can be reduced to 4.5 m so the luminosity is doubled to above 10^{34} cm^{-2}s^{-1}.

Table 1: MEIC Parameters at a design point of 60×5 GeV2 e-p collision for a Full-Acceptance Detector.

		Proton	Electron
Beam energy	GeV	60	5
Collision frequency	GHz	0.75	
Particles per bunch	10^{10}	0.416	2.5
Beam current	A	0.5	3
Polarization	%	>70	~80
RMS bunch length	mm	10	7.5
Normalized emit. (ε_x / ε_y)	mm	0.35/0.07	53.5/10.7
Horizontal beta-star	cm	10 (4)	
Vertical beta-star	cm	2 (0.8)	
Vert. beam-beam tune-shift		0.015	0.03
Laslett tune-shift		0.06	Small
Detector space	m	±7 (4.5)	±3.5
Luminosity per IP (10^{33})	cm^{-2}s^{-1}	5.6 (14.2)	

(Values for a high-luminosity detector are given in parentheses)

Table 2: MEIC *e-A* luminosities for different ion species.

		Proton	Deuteron	Helium	Carbon	Calcium	Lead
Ion species		P	d	$^{3}He^{++}$	$^{12}C^{6+}$	$^{40}Ca^{20+}$	$^{208}Pb^{82+}$
Ion energy	GeV/u	100	50	66.7	50	50	40
Ion current	A	0.5					
Ions per bunch	10^9	4.2	4.2	2.1	0.7	0.2	0.05
Ion β* (*x/y*)		6/2 (2.4/0.8)					
Ion beam-beam tune shift (vertical)		0.014	0.008	0.01	0.008	0.008	0.006
Electron beam	Energy: 6 GeV; Current: 3 A; Electrons per bunch: 2.5×10^{10} Vertical β*: 1.55 to 2.8 cm (0.61 to 1.1 cm) Vertical beam-beam tune-shift: 0.022 to 0.029						
Luminosity/IP (10^{33})	$cm^{-2}s^{-1}$	7.9 (20)	5.5 (14)	7.3 (19)	5.5 (14)	5.5 (14)	4.4 (11)

(Values for a high-luminosity detector are given in parentheses)

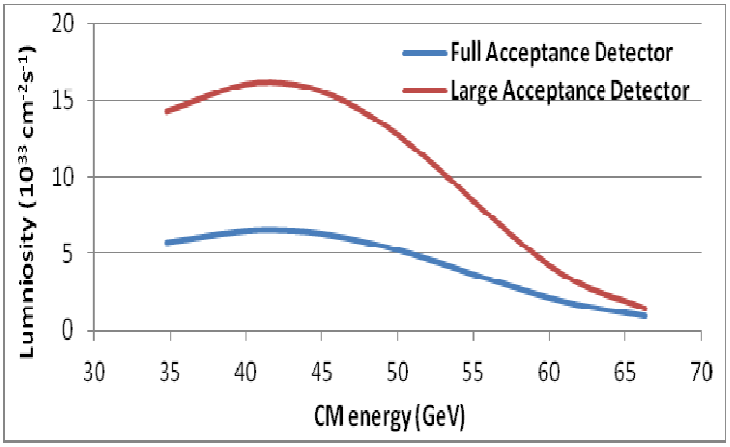

Figure 3: MEIC *e-p* collision luminosity.

4.4.3 Technical and Design Choices

The high luminosity of MEIC relies on high bunch repetition colliding beams [7], a key ingredient of a luminosity concept spearheaded by several modern lepton-lepton colliders [8] which have achieved unprecedented high luminosities. In MEIC, the electron beam from CEBAF has a bunch repetition rate of 1.5 GHz, while the ion beams from a specially designed ion complex will match the electron beams. MEIC thus holds a promise to replicate the luminosity success in colliders involving hadron beams. A 750 MHz has been chosen as a base frequency for the present design.

The MEIC collider rings stores several thousand ion or electron bunches with very small bunch spacing under a 750 MHz base frequency for the present design. The bunch charges of such beams are very small (as low as several of 10^9 protons per bunch); however, a moderate current can be achieved by the large number of bunches in the rings. This is very different from a typical hadron storage ring whose bunch number is usually small; therefore the bunch length is usually long in order to hold a very large

number of particles (~10^{11}) per bunch for maintaining even a modest beam current. In MEIC, an ultra small bunch charge allows a dramatic reduction of the bunch length (as low as 1 cm RMS) with assistance of electron cooling, therefore permitting beta-stars hundreds times smaller than those of the typical hadron colliders. With appropriate interaction region designs, the combination of a high bunch repetition rate and ultra-small beta-stars could lead to a very high luminosity [7].

Initially, the Jefferson Lab electron-ion collider was designed naturally as an ERL-ring collider [9] due to the existing CEBAF SRF linac and also the successful experience of ERL technology. It later evolved into a traditional ring-ring collider after the realization that the ERL-ring collider scenario, in fact, does not provide additional and significant advantages in achieving a higher luminosity with high bunch repetition rate beams [7]. It would in actuality add tremendous burdens on technology development including high current polarized electron sources and high current/energy ERLs.

A unique design feature of MEIC is its figure-8 shape for all the booster and collider rings. Such a design greatly improves the preservation of the ion polarization during acceleration and storage, and also significantly simplifies the spin control [10]. An additional and important advantage of the figure-8 design is that it allows the acceleration and storage of polarized deuterons, thus expanding its science reach enormously [2].

The MEIC design is derived with certain limits on parameters of stored beams due to collective beam effects [5]: the ion beam space-charge tune-shift should be less than 0.1; the total beam-beam tune-shift summed over all the IPs must not be larger than 0.03 and 0.1 for ion and electron beams respectively. We have also imposed limits on other machine parameters [5] based largely on previous lepton and hadron collider experience and the present state of the art of accelerator technologies in order to reduce R&D challenges and to improve robustness of the design. As an example, the stored beam currents are up to 0.5 and 3 A for ions and electrons respectively, and the electron synchrotron radiation power should not exceed 20 kW/m.

4.4.4 **Electron and Ion Collider Rings**

The two collider rings have nearly identical footprints (shown in Figure 4) and intersect at two symmetric points in the two long straights of the figure-8 for medium energy collisions. The figure-8 has a crossing angle of 60°, thus partitioning the ring roughly equally into two arcs and two long straights. The long straights also accommodate utility components such as injection, RF systems, and electron cooling. There are two short (20 m) straights in the middle of the two arcs of the ion ring for two Siberian snakes. Table 3 summarizes the parameters of the ion and electron collider rings.

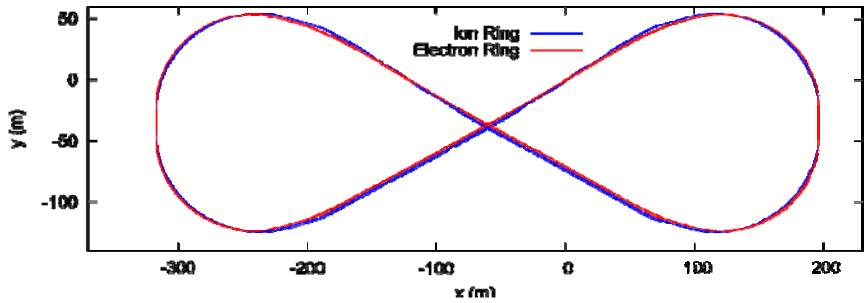

Figure 4: The layout of the MEIC electron and ion collider rings using MAD-X output.

Table 3: Main design parameters of the MEIC collider rings.

		Proton (ion)	Electron
Proton kinetic energy	GeV/u	20 to 100 (40)	3 to 11
Circumference	m	1340.9	1340.4
Figure-8 crossing angle	deg	60	
Arc length[#] and average radius	m	391.0 / 93.3	405.8 / 96.9
Length of long and short straight	m	279.5 / 20	264.5 / 25.9
Electron universal spin rotator	m		47.6
Base lattice		FODO	
Length of cell in arc / straight	m	9 / 9.3	5.25 / 5.58
Phase advance per cell, hori. / vert.	deg	60 / 60	120 / 120
Number of cells in arc / straight		52 / 20	54 / 48.5
Dispersion suppression		Adjusting quadrupole strength	

An electron arc also includes short straight section and two Universal Spin Rotators

Both MEIC collider rings are designed as FODO lattices in arcs and straights. The functional blocks such as spin rotators, Siberian snakes, interaction regions and RF systems will be treated as isolated insertions into the base lattices and optics matching is required. The electron arc lattice is designed mirror symmetrically about the short straight in the center. Each half arc contains 27 cells including 2.5 and 3.5 cells for dispersion suppression near the short straight, and for matching optical functions to those of the spin rotator, respectively. The filling factor of the arc cell is 57%. There are 48.5 cells in one long straight; 5 of them are in two identical optics matching blocks at both ends. The electron ring optics function is shown in Fig. 5.

In the ion collider ring, the four 120º arc sections separated by two long and two short straights are designed identically with a FODO lattice. The 9 m long arc base unit is filled with two 3 m long SC dipoles of 3.236° bending; 33 such dipoles in one arc section provide 106.8° bending. Three more SC dipoles providing total 13.2° bending are placed 21 m away from the regular arc cells in order to match the footprint of an electron spin rotator. The ion collider optical functions are also plotted in Fig. 5.

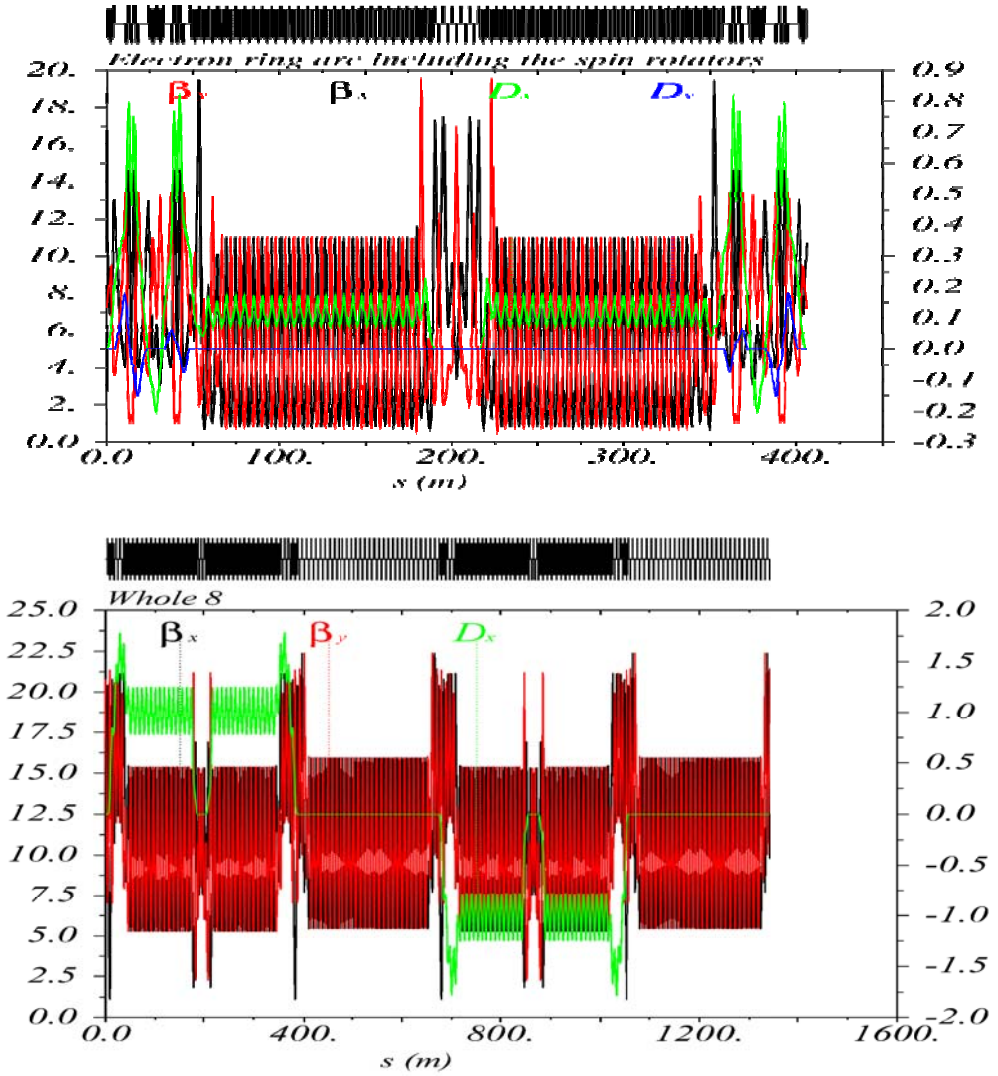

Figure 5: Optical functions of the electron (upper) and ion (lower) collider rings.

Beam synchronization in MEIC is a challenging issue. In the medium energy range, ions are not fully relativistic yet; thus the revolution time of the collider ring is energy dependent. On the other hand, electrons with energies of 3 GeV and above are already ultra-relativistic so the revolution time is a constant. The circumferences of two collider rings can be adjusted such that the revolution times are matched (or identical) for one particular ion energy. Nevertheless, this matched condition could not be maintained for the whole ion energy range. The beam synchronization problem can be further complicated with multiple IPs.

Presently, a scheme has been developed [5] for ensuring beam synchronization in the MEIC collider rings. It consists of two parts. At a sufficiently low (< 40 GeV) proton energy and over the whole range of heavy ions, variation of number of ion bunches (harmonic numbers) in the collider ring provides a set of discrete ion energies which satisfy the beam synchronization condition. For proton energy between 40 to 100 GeV, variation of electron ring circumference combined with variation of RF frequency provides a working solution. The main advantage of this scheme is that, being a normal

conducting magnet ring, the variation of the electron ring circumference is far easier since apertures of the magnets could be made large enough for a shift of the magnetic center up to 1.2 cm for one IP or 2.4 cm for two IPs. The scheme requires a variation of frequency of SRF modules by up to 0.012%. Though it has never been done before, it is believed achievable.

4.4.5 **Ion Injector**

The schematic layout [5] of the MEIC ion injector in Figure 6 illustrates the scheme [11] for ion beam formation and acceleration. The ions, coming out of the polarized or un-polarized sources, will be accelerated step-by-step to the colliding energy in the following machine components: a 285 MeV pulsed SRF linac, a 3 GeV pre-booster, a 20 GeV large booster and finally a medium-energy collider ring of 20 to 100 GeV. The energy values above are the design parameters for protons, and should be scaled appropriately for other ion species using a charge-to-mass ratio. All rings are in figure-8 shape for benefit of ion polarization.

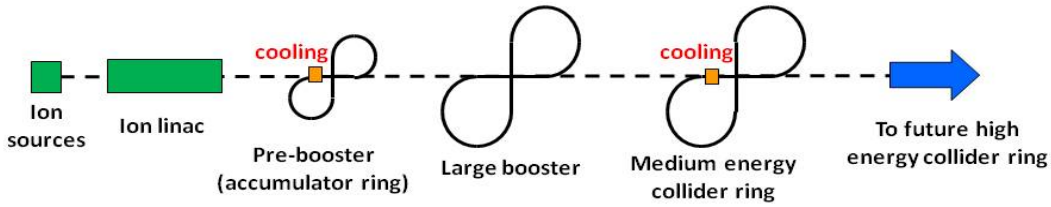

Figure 6: A schematic layout of MEIC ion injector complex.

The MEIC ion sources will rely on existing and mature technologies: an Atomic Beam Polarized Ion Source (ABPIS) with Resonant Charge Exchange Ionization for producing polarized light ions H^-/D^- and $^3He^{++}$, and an Electron-Beam Ion Source (EBIS) currently in operation at BNL for producing unpolarized light to heavy ions. Alternatively, an Electron Cyclotron Resonance Source (ECR) can generate ions with 10 or more times charge per pulse than an EBIS source.

The technical design of a pulsed SRF ion linac, originally developed at ANL as a heavy-ion driver accelerator for FRIB [12] and shown in Figure 7, has been adopted for the MEIC proposal. Figure 8 shows the three types of SRF cavities used in this linac. This linac is very effective in accelerating a wide variety of ions from H^- to $^{208}Pb^{30+}$.

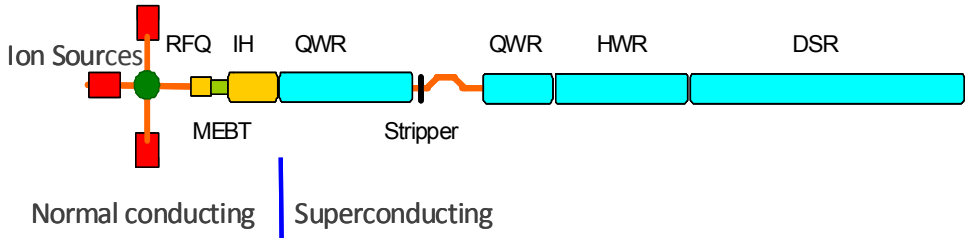

Figure 7: A schematic layout of the MEIC ion linac.

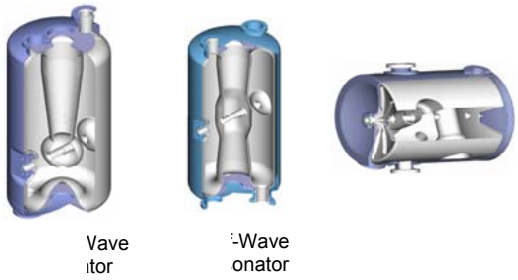

Figure 8: SRF cavities for the MEIC ion linac: quarter wave resonator (left), half wave resonator (center) and double-spoke resonator (right).

The pre-booster synchrotron accepts ion pulses from the linac, and after accumulation and acceleration, transfers them to the large booster. Figure 9 shows a layout of this pre-booster ring. It is designed [13,14] with three arc sections (two on the right side are identical) connected by two straights of the figure-8. The circumference of the pre-booster is one-fourth that of the large booster. The mechanisms of pre-booster operation depend on the ion species, relying on either the combined longitudinal and transverse painting technique for H^-/D^-, or conventional DC electron cooling for lead or other heavy ions during multi-turn injection from the linac. The optics design ensures a sufficiently high transition gamma such that the ions never cross the transition energy during acceleration in order to prevent particle loss associated with such crossing.

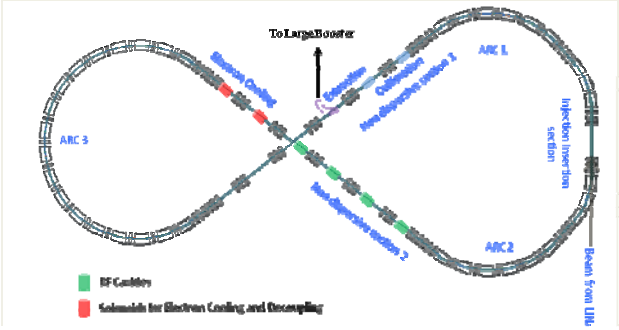

Figure 9: The layout of the MEIC pre-booster synchrotron.

The large booster synchrotron shares the tunnel with the collider rings, and will be responsible for accelerating protons from 3 to 20 GeV or ions with the same magnetic rigidity before transporting them to the collider ring. It is meticulously designed [15] to match the collider ring footprints including such special geometric features of electron spin rotators, ion Siberian snakes and interaction regions. The large booster has also adopted a FODO lattice as its base optics in the interests of simplicity and attaining relatively high transition energy. The latter is an important design goal for ensuring no crossing of the transition energy for any ion species, in order to avoid associated particle loss. The optics is broken down into large sections including four 120° arc sections, two long and two short straights, with optics matching between them and dispersion suppression at the end of each arc section. A preliminary analysis gives a dipole magnet ramping rate of 1.5 T/s; thus it takes 0.95 s to ramp the field to the peak value of 1.65 T. To boost the beam energy, two RF cavities, each having 120 kV voltage assuming it is operated at 45° off-crest, are placed in a dispersion free region of one long straight, requiring total 60 kW RF power [15].

4.4.6 **Electron Cooling and ERL Circulator Cooler**

MEIC has adopted a concept of multi-stage electron cooling of bunched medium energy ion beams [16,17]. First, low energy electron cooling will assist ion accumulation in the pre-booster. Next, in the collider ring, electron cooling is applied after injection, and then after the acceleration of ions to the collision energy for reduction of ion beam emittances and bunch length. Finally, cooling will be continued during collisions for the suppression of emittance growth induced by intra-beam scattering. Shortening the bunch length (1 cm or less) that results from electron cooling of the ion beam captured in a high voltage SRF field is critical for high luminosity in MEIC since it facilitates an extreme focusing and also crab crossing of the colliding beams at the IPs.

The multi-stage cooling scheme requires two electron coolers. One is a low energy cooler with a DC electron beam, based on mature technologies. The other is a medium energy cooler which demands new technologies for delivering a high current and high bunch repetition rate electron beam with energy up to 55 MeV. Presently this medium energy electron cooler is designed by utilizing several new technologies: a magnetized photo-cathode SRF gun, an SRF ERL, and a compact circulator ring [17]. A schematic drawing in Figure 10 illustrates this ERL circulator cooler design concept. These technologies play critical roles in the success of this cooling facility by providing most promising solutions to two bottlenecks of the facility: the high current and high power of the cooling electron beam. The first challenge is high RF power, up to 81 MW, for accelerating a 1.5 A, 55 MeV electron beam. Delivery of such high power without an ERL demands not only very high capital costs for hardware, but also unacceptably high operation costs. Furthermore, safely dumping a beam with such high power, about a hundred times that of the CEBAF 12 GeV beam, is technically unfeasible. With an ERL, nearly all beam power is recaptured in a decelerating pass and is then used for accelerating a new bunch. The second challenge is a need for a long cathode lifetime, in terms of the total extracted charge, which greatly exceeds the present state-of-the-art. A compact circulator ring, in which the cooling electron bunches will circulate multiple times while continuously cooling an ion beam, could lead to a reduction of beam current from the cathode by a factor equal to the number of circulations, thus extending the effective injector lifetime.

Currently, as a design optimization, this ERL circulator cooler is placed at the vertex of the figure-8 of the ion collider ring, as shown in Figure 10, by taking advantage of this unique shape. It provides two 30 m long cooling channels for gaining higher cooling rates.

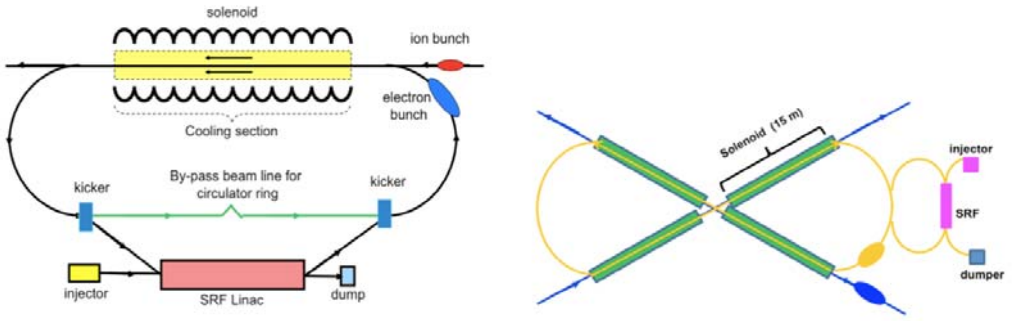

Figure 10: A schematic layout of an ERL circulator electron cooler (left) and an optimized location (right) in the MEIC ion collider ring.

Recently, a proof-of-principle experiment [18] has been proposed to demonstrate the ERL circulator cooler concept. The Jefferson Lab FEL is selected as the test facility for this experiment since it can provide a high quality electron beam with an energy range and bunch repetition rate similar to the cooler; therefore it allows maximum reuse of existing hardware, dramatically reducing the capital cost of this experiment. As shown in Figure 11, the presence of the two parallel IR and UV beam lines provides an opportunity for implementation of a compact circulator ring with two 180° bends already available. The purpose of this experiment is to demonstrate circulations of an electron beam in a circulator ring while the beam quality is satisfactorily preserved. Specifically, we will (1) demonstrate a scheme for bunch exchange between the ERL and the circulator ring, (2) develop and test support technologies such as ERL and faster kickers, (3) study beam dynamics and collective effects in the circulator ring, and (4) test bunch length change and longitudinal phase matching between the ERL and the circulator ring. We expect this experiment will be completed in less than three years.

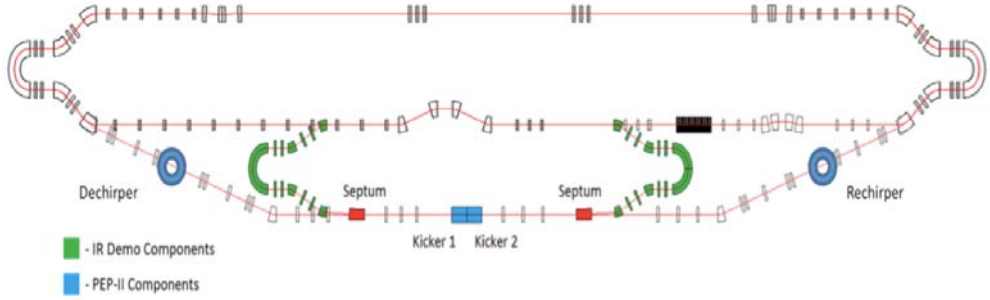

Figure 11: A test facility for an ERL circulator electron cooler.

4.4.7 **Polarization**

The unique figure-8 shape [5,10] for all the booster synchrotrons and collider rings is chosen for its advantage of preserving the ion polarization during acceleration and storage and for greatly simplifying the spin control. The mechanism is simple: the total spin procession (and the spin tune) in a figure-8 ring is zero. Further, a Siberian snake could shift the spin tune to a non-zero constant, thus retaining the energy independence, as a consequence, effectively by-passing all spin resonances during acceleration. Such a figure-8 design is also advantageous for the booster synchrotrons where polarization of protons and $^{3}He^{++}$ ions can be preserved by making the spin tune energy independent

with a partial snake if the space is too limited to accommodate full snakes, while this is not possible in a conventional circular synchrotron.

The figure-8 design is the only practical way [5] presently to preserve the deuteron polarization at the medium energy range. It allows acceleration and storage of polarized deuterons in a synchrotron, which is not possible in a circular synchrotron since the required Siberian snakes would be impractical due to the deuteron small anomalous magnetic moment.

The MEIC science program demands both longitudinal and transverse polarization of light ions at all IPs. Schemes for arranging ion polarizations in the two long straights (where one to two IPs are located) of the figure-8 collider ring have been developed [19]. For polarized protons and $^3He^{++}$ ions, three polarization configurations—namely, longitudinal at all IPs, transverse at all IPs, and alternately longitudinal in one straight and transverse in the other straight—are achievable, as illustrated in Figure 12. Using multiple Siberian snakes provides a high flexibility for science programs at the multiple detectors. For polarized deuterons, we can deliver a transverse polarization in both long straights; however, a longitudinal polarization is only possible in one straight while the spin orientation at the other straight will have an angle depending on the beam energy. Figure 13 illustrates the design of deuteron polarization in a figure-8 collider ring.

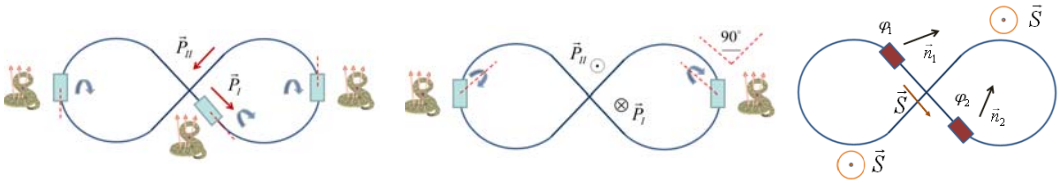

Figure 12: Polarization configurations of proton and $^3He^{++}$ ions in a figure-8 ring with Siberian snakes: longitudinal (left) and transverse (middle) polarization at all IPs. The right drawing shows a transverse polarization in one straight and a longitudinal polarization in the other.

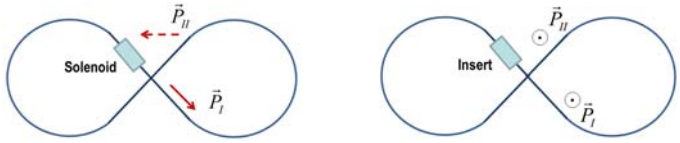

Figure 13: Polarization configurations of deuterons in a figure-8 ring with an SC solenoid or a special magnetic insert: longitudinal in one straight (left) and transverse polarization in both straights (right).

The MEIC electron ring also has a figure-8 shape since it is housed in a common tunnel as the ion collider ring. It should provide similar advantages to electron polarization after the future energy upgrade of MEIC, in which the electron energy will be ramped to 20 GeV in the ring. At the first stage, such advantages are not as significant or critical to the electron polarization as they are to the ion beam polarization.

In MEIC, the polarization of the electron beam originates in a polarized photo-cathode DC gun and can be easily preserved during acceleration in five passes of the CEBAF recirculating SRF Linac. CEBAF operations have shown that the polarization at 6 GeV is above 85%. It is expected that a similar high polarization will be achieved after the 12 GeV CEBAF upgrade. The design strategy of MEIC is to utilize the Sokolov-Ternov effect to preserve this high polarization and improve its lifetime in the

storage ring [5,20]. This requires aligning the electron spin in the vertical direction in arcs, and anti-parallel to the magnetic field of arc bending dipoles, as shown in the Figure 14. This, in turn, demands four energy-independent 90° universal spin rotators on each end of the two arcs to achieve longitudinal orientation at IPs. The first spin rotator rotates a downward spin to the longitudinal direction at one long straight; the second spin rotator then rotates the spin another 90° to upward orientation at the other half ring. This spin manipulation is repeated for the second long straight, and the electron will finally return to the original state of downward spin in the original half ring. The total spin tune is energy dependent, and to move the tune away from resonances, one or more spin tuning solenoids are placed in one long straight.

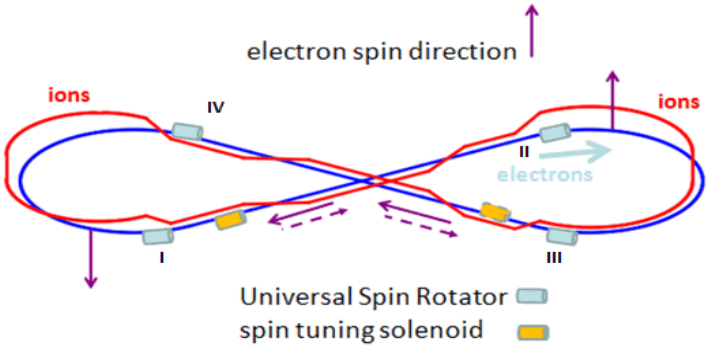

Figure 14: Illustration of spin orientation in the MEIC electron collider ring.

A concept of a universal spin rotator [5] has been developed to provide rotation of spin vectors. The term *universal* is used for referring its orbital and energy independence. As shown in Figure 15, it utilizes two solenoids and two (sets) of arc dipoles.

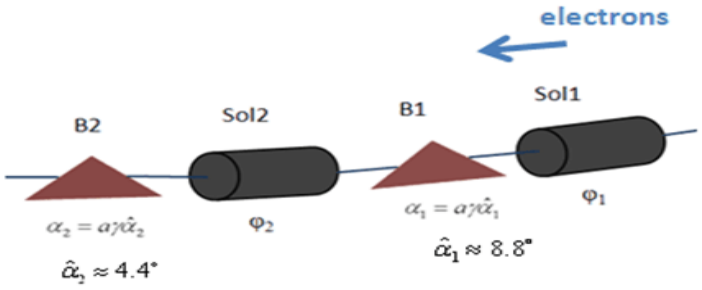

Figure 15: A schematic drawing of a universal spin rotator. B1 and B2 are the arc bends rotating spins by α_1 and α_2. Sol1 and Sol2 are solenoids with spin rotation angles φ_1 and φ_2.

4.4.8 **Interaction Region**

The design of the interaction region (IR) associated to the primary full acceptance detector is aimed for the detection of scattered electrons, mesons, and baryons without holes in the acceptance, even in forward regions, and operation in a high-luminosity environment with moderate event multiplicities and acceptable background conditions.

It should be pointed out that a full acceptance detector literally is capable of detecting particles with angles from 0 to 180°. The particles with a very small forward

angle (less than 1° with respect to the out-going ions), which are in abundance due to the high energy asymmetry of MEIC and carry rich information of great physical interest, are detected through a forward detector [21]. This new design concept allows these particles to pass through the apertures of the final focusing elements in an IR, and are then collected and analyzed by detectors placed after the final focusing block. Figure 16 shows the MEIC IR design that supports such forward particle detection.

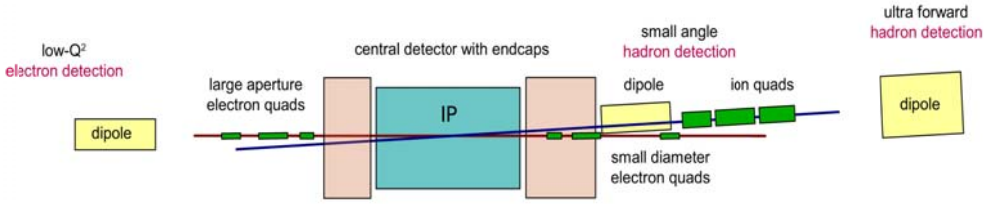

Figure 16: A layout of the interaction region of MEIC.

Additional issues were also taken into consideration in mapping the IR layout. Synchrotron radiation of the electron beam at or near the IR could cause serious background problems for the detector; thus bending of the electron beam in the IR has been minimized. It is designed such that the electron beam travels along a straight line (except inside a chromatic compensation block which has two weak dipoles for introducing and suppressing dispersion) after exiting the arc until reaching the IP. In the crab crossing scheme, the electron beam line is aligned with the detector solenoid, as shown in Figure 16. Further, to reduce the random background from the interactions between the ion beam and residual gas inside the beam pipe, the IPs are located as close as possible to the arc where the ion beam comes.

The MEIC IR consists of three function blocks, namely, final focusing block, chromaticity compensation block (CCB) and beam extension section, distributed from the IP toward the arc, with the optical functions for each block shown in Figure 17 for the ion beam. Figure 18 shows the optics functions over the complete ion and electron IRs [5].

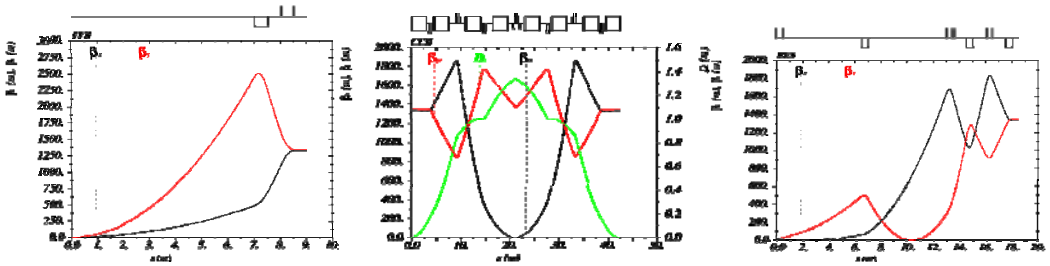

Figure 17: Optical functions of the ion beam at Final Focusing Block (left), Chromatic Correction Block (middle) and Beam Extension Block (right).

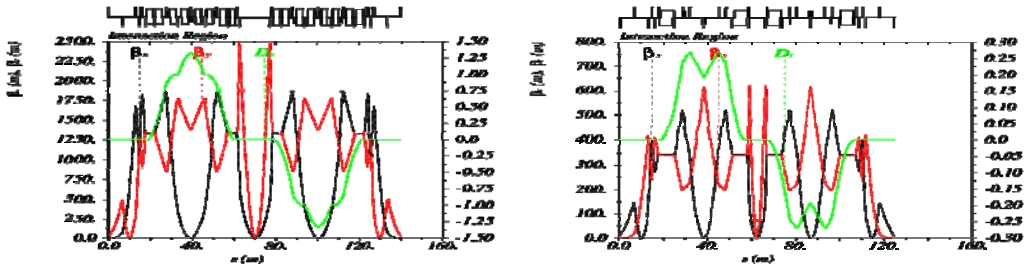

Figure 18: Complete optics of an ion interaction region (left) and electron interaction region (right).

A low-β insertion in an IR induces serious chromatic effects. The present approach of MEIC is a local correction scheme utilizing two CCBs placed on the both sides of an IP, as shown in Figure 18. A CCB for the ion beam is made of eight alternating horizontal dipoles sandwiched with seven quadrupoles, all arranged symmetrically as shown in the middle plot of Figure 18. The quadrupole strengths are adjusted to produce a total transfer matrix of the CCB that meets the symmetry requirements. Two sextupole pairs are inserted in each CCB; each pair is identical and placed symmetrically with respect to the center of the CCB. Such a scheme can simultaneously compensate the 1st order chromaticity and chromatic beam spot smear at the IP without inducing significant 2nd order aberrations [22].

For ion collider ring with two IPs, the horizontal and vertical chromaticities before compensation are - 278 and - 268, respectively. The strengths of two sextupole families in the CCB are adjusted to reduce slopes of the chromatic betatron tune curves to zero. As shown in the left plot of Figure 19, the tune variations are less than 0.005 and 0.01 in the horizontal and vertical directions respectively over a ± 0.2% range of $\Delta p/p$, and further within 0.02 and 0.03 over a wide $\Delta p/p$ range of ± 0.4% [9]. A frequency map analysis based on the tracking simulation results has demonstrated in the middle plot of Figure 19 that the momentum acceptance can easily reach ± 0.4%, about 14 times the ion beam momentum spread, with only the linear chromaticity compensation [23].

The dynamic apertures of the collider rings are explored by tracking particles for 1000 turns with increasing initial transverse amplitudes until a boundary between survival and loss is found. Simulations show the particles having large initial amplitudes experience stronger non-linear sextupole fields, resulting in a 3rd order aberration in the form of amplitude dependent tune-shifts [23]. Therefore, families of octupoles are introduced and placed in large betatron function but dispersion-free regions. These leave the linear chromatic correction unaffected, but compensate this 3rd order aberration. With this additional compensation, the dynamic aperture is increased significantly [23], as shown in the right plot of Figure 19.

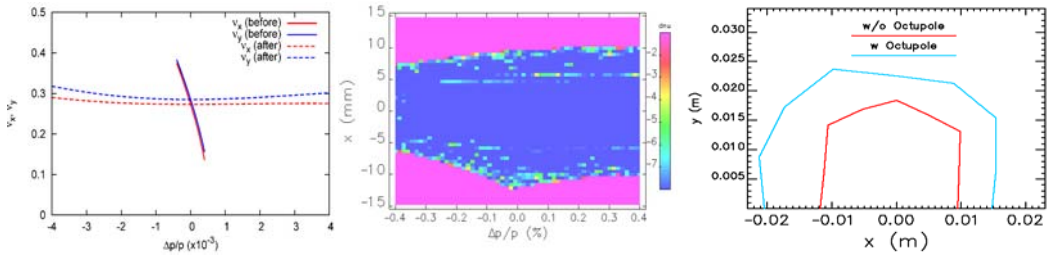

Figure 19: (Left) Chromatic dependence of the fractional betatron tunes before and after compensation. (Middle) Frequency map in the (x-Δp/p) space. The color reflects the tune change. (Right) Dynamic aperture of the ion ring without (red) and with (blue) octupole minimization of the 1st order amplitude-dependent tune-shift.

4.4.9 **Outlook**

MEIC is the primary future of the nuclear science program at Jefferson Lab beyond the 12 GeV CEBAF fixed target program. By incorporating several unique and advanced design features including figure-8 shape rings, staged electron cooling, and high bunch repetition rate beams, it holds a promise to deliver high performance including high luminosity above 10^{34} $cm^{-2}s^{-1}$ per detector for two IPs and higher than 70% polarization of electron and light ion beams. The two-step staging approach enables a physics program with CM energy range up to 66 GeV immediately and ultimately reaches a higher medium CM energy up to 140 GeV in a future upgrade. The first conceptual design of MEIC has been completed recently and a comprehensive design report is now available online and will be officially published soon.

The focus of the Jefferson Lab study group is now the accelerator R&D for both the technology development and demonstration and for beam physics studies. For the next two years, we will focus on the following topics: collective beam physics including beam-beam and electron clouds; election cooling simulation study and ERL circulator cooler technology development and demonstration; IR development and dynamic aperture optimization; and a demonstration of the advantages of the figure-8 ring on ion polarizations and a satisfactory electron polarization lifetime.

4.4.10 **References**

1. **"**Gluons and the quark sea at high energies: Distributions, polarization, tomography**",** D. Boer *et al*., arXiv:1108.1713 [nucl-th] (2011).
2. A. Accardi, V. Guzey, A. Prokudin and C. Weiss, "Nuclear Physics with a Medium-Energy Electron-Ion Collider", Eur. Phys. J. A 48: 92 (2012).
3. S. Ahmed, *et al.*, "Conceptual Design of A Polarized Medium Energy Electron-Ion Collider at JLab", Proceedings of PAC11, NY, NY, p2306 (2011).
4. S. Ahmed, *et al.*, "MEIC Design Progress", proceedings of IPAC12, New Orleans, LA (2012).
5. "MEIC - An Intermediate Design Report of A Polarized Ring-Ring Electron-Ion Collider at Jefferson Lab", edited by J. Bisognano & Y. Zhang (2012).
6. Ya. Derbenev, "Advanced Concepts for Electron-Ion Collider", Proceedings of EPAC 2002, Paris, France, p315, (2002).
7. Ya. Derbenev, G. Krafft, B. Yunn and Y. Zhang, "Achieving High Luminosity In An Electron-Ion Collider", Proceedings of HB2010, Morschach, Switzerland, p49 (2010).
8. For example, Y. Funakoshi, *et al.*, "Recent Progress of KEKB", Proceedings of

IPAC'10, Japan, p2372 (2010).
9. Ya. Derbenev, *et al.*, "ELIC at CEBAF", Proceedings of PARC2005, Knoxville, Tennessee, TPPP015 (2005).
10. Ya. Derbenev, "The Twisted Spin Synchrotron", University of Michigen Report UM HE 96-05 (1996).
11. S. manikonda, B. Erdelyi and P. Ostroumov, "Formation of Beams in the Accelerator Complex of The Medium Energy Electron Ion Collider Facility at JLab", Proceedings of IPAC12, New Orleans, LA (2012).
12. P. Ostroumov, *et al.*, "Design of the Driver Linac for the Rare Isotope Accelerator", Proceedings of HB2006, Tsukuba, Japan, p89 (2006).
13. B. Erdelyi, S. Mamnikonda, P. Ostroumov, S. Abeyratne, Y. Derbenev, G. Krafft and Y. Zhang, "An Accumulator/Pre-booster for the Medium Energy Electron Ion Collider at JLab", proceedings of PAC 2011, New York, NY, p1873 (2011).
14. S. Abeyratne, S. Manikonda, B. Erdelyi, "Design Studies of Pre-boosters of the Different Circumference for An Electron Ion Collider at JLab", Proceedings of PAC 2011, New York, NY, p954 (2011).
15. E. Nissen, T. Satogate and Y. Zhang, "The Design of A Large Booster Ring for the Medium Energy Electron-Ion Collider at JLab", Proceedings of PAC 2011, New York, NY, p954 (2011).
16. Ya. Derbenev, J. Musson and Y. Zhang, "Electron Cooling for a High Luminosity Electron-Ion Collider", Proceedings of COOL07, Kreuznach, Germany, p187 (2007).
17. Ya. Derbenev and Y. Zhang, "Electron Cooling for Electron-Ion Collider", Proceedings of COOL09, Lanzhou, China, p181 (2009).
18. Ya. Derbenev, D. Douglas, A. Hutton, G. Krafft , E. Nissen and Y. Zhang, "A Test Facility for MEIC ERL Circulator Ring Based Electron Cooler Design", Proceedings of IPAC12, New Orleans, LA (2012).
19. V. Morozov, Ya. Derbenev, Y. Zhang, P. Chevtsov, A. Kondratenko, M. Kondratenko and Yu. Filatov, "Ion Polarization in the Figure-8 Ion Collider Ring", Proceedings of IPAC12, New Orleans, LA (2012).
20. F. Lin, Ya. Derbenev, V. Morozov, Y. Zhang and D. Barber, "Electron Polarization in the Medium Energy Electron-Ion Collider at JLab", Proceedings of IPAC12, New Orleans, LA (2012).
21. V. Morozov, P. Nadel-Turonski, R. Ent and C. Hyde, "Integration of Detector into Interaction Region at MEIC", Proceedings of IPAC12, New Orleans, LA (2012).
22. V. Morozov and Ya. Derbenev, "Achromatic Low-Beta Interaction Region Design for An Electron-Ion Collider", Proceedings of IPAC12, New Orleans, LA (2012).
23. F. Lin, Ya. Derbenev, V. Morozov, Y. Zhang and K. Beard, "Optimization of Chromaticity Compensation and Dynamic Aperture in MEIC Collider Rings", Proceedings of IPAC12, New Orleans, LA (2012).

4.5 High-Energy, High-Luminosity Electron-Ion Collider, eRHIC

Vladimir N. Litvinenko[1,2], Sergey Belomestnykh[1,2], Ilan Ben-Zvi[1,2], Michael M. Blaskiewicz[1], Kevin A. Brown[1], Jean Clifford Brutus[1], Andrey Elizarov[1,2], Alexei Fedotov[1], Pei Kuan Feng[1], David Gassner[1], Harald Hahn[1], Yue Hao[1,2], Ping He[1], Lawrence T. Hoff[1], William Jackson[1], Animesh Jain[1], Yichao Jing[1], Dmitry Kayran[1], Robert Lambiase[1], Chuyu Liu[1], Yun Luo[1], Michael Mapes[1], George Mahler[1], Gary McIntyre[1], Wuzheng Meng[1], Michiko Minty[1], Robert Michnoff[1], Brett Parker[1], Alexander Pendzick[1], Alexander Pikin[1], Igor Pinayev[1], Vadim Ptitsyn[1], Triveni Rao[1],Eric Riehn[1], Thomas Roser[1], Jon Sandberg[1], John Skaritka[1], Brian Sheehy[1], Kevin Smith[1], Steven Tepikian[1], Oleg Tchoubar[1], Yatming Than[1], Charles Theisen[1], Dejan Trbojevic[1], Evgeni Tsentalovich[3], Nicholaos Tsoupas[1,2], Joseph Tuozzolo[1], Gang Wang[1], Qiong Wu[1], Wencan Xu[1], Alex Zaltsman[1], Wu Zhang[1], Anatoly Zelenski[1]

[1] Brookhaven National Laboratory, Upton, NY 11973
[2] Department of Physics and Astronomy, Stony Brook University, Stony Brook, 11784
[3] MIT-Bates, Middleton, MA 01949

Mail to vl@bnl.gov

4.5.1 Introduction

In this paper, we describe our planned future electron-ion collider (EIC), based on the existing Relativistic Heavy Ion Collider (RHIC) hadron facility, with two intersecting superconducting rings, each 3.8 km in circumference [1]. We plan adding a polarized electron-beam with energy tunable within the 5-30-GeV range to collide with variety of species in the existing RHIC-accelerator complex, from polarized protons with a top energy of 250 GeV, to heavy fully striped ions with energies up to 100 GeV/u. Using the present significant margin of the RHIC superconducting magnets, we should be able to increase the maximum beam energy by 10 to 25 percent;[1] correspondingly, this would bring the energy's reach to 325 GeV and 130 GeV/u.

Brookhaven's innovative design, (Fig. 1) is based on one of the RHIC's hadron rings and a multi-pass energy-recovery linac (ERL). Using the ERL as the electron accelerator assures our ultimately reaching high luminosity up to 10^{34}-10^{35} cm^{-2} sec^{-1} and a c.m. energy range from 30 GeV to 200 GeV.

The eRHIC will support the collision of highly polarized electrons with polarized protons or He3 ions, or with un-polarized heavy-ion beams up to uranium. The eRHIC will offer up to three interaction regions for electron-hadron collisions. If needed, a dedicated cooling ring would deliver polarized positrons for the ERL to collide with the ions. The luminosity of these collisions will be modest.

[1] In a dedicated test, RHIC demonstrated that 260 GeV operation is possible. A further increase for eRHIC used may require our combining better performing magnets from both rings.

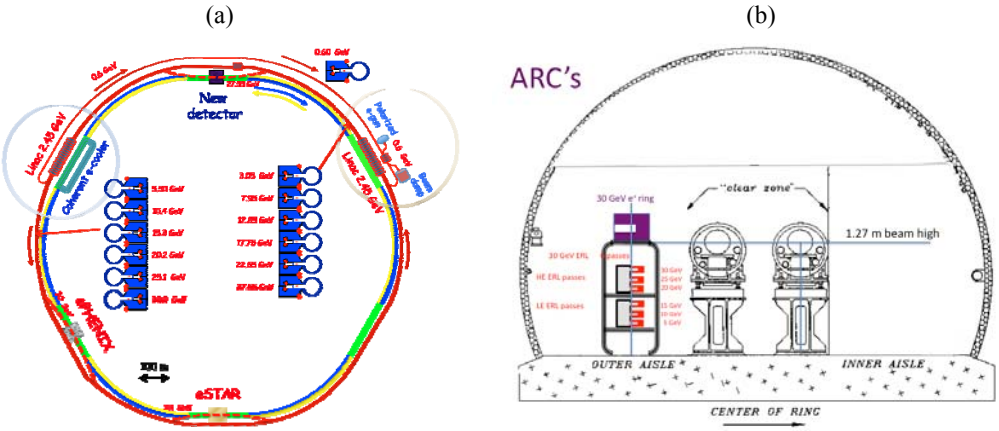

Figure 1: (a) Layout of the ERL-based, all-in-RHIC-tunnel, 30 GeV x 325 GeV high-energy high-luminosity eRHIC. (b) Location of eRHIC's six recirculation arcs in the RHIC tunnel.

Cost is the major factor in assuring the realization of the EIC facility, and hence, our design for the eRHIC highly cost effective. It fully utilizes the existing hadron RHIC facility whose replacement cost is about two billion US dollars[2].

Furthermore, the eRHIC's ERL is located inside the existing RHIC tunnel, thereby which significantly reduces cost of its civil construction. The extremely small size of the electron beam in the ERL allows us to install cost-effective small (few mm) gap magnets and a vacuum chamber for its recirculating loops [2] or novel permanent-magnet FFAG arcs [3] accommodating multiple turns.

The eRHIC's ERL has natural staging scenario of increasing, in stages, the electron-beam's top energy from an initial value of 5-10 GeV to its final energy of 30 GeV by adding additional cavities to its SRF linacs and increasing settings in the magnet's power supplies. The eRHIC design includes a number of scenarios for staging its luminosity and its detectors. For example, the two existing RHIC detectors are considering upgrades to serve as initial detector(s) for eRHIC.

The first phase of eRHIC aiming at keeping the cost below 0.5B US$, will provide luminosity in the range of 10^{33}-10^{34} cm^{-2} sec^{-1} with a c.m. energy-range from 30 to 100 GeV. We detail the eRHIC's performance in Section 4.5.5.

4.5.2 Choice of the Scheme for the EIC

Since first paper on eRHIC was published in 2001 [4], its design underwent several iterations. Initially, the main option (the so-called ring-ring (RR) design) was based on an electron ring, with the linac-ring (LR) option as its backup. In 2004, we published the detailed "eRHIC 0th-Order Design Report" [5]. After comprehensive explorations, we found that an LR eRHIC has about a 10-fold higher luminosity than the RR; hence, since 2007, the LR, with its natural staging strategy and full transparency for polarized electrons, became the main choice for eRHIC. In 2009, we completed technical studies of the design and dynamics for MeRHIC with a 3-pass 4-GeV ERL. We learned much

[2] It is established that building a 200 GeV/c hadron facility is significantly more expensive than constructing a 20 GeV electron accelerator. Indeed, the cost of a hadron facility with top energy in hundreds of GeVs is measured in billions of US$ (examples are the RHIC and TEVATRON), while the outlay for an electron beam accelerator and colliders of a few tens of GeV amounts to hundreds of millions US$ (examples are the CEBAF upgrade and the B-factory).

from this evaluation, completed a bottom-up cost-estimate for this $350M machine, but then shelved the design.

eRHIC is based on a ring-linac collider design, which, within a given set of conditions, is superior to an optimized ring-ring design. In eRHIC, the electron beam is provided by a six-pass super-conducting RF (SRF) energy-recovery linac (ERL) that accelerates polarized electrons to the top energy, collides them with the hadron beam, and then decelerates them by removing their energy; finally, they are dumped at very low energy of few MeV.

The single use of the electron beam, in contrast with its repetitive use in a ring-ring collider, allowed us to increase by two orders-of-magnitude beam-beam effects on the electrons. Detailed studies of eRHIC design had revealed that a linac-ring configuration assures a 10- to 50-fold higher luminosity than the optimized ring-ring design does [6]. These advantages especially are evident for high electron-beam energies. Here, we briefly review the main arguments and considerations that resulted in our switching from the early ring-ring design [5] for the eRHIC to the linac-ring one.

The most generic formula for collider luminosity is the well-known one,

$$L = f_c \frac{N_1 N_2}{4\pi\sigma_x\sigma_y} \cdot h, \tag{1}$$

where f_c is the frequency of the bunch collision , $N_{1,2}$ represents the number of particles per bunch in the corresponding beams, $\sigma_{x,y} = \sqrt{\beta^*_{1x,y}\varepsilon_{1x,y}} = \sqrt{\beta^*_{2x,y}\varepsilon_{2x,y}}$ are transverse beam sizes[3], and $h \sim 1$ is a luminosity-suppression factor. The latter can be kept near unity with the proper design of the IR and choice of the bunches' length. From simply observing formula (1), it is apparent that luminosity can be enhanced by increasing the frequency of collisions, the number of particles in bunches, or by reducing transverse beam sizes at the collision point. Since the limitations in luminosity are similar for flat- and round-beams, for simplicity, we focus here on round beams with equal emittances ε and β^*: $\sigma_x = \sigma_y = \sqrt{\beta^*\varepsilon}$

$$L = f_c \frac{N_1 N_2}{4\pi\beta^*\varepsilon} \cdot h. \tag{2}$$

In practice all of these increases have confines that often are specific to a type of collider. For example, restrictions for lepton colliders differ from those for hadron colliders. The EIC, being a lepton-hadron collider, has limitations from both sides.

First, in contrast with lepton colliders wherein the collision frequency can be as high as 500 MHz [7], that in hadron colliders is restrained by the need to have a detector trigger to avoid an otherwise intolerable background. At present, LHC detectors have the fastest electronics, supporting a collision frequency up to 40 MHz. Furthermore, existing RHIC detectors limit this frequency to 10 MHz. The EIC detector would have the same or nearly the same limitation in the collision frequency as hadron detectors. The eRHIC design takes these boundaries into consideration: the first eRHIC phase will support a collision rate of 9 MHz, while its ultimate performance (discussed later) could be extended to 56 MHz, so increasing six-fold the attainable luminosity.

[3] It was proven experimentally that both beams should have same transverse sizes in the point of collision.

Second, the intensities and densities of the colliding beams are limited by non-linear effects occurring during the beam-beam collisions. In storage rings, these beam-beam effects are characterized by the tune shift

$$\xi_1 = \frac{N_2}{\gamma_1}\frac{r_1}{4\pi\varepsilon}; \quad \xi_2 = \frac{N_1}{\gamma_2}\frac{r_2}{4\pi\varepsilon}; \tag{3}$$

$\gamma_{1,2} = E_{1,2}/m_{1,2}c^2$ are beam's relativistic factors, and $r_e = e^2/m_e c^2; r_p = e^2/m_p c^2$ are the corresponding classical radii of colliding particles that we assume to be electrons and protons[4]. In a ring-ring collider both of the beam-beam tune shifts are limited

$$\frac{N_e}{4\pi\varepsilon} \le \frac{\gamma_p \cdot \xi_{p\max}}{r_p}; \quad \frac{N_p}{4\pi\varepsilon} \le \frac{\gamma_e \cdot \xi_{e\max}}{r_e}; \tag{4}$$

with $\xi_{e\max} \le 0.1; \quad \xi_{p\max} \le 0.03$. This limitation means that in a ring-ring EIC both the increase of the number of colliding particles and reduction of the beam emittance are limited by the above, and the maximum attainable luminosity can be written as

$$L_{\max R-R} \le f_{c\max} \cdot \min\left\{\gamma_e \frac{N_e}{\beta^* r_e}\xi_{e\max}, \gamma_p \frac{N_p}{\beta^* r_p}\xi_{p\max}\right\} \sim \frac{\varepsilon}{\beta^*}. \tag{5}$$

Hence, the remaining optimization would require either increasing the beam's emittance or reducing β^*. Since the ε/β^* represents nothing else but the opening solid angle of the beams in the interaction point, increasing emittance and reducing β^* would create problems with the acceptance of the final focusing elements, and the detector's hermeticity.

In contrast, the single use of the electron beam in the linac-ring EIC collider removes the limitation on the beam effect imposed on the electron beam (i.e., in eRHIC $\xi_e \sim 10$) and luminosity is only limited by available parameters of the hadron beam:

$$L_{\max L-R} \le f_{c\max} \cdot \gamma_p \frac{N_p}{\beta^* r_p}\xi_{p\max} \cdot h \quad . \tag{6}$$

In hadron storage rings operating at hundreds of GeV, the final focusing quadrupoles impose serious restrictions on the attainable β^*. Opening their apertures assures reducing focusing strength and, therefore, opposes the reduction of β^*. In contrast with lepton colliders where β^* of few mm was achieved, the smallest $\beta^* = 25cm$ was attained in TEVATRON. New superconducting quadrupoles developed for LHC up-grade should allow about a 5-fold reduction of β^* at eRHIC energies, while keeping chromatic effects under control [8]. Hence, we assume $\beta^* = 5cm$ for eRHIC operations.

Third, in contrast with 100-GeV-scale hadron beams, electrons at 10-30 GeV lose much energy via synchrotron radiation, which can seriously limit the attainable luminosity in ring-ring EIC:

[4] While the generalization for the case of ions with charge Ze and atomic number A is straight forward, to assure the clarity of the concept we use single-charge particles.

$$P_{SR} = \frac{4\pi}{3} f_c N_e \cdot \frac{e^2}{\rho} \gamma_e^4, \quad (7)$$

where ρ is the bending radius, and $I_e = e f_c N_e$ is the electron beam current. Imposing a reasonable limit on the power of synchrotron radiation (which must be compensated for by the RF system with about 50% plug efficiency) in the EIC, we can derive the limitation on the maximum attainable luminosity in ring-ring EIC:

$$L_{\max R-R} \le \gamma_e^{-3} \frac{3}{4\pi} \frac{P_{SR} \cdot \rho}{m_e c^2} \frac{\xi_{e\max}}{\beta^* r_e^2}. \quad (8)$$

Thus, restricting synchrotron losses for 20 GeV electron beam to 10 MW in a reasonably sized storage collider with a 200 m bending radius (i.e. ~ 2 km in circumference) limits the maximum attainable luminosity to $2.45 \cdot 10^{33}$ cm^{-2} sec^{-1}, subject to the overall limitation in eq. (5). We assumed $\beta^* = 5cm$ for this estimation.

The luminosity of the linac-ring would continue to be limited by Eq. (6) and can exceed the ring-ring limit by one-to-two orders of magnitude. Hence, we conclude that within a given set of parameters, the linac-ring EIC always would have higher luminosity than the ring-ring version.

An asymmetric IR design as well as issues with beam stability may apply further limitations that can limit the EIC's luminosity. The eRHIC team undertook an in-depth comparison of highly optimized ring-ring- and linac-ring-scenarios for eRHIC and found that the luminosity in the latter would exceed that in the former by a factor from ten to fifty, depending on the e-beam's energy.

4.5.3 **eRHIC Design**

Injector. As shown in Fig.1, an electron gun will provide fresh electron beams. In the phase I, we will employ a 50-mA polarized electron gun, based either on single large-sized GaAs cathode [9] (Fig. 2 (a)), or on a Gatling gun [10,11], an approach combining beams from a large array of GaAs cathodes (Fig.2 (b)). Illuminated by a circular polarized IR laser-light, a strained or a super-lattice GaAs cathode will produce longitudinally polarized electrons with polarization as high as 85-90%. The direction of electron's spin can be flipped on a bunch-to-bunch basis by changing the helicity of the laser photons.

(a) (b)

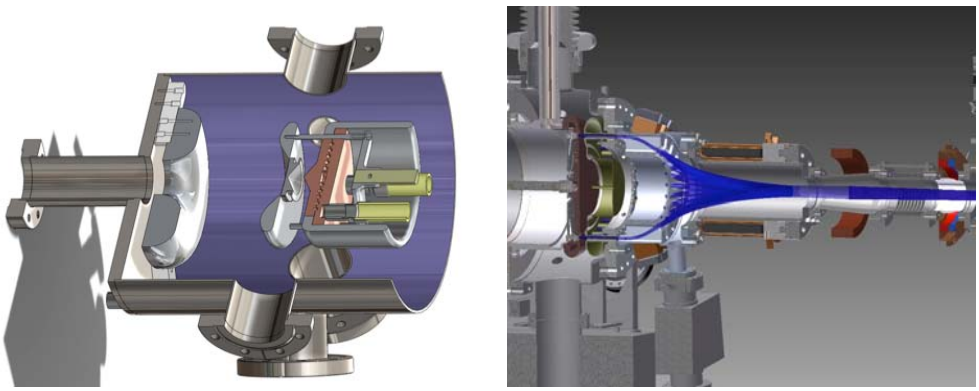

Figure 2: Two candidates for eRHIC polarized electron gun: (a) With a large-sized GaAs cathode gun; (b) Gatling gun, combing beams from an array of 24 GaAs cathodes.

If needed, we will utilize a dedicated un-polarized SRF electron gun, similar to that designed for BNL's R&D ERL [12] to generate a significantly higher beam current (up to 250 mA CW).

Thereafter, the electrons will be accelerated in a pre-injector linac and then will pass six times around RHIC tunnel, gaining energy from two super-conducting RF (SRF) linacs located in two of RHIC's straight sections (see Fig. 1a, wherein the linacs are located in the 2- and 10-o'clock straight sections). They can accommodate SRF 703 MHz linacs up to maximum length of 201 m that suffice for a 2.45-GeV linac operating with a real-estate gradient of 12.45 MeV per meter, corresponding to 20.4 MeV gain per 5-cell 703 MHz cavity.

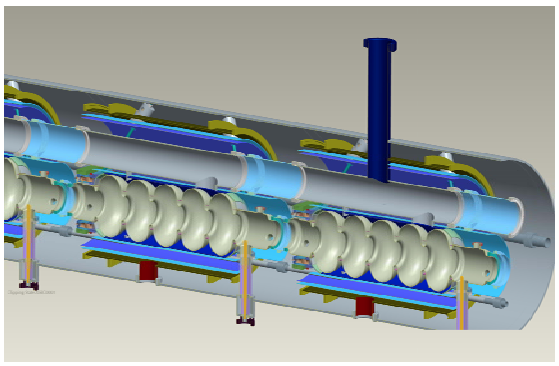

Figure 3: A cross-section of eRHIC SRF cryomodule showing two 5-cell SRF cavities.

The Main ERL. While we will install the eRHIC magnets from the start of operations, the top energy of electron beam will be raised in stages by increasing the length (and the energy gains) of each linac in the ERL chain. At the final stage with six passes, the two main linacs each will have energy gain of 2.45 GeV, while the injection SRF linac will provide 0.6-GeV of energy. At all intermediate stages, the energy gains of all linacs will be proportionally lower, i.e., for the 10-GeV stage, the e-beam will be injected at 0.2-GeV into the main ERL, and each main linac will provide a gain of 0.817 GeV.

We plan to build the eRHIC's linacs from modules comprising six 5-cell 703-MHz SRF cavities. Fig.3 is a 3D rendering of such modules with the HOM-dumped 5-cell cavities.

At their peak energy, the electrons collide with hadrons and then the same linacs recover their energy. The latter process is assured by the additional 180-degrees delay of the electrons at the top energy; such a delay switches acceleration to deceleration.

Dedicated combiners and splitters assure that beams at all energies pass through the same linacs while propagating in their individual beam-lines around the arcs. Figure 4 depicts the arrangement in the 10 o'clock straight section; there is a similar system in the 2 o'clock section.

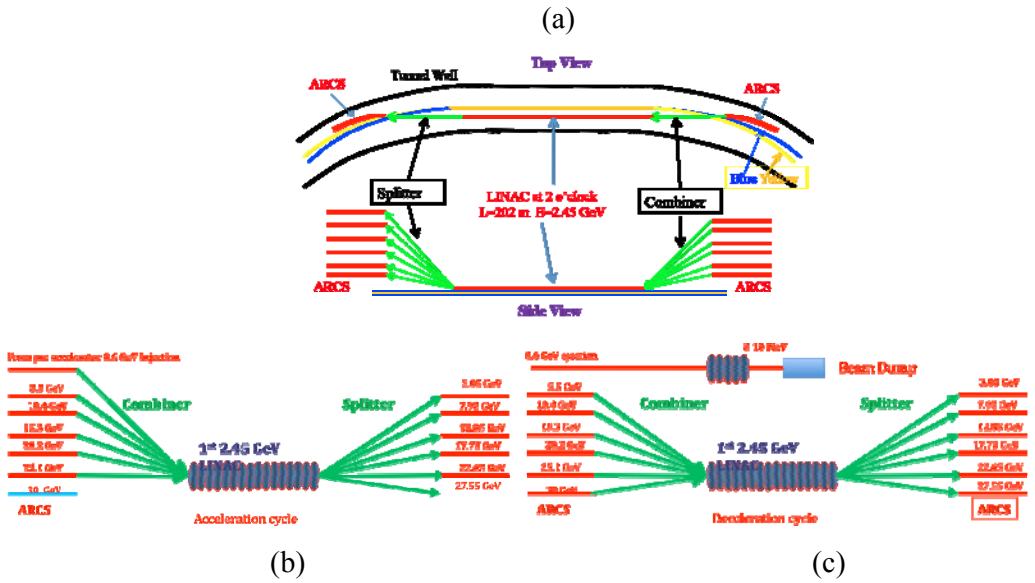

Figure 4: Scheme for the combiners and the splitters providing for 6-pass acceleration and 6-pass deceleration of the electron beam in eRHIC's ERL. The beams are separated vertically. (a) Overall layout with top and side views of the 10 o'clock RHIC straight section with the eRHIC linac; (b) action of the combiner and the splitter for accelerating beams; and, (c) their action for decelerating beams.

Except at their top energy, the accelerating- and decelerating-beams share the arcs, though separated in time. For example, electron beams at 15.3-GeV traverse the same arc between IP2 and IP10, wherein the energy of accelerating beam increases to 17.75 GeV. It enters the 17.75-GeV arc together with the beam that just was decelerated from 20.2-GeV. In contrast, after passing through the linac, the decelerating 15.3 GeV beam passes into the 12.85 GeV arc, sharing it with the beam that just was accelerated in the same linac from 10.4 GeV. Two linacs having equal energy gains maintain this important ratio between the accelerating- and decelerating- beams. The process of the energy recovery in SRF linacs is extremely efficient, such that only about one kilowatt of RF power per 2.45 GeV linac is absorbed by the SRF surfaces. Main part of the RF transmitter power is reactive and is used to combat the micro-phonic effects in the SRF cavities.

The main beam-energy losses come from synchrotron radiation, resistive losses in the walls of vacuum chambers, and HOM losses in the SRF linacs. Figure 5 shows the values for this power loss. They must be compensated for either by a special (second-

harmonic) RF system, or by specially tuning the main linacs [13]. Additional non-compensated beam-energy results from dumping the beam at about 10 MeV; this energy is generated by the pre-injector.

The size of the electron beam in ERL is so small that the sizes of the vertical gaps in the arcs can be about a few mm; hence, this warrants our using small-gap magnets. They are an important cost-saving factor for eRHIC; we discuss the prototyping of such magnets in section 4.5.6. The vacuum pipe will be made from extruded aluminum with a typical keyhole antechamber design characteristic of modern light-sources. In practice, the minimal vertical gap of the vacuum chamber (and, therefore, that of the magnets) is likely to be influenced by the tolerable wakefield effects from resistive walls and roughness; their exact value will be determined when we complete our theoretical- and experimental-studies of them.

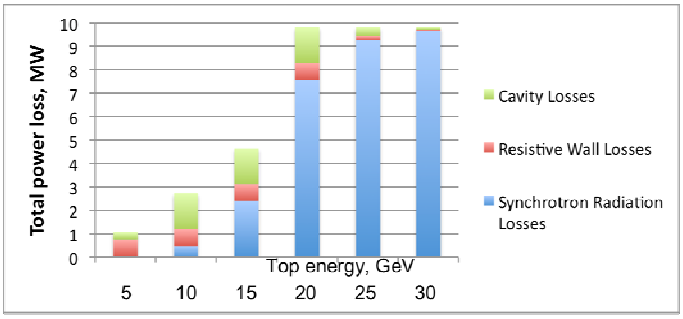

Figure 5: Electron beam's power loss for various top energies of eRHIC operating with polarized electrons. Note, the losses for synchrotron radiation are kept at a fixed level for e-beam energies above 20 GeV by proportionally reducing the electron beam's current to about the fourth power of the energy.

Preserving polarization. We will preserve in the ERL the high degree of the electrons' polarization originating from the polarized electron gun [14], and provide the desirable direction, i.e., longitudinal, of the electron's polarization in the interaction point (IP). The easiest (and most economical) way of doing so is to keep the spin in the horizontal plane. In this condition, the angle between the direction of electron's velocity and its spin grows according a very simple equation:

$$\varphi(\Theta) = \varphi_0 + \alpha \int_0^{\Theta} \gamma(\theta)\, d\theta, \qquad (9)$$

where φ_0 is the initial angle at the source, θ is the angle of trajectory rotation in the bending magnetic field, $\gamma = E_e / m_e c^2$ is the relativistic factor of the electron beam, and α is the anomalous magnetic moment of the electron. Selecting the energy of electron providing for an $m\pi$ total rotation angle, where m is integer between the polarized gun and the collision point, will ensure the longitudinal polarization of electrons in the IP[5]. With six passes in the ERL and layout shown in Fig. 6, the required condition will be satisfied at IP6 for collisions at electron energies of $E_e = N \cdot 0.07216\ \ GeV$, where N is an integer. This signifies that tuning the energy for 0.24% of a top energy of 30 GeV will assure such a condition.

[5] There is no need for the transverse polarization of electrons in exploring the physics processes of interest.

RHIC is the only high-energy polarized proton collider. It had demonstrated polarization of protons at the collision energy of 250 GeV at the 55% level. There are plans, and means, to bring the polarization to the 70% level, that we plan to use in eRHIC. Proton polarization in the IP is controlled by spin rotators and can be directed either longitudinally or transversely. The direction of proton beam in RHIC is controlled, and can be switched on a bunch-by-bunch basis. As discussed above, the direction of electron spin will be changed by reversing the helicity of the laser photons in the gun on the bunch-by-bunch basis to provide any desirable spin-bunch pattern. This flexibility affords an important opportunity to lower systematic errors in data analysis.

This option is impossible to achieve in a ring-ring scenario wherein the polarization and depolarization of electron beams depend upon their spin direction.

Arcs lattice. The eRHIC's arc lattice has two components, viz., that of the Blue hadron ring, and of the ERL lattice. The lattice of RHIC's blue ring would be modified significantly only in the IR straight sections. We discuss this in the next section. The lattice of 6-passes for eRHIC's ERL is based on a low-emittance near-isochronous lattice module. The concept of such a lattice originated from the early work of Dejan Trbojevic [15]. In addition to having an excellent filling factor, this lattice supports the fine-tuning of the R_{56} elements in the transport matrix, so supporting the perfect isochronism of the complete paths. Figure 7 illustrates the main building block of the arc lattice. Similar blocks at the both sides of the arc lattice make it perfectly achromatic. The lattice of the regular arcs is identical for all passes, independent of their energy. The differences arise only from the splitters and combiners in the SRF linac straights, as well as from the by-pass sections in the other straights.

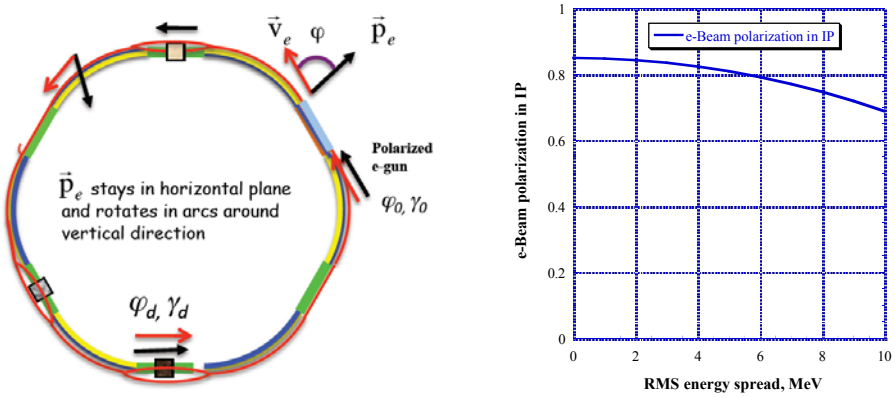

(a) (b)

Figure 6: (a) Electron spin dynamics in eRHIC; (b) Degree of longitudinal polarization as a function of RMS energy-spread averaged along the six paths.

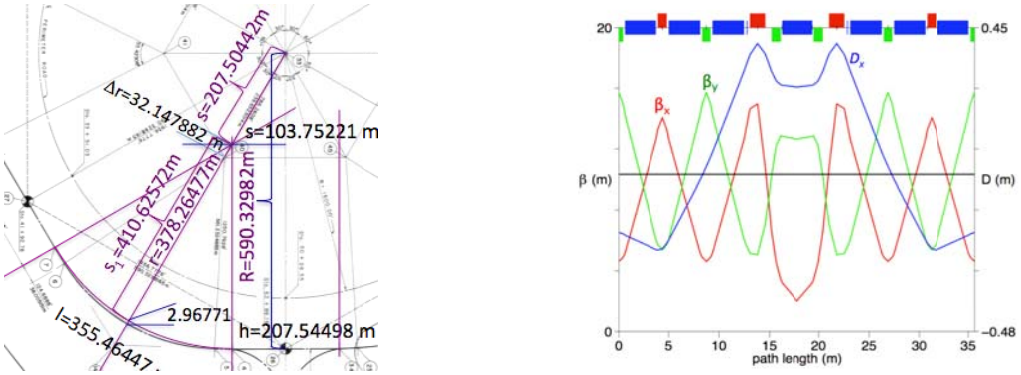

(a) (b)

Figure 7: Geometry (a), and lattice functions (b) for the standard building block.

As evident from Fig. 4, the ERL linacs will be located inside the RHIC rings, while ERL arcs are located outside them. This transition, as well as other peculiarities of the RHIC tunnel's geometry, is accommodated by using two types of the same basic section (Fig.7) with slightly different radii of curvature. Similar basic blocks are used for the straight passes and for by-passes around the detectors. Fig. 8 shows such a design for the by-pass around the eSTAR detector.

Presently, we are considering using a linac lattice without quadrupoles and with values of β-function of about 200 meters at its ends. Splitters and combiners serve an additional role as matching sections between linacs and arcs. Figure 9 shows the 30-GeV splitter matching the β-functions from the linac to the arcs. At present, the lattices of all six passes of eRHIC ERL are completed, and the exact location of each ERL magnet inside the RHIC tunnel identified.

One very important issue is finding a solution for synchronizing the electron beam with the hadron beam circulating in RHIC at different energies from 50 to 325 GeV/u. Because it is based on the ERL, eRHIC does not suffer from standard ring-ring limitations. One elegant solution identified is operating the RHIC at energies corresponding to the hadron beam's repetition frequency, i.e., various sub-harmonics of the ERL RF frequency (Fig. 10 b). The remaining tunability of the ERL's circumference can be realized by installing a standard eRHIC bypass in one of the free straight sections (specifcally, in IP4).

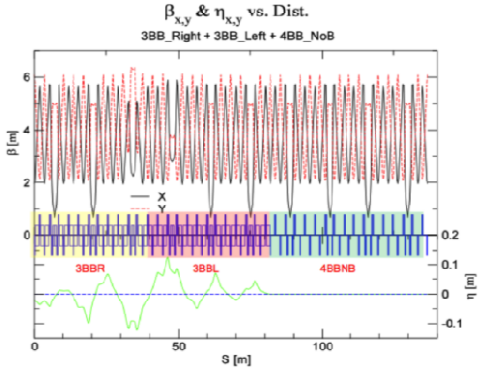

Figure 8: Half of the bilaterally symmetric lattice of the bypass around eRHIC detector at 6 o'clock.

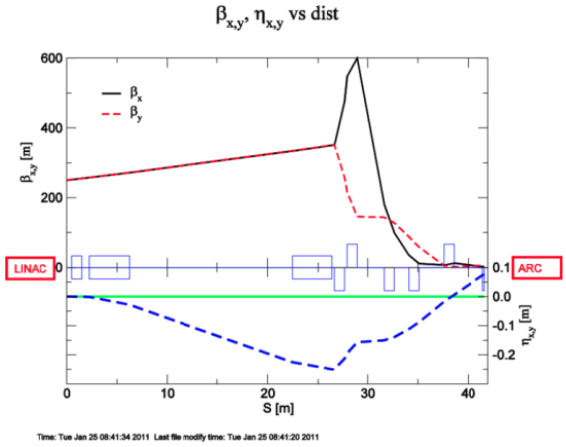

Figure 9: Lattice of the 30-GeV splitter matching the optical functions of the SRF linac and the arc.

We explored many issues in beam dynamics for the eRHIC ERL, identifying no major deterrents [16]. We detailed the effects of synchrotron radiation (both its energy spread and growth of emittance wake-fields from SRF linacs, resistive walls, and the transverse beam's (TBBU's) stability. We will address a few remaining questions before releasing the final eRHIC design. One such question is about the effect on energy spread of the wakefields from the wall's roughness. These issues and their remedies are under investigation.

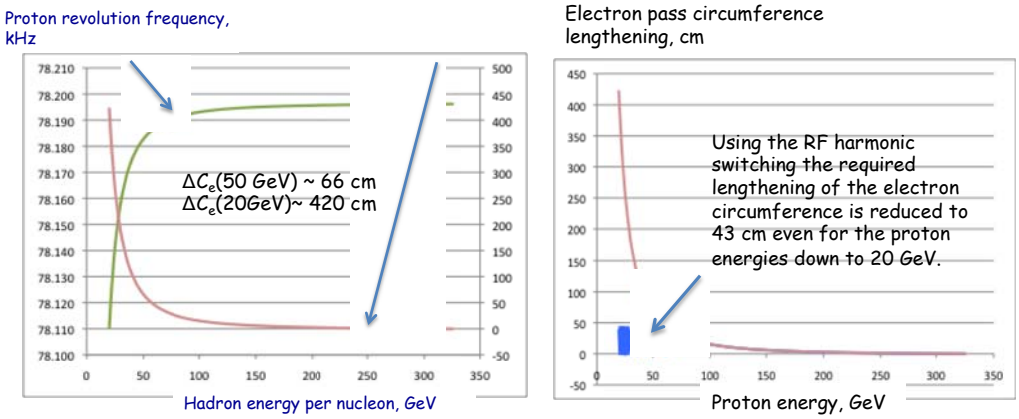

(a) (b)

Figure 10: (a) Change in the revolution frequency of hadron beams in the RHIC as function of their energy; (b) Red line - the required change for the e-beam circumference without harmonic switching (i.e. ring-ring case); Blue – the same curve with switching the harmonic number.

4.5.4 eRHIC Interaction Region

The current high-luminosity eRHIC IR design incorporates a 10-mrad crab-crossing scheme; thus, hadrons traverse the detector at a 10-mrad horizontal angle, while electrons go straight through. Figure 11 plots this scheme. The hadron beam is focused to $\beta^* = 5$ cm by a special triplet, wherein first magnet is a combined function magnet (1.95 m long with 2.23T magnetic fields and a -88 T/m gradient). It has two functions;

it focuses the hadron beam while bending it by 4 mrad. Two other quadrupoles do not bend the hadron beam but serve only for focusing it. Importantly, all three magnets provide zero magnetic fields along the electron beam's trajectory. Quadrupoles for this IR require very high gradients, and can be built only via modern superconducting technology [17,18].

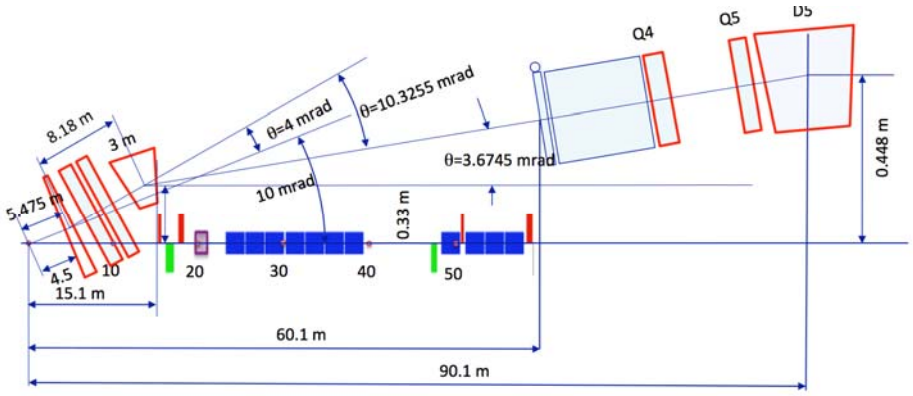

Figure 11: Layout of the right side of eRHIC IR from the IP to the RHIC arc. The spin rotator is the first element of the existing RHIC lattice remaining in place in this IR design.

This configuration guarantees the absence of harmful high-energy X-rays from synchrotron radiation. Further, the electron beam is brought into the collision via a 130-meter long merging system (Fig. 12). The radiation from regular bending magnets would be absorbed. The last 60 meters of the merging system use only soft bends: the downwards magnets have strength of 84 Gs (for 30 GeV beam), and the final part of the bend uses only a 24-Gs magnetic field. Only 1.9 W of soft radiation from the latter magnets would propagate through the detector.

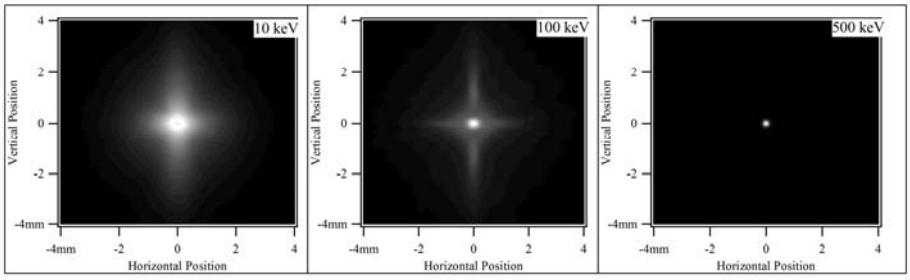

Figure 12: Distribution of synchrotron radiation from the final focusing triplet in the center of the IP.

One important factor in the IR design with low β*=5 cm is that the chromatism of the hadron's optics in the IR should be controlled, as reflected in the maximum β-function of the final focusing quadrupoles. Figure 13a shows the designed β- and dispersion-functions for hadron beam. The values of β-function are kept under 2 km, and the chromaticity is held at the level typical for RHIC operations with β* ~ 1m. We are starting a full-fledged program of tracking of hadron beams in the RHIC, including characterizing beam-beam effects and all known nonlinearities of RHIC magnets: we do not anticipate any serious chromatic effects originating from our IR design.

Furthermore, we introduced the bending field in the first quadrupole for the hadrons, thereby to separate them from the neutrons. Physicists considering processes of interest for electron-ion collider (EIC) science requested this configuration.

Since the electrons are used only once, the optics for them is much less constrained, and hence, does not present any technical- or scientific-challenges; therefore, even though it is designed, we do not describe it here.

Finally, beam-beam effects play important role in the eRHIC's performance. While we will control these effects on the hadron beam, i.e., we will limit the total tune shift for hadrons to about 0.015, the electron beam is used only once, and will be strongly disrupted during its single collision with the hadron beam. Consequently, the electrons are strongly focused by the hadron beam (pinch effects), and the e-beam's emittance grows by about a factor of two (disruption) during the collision. These effects, illustrated in Fig. 14, do not represent a serious problem, but will be studied carefully and taken into account in designing the optics and the aperture.

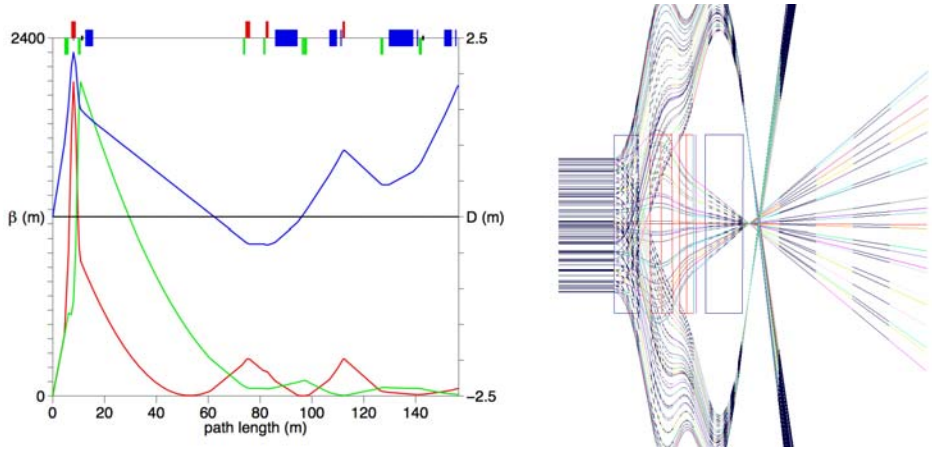

(a) (b)

Figure 13: (a) Hadron beam's optics at the eRHIC IR. The 5 cm β* is matched into the RHIC's arc lattice that starts about 60m from the IR. (b) Tracking hadrons with an energy deviation of +/- 0.1% through the first four magnets at the IR.

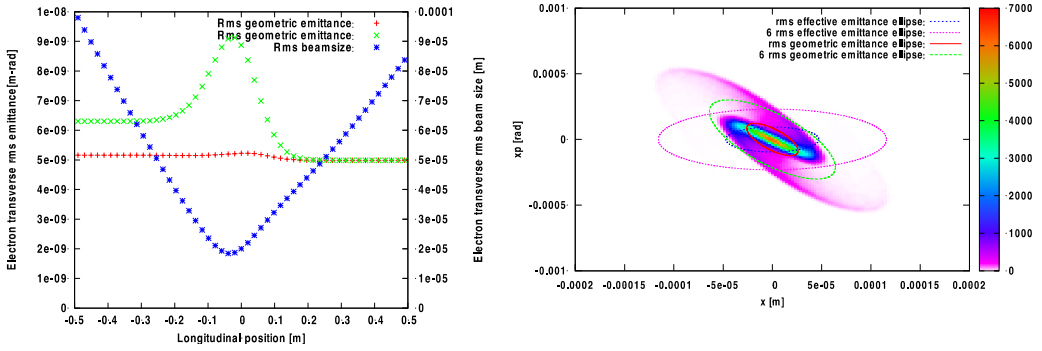

(a) (b)

Figure 14: (a) The optimized e-beam envelope during collision with the hadron beam in eRHIC; (b) distribution of electrons with initial Gaussian distribution after colliding with the hadron beam in eRHIC.

One of the important effects arising in a linac-ring collision is a potential for the so-called kink instability. Our detailed studies showed that using broad-band feedback suppresses this potentially dangerous instability within all ranges of the eRHIC parameters [19]. More details on the lattice and IR design appear in Ref. [20].

4.5.5 eRHIC Luminosity

As we discussed above, eRHIC energy as well as its luminosity will be staged. Hence, here we initially describe the Phase I eRHIC performance. After detailed studies, and considering the expense of its construction and running costs, we set the following limits for the eRHIC:

1. Beam-intensity limits: For protons: $4\ 10^{11}$
   For Au ions: $3\ 10^{9}$
   Electron-beam current: 50 mA
2. Minimum $\beta^* = 5$ cm for all species
3. Space-charge tune shift for hadrons is compensated by electron column
4. Maximum proton (ion) beam-beam parameter: 0.015
5. Coherent e-cooling will cool and maintain the hadron beam at
   a. Hadron beam 95% normalized emittance: 1.2 mm mrad
   b. RMS bunch length 4.9 cm
6. Synchrotron radiation's intensity limit is defined at 10 MW
7. Collision repetition-rate : 9 MHz

With 50 mA of beam current, the phase I eRHIC luminosity does not depend on the e-beam's energy but is proportional to that of the hadrons. Table 1 lists the typical eRHIC phase I's luminosity.

Table 1: Phase I eRHIC luminosity.

	e	p	$^{3}_{2}$He	$^{197}_{79}$Au	$^{238}_{92}$U
Energy, GeV	10	250	167	100	100
CM energy, GeV		100	82	63	63
Number of bunches/distance between bunches	107 nsec	111	111	111	111
Bunch intensity (nucleons)	$0.24\cdot10^{11}$	$4\cdot10^{11}$	$6\cdot10^{11}$	$6\cdot10^{11}$	$6.3\cdot10^{11}$
Bunch charge, nC	5.8	64	60	39	40
Beam current, A	0.05	0.556	0.556	0.335	0.338
Normalized emittance of hadrons 95% , mm mrad		1.2	1.2	1.2	1.2
Normalized emittance of electrons, rms, mm mrad		16	24	40	40
Polarization, %	80	70	70	none	none
RMS bunch length, cm	0.2	5	5	5	5
β^*, cm	5	5	5	5	5
Luminosity per nucleon, $cm^{-2}\ s^{-1}$		**2.7×10^{34}**	**2.7×10^{34}**	**1.6×10^{34}**	**1.7×10^{34}**

We included in the luminosity numbers the hourglass effect of 0.851 and the e-beam's pinch effect. This effect raises luminosity by 20- to 30-percent, depending on the ratio between the energies of the electron- and hadron-beams. For simplicity we use the lowest value of 1.2 in the table.

An increase in the e-beam's energy up to 20 GeV would not affect luminosity; above it, the SR would exceed the 10 MW level so that the e-beam current and luminosity must be reduced inversely in proportion to the fourth power of its energy. Figure 15 illustrates the eRHIC phase I luminosity in polarized e-p collision as functions of the particles' energy E_e and E_p , as well as the c.m. energy and E_e / E_p.

Ultimately, we could raise the eRHIC's luminosity and the c.m. energy reach by increasing the collision frequency to 56 MHz and taking advantage of up to a 25% enhancement of RHIC's energy. Table 2 shows the ultimate reach of the eRHIC luminosity that necessitates an enhancement in the beams' currents.

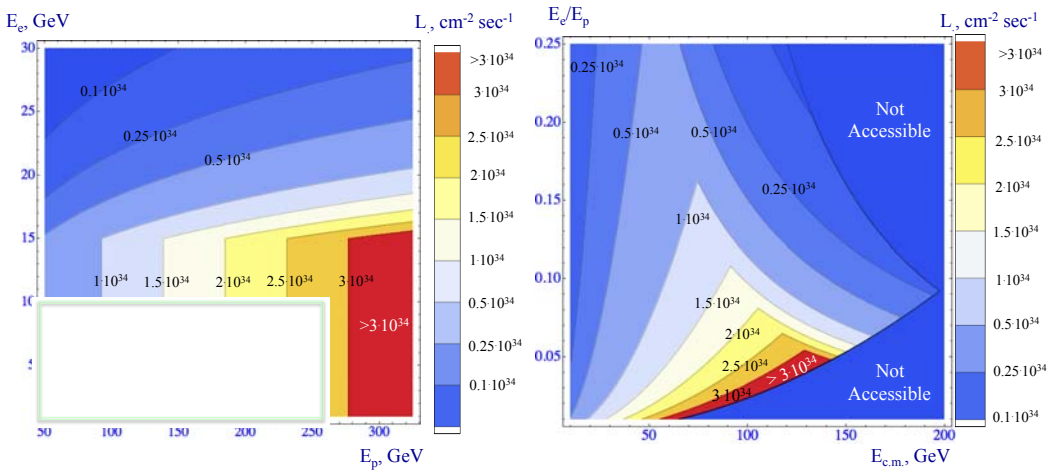

Figure 15: The contour plots of eRHIC luminosity with phase I beam parameters a function of the electron- and proton-energies (a), and the c.m. energy and the ratio of the e-beam's and the proton beam's energies (b). The box in (a) shows the reach of energy phase I.

Table 2: Ultimate eRHIC luminosity

	e	p	$^{2}_{3}$He	$^{79}_{197}$Au	$^{92}_{238}$U
Energy, GeV	≤ 15	325	215	130	130
CM energy, GeV		80-161	131	102	102
Number of bunches/distance between bunches	18 nsec	666	666	666	666
Bunch intensity (nucleons)	$0.24\cdot10^{11}$	$4\cdot10^{11}$	$6\cdot10^{11}$	$6\cdot10^{11}$	$6.3\cdot10^{11}$
Bunch charge, nC	3.8	64	60	39	40
Beam current, A	0.22	3.33	3.33	2.00	2.03
Normalized emittance of hadrons 95% , mm mrad		1.2	1.2	1.2	1.2
Normalized emittance of electrons, rms, mm mrad	Matches hadron beam	5.8-23	7-35	12-57	12-57
Polarization, %	80	70	70	none	none
RMS bunch length, cm	0.2	4.9	4.9	4.9	4.9
β*, cm	5	5	5	5	5
Luminosity per nucleon, $cm^{-2}\ s^{-1}$		**1.4×10^{35}**	**1.4×10^{35}**	**0.84×10^{35}**	**0.88×10^{35}**

We included the hourglass effect of 0.851 and 1.2 for the pinch effect into the luminosity numbers. With these beam parameters, the 10 MW limit for synchrotron radiation power will be attained at 15 GeV e-beam's energy, above which the luminosity would fall with the decline in the power of the e-beam's energy. The plots below (Fig. 16) depict the dependence of luminosity on electron energy for the top energy of the hadron beams, and on the hadron energy for an electron energy of 15 GeV or less.

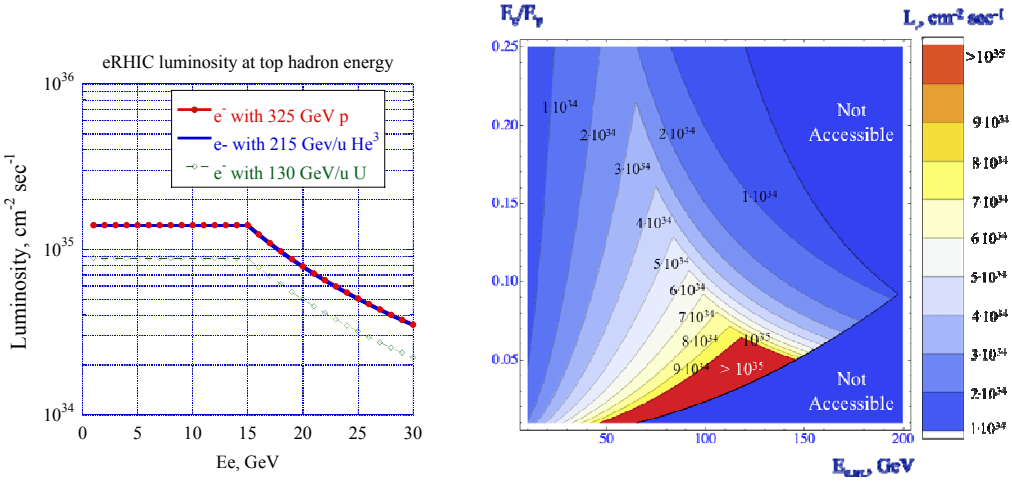

(a) (b)

Figure 16: The dependence of the ultimate eRHIC luminosity on the e-beam's energy (a). The luminosity contours is plotted as function the c.m. energy and the ratio of the energies of the e-beam and the proton beam (b).

Finally, eRHIC's maximum luminosity also can be calculated using following formulae

$$L_{ep} = 1.40 \cdot 10^{35} \cdot \frac{E_p}{325\,GeV} \cdot \min\left(1, \left(\frac{15\,GeV}{E_e}\right)^4\right); \quad L_{eHe3} = 1.39 \cdot 10^{35} \cdot \frac{E_{He3}/u}{215\,GeV} \cdot \min\left(1, \left(\frac{15\,GeV}{E_e}\right)^4\right);$$

$$L_{eU} = 0.884 \cdot 10^{35} \cdot \frac{E_U/u}{130\,GeV} \cdot \min\left(1, \left(\frac{15\,GeV}{E_e}\right)^4\right).$$

as function of the beam's energies. Using these formulae

$$L_{ep}\left(E_{c.m.},\alpha\right) = 1.40 \cdot 10^{35} \cdot \frac{E_{c.m.}}{\sqrt{\alpha} \cdot 650\,GeV} \cdot \min\left(1, \left(\frac{30\,GeV}{\sqrt{\alpha} \cdot E_{cm}}\right)^4\right); \quad L_{eHe3}\left(E_{c.m.},\alpha\right) = 1.39 \cdot 10^{35} \cdot \frac{E_{c.m.}}{\sqrt{\alpha} \cdot 430\,GeV} \cdot \min\left(1, \left(\frac{30\,GeV}{\sqrt{\alpha} \cdot E_{cm}}\right)^4\right);$$

$$L_{eU}\left(E_{c.m.},\alpha\right) = 0.884 \cdot 10^{35} \cdot \frac{E_{c.m.}}{\sqrt{\alpha} \cdot 260\,GeV} \cdot \min\left(1, \left(\frac{30\,GeV}{\sqrt{\alpha} \cdot E_{cm}}\right)^4\right).$$

gives the luminosity as function of the c.m. energy $E_{c.m.} \cong 2\sqrt{E_e E_h}$ and the beam energy ratio $\alpha = E_e / E_h$ with natural kinematic limits of (with h here standing for hadrons instead of protons)

$$E_{c.m.} \le 2\min\left(\sqrt{\alpha} E_{h\max}, E_{e\_\max} / \sqrt{\alpha}\right) \left(\frac{E_{c.m.}}{2E_{h\max}}\right)^2 \le \alpha \le \left(\frac{2E_{e\max}}{E_{c.m.}}\right)^2.$$

4.5.6 **eRHIC R&D**

The list of the needed accelerator R&D on the eRHIC ranges from the 50 mA CW polarized source to Coherent Electron Cooling [21]. It includes also designing and testing multiple aspects of SRF ERL technology in BNL's R&D ERL [22].

Coherent Electron Cooling (Fig. 17) promises to cool both the ion and proton beams to an order-of- magnitude smaller beams (both transversely and longitudinally) in under half an hour. Traditional stochastic- or electron- cooling techniques could not satisfy this demand. Being a novel unverified technique, the CeC will be tested in a proof-of-principle experiment at RHIC in collaboration with scientists from JLab, Daresbury Lab, BINP and TechX [23].

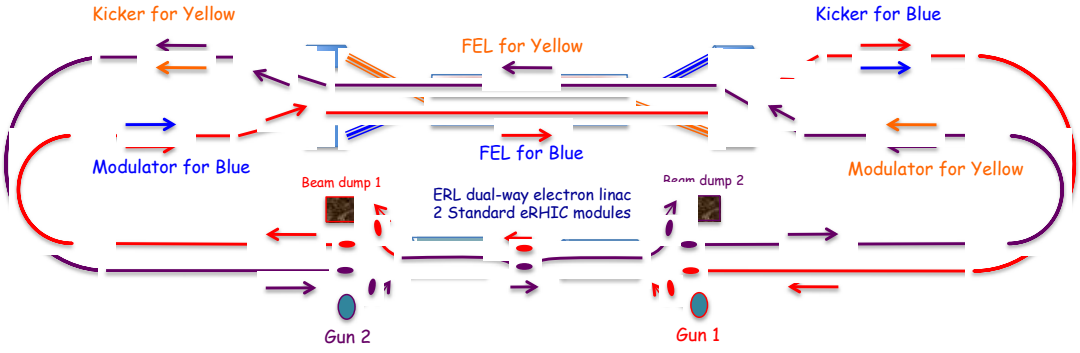

Figure 17: Possible layout of RHIC CeC system's cooling for both the yellow- and blue-beams.

Other important R&D effort, supported by an LDRD grant, focuses on designing and prototyping small-gap magnets and a vacuum chamber for cost-effective eRHIC arcs [2]. In addition to their energy efficiency and cheapness, small-gap magnets assure a very high gradient as room-temperature quadrupole magnets. Figure 18 shows two such prototypes; they were carefully tested and their fields were mapped using high-precision magnetic measurements. While the quality of their dipole field is close to satisfying our requirements, the quadrupole prototype was not manufactured to our specifications. We will continue this study, making new prototypes employing various manufacturers and techniques.

(a) (b)

Figure 18: (a) A prototype of eRHIC quadrupole with 1 cm gap; (b) Assembled prototype of eRHIC dipole magnet with 5 mm gap.

Cooling the hadron beams in eRHIC significantly increases the space-charge tune shift to level that dedicated compensation by an electron beam is required [24]. The detailed studies and simulations of this scheme are also part of eRHIC R&D.

The FFAG arc, including those with a permanent magnets lattice, may provide an inexpensive option for eRHIC. We are intensively investigating this option for phase I of eRHIC.

Another part of our R&D encompasses testing the RHIC in the various modes that will be required for the eRHIC's operation.

4.5.7 **Conclusions and Acknowledgements**

We are making steady progress in designing the high-energy, high-luminosity cost-effective electron-ion collider eRHIC and plan to continue our R&D projects and studies of various effects and processes (see for example [25,26]). So far, we have not encountered a problem in our proposed design that we cannot resolve. Being an ERL-based collider, eRHIC offers a natural staging of the electron beam's energy from 10 to 30 GeV. During this year we are continuing exploring various options for low-cost phase I designs.

The authors would like to acknowledge contributions and advice from E.-C. Aschenauer, D. Bruhwiler, G. Bell, A. Cadwell, A. Deshpande, R. Ent, W. Gurin, H. Kowalsky, M. Lamont, T.W. Ludlam, R. Milner, M. Poelker, B. Surrow, B. Schwartz, T. Ulrich, S. Vigdor, R. Venugopalan, and W. Vogelsan.

4.5.8 References

1. RHIC, http://www.bnl.gov/rhic/.
2. Y. Hao, P. He, A.K. Jain, V.N. Litvinenko, G. Mahler, W. Meng, J. Tuozzolo, Proceedings of First International Particle Accelerator Conference, IPAC'10, Kyoto, Japan, May 23-28, 2010, p.1614.
3. D. Trbojevic, S. J. Berg, I. Ben-Zvi, M. Blaskiewicz , V. Litvinenko, W. MacKay, V. Ptitsyn, T. Roser, and A. G. Ruggiero, In the Proceedings of Particle Accelerator Conference (PAC 07), Albuquerque, New Mexico, 2007, p.3205.
4. I. Ben-Zvi, J. Kewisch, J. Murphy and S. Peggs, Nuclear Instruments and Methods in Physics Research A **463**, 94 (2001).
5. eRHIC - 0th Order Design Report, Editors: M. Farkhondeh and V.Ptitsyn, BNL, 2004, http://www.bnl.gov/cad/eRhic/eRHIC_ZDR.asp.
6. V. Ptitsyn, J. Beebe-Wang, I. Ben-Zvi, A. Fedotov, W. Fischer, V.N. Litvinenko, W.W. MacKay, C. Montag, S. Ozaki, T. Roser, S. Tepikian, D. Trbojevic, W. Franklin, W. Graves, R. Milner, B. Surrow , C. Tschalaer, E. Tsentalovich, J. van der Laan, A.V. Otboev, Yu.M. Shatunov, D.P. Barber, Proceedings of EPAC 2006, Edinburgh, Scotland, June 26-30, 2006, p. 676 http://accelconf.web.cern.ch/AccelConf/e06/PAPERS/MOPLS058.PDF.
7. SuperB Conceptual Design Report, http://superb.infn.it/cdr.
8. D. Trbojevic, J. Beebe-Wang, Y. Hao, D. Kayran, V.N. Litvinenko, Y.Luo, V. Ptitsyn, and N. Tsoupas, eRHIC Interaction Region Design, Proc. of Second International Particle Accelerator Conference, San Sebastian, Spain, September 4-9, 2011, p. 3729, http://accelconf.web.cern.ch/AccelConf/IPAC2011/papers/thpz020.pdf.
9. E.Tsentalovich, High Intensity Polarized Electron Gun Studies at MIT-Bates, E. Tsentalovich, AIP Conference Proceedings Volume 1149, SPIN PHYSICS: 18th International Spin Physics Symposium Charlottesville (Virginia), 6–11 October 2008, p. 997.
10. V.N. Litvinenko, Gatling Gun: High Average Polarized Current Injector for eRHIC, C-A/AP/417 note, January 2011, http://www.cadops.bnl.gov/AP/ap_notes/ap_note_417.pdf.
11. X. Chang, I. Ben-Zvi, J. Kewisch, V. Litvinenko, A.I. Pikin, V. Ptitsyn, T. Rao, B. Sheehy, J. Skaritka, Q. Wu, E. Wang, T. Xin, A Multiple Cathode Gun Design for the eRHIC Polarized Electron Source, Proceedings of 2011 Particle Accelerator Conference, New York, NY, USA, March 25-April 1, 2011, p. 1969, http://accelconf.web.cern.ch/AccelConf/PAC2011/papers/wep263.pdf.
12. R. Calaga, I. Ben-Zvi, M. Blaskiewicz, X.Chang, D. Kayran, V.Litvinenko, Physica C **441** (2006) 159.
13. ERL option for LHeC, Y. Hao, D. Kayran, V.N. Litvinenko, V.Ptitsyn, D. Trbojevic, N. Tsoupas, CERN-LHeC-Note-2010-010 ACC (2010) http://cdsweb.cern.ch/record/1323297/files/ERL%20for%20LHeC%20-%20BNL%20paper%20-%20January%202011.pdf.
14. V.N. Litvinenko, L. Ahrens, M. Bai, J. Beebe-Wang, I. Ben-Zvi, M. Blaskiewicz, J.M. Brennan, R. Calaga, X. Chang, A.V. Fedotov, W. Fischer, D. Kayran, J. Kewisch, W.W. MacKay, C. Montag, B. Parker, S. Peggs, V. Ptitsyn, T. Roser, A. Ruggiero, T. Satogata, B. Surrow, S. Tepikian, D. Trbojevic, V. Yakimenko, S.Y. Zhang, M. Farkhondeh, A. Deshpande, Proc. of 2005 Particle Accelerator Conference, May 2005, Knoxville, TN, 2768 http://cern.ch/AccelConf/p05/PAPERS/TPPP043.PDF.
15. D.Trbojevic, E/.D. Courant, A. Garren,, AIP Conference Proceedings, V. **530**, (2000) p. 333.
16. G. Wang, M. Blaskiewicz, A.V. Fedotov, Y. Hao, J. Kewisch, V.N. Litvinenko, E. Pozdeyev, V. Ptitsyn, Proceedings of First International Particle Accelerator Conference, IPAC'10, Kyoto, Japan, May 23-28, 2010, p.1889,

http://accelconf.web.cern.ch/AccelConf/IPAC10/papers/tupec075.pdf.
17. H. Felice, S. Caspi, D. Cheng, D. Dietderich, P. Ferracin, R. Hafalia, J. Joseph, J. Lizarazo, G.L. Sabbi, X. Wang, M. Anerella, A.K. Ghosh, J. Schmalzle, P. Wanderer, G. Ambrosio, R. Bossert, A. V. Zlobin, Proceedings of First International Particle Accelerator Conference, IPAC'10, Kyoto, Japan, May 23-28, 2010, p.403, http://accelconf.web.cern.ch/AccelConf/IPAC10/papers/mopeb059.pdf.
18. P. Wanderer, IEEE Appl. Superconductivity, Vol. **19**, no. 3, June 2009, p. 1208.
19. Y. Hao, V.N. Litvinenko and V. Ptitsyn, Kink Instability Suppression with Stochastic Cooling Pickup and Kicker, In Proceedings of IPAC12, New Orleans, Louisiana, USA, 2012.
20. D. Trbojevic, J. Beebe-Wang, X. Chang, Y. Hao, A. Kayran, V.N. Litvinenko, B. Parker, V. Ptitsyn, N. Tsoupas, In Proceedings of IPAC'10, Kyoto, Japan, May 2010, p. 127 http://accelconf.web.cern.ch/accelconf/IPAC10/papers/mopea028.pdf.
21. V.N.Litvinenko, Y.S.Derbenev, Physical Review Letters 102, 114801 (2009).
22. I. Ben-Zvi, Z. Altinbas, D. Beavis, S. Belomestnykh, J. Dai, L. DeSanto, D. Gassner, L. Hammons, Ha. Hahn, A. Hershcovitch, A. Jain, P. Jain, J. Jamilkowski, D. Kayran, N. Laloudakis, R. Lambiase, D. Lederle, E. Lessard, X. Liang, V. Litvinenko, C. Liu, G. Mahler, M. Mapes, G. McIntyre, R. Michnoff, W. Meng, T. Miller, D. Pate, P. Pile, D. Phillips, S. Pontieri, J. Reich, T. Roser, M. Ruiz Osés, C. Schultheiss, T. Seda, B. Sheehy, J. Smedley, T. Rao, K. Smith, R. Than, R. Todd, J. Tuozzolo, E. Wang, D. Weiss, M. Wilinski, W. Xu, A. Zaltsman, The Status of the BNL R&D ERL, in this ICFA newsletter.
23. V.N. Litvinenko, J. Bengtsson, I. Ben-Zvi, A.V. Fedotov, Y. Hao, D. Kayran, G. Mahler, W. Meng, T. Roser, B. Sheehy, R. Than, J. Tuozzolo, G. Wang, S. Webb, V. Yakimenko, A. Hutton, G. Krafft, M. Poelker, R. Rimmer, G.I. Bell, D.L. Bruhwiler, B.T. Schwartz, Proceedings of 2011 Particle Accelerator Conference, New York, NY, USA, March 25-April 1, 2011, p. 2064 http://accelconf.web.cern.ch/AccelConf/PAC2011/papers/thobn3.pdf.
24. V. Shiltsev, A.Valishev, G.Kuznetsov, V.Kamerdzhiev, A.Romanov, FERMILAB-CONF-09-152-APC, http://lss.fnal.gov/archive/2009/conf/fermilab-conf-09-152-apc.pdf.
25. Y. Hao and V. Ptitsyn, Physics Review Special Topics: Accelerators and Beams **13**, 071003 (2010).
26. Y. Hao, V.N. Litvinenko, V. Ptitsyn, Proceedings of 2009 Particle Accelerator Conference, Vancouver, Canada, May 4-8, 2009, p.2868 , http://accelconf.web.cern.ch/AccelConf/PAC2009/papers/we6pfp057.pdf.

4.6 LHeC at CERN

Oliver Brüning, CERN, CH-1211 Geneva 23, Switzerland
Mail to: oliver.bruning@cern.ch

4.6.1 Introduction

The Large Hadron electron Collider (LHeC) project provides the unique possibility of exploring lepton-proton collisions in the TeV Center of Mass (CM) regime. The LHeC would use one of the proton beams of the LHC and therefore represents an interesting possibility for a further exploitation of the existing LHC infrastructure investment. Aiming at CM collision energies in the TeV range by using one of the 7 TeV proton (and a few TeV energy ion) beams of the LHC implies lepton beam

energies significantly exceeding the electron beam energy of HERA, the first ep collider built.

The LHeC study started at CERN in 2007 with an invitation by the CERN SPC and ECFA to work out a conceptual design study. The LHeC study was later also supported by NuPECC. The LHeC study conducted in total four workshops in the time between 2008 (first LHeC-CERN-ECFA workshop in Divonne, Switzerland) and 2012 (fourth LHeC-CERN-ECFA-NuPECC workshop in Chavannes-de-Bogis, Switzerland). The study prepared a Conceptual Design Report, which was published internally at CERN as a draft version in 2011 [1]. An external panel of experts reviewed the accelerator solutions, the auxiliary systems and the detector design that are presented in the study. The accelerator review confirmed, that both options that are described in the study are feasible and can reach the requested performance level within the given parameter constraints. The final version of the Conceptual Design Study is published in the Journal of Physics G, Nuclear Physics [2].

The CDR describes the LHeC exploitation in parallel with the HL-LHC operation (at a time scale of approximately 10 years). Synchronous pp and ep operation provides the possibility for collecting a total integrated luminosity of the order of 100 fb^{-1} based on peak e-p luminosities of the order of $L = 10^{33}$ cm^{-2} s^{-1}. The luminosity prospects are thus exceeding the HERA achievements by a factor of 100. In order to keep the total power consumption of the facility at a realistic level, a limit of the total LHeC power is set at 100 MW. A electron beam energy of 60 GeV was chosen for the Conceptual Design Report, an energy between the beam energies of LEPI and LEPII. A team of nearly 200 physicists and engineers worked out the CDR with the support of ECFA and NuPECC. The CDR describes two options for the LHeC implementation in some detail: a Ring-Ring option and a Linac-Ring option.

The Ring-Ring option features the installation of a new lepton storage ring inside the LHC tunnel, on top of the existing LHC ring. This option is technically relatively straightforward (in between LEP-I and LEP-II). However, it requires additional bypasses around the existing experiments for the HL-LHC (minimum number of 2 bypasses around ATLAS and CMS and more if other experiments continue to run during the HL-LHC phase [e.g. LHCb]) and challenging installation work inside a tunnel with an already operational accelerator infrastructure that will be pushed to the highest performance levels during the HL-LHC exploitation phase.

The Linac-Ring option requires the construction of a new linear accelerator for the electron beam that intersects in one location, most likely at IP2, with the existing LHC machine. Several options have been considered for the linear accelerator (pulsed linac, re-circulating linac and Energy Recovery Linac configurations) that provide a range of energy and luminosity combinations.

Recent discussions at CERN and at the 2012 CERN-ECFA-NuPECC Workshop on the LHeC, held in Chavannes de Bogis, Switzerland in June 2012, have underlined that the integration and planning aspects for the installation of a new machine inside the LHC tunnel represent a major challenge for the Ring-Ring option. This led to the decision to concentrate on the technical R&D work for the Linac-Ring option for further studies over the coming 3 to 4 years. This strategy should allow demonstrating the technical feasibility of the Linac-Ring options by 2015, in time for a final decision once first results become available from the LHC at close to nominal beam energies, between 6 TeV and 7 TeV. The CERN management mandated the LHeC study group to develop international collaborations for the above studies and to prepare a project

proposal for the European Strategy group so that the LHeC project can be part of the ongoing evaluation round of the European strategy group [3].

Table 1 summarizes the main parameters for two options for the Linac-Ring implementation of the LHeC: one version with a pulsed linac offering the highest beam energy reach but only modest luminosities and one version with CW linac operation offering the highest luminosity reach by exploiting an energy-recovery operation mode.

Table 1: Key parameters for two options for the Linac-Ring implementation of the LHeC.

LINAC Parameters for the Linac-Ring Option		
Operation mode	CW	Pulsed
Beam Energy [GeV]	60	140
Peak Luminosity [$cm^{-2}s^{-1}$]	10^{33}	$4\ 10^{31}$
Cavity gradient [MV/m]	20	32
RF Power Loss [W/cavity]	28	11
W per W (1.8K to RT)	700	700
Cavity Q_0	$2.5\ 10^{10}$	$2.5\ 10^{10}$
Power loss/GeV at RT	0.90	0.24
RF length [km]	2	7.9
Total length (including return arcs) [km]	9	7.9
Beam current [mA]	6.4	0.27
Repetition rate	-	10 Hz
Pulse length	-	5ms

4.6.2 **Technical Systems**

4.6.2.1 ***Warm Magnets***

Two compact normal conducting magnet designs (diameter of 35 cm and weight of 280 kg per meter magnetic length) have been developed at BINP (Novosibirsk) and at CERN and first prototypes have been produced for both design proposals. Both models demonstrated that theses magnets can achieve a high field quality and reproducibility of 10^{-4} at an operating range of approximately 125 Gauss to 800 Gauss, as is required by the Ring-Ring version of the LHeC and assuming a 10 GeV injection beam energy. With such parameters, these normal conducting magnets are also close to the specifications required for the dipoles in the return arcs of the Energy Recovery Linac option of the LHeC. However, the magnet design could be further optimized for the case of the Linac-Ring option as the magnets are operated at constant field strength and do not need to be cycled during the LHeC operation. The racetrack linac configuration comprises 3-fold return arcs in about 7 km tunnel. Each arc element has 600 four-meter long dipole magnets, with field strength between 0.046T and 0.264 T corresponding to the electron beam energy in the arc, and 240 quadrupole magnets (of 4 different types). These magnets are less demanding in terms of field reproducibility than for the Ring-Ring option. For the preparation of the ERL configuration it is of interest to find a cheap and reliable solution. One option worth pursuing is whether such magnets, quadrupoles and possibly dipoles, could be permanent magnets, which would relax the demands on the operation and tunnel infrastructure.

4.6.2.2 *Superconducting Magnets*

The simultaneous operation of a pp and ep collider facility within the same collider installation requires the development of novel superconducting magnet designs with apertures for three beams with widely different beam energies (two proton beams at 7 TeV and one lepton beam at 60 GeV). A conceptual design for such magnets, documented in the CDR, has been developed at CERN and is sketched in Figure 1. However, more studies (mechanical stress analysis) and magnet R&D (prototype with NbTi cables and prototypes with Nb_3Sn technology as demanded for the Linac-Ring option of the LHeC) are required before such magnets could be ready for the use in an operational collider.

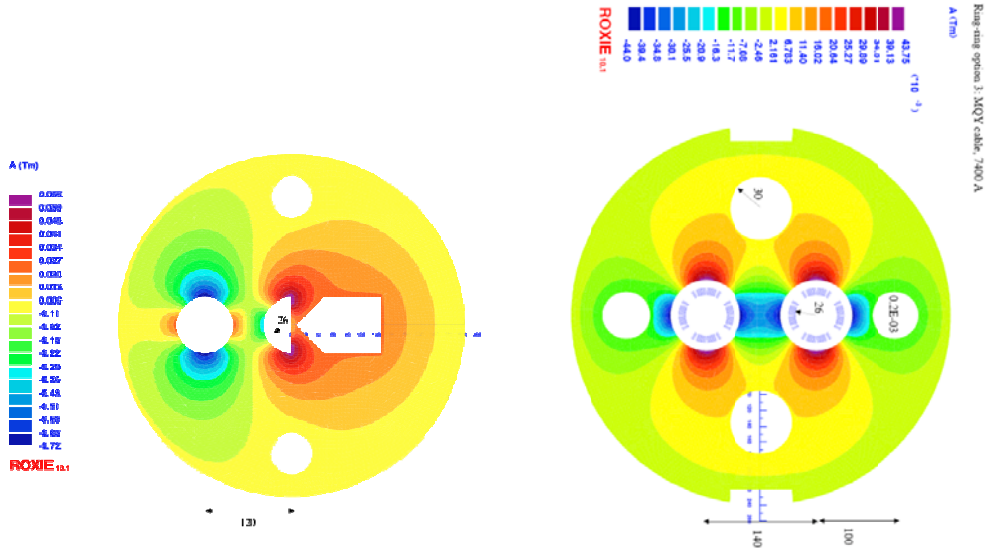

Figure 1: Conceptual cross section design of the superconducting interaction region magnets with three beam apertures. Left (right) the magnet closest (next to closest) to the interaction point Q1 (Q2).

4.6.2.3 *Superconducting RF*

The Energy Recovery Linac option of the LHeC constitutes the highest energy application of the energy recovery technique worldwide. The construction of an efficient Energy Recovery Linac requires the development of:

- High gradient Superconducting cavities (the RF gradient translates for a given beam energy directly into the required number and length of superconducting cavities and thus to the cost of the project);
- RF coupler design that is optimized for ERL operation;
- The highest possible Q_0 values (the Q-value directly impacts on the required cryogenics power for the facility and thus on the total power consumption of the LHeC). The LHeC power consumption estimates in the CDR assume Q_0 values higher than $2\ 10^{10}$ compared to design Q_0 values of 2 to $9\ 10^{10}$ for the SPL and $2.5\ 10^{10}$ for the TESLA cavity development. Both these projects have launched

dedicated R&D projects and prototype developments for demonstrating the above cavity performance values;
- Development of RF diagnostics and feedback loops for operating a multi-pass ERL over a wide range of beam energies (a few MeV to 60 GeV).

The LHeC design aims at maximum cavity gradients of 18 MV/m (compared to approximately 7 MV/m for the LEP SC RF system), which is close to the limit of state of the art RF developments (e.g. SPL cavity design with 25 MV/m in pulsed operation mode) and at Q_0 values above $2\ 10^{10}$. The feasibility of these parameters needs to be demonstrated in a prototype cavity that is optimized for the LHeC application with RF couplers designed for ERL operation. Furthermore, it needs to be demonstrated that the design parameters are within reach for a realistic series production of the cavities and new RF tools for the operation of a multi-turn re-circulating ERL (diagnostics tools, feedback loops etc.) need to be tested in operation in a dedicated ERL test facility.

4.6.2.4 *Energy Recovery Linac Operation*

Several Energy Recovery Linac projects and Test facilities are currently being pursued around the world. But most of these studies look at an ERL operation at relatively low beam energies (MeV regime) and more studies are required for studying the ERL operation at multi GeV beam energies. The development of a dedicated LHeC ERL test facility represents therefore an important goal for the future LHeC project development.

4.6.3 **Timeline of the LHeC**

Based on the experience with other projects such as LEP, LHC, LINAC4 at CERN, HERA and the XFEL at DESY, one should plan for approximately 10 years from the CDR to the project finalization. Smaller projects such as ESS and PSI XFEL plan for 8 to 9 years [TDR to project start] and the EU XFEL plans for 5 years from construction to operation start. HERA required approximately 10 years from project proposal to start of operation. A time line of 10 years for a project of the scale of the LHeC is ambitious but appears to be feasible and necessary to be consistent with the LHC planning and a project exploitation start by the mid 2020ies. Figure 2 shows the schematic schedule for the LHeC along these lines, as has been part of the CDR. It illustrates that keeping the option of an LHeC exploitation by 2025 requires the start of R&D activities for key technical developments (SC magnets and SC RF) by 2012.

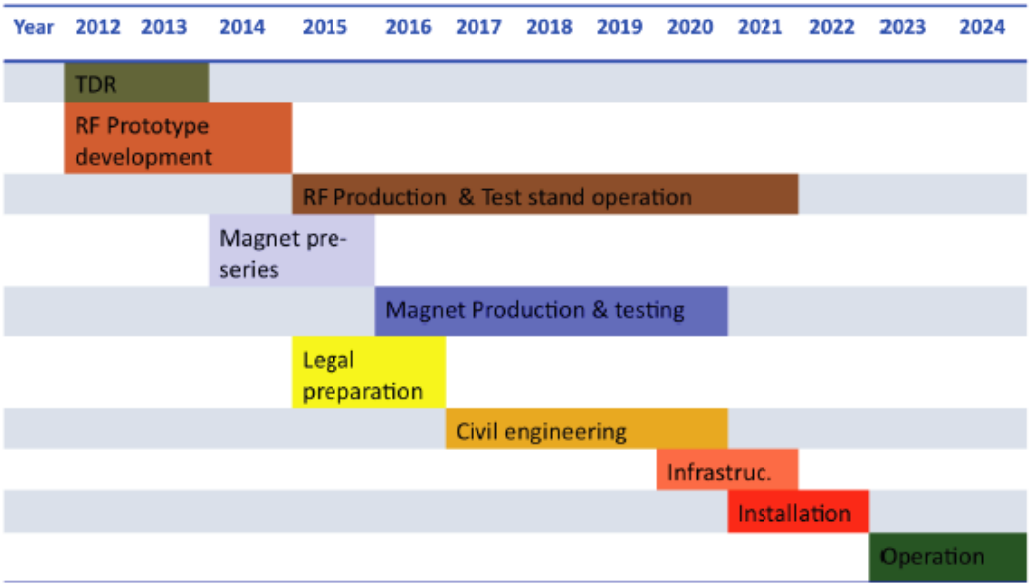

Figure 2: Schematic schedule for the LHeC, from the LHeC CDR.

4.6.4 References

1. LHeC-Note-2011-003 GEN.
2. J.L.Abelleira Fernandez et al.,
   LHeC Study Group, A Large Hadron Electron Collider at CERN,
   CERN-OPEN-2012-015, arXiv:1206.2913, submitted to J.Phys.G (2012).
3. http://europeanstrategygroup.web.cern.ch/europeanstrategygroup/.

4.7 LHeC Ring-Ring option

Helmut Burkhardt on behalf of the LHeC RR Team, CERN
Mail to: Helmut.Burkhardt@cern.ch

4.7.1 Introduction

In the earlier phases of the LEP and LHC designs there were plans to install both machines in the same tunnel and it was natural to also consider the possibility of ep collisions between the two rings [1, 2]. This turned out to be not practical and it was decided to install the LHC in the LEP tunnel after complete removal of the LEP machine.

The interest in a high energy ep collider increased when it became clear that HERA would stop operation in 2007. A proposal was made to re-install a lighter, compact, lower energy 70 GeV (compared to 104 GeV in LEP2) electron ring on top of the LHC [3], providing a luminosity of 10^{33} $cm^{-2}s^{-1}$ at a centre-of-mass energy of 1.4 TeV in collisions with the protons of the LHC.

This was followed by a conceptual design study, considering both a ring-ring (RR) option, described in this chapter, as well as a 60 GeV linac-ring (LR) option, described in the following chapter. To allow for a better comparison, it was decided to reduce the

electron ring energy to 60 GeV for the studies described in the conceptual design report (CDR). With extra efforts and investments, one might increase the electron ring energy to over 100 GeV, as had been achieved for LEP [4].

The main beam parameters of the LHeC RR option as considered for the CDR are listed in Table 1.

Table 1: Main LHeC RR parameters

Parameter	**Value**
Electron beam energy	60 GeV
Proton beam energy	7 TeV
e+, e- intensity per bunch	2×10^{10}
Total e+, e- beam current	100 mA
#bunches	2808
ep Luminosity (HL-layout)	1.3×10^{33} $cm^{-2}s^{-1}$
Total wall plug power	100 MW
Transverse normalized emittance $\varepsilon_{N\,x,y}$	0.59, 0.29 mm

Details of both the LR and RR options can be found in the CDR, which has just been published [5]. The advantages of the ring-ring configuration are that it uses known technology, with much experience from HERA and LEP, and that intense beams of both electrons and positrons are available.

4.7.2 **Layout, Optics and Integration**

The main constraint for the electron ring is to design it so that it fits in the existing tunnel without compromising the LHC performance to allow for ep collisions in one interaction point, simultaneously with high-luminosity pp collisions in the other interaction regions. This requires the active pp interaction regions to be bypassed with separate tunnels housing the RF in adjacent caverns. Excavation of such tunnels could proceed in parallel with LHC operation, just as the CMS cavern was excavated while LEP ran. Because of machine hardware placements and geological conditions, none of the 4 machine points (3, 4 and 6, 7) could house the LHeC interaction region (IR). For the CDR study, IP2 was chosen as the ep IR, currently housing the ALICE experiment, and bypasses were studied for ATLAS (IP1) and CMS (IP5).

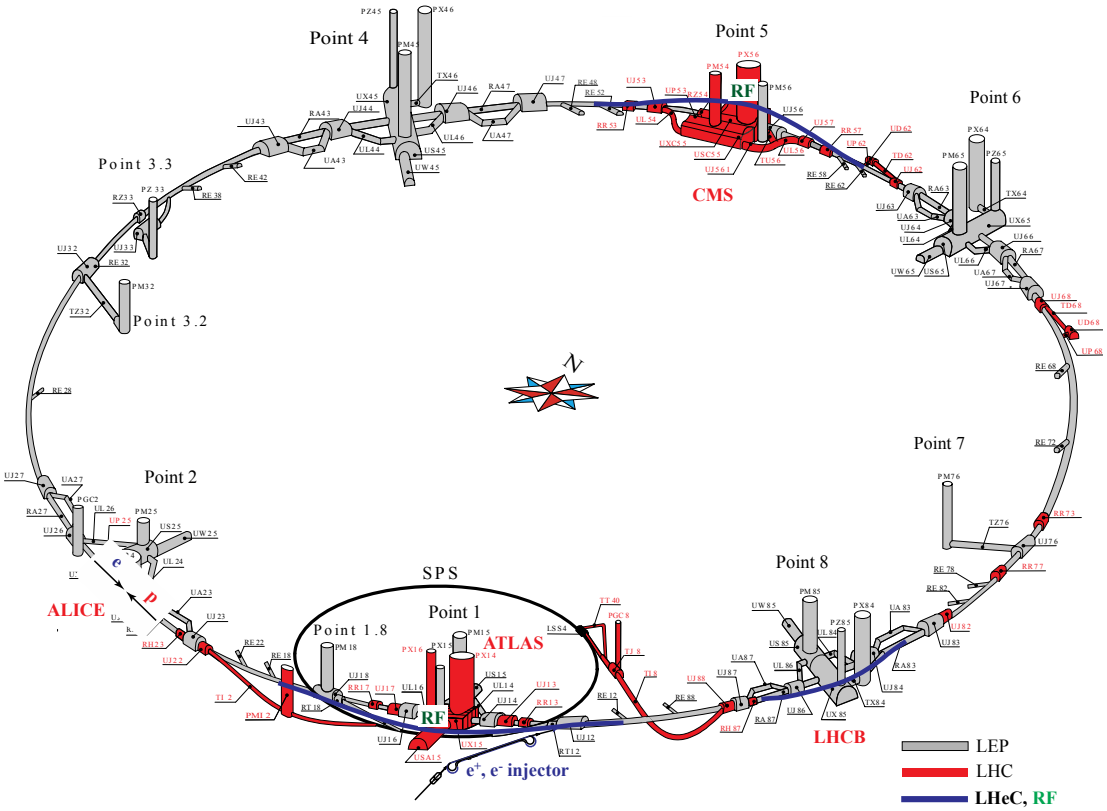

Figure 1: Schematic layout of the LHeC: In grey the LEP tunnel now used for the LHC, in red the LHC extensions. The three LHeC bypasses are shown in blue. The RF is installed in the central straight sections of the bypasses around Points 1 and 5. The bypass around Point 1 hosts in addition the injection.

The schematic layout of the LHeC RR option is shown in Fig.1. Horizontal outer bypasses for IR1 and IR5 were studied in detail for the CDR. The lengths of these bypasses are shown in Table 2.

Table 2: Length of the bypasses for IR1 and 5

	IR 1	IR 5
Bypass length	1303.3 m	1303.7 m
Separation	16.25 m	20.56 m
Dispersion free straight sections	172 m	297 m

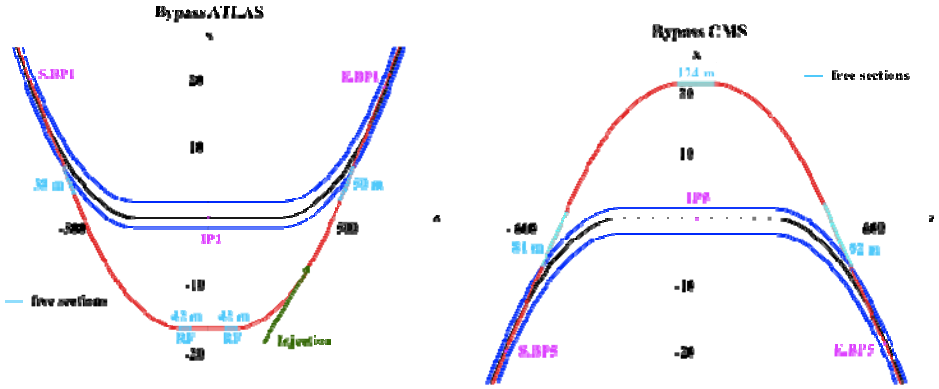

Figure 2: Horizontal bypass in Point 1 and Point 5. The LHC proton ring is shown in black, the electron ring in red and the tunnel walls in blue. Dispersion free sections reserved for the installation of RF, wiggler(s), injection and other equipment are marked in light blue. Beginning and end of the bypass are marked with S.BP and E.BP.

The geometry of the bypasses for ATLAS and CMS are shown in Fig. 2. The increase in circumference of the electron ring by the bypasses for IR1 and IR5 could be compensated by reducing the radius of the electron ring by 61 cm. In case LHCb will continue to run during the LHeC operation period, another bypass would be needed for IR8 and make it more difficult to compensate the increase in circumference.

It would then be more practical to install the electron ring on top of the proton ring as shown in Fig. 3. This would result in unequal circumferences of the electron and proton rings. The emittance increase by Hirata-Keil resonance effects [6] is believed to be tolerable (to be confirmed by detailed simulations).

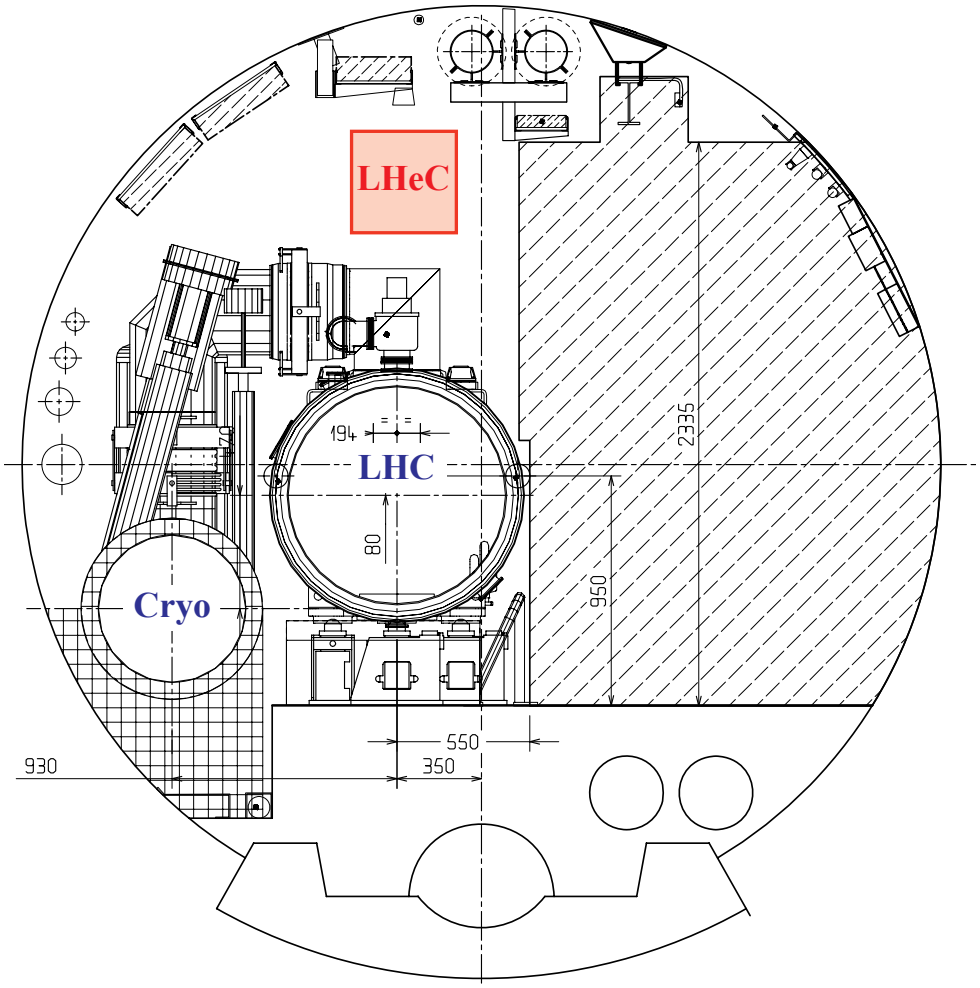

Figure 3: Representative cross section of the LHC tunnel. The possible location of the electron ring is indicated in red.

A complete lattice has been designed for the new electron ring. The main constraint was to design the lattice so that the new machine can be installed in the existing tunnel and available space. To achieve this, we chose an asymmetric FODO cell, of half the LHC FODO cell length, which conserves the space for the LHC service modules. The lattice in the straight sections was adapted to minimize the integration issues with the electrical distribution feedboxes (DFBs), which supply the currents to the superconducting LHC magnets. The basic FODO cell optics is shown in Fig. 4. The phase advance per half-cell for the horizontal plane was chosen to be 90^{o}, which allows for sufficiently small emittances to match the proton beam sizes at the interaction points. Based on LEP experience, we chose a different, 60^{o} phase advance for the vertical plane.

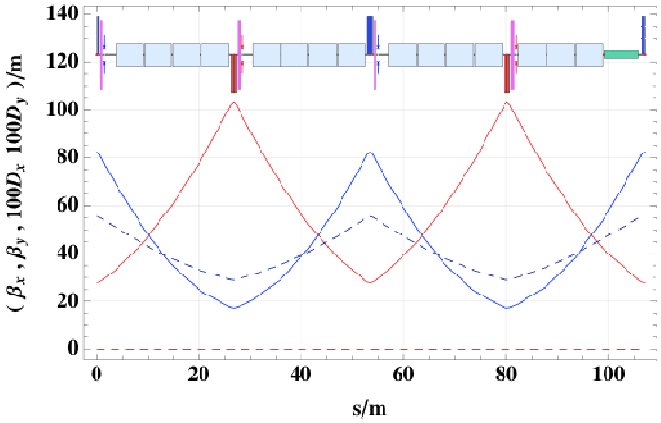

Figure 4: Electron ring arc cell optics. One arc cell consists of two FODO cells symmetric in the placement of the quadrupoles and asymmetric for the dipoles.

The main optics and emittance parameters are listed in Table 3. It is planned to adjust the vertical emittance to match the vertical proton beam size at the ep interaction point using transverse coupling ($\kappa = 0.5$).

Table 3: Optics parameters of the LHeC e-ring lattice

Electron beam energy	60 GeV
Phase advance per half cell, H/V	$90^o/60^o$
Cell length	106.881 m
Dipole fill factor	0.75
Damping partition J_x / J_y / J_e	1.5 / 1 / 1.5
Coupling constant κ	0.5
Horizontal emittance (no coupling)	5.5 nm
Horizontal emittance ($\kappa = 0.5$)	4.2 nm
Vertical emittance ($\kappa = 0.5$)	2.1 nm

A non-standard solution using eight individually powered quadrupoles was required for the dispersion matching regions to allow them to fit in the available space.

Chromaticity correction is achieved with 5 interleaved sextupole families, 2 horizontal and 3 vertical. The tune working point can be adjusted using IR3 and IR7 or the main arc quadrupoles.

4.7.3 **Injectors**

The LEP pre-injectors have been dismantled and the space and infrastructure are no longer available. Therefore, new injectors are required.

Table 4: Main parameters for the LHeC RR injector

Particle types	e+,e-
Injection energy	10 GeV
Bunch intensity	2×10^{10} = 3.2 nC
Filling time for 2808 bunches into the LHeC	< 10 min.

The main injector parameters are given in Table 4. They are within the reach of proven technology and concepts. Rebuilding the LEP source, pre-accelerators and electron-positron accumulators (EPA) would be fully adequate for the first stage of the injection system to 0.6 GeV [7]. This system could fill the electron ring with 2808 electron bunches in 6.7 minutes using groups of 8 bunches from the accumulator operating at a 1.14 s cycle time. The bunch intensity of 2×10^{10} in the LHeC (RR) is much lower than the 4×10^{11} which was required for LEP. It allows for direct injection without accumulation and a lower injection energy of 10 GeV, compared to the 22 GeV used for LEP. In the 30 years since the design of the LEP injectors, there has been substantial progress in superconducting RF technology. It is now feasible to design a very compact and efficient 10 GeV injector based on the principle of a recirculating Linac and to take advantage of the studies for ELFE at CERN [8]. A schematic view of this system is shown in Fig.5.

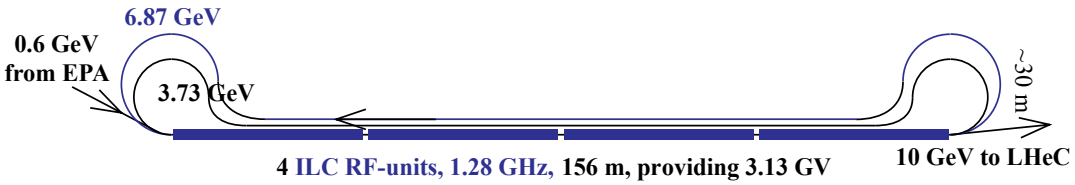

Figure 5: LHeC (RR) injector : The 0.6 GeV e+ or e- beams are accelerated in 3 passes through a re-circulating Linac to the injection energy of 10 GeV into the LHeC.

4.7.4 **Electron Ion Collisions**

The LHC has already operated in 2010 and 2011 as a heavy ion collider, producing collisions of fully ionized lead nuclei $^{208}Pb^{82+}$. The LHC will operate as proton – lead ion collider at the end of the present run period at the beginning of 2013.

With the additional electron ring of the LHeC, it will be possible to also collide electrons or positrons with heavy ions in the LHC. Ion operation is done with at most 592 bunches or roughly 5 times less bunches than used for proton operation. The number of electron bunches will be reduced accordingly. At constant synchrotron radiation power, the electron intensity per bunch could in this mode be increased by the same factor of about 5 to 10^{11}. This is still much lower than the maximum bunch intensities of 4.2×10^{11} used in LEP but may already require extra efforts to keep the ring impedance sufficiently low to remain below the transverse mode coupling threshold at 10 GeV and accumulation at injection into the electron ring.

4.7.5 **Polarization**

Transverse spin polarization naturally builds up for the stored electron or positron beams at high energy: there is small imbalance in spin-flip probabilities in synchrotron radiation that preferentially aligns the spins with the field of the main bending magnets. This is known as the Sokolov-Ternov effect. Imperfections and, in particular, vertical dispersion from magnet misalignment will reduce the equilibrium level of polarization. The depolarization increases with beam energy. Simulation results are shown in Fig. 6. High (50 to 80%) transverse polarization is expected at beam energies below 50 GeV [9]. Longitudinal polarization of the electrons or positrons at the ep interaction point will be obtained using a pair of spin rotators.

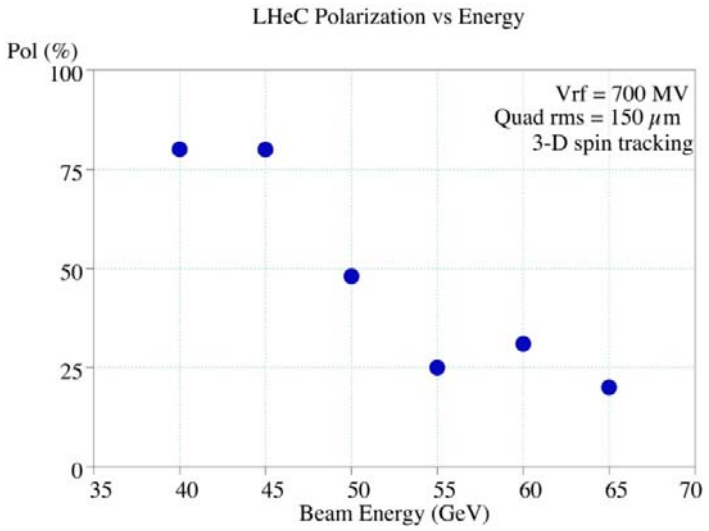

Figure 6: Equilibrium polarization as a function of ring energy, predicted by full 3-D spin tracking with imperfections.

4.7.6 **IR Layout**

Maximum luminosity can be achieved with focussing magnets placed close to the interaction point. However this limits the polar angle acceptance. Two principal interaction optics solutions have been developed, a high luminosity (HL) optics, with acceptance down to about 10^{o}, and a high acceptance (HA) optics, covering polar angles down to 1^{o}.

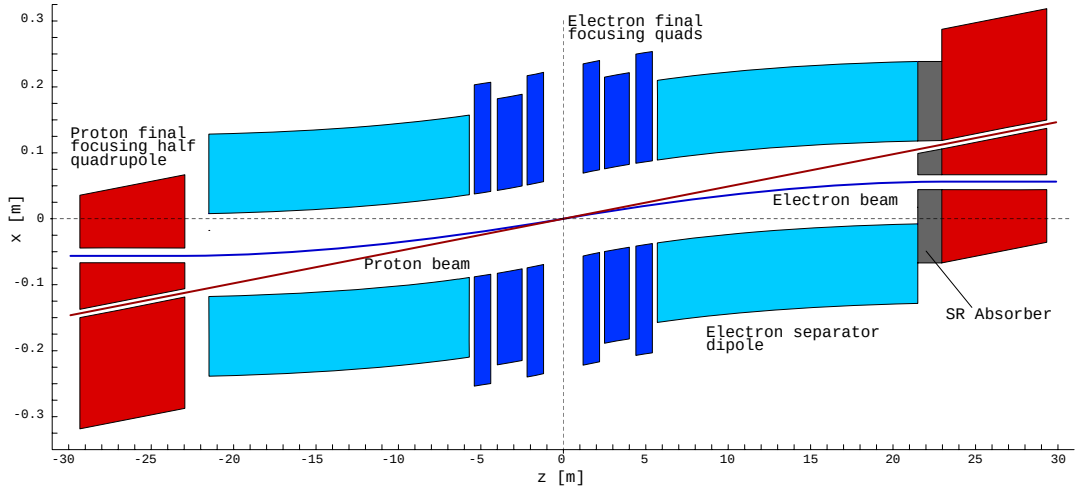

Figure 7: Schematic layout of the LHeC (RR) 10^{o} interaction region. The electron final focus quadrupole and separation dipole magnets (blue) are placed in the region within the superconducting mini-beta proton quadrupoles (red).

A schematic view of the interaction layout for the high-luminosity solution is shown in Fig. 7. The electron mini-beta quadrupoles are embedded into the detector opening angle and, in order to obtain the required separation effect, they are shifted in the horizontal plane and act effectively as combined function magnets. Thus focusing and separation of the electron beam are combined in a very compact lattice structure, a prerequisite for luminosity values in the range of 10^{33} $cm^{-2}s^{-1}$. The crossing angle between the colliding proton and electron beam is 1 mrad for both IR options.

The nearest proton quadrupole to the IP is a specially designed superconducting half-quadrupole illustrated in Fig. 8.

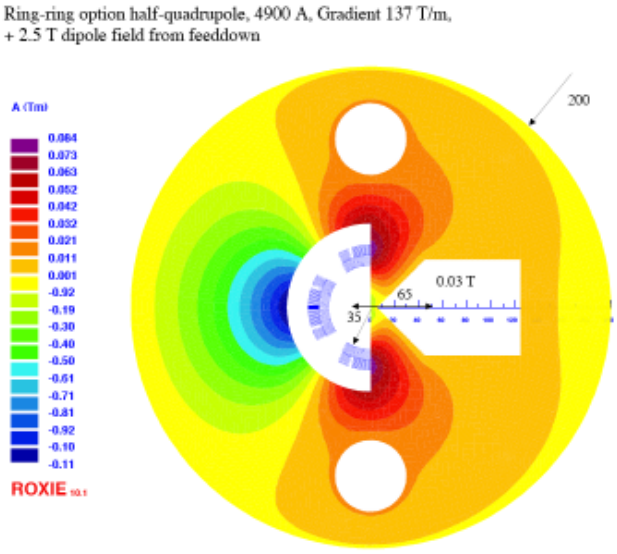

Figure 8: Super conducting half quadrupole in the proton lattice. The electron beam will pass on the right hand side of the mirror plate in a quasi-field free region.

The synchrotron radiation power lost by the electron beam in its passage through the fields of the warm insertion magnets is substantial: 33 kW for the HL and 51 kW for the

HA optics. The radiation is emitted in a very narrow forward cone and mainly impacts on the synchrotron radiation absorbers placed in front of the superconducting half-quadrupole.

An additional complication (not present at HERA) is that we have in the LHC two counter rotating proton beams and that we must allow for a clean passage for the second, non-colliding proton beam through the ep interaction region. The second proton beam is guided through the same aperture as the electron beam but experiences essentially no focusing due to its much higher energy. It then passes through the half-quadrupole in the field free region.

The main IR-layout parameters are shown in Table 5. The luminosities include the reduction by about 20% due to the crossing angle. Table 5 also gives the unperturbed β-values at the interaction point and the beam-beam parameters ξ. The luminosity and ξ values include the expected increase in the dynamic reduction in β* by the beam-beam effect. The beam-beam parameters quoted for the electrons correspond about to the best values reached in LEP simultaneously in four interaction regions. The beam-beam parameter ξ for the protons is much lower than has already been achieved in pp collisions in the LHC and leaves room for a further luminosity performance increase for the LHeC RR option.

Table 5: Parameters for the HL and HA IR optics layouts

Parameter	**HL**		**HA**	
	e	p	e	p
Energy	60 GeV	7 TeV	60 GeV	7 TeV
β^*_x	0.18 m	1.8 m	0.4 m	4.05 m
β^*_y	0.1 m	0.5 m	0.2 m	0.97 m
ξ_x	0.085	0.0008	0.086	0.0008
ξ_y	0.088	0.0004	0.090	0.0004
σ^*_x	30 μm		45 μm	
σ^*_y	15.8 μm		22 μm	
Luminosity	1.3×10^{33} cm^{-2}s^{-1}		0.7×10^{33} cm^{-2}s^{-1}	
Crossing angle	1 mrad		1 mrad	
SR Power	33 kW		51 kW	

4.7.7 **Conclusion**

As described in the recent CDR [3] and summarized here, we conclude that it is feasible to re-install a high energy electron ring in the LHC tunnel to allow for ep collisions in one interaction region simultaneously with high-luminosity pp operation on the other interaction regions. The electron ring design has been designed as a relatively light, compact machine consisting of a conventional magnet lattice, which can be installed on top of the existing LHC proton ring. The new superconducting RF-system of the electron ring will be installed in the new bypass tunnels and not interfere with the LHC.

4.7.8 References

1. A. Verdier, “An optimized e-p insertion for LEP and LHC”, Proc. PAC 1991
2. E. Keil, “LHC e-p Otion”, LHC Project Report 93, March 1997
3. J. B. Dainton, M. Klein, P. Newman, E. Perez, and F. Willeke, “Deep inelastic electron nucleon scattering at the LHC,” JINST 1 (2006) P10001
4. A. Butterworth et al., “The LEP2 superconducting RF system”, NIM A587 (2008) pp. 151-177
5. LHeC Study Group, “A Large Hadron Electron Collider at CERN”, CERN-OPEN-2012-015, June 2012
6. Hirata, Keil, “Barycenter motion of beams due to beam-beam interaction in asymmetric ring colliders”, NIM A292 (1990) pp. 156-168
7. The LEP injector chain, CERN-LEP/TH/83-29, June 1983
8. ELFE at CERN, Conceptual Design Report, H. Burkhardt (Ed.), CERN 99-10
9. D. P. Barber, H.U. Wienands et al., J. Phys. Conf. Ser. 295 (2011) 012145.

4.8 LHeC ERL/Linac-Ring Option

Frank Zimmermann, CERN, CH-1211 Geneva 23, Switzerland
Mail to: frank.zimmermann@cern.ch

4.8.1 General Considerations

A high-energy electron-proton collider can be realized by accelerating electrons (or positrons) in a linear accelerator (linac) to 60 – 140 GeV and colliding them with the 7-TeV protons circulating in the Large Hadron Collider (LHC). Except for the collision point and the surrounding interaction region, the tunnel and the infrastructure for such a linac are separate and fully decoupled from the LHC operation, from the LHC maintenance work, and from other LHC upgrades (e.g., High Luminosity - LHC and High Energy - LHC).

The technical developments required for this type of collider can both benefit from and be used for many future projects. In particular, to deliver a long or continuous beam pulse, as required for high luminosity, the linac must be based on superconducting (SC) radio frequency (RF) technology. The development and industrial production of its components can exploit synergies with numerous other advancing SC-RF projects around the world, such as the European XFEL at DESY, eRHIC, ESS, ILC, CEBAF upgrade, CESR-ERL, JLAMP, and the CERN HP-SPL.

For high luminosity operation at a beam energy of 50 – 70 GeV the linac should be operated in continuous wave (CW) mode, which restricts the maximum RF gradient through the associated cryogenics power, to a value of about 20 MV/m or less. In order to limit the active length of such a linac and to keep its construction and operating costs low, the linac should, and can, be recirculating. For the sake of energy efficiency and to limit the overall site power, while boosting the luminosity, the SC recirculating CW linac can be operated in energy-recovery (ER) mode.

Electron-beam energies higher than 70 GeV, e.g. 140 GeV, can be achieved by a pulsed SC linac, similar to the XFEL, ILC or SPL. In this case the accelerating gradient can be larger than for CW operation, i.e. above 30 MV/m, which minimizes the total length, but recirculation is no longer possible at this beam energy due to prohibitively high synchrotron-radiation energy losses in any return arc of reasonable dimension. As

a consequence the standard energy recovery scheme using recirculation cannot be implemented and the luminosity of such a higher-energy lepton-hadron collider would be more than an order of magnitude lower than the one of the lower-energy CW ERL machine, at the same wall-plug power.

For a linac it is straightforward to deliver an electron beam with 80–90% polarization.

The production of a sufficient number of positrons to achieve positron-proton collisions at a similar luminosity as for electron-proton collisions is challenging for a linac-ring collider. A conceivable path towards decent proton-positron luminosities would include a recycling of the spent positrons, together with the recovery of their energy.

The development of a CW SC recirculating energy-recovery linac (ERL) for LHeC would prepare the ground, the technology and the infrastructure for many possible future projects, e.g., for an International Linear Collider, for a Muon Collider, for a neutrino factory, or for a proton-driven plasma wake field accelerator.

A ring-linac LHeC would, therefore, promote a variety of conceivable long-term high-energy physics projects, while pursuing an attractive forefront high-energy physics programme in its own right.

4.8.2 **ERL-Ring Collider Performance and Layout**

Particle physics imposes the following performance requirements for the LHeC. The lepton beam energy should be 60 GeV or higher and the electron-proton (*ep*) luminosity of order 10^{33} $cm^{-2}s^{-1}$. Positron-proton collisions are also required, with at least a few percent of the electron-proton luminosity. Since the LHeC should operate simultaneously with LHC *pp* physics, it should not degrade the *pp* luminosity. Both electron and positron beams should be polarized. Lastly, the detector acceptance should extend down to 1^{o} or less. In addition, the total electrical power for the lepton branch of the LHeC collider should stay below 100 MW.

For round-beam collisions, the luminosity of the linac-ring collider [1] is written as

$$L = \frac{1}{4\,\pi\,e}\,\frac{N_{b,p}}{\varepsilon_p}\,\frac{1}{\beta_p^*}\,I_e\,H_{hg}\,H_D\,, \qquad (1)$$

where e denotes the electron charge, $N_{b,p}$ the proton bunch population, β_p^* the proton beta function at the interaction point (IP), ε_p the proton beam transverse geometric emittance (round beams are assumed), I_e the average electron beam current, H_{hg} the geometric loss factor arising from crossing angle and hourglass effect, and H_D the disruption enhancement factor due to the electron pinch in collision, or luminosity reduction factor from the anti-pinch in the case of positrons. In the above formula, it is assumed that the electron bunch spacing is a multiple of the proton beam bunch spacing. The latter could be equal to 25 or 50 ns, without changing the luminosity value.

The ratio $N_{b,p}/\varepsilon_p$ is also called the proton beam brightness. Among other constraints, the LHC beam brightness is limited by the proton-proton beam-beam limit. For the LHeC design we assume the brightness value obtained for the ultimate bunch intensity, $N_{b,p}$ =1.7x10^{11}, and the nominal proton beam emittance, ε_p =0.5 nm ($\gamma\varepsilon_p$ =3.75μm). This corresponds to a total *pp* beam-beam tune shift of 0.01 with two collisions per turn.

More than two times higher values have already been demonstrated with good *pp* luminosity lifetime, during initial LHC beam commissioning, indicating a potential for higher *ep* luminosity.

To maximize the luminosity, for the LHeC linac-ring collider the proton IP beta function is chosen as 0.1 m. This is considerably smaller than the 0.55 m for the *pp* collisions of the nominal LHC. The reduced beta function can be achieved by reducing the free length between the IP and the first proton quadrupole (10 m instead of 23 m), and by squeezing only one of the two proton beams, namely the one colliding with the leptons, which increases the aperture available for this beam in the last quadrupoles. In addition, it is assumed that the final quadrupoles could be based on Nb_3Sn superconductor technology instead of Nb-Ti. The critical field for Nb_3Sn is almost two times higher than for Nb-Ti, at the same temperature and current density, allowing for correspondingly larger aperture and higher quadrupole gradient. Nb_3Sn quadrupoles are presently under development for the High-Luminosity LHC upgrade (HL-LHC).

The geometric loss factor H_{hg} due to hourglass effect and possible crossing angle needs to be optimized as well. For round beams with $\sigma_{z,p} >> \sigma_{z,e}$ (well fulfilled for $\sigma_{z,p} \sim$ 7.55 cm, $\sigma_{z,e} \sim$300 μm) and $\theta_c << 1$, it can be expressed as (see also [2,3])

$$H_{hg} = \frac{\sqrt{\pi}\; z\, e^{z^2}\, \mathrm{erfc}\,(z)}{S}, \tag{2}$$

where

$$z \equiv 2\,\frac{\left(\beta_e^* / \sigma_{z,p}\right)\left(\varepsilon_e / \varepsilon_p\right)}{\sqrt{1+\left(\varepsilon_e / \varepsilon_p\right)^2}}\,S \qquad \text{and} \qquad S \equiv \sqrt{1+\frac{\sigma_{x,p}^2\,\vartheta_c^2}{8\,\sigma_p^{*2}}}\ . \tag{3}$$

Luminosity loss from a crossing angle θ_c is avoided by head-on collisions. The luminosity loss from the hourglass effect, due to the long proton bunches and potentially small electron beta functions, is kept small, thanks to a "small" linac electron beam emittance of 0.43 nm ($\gamma\varepsilon_e$=50 μm). We note that the assumed electron-beam emittance, though small when compared with a storage ring of similar energy, is still very large by linear-collider standards. Figure 1 illustrates the hourglass effects for an LHeC linac-ring and ring-ring collider. The difference in the optimized IP configuration arises from the much smaller emittance of the linac beam.

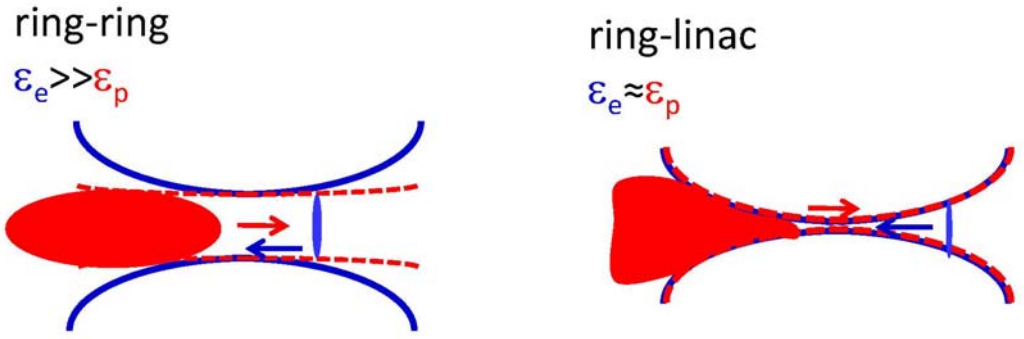

Figure 1: Bunch lengths and beam envelopes at the collision point of two unequal beams for a ring-ring (left) and linac-ring ep collider (right). For the ring-ring IP the minimum beta function and, thereby, the minimum beam size are limited by the hourglass effect, a small crossing angle is acceptable, and the colliding lepton beam is barely disrupted. For the linac-ring collider

smaller beta functions and beam sizes are possible, head-on collision is required, and the disruption of the lepton beam is significant.

The disruption enhancement factor for the ERL-Ring electron-proton collisions is about H_D ~1.35, according to Guinea-Pig simulations [4] and also from a simple estimate based on the fact that the average rms size of the electron beam during the collision approaches a value equal to $2^{-1/2}$ of the proton beam size. On the other hand, for positron-proton collisions the disruption of the positrons leads to a significant luminosity reduction, by roughly a factor H_D ~0.3, similar to the case of electron-electron collisions [5].

The final parameter determining the luminosity is the average electron (or positron) beam current I_e. It is closely tied to the total electrical power available, which is taken to be 100 MW.

4.8.2.1 *Crossing Angle and IR Layout*

The colliding electron and proton beams need to be separated by about 7 cm at a distance of 10 m from the IP in order to enter through separate holes in the first proton quadrupole magnet. This separation could be achieved with a crossing angle of 7 mrad and crab cavities. The required crab voltage would, however, need to be of order 200 MV, which is 20–30 times the voltage needed for *pp* crab crossing at the HL-LHC. Therefore, crab crossing is not considered an option for the L-R LHeC. Without crab cavities, any crossing angle should be smaller than 0.3 mrad. A crossing angle so small is not useful compared with the 7 mrad angle required for the separation. The R-L interaction region (IR), therefore, uses detector-integrated dipole fields around the collision point, to provide head-on *ep* collisions (θ_c=0 mrad) and to separate the beams by the required amount. A dipole field of about 0.3 T over a length of ±9 m accomplishes these goals.

The IR layout with separation dipoles, superconducting (SC) final proton quadrupoles and 3 beams is sketched in Fig. 2.

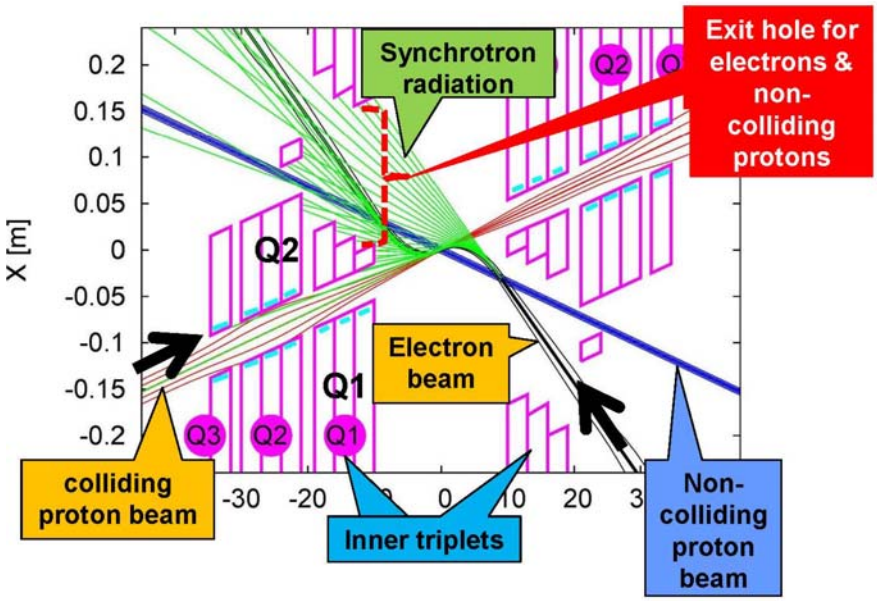

Figure 2: LHeC interaction region with a schematic view of synchrotron radiation [6] (courtesy R. Tomas). Beam trajectories with 5σ and 10σ envelopes are shown. The parameters of the Q1

and Q2 quadrupole segments correspond to Nb_3Sn half-aperture and single-aperture (with holes) quadrupoles.

Significant synchrotron radiation, with 48 kW average power, and a critical photon energy of 0.7 MeV, is emitted in the detector-integrated dipole fields. A large portion of this radiation is extracted through the electron and proton beam pipes. The SC proton magnets can be protected against the radiation heat load by an absorber placed in front of the first quadrupole and by a liner inside the beam pipe. Backscattering of synchrotron radiation into the detector is minimized by shaping the surface of absorbers and by additional masking. Except for the horizontally outward direction of the synchrotron radiation fan, the geometric detector acceptance can go down to values as low as 0.5°.

The separation dipole fields modify, and enhance, the geometric acceptance of the detector. Figure 3 illustrates that scattered electrons with energies of 10–50 GeV might be detected at scattering angles down to zero degrees.

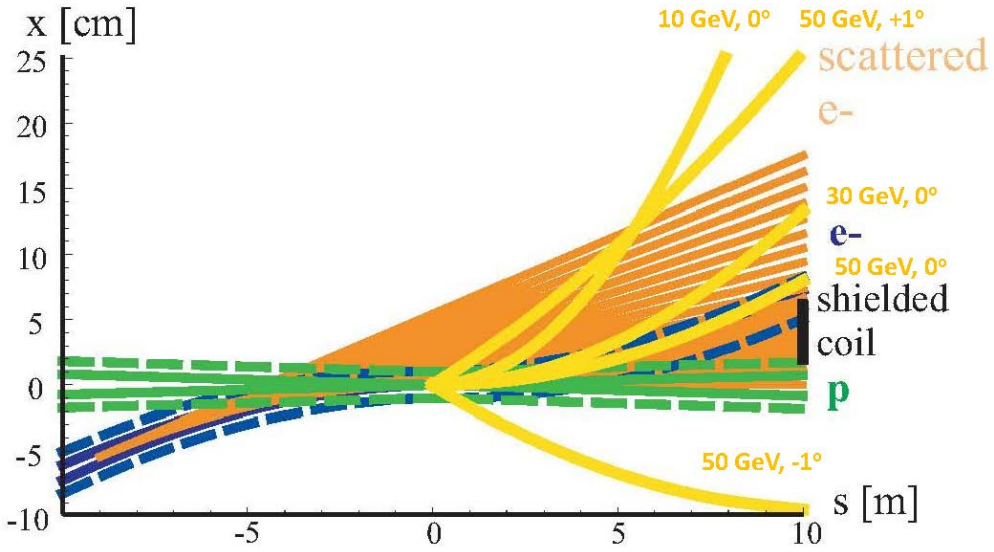

Figure 3: Example trajectories in the detector dipole fields for electrons of different energies and scattering angles, suggesting an enhancement of the detector acceptance by the dipoles.

4.8.2.2 *Electron Beam and the Case for Energy Recovery*

The electron-beam emittance and the electron IP beta function are not critical, since the proton beam size is large by electron-beam standards (namely about 7 μm rms compared with nm beam-sizes for linear colliders). The most important parameter for high luminosity is the average beam current, I_e, which linearly enters into the luminosity formula. In addition to the electron beam current, also the bunch spacing (which should be a multiple of the LHC 25-ns proton spacing) and polarization (80–90% for the electrons) need to be considered.

Having pushed all other parameters in the luminosity expression an average electron current of about 6.4 mA is required to reach the target luminosity of 10^{33} $cm^{-2}s^{-1}$.

For comparison, the CLIC main beam has a design average current of 0.01 mA [7], so that it falls short by a factor 600 from the LHeC requirement. For other applications

it has been proposed to raise the CLIC beam power by lowering the accelerating gradient, raising the bunch charge by a factor of two, and increasing the repetition rate up to three times, which raises the average beam current by a factor 6 to about 0.06 mA (this type of CLIC upgrade is described in [8]. This ultimate CLIC main beam current is still a factor 100 below the LHeC target. On the other hand, the CLIC drive beam would have a sufficiently high current, namely 30 mA, but at the low energy 2.37 GeV, which would not be useful for high-energy *ep* physics. Due to this low energy, also the drive beam power is still a factor of 5 smaller than the one required by LHeC. Finally, the ILC design current is about 0.04 mA [9], which also falls short of the goal by more than a factor 100.

Fortunately, SC linacs can provide higher average current, e.g. by increasing the linac duty factor 10 – 100 times, or even running in continuous wave (CW) mode, at lower accelerating gradient. Example average currents for a few proposed designs illustrate this point: the CERN High-Power Superconducting Proton Linac aims at about 1.5 mA average current (with 50 Hz pulse rate) [10], the Cornell ERL design at 100 mA (cw) [11], and the eRHIC ERL at about 50 mA average current at 20 GeV beam energy (cw) [12]. All these designs are close to, or exceed, the LHeC requirements for average beam current and average beam power (6.4 mA at 60 GeV). It is worth noting that the JLAB UV/IR 4th Generation Light Source FEL is routinely operating with 10 mA average current (135 pC pulses at 75 MHz) [13]. The 10-mA current limit in the JLAB FEL arises from well understood bream break up [14] and significantly larger currents would be possible with suitably designed cavities. It is, therefore, believed that more than 6.4 mA would be feasible for the LHeC ERL.

The target LHeC IP electron-beam power is 384 MW. With a standard wall-plug-power to RF conversion efficiency around 50%, this would imply about 800 MW electrical power, far more than available. This highlights the need for energy recovery where the energy of the spent beam, after collision, is recuperated by returning the beam 180^{o} out of phase through the same RF structure that had earlier been used for its acceleration, again with several recirculations.

An energy recovery efficiency η_{ER} reduces the electrical power required for RF power generation at a given beam current by a factor $(1-\eta_{ER})$. An efficiency η_{ER} above 90% is needed to reach the LHeC linac-ring beam-current goal of 6.4 mA with less than 100 MW total electrical power.

The above arguments have given birth to the LHeC Energy Recovery Linac high-luminosity baseline design.

4.8.2.3 *Choice of RF Frequency*

Two candidate RF frequencies exist for the SC linac. One possibility is operating at the ILC and XFEL RF frequency around 1.3 GHz, the other choosing a frequency of about 720 MHz, close to the RF frequencies of the CERN High-Power SPL, eRHIC, and the European Spallation Source (ESS).

The ILC frequency would have the advantage of synergy with the XFEL infrastructure, of profiting from the high gradients reached with ILC accelerating cavities, and of smaller structure size, which could reduce the amount of high-purity niobium needed by a factor 2 to 4.

Despite these advantages, the present LHeC baseline frequency is 720 MHz, or, more precisely, 721 MHz to be compatible with the LHC bunch spacing.

The arguments in favor of this lower frequency are the following:

- A frequency of 721 MHz requires less cryo-power (about two times less than at 1.3 GHz according to BCS theory; the exact difference will depend on the residual resistance [15]).
- The lower frequency will facilitate the design and operation of high-power couplers [16], though the couplers might not be critical [17].
- The smaller number of cells per module (of similar length) at lower RF frequency is preferred with regard to trapped modes [18].
- The lower-frequency structures reduce beam-loading effects and transverse wake fields.
- The project can benefit from synergy with SPL, eRHIC and ESS.
- Other projects, e.g. low-emittance ERL light sources, can reduce the bunch charge by choosing a higher RF frequency. This is not the case for the LHeC, where the bunch distance is not determined by the RF frequency, but by the distance between proton bunches.

The 721 MHz parameters can be derived from eRHIC [19]. In case the cavity material costs at 721 MHz would turn out to be a major concern, they could be reduced by applying niobium as a thin film on a copper substrate, rather than using bulk niobium. Establishing the necessary cavity performance with thin-film coating will require further R&D. It is expected that the thin-film technology may also enhance the intrinsic cavity properties, e.g. increase the Q_0 value.

4.8.2.4 *ERL Electrical Site Power*

The cryopower for two 10-GeV accelerating SC linacs is 22 MW, assuming 28 W/m heat load at 1.8 K for 20 MV/m cavity gradient and 700 “W per W” cryo efficiency as for the ILC. The RF electrical power needed to compensate synchrotron radiation losses (12 MW SR power) and to control microphonics is estimated at about 68 MW [20], with an RF generation efficiency of 50%. In addition, with an injection energy of 500 MeV and 6.4 mA beam current, the electron injector consumes about 6 MW. A further 4 MW is budgeted for the recirculation-arc magnets [21].Together this gives a grand total of 100 MW electrical power for the electron branch of the LHeC.

4.8.2.5 *ERL Configuration*

The ERL configuration is depicted in Fig. 4. The shape, arc radius and number of passes have been optimized with respect to construction cost and with respect to synchrotron-radiation effects [22].

The ERL is of racetrack shape. A 500-MeV electron bunch coming from the injector is accelerated in each of the two 10-GeV SC linacs during three revolutions, after which it has obtained an energy of 60 GeV. The 60-GeV beam is focused and collided with the proton beam. It is then bent by 180^o in the highest-energy arc beam line before it is sent back through the first linac, at a decelerating RF phase. After three revolutions with deceleration, re-converting the energy stored in the beam to RF energy, the beam energy is back at its original value of 500 MeV, and the beam is now disposed in a low-power 3.2-MW beam dump. A second, smaller (tune-up) dump could be installed behind the first linac.

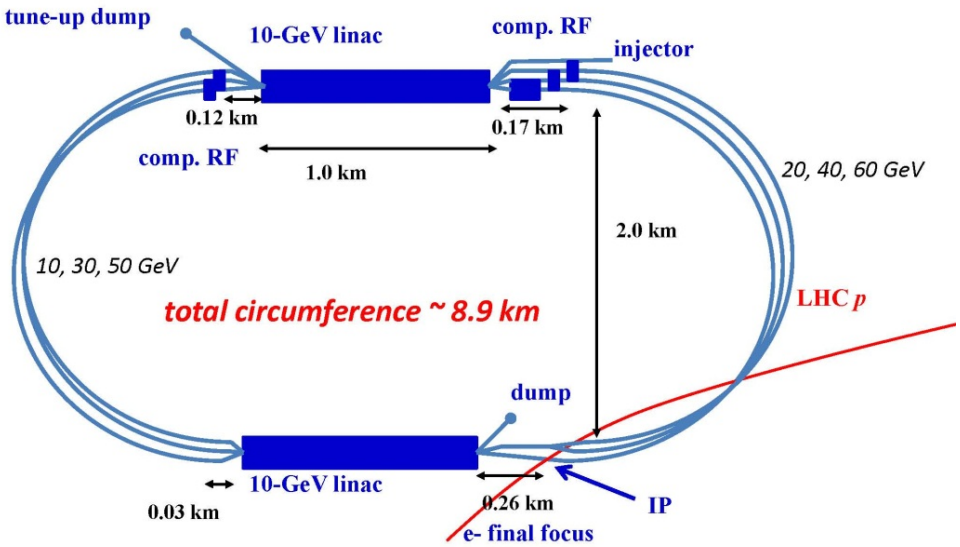

Figure 4: LHeC ERL layout including dimensions.

Strictly speaking, with an injection energy into the first linac of 0.5 GeV, the energy gain in the two accelerating linacs need not be 10 GeV each, but about 9.92 GeV, in order to reach 60 GeV after three passages through each linac. Considering a rough value of 10 GeV means that we overestimate the electrical power required by about 1%.

Each arc contains three separate beam lines at energies of 10, 30 and 50 GeV on one side, and 20, 40 and 60 GeV on the other. Except for the highest energy level of 60 GeV, at which there is only one beam, in each of the other arc beam lines there always co-exist a decelerating and an accelerating beam. The effective arc radius of curvature is 1 km, with a dipole bending radius of 764 m [23].

The two straight sections accommodate the 1-km long SC accelerating linacs. In addition to the 1-km linac section, there is an additional space of 290 m in each straight section of the racetrack. In one straight of the racetrack 260 m of this additional length is allocated for the electron final focus (plus matching and splitting), the residual 30 m on the other side of the same straight allows for combining the beam and matching the optics into the arc. In the second straight section of the racetrack the additional length of the straight sections houses the additional linacs for compensating the 1.88 GeV energy loss in the return arcs [24]. For the highest energy, 60 GeV, there is a single beam and the compensating RF (750 MV) can have the same frequency, 721 MHz, as in the main linac [24]. For the other energies, a higher harmonic RF system, e.g. at 1.442 GHz, can compensate the energy loss for both decelerating and accelerating beams, which are 180^{o} out of phase at 721 MHz. On one side of the second straight one must compensate a total energy loss of about 907 MeV per particle (=750+148+9 MeV, corresponding to the energy loss at 60, 40 and 20 GeV, respectively), which should easily fit within a length of 170 m. On the other side of the same straight one has to compensate 409 MeV (=362+47 MeV, corresponding to SR energy losses at 50 and 30 GeV), for which plenty of free space, with a length of 120 m, is available.

The total circumference of the ERL racetrack is chosen as 8.9 km, equal to one third of the LHC circumference. This choice has the advantage that one could introduce ion-clearing gaps in the electron beam which would match each other on successive revolutions (e.g. for efficient ion clearing in the linacs that are shared by six different

parts of the beam) and which would also always coincide with the same proton bunch locations in the LHC, so that in the latter a given proton beam would either always collide or never collide with the electrons [25]. Ion clearing may be necessary to suppress ion-driven beam instabilities. The proposed implementation scheme would remove ions while minimizing the proton emittance growth which could otherwise arise when encountering collisions only on some of the turns. In addition, this arrangement could be exploited for tailoring the electron bunch pattern so as to match the one of the protons (i.e. with gaps of variable size between successive bunch trains), potentially increasing the luminosity by up to a factor 3564/2808~1.27 at constant electron beam current (3564 is 1/10th of the harmonic number, i.e. the maximum number of LHC proton bunch places with 25 ns spacing; and 2808 the nominal number of proton bunches per beam). Alternatively, or in addition, the scheme allows for some non-colliding proton bunches, which could be useful for investigating the proton emittance growth induced by the electron beam (if any).

The length of individual components is as follows. In the optics design the exact length of the 10-GeV linac is 1008 m, the individual cavity length is taken to be 1 m, the optics consists of 56-m long FODO cells with 32 cavities, the number of cavities per linac is 576, and the linac cavity filling factor is 57%. The RF specialists assume slightly different numbers: cavity length 1.06 m, FODO cell length 66 m, 480 cavities per linac, and a cavity filling factor of 15% (requiring a cavity gradient of 20 MV/m instead of 18 MV/m) [26]. The effective arc bending radius is set to be 1000 m. The bending radius of the dipole magnets is 764 m, corresponding to a dipole filling factor of 76.4% in the arcs. The longest SR compensation linac has a length of 84 m (replacing the energy lost by SR at 60 GeV). Combiners and splitters between straights and arcs require about 20–30 m space each. The electron final focus may have a length of 200–230 m.

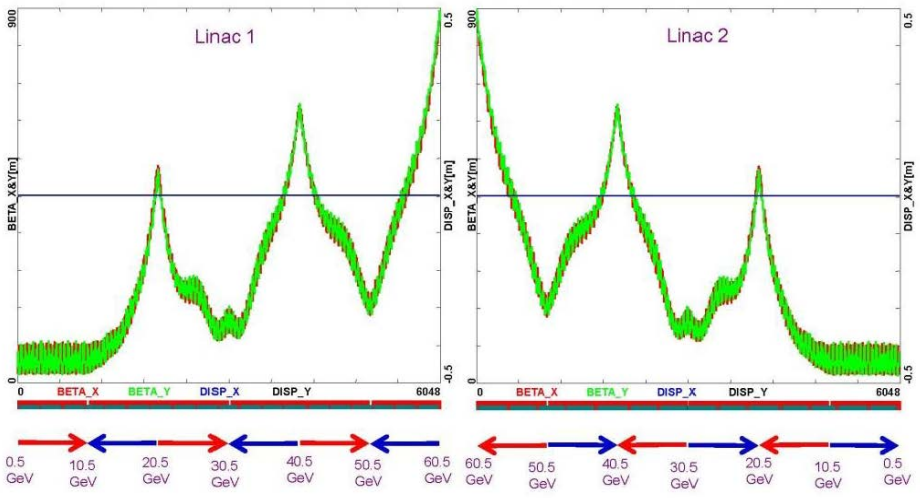

Figure 5: Optics for the two linacs of the LHeC ERL [27] (courtesy A. Bogacz). The two linacs are symmetric and the optics was chosen to minimize the integral of β/E.

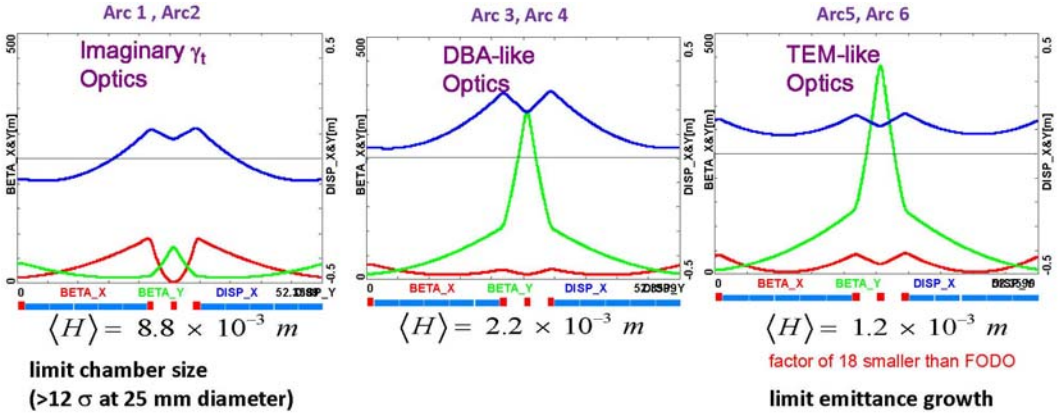

Figure 6: ERL arc optics [27] (courtesy A. Bogacz). The flexible momentum compaction cell; tuned for small beam size in the low-energy arcs and for low emittance growth from synchrotron radiation at high energy.

Figure 5 illustrates the optics for the two linacs [26], and Fig. 6 shows the optics for the return arcs [27]. Details of the optics design and ERL beam dynamics issues, such as transverse beam break up and ion instabilities, are discussed in the LHeC Conceptual Design Report [28].

4.8.2.6 *IP Parameters and Beam-Beam Effects*

Table 1 presents interaction-point (IP) parameters for the proton and electron beams.

Table 1: IP beam parameters for the LHeC ERL-Ring collider.

	protons	electrons
beam energy [GeV]	7000	60
Lorentz factor γ	7460	117400
transverse normalized emittance $\gamma\varepsilon_{x,y}$ [μm]	3.75	50
transverse geometric emittance $\varepsilon_{x,y}$ [mm]	0.50	0.43
IP beta function $\beta^*_{x,y}$ [m]	0.10	0.12
rms IP beam size $\sigma^*_{x,y}$ [μm]	7	7
initial IP rms beam divergence $\sigma'^*_{x,y}$ [μm]	70	58
beam current [mA]	>430	6.4
bunch spacing [ns]	25 or 50	(25 or) 50
bunch population [10^{10}]	17	(0.1 or) 0.2
rms bunch length [mm]	75.5	0.3 or 0.6
beam-beam tune shift ΔQ_p	+0.0001	N/A
hourglass factor H_{hg}	0.91	
disruption enhancement factor H_D	~1.3	
ep luminosity [10^{32} cm^{-2}s^{-1}]	~10	

Due to the low charge of the electron bunch, the proton head-on beam-beam tune shift is tiny, namely ΔQ_p=+0.0001, which amounts to only about 1% of the LHC *pp* design tune shift (and is of opposite sign). Therefore, the proton-beam tune spread

induced by the *ep* collisions is negligible. In fact, the electron beam acts like an electron lens and could conceivably increase the *pp* tune shift and luminosity, albeit by about 1% only. Long-range beam-beam effects are equally insignificant for both electrons and protons, since the detector-integrated dipoles separate the electron and proton bunches by about $36\sigma_p$ at the first parasitic encounter, 3.75 m away from the IP.

One further item to be looked at is the proton beam emittance growth. Past attempts at directly simulating the emittance growth from *ep* collisions were dominated by numerical noise from the finite number of macroparticles and could only set an upper bound [28], nevertheless indicating that the proton emittance growth due to the pinching electron beam might be acceptable for centered collisions. Proton emittance growth due to electron-beam position jitter and simultaneous *pp* collisions is another potential concern. For a 1σ offset between the electron and proton orbit at the IP, the proton bunch receives a deflection of about 10 nrad (approximately $10^{-4}\sigma_{x',y'}^{*}$). Beam-beam simulations for LHC *pp* collisions have determined the acceptable level for random white-noise dipole excitation as $\Delta x/\sigma_x<0.1\%$ [29]. This translates into a very relaxed electron-beam random orbit jitter tolerance of more than 1σ. The tolerance on the orbit jitter will then not be set by beam-beam effects, but by the luminosity loss resulting from off-center collisions, which, without disruption, scales as $\exp[-\Delta x^2/(4\sigma_{x,y}^{*2})]$. The random orbit jitter observed at the SLAC SLC had been of order $0.3 – 0.5\ \sigma$ [30,31]. A 0.1σ offset at LHeC would reduce the luminosity by at most 0.3%, a 0.3σ offset by 2.2%. Disruption further relaxes the tolerance.

A much stronger beam-beam effect is encountered by the electron beam, which is heavily disrupted. The electron disruption parameter is $D_{x,y}= N_{b,p}r_e\sigma_{z,p}/(\gamma_e\sigma^{*2})\sim6$, and the "nominal disruption angle" $\theta_0=D\sigma^{*}/\sigma_{z,p}$ [32] is about 600 μrad (roughly $10\sigma_{x',y'}^{*}$), which is huge. Simulations show that (1) the actual maximum angle of the disrupted electrons is less than half θ_0, (2) due to head-on collision with a "strong" proton bunch, the intrinsic emittance grows by only about 15%, and (3) there is an additional 180% optical mismatch. Therefore, without any adjustment of the extraction line optics to the parameters of the disrupted beam the emittance growth would be about 200%. This would still be acceptable since the arc and linac physical apertures have been determined assuming up to 300% emittance growth for the decelerating beam [23,27]. However, if the optics of the extraction line is rematched for the colliding electron beam (corresponding to an effective β_e^{*} of about 3 cm rather than the nominal 12 cm, the net emittance growth can be much reduced, to about 20%.

4.8.3 **Polarization**

The electron beam can be produced from a polarized DC gun with about 90% polarization, and with, conservatively, 10–50 μm normalized emittance [33]. Spin-manipulation tools and measures for preserving polarization, like Wien filter and/or spin rotators [34], and polarimeters are included in the optics design of the injector, the final focus, and the extraction line.

As for the positrons, up to about 60% polarization can be achieved either with an undulator or with a positron source based on Compton scattering (e.g. again with an ERL). However, the primary challenge for positrons is to produce them at all, in sufficient numbers and with a small enough emittance.

4.8.4 **Pulsed Linacs**

For beam energies above about 140 GeV, due to the growing impact of synchrotron radiation, the construction of a single straight linac is cheaper than that of a recirculating linac [22]. This linac could be either of ILC type (1.3 GHz RF frequency) or operate at 721 MHz, like the preferred ERL version. This type of linac would be extendable to ever higher beam energies and could conceivably later become part of a linear collider. In its basic, simplest and conventional version no energy recovery is possible for this configuration, since it is impossible to bend the 140-GeV beam around. The lack of energy recovery leads to significantly lower luminosity. For example, with 10 Hz repetition rate, 5 ms pulse length (longer than ILC), a geometric reduction factor H_{hg}=0.94 and $N_{b,e}$=1.5x10^9 per bunch, the average electron current would be 0.27 mA and the luminosity 4x10^{31} cm^{-2}s^{-1}.The construction of the 140-GeV pulsed straight linac could be staged, e.g. so as to first feature a pulsed linac at 60 GeV, which could also be used for γ–p/A collisions.

The linac length decreases directly in proportion to the beam energy. For example, at 140-GeV the pulsed linac measures 7.9 km, while at 60 GeV its length would be 3.4 km. For a given constant wall-plug power, of 100 MW, both the average electron current and the luminosity scale roughly inversely with the beam energy. At 60 GeV the average electron current becomes 0.63 mA and the pulsed-linac luminosity, without any energy recovery, would be close to 10^{32} cm^{-2}s^{-1}.

The simple straight linac layout can be expanded by decelerating the electron beam after collision in a second linac [35]. By transferring the RF energy back to the first accelerating linac, with the help of multiple, e.g. 15, 10-GeV "energy-transfer beams," a novel type of energy recovery is realized without bending of the spent beam. With two straight linacs facing each other this configuration could easily be converted into a linear collider, or vice versa, pending on geometrical and geographical constraints of the LHC site. As there are negligible synchrotron-radiation losses the energy recovery could be more efficient than in the case of the 60-GeV recirculating linac. Such novel form of ERL could push the LHeC luminosity to the 10^{35} cm^{-2}s^{-1} level [35]. In addition, it offers ample synergy with the CLIC two-beam technology.

4.8.5 ***γ-p/A Option***

In case of a (pulsed) linac without energy recovery the electron beam can be converted into a high-energy photon beam, by backscattering off a laser pulse. The rms laser spot size at the conversion point should be similar to the size of the electron beam at this location, that is σ_γ~10 mm. With a laser wavelength around λ_γ~250 nm ($E_{\gamma,0}$~ 5eV), as obtained e.g. from a Nd:YAG laser with frequency quadrupling, the Compton-scattering parameter x [36,37] is close to the optimum value 4.8 for an electron energy of 60 GeV (for x>4.8 high-energy photons get lost due to the creation of e^+e^- pairs). The maximum energy of the Compton scattered photons is larger than 80% of the initial electron-beam energy, for the chosen LHeC parameters. The cross section and photon spectra depend on the longitudinal electron polarization and on the circular laser polarization. With proper orientation the photon spectrum is concentrated near the highest energy.

The laser pulse energy corresponding to a conversion efficiency of 65%, is estimated as about 16 J. To set this into perspective, for a γγ collider at the ILC, Ref. [38] considered a pulse energy of 9 J at a four times longer wavelength of $\lambda_\gamma \sim 1$ μm.

The energies of the leftover electrons after conversion extend from about 10 to 60 GeV. This spent electron beam, with its enormous energy spread, must be safely extracted from the interaction region. The detector-integrated dipole magnets will assist in this process. They will also move the scattered electrons away from the interaction point. A beam dump for the high-energy photons should also be installed, behind the downstream quadrupole channel.

The much larger interaction-point spot size and the lower electron beam energy at the LHeC compared with γγ collisions at a linear collider allow placing the conversion point at a much greater distance, ~0.1 m, from the interaction point, which could simplify the integration in the detector, and is also necessary, since otherwise, with e.g. a mm-distance between CP and IP, the conversion would take place inside the proton bunch.

To achieve the required laser pulse energy, external pulses can be stacked in a recirculating optical cavity. For an electron bunch spacing of, e.g, 200 ns, the path length of the recirculation could be 60 m.

4.8.6 **Summary of LHeC Linac-Ring Parameters and Configurations**

The baseline 60-GeV ERL-ring option for the LHeC can provide an *ep* luminosity of 10^{33} $cm^{-2}s^{-1}$, at about 100 MW total electrical power for the electron branch of the collider, and with less than 9 km circumference. The 21 GV of SC-RF installation represents its main hardware component.

A pulsed 140-GeV linac, without energy recovery, could achieve a luminosity of 1.4×10^{31} $cm^{-2}s^{-1}$, at higher c.m. energy, again with 100 MW electrical power, and shorter than 9 km in length. The pulsed linac can accommodate a γ-*p/A* option. An advanced, novel type of energy recovery, proposed for the case of a single straight high-energy linac, includes a second decelerating linac, and multiple 10-GeV "energy-transfer beams". This type of collider could reach luminosities of 10^{35} $cm^{-2}s^{-1}$.

High polarization is possible for all linac-ring options. Beam-beam effects are benign, especially for the proton beam, which should not be affected by the presence of the (extremely weak) electron beam.

Producing the required number of positrons needed for high-luminosity proton-positron collisions is the main open challenge for a linac-ring LHeC. Recovery of the positrons together with their energy, as well as fast transverse cooling schemes, are likely to be essential ingredients for any linac-based high-luminosity *ep* collider involving positrons. As an example, Fig. 7 shows a 3-ring scheme which transforms a cw beam into a pulsed beam, which could be cooled (in the center ring) and then converts the cold positron beam back into a cw beam.

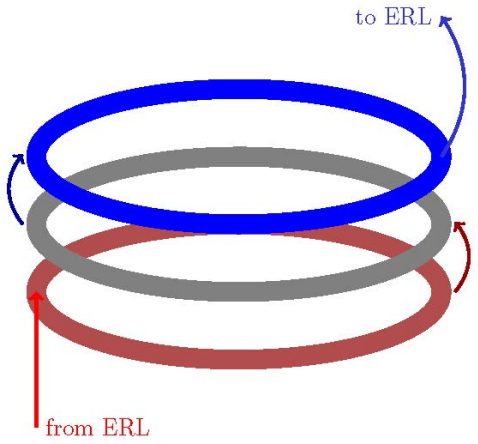

Figure 7: Tri-ring scheme for positron recycling and cooling, cw→pulse converter (red), cooling ring (grey), and pulse→cw transformer (blue) [39] (courtesy E. Bulyak).

4.8.7 References

1. P. Grosse-Wiesmann, Colliding a Linear Electron Beam with a Storage Ring Beam, NIM A 274 (1989) 21.
2. F. Ruggiero and F. Zimmermann, Luminosity Optimization near the Beam-Beam Limit by Increasing Bunch Length or Crossing Angle, PRST-AB 5 (2002) 061101.
3. F. Zimmermann et al, Linac-LHC ep Collider Options, Proc. EPAC'08 Genoa (2008) 2847.
4. D. Schulte, LHeC Ring-Linac Lattice and Beam Dynamics, 3rd CERN-ECFA-NuPECC LHeC Workshop Chavannes-de-Bogis, December 2010.
5. F. Zimmermann, K.A. Thompson, K.A. and R.H. Helm, Electron-Electron Luminosity in the Next Linear Collider, Int.J.Mod.Phys. A 13 (1998) 2443.
6. J. Abelleira, N. Bernard, S. Russenschuck, R. Tomas, F. Zimmermann, Design Status of the LHeC Ling-Ring Interaction Region, Proc. IPAC'11 San Sebastian (2011) 2796.
7. H. Braun, et al, CLIC 2008 Parameters, CLIC-Note-764 (2008).
8. H. Aksakal, A.K. Ciftci, Z. Nergiz, D. Schulte, and F. Zimmermann, Conversion efficiency and luminosity for gamma proton colliders based on the LHC-CLIC or LHC-ILC QCD Explorer scheme, NIM A 576 (2007) 287.
9. N. Phinney, N. Toge, and N. Walker, LC Reference Design Report Volume 3 – Accelerator (2007) eprint 0712.2361 arXiv physics.acc-ph.
10. F. Gerigk et al, Conceptual Design of the SPL II, CERN-2006-006 (2006).
11. C.E. Mayes and G.H. Hoffstaetter, Cornell Energy Recovery Linac Lattice and Layout, Proc.~IPAC'10 Kyoto (2010).
12. V. Litvinenko, Future Electron-Hadron Colliders, Proc. IPAC'10 Kyoto (2010).
13. G.R. Neil, Free Electron Lasers from THz to X-rays, Invited Talk at UPHUK4, Bodrum, Turkey, 30 August 2010.
14. C. Tennant, et al, Experimental Investigation of Beam Breakup in the Jefferson Laboratory 10 kW FEL Upgrade Driver, Proc. PAC2005 Knoxville.
15. T. Linnecar, and J. Tückmantel, private communication, 28 May 2008.
16. P. Napoly, private communication, 6th EuCARD Steering Meeting, Malta, 12 –13 October 2010.
17. E. Ciapala, RF for the LHeC, 3rd CERN-ECFA-NuPECC LHeC Workshop Chavannes-de-Bogis, December 2010.
18. J. Tückmantel, comment at 2nd RFTech meeting, PSI, Villigen, 2 –3 December 2010.
19. V. Litvinenko, and I. Ben-Zvi, private communications, 2010.

20. E. Jensen, SC Cavities R&D for LHeC and HE-LHC, LHC Performance workshop Chamonix'12.
21. D. Tommasini, RR+RL Magnets, 3rd CERN-ECFA-NuPECC LHeC Workshop Chavannes-de-Bogis, December 2010.
22. J. Skrabacz, Optimizing Cost and Minimizing Energy Loss in the Recirculating Race-Track Design of the LHeC Electron Linac, CERN-AB-Note-2008-043 (2008).
23. A. Bogacz, LHeC Recirculator with Energy Recovery – Beam Optics Choices, JLAB-TN-10-040 (2010).
24. D. Schulte and F. Zimmermann, private discussions, 2010.
25. D. Schulte, private communication, 2010.
26. LHeC Study Group, A Large Hadron Electron Collider at CERN, CERN-OPEN-2012-015, arXiv:1206.2913, submitted to J.Phys.G (2012).
27. A. Bogacz, I. Shin, D Schulte, F. Zimmermann, LHeC ERL Design and Beam-Dyanmics Issues, Proc. IPAC'11 San Sebastian (2011) 1120.
28. D. Schulte and F. Zimmermann, QCD Explorer Based on LHC and CLIC-1, Proc. EPAC'04, Lucerne, and CERN-AB-2004-079.
29. K. Ohmi, R. Calaga, W. Hofle, R. Tomas, R. and F. Zimmermann, Beam-Beam Effects with External Noise in LHC, Proc.~PAC07, Albuquerque (2007) 1496.
30. F. Zimmermann et al, First Bunch Length Studies in the SLC South Final Focus, Proc. EPAC 1998 Stockholm (1998) 487.
31. C. Adolphsen et al, Pulse-to-Pulse Stability Issues at the SLC, Proc. IEEE PAC 1995 Dallas.
32. P. Chen and K. Yokoya, Disruption Effects from the Interaction of Round e+e- Beams, Phys.Rev.D 38 (1988) 987.
33. M. Yamamoto and M. Kuwahara, Superlattice Photocathode Development for Low Emittance, Photocathode Physics for Photoinjectors Workshop, BNL, October 2010.
34. M. Bai, Spin Rotator, at the 4th CERN-ECFA-NuPEC LHeC workshop held at Chavannes de Bogis, Switzerland, 14-15 June 2012.
35. V. Litvinenko, Recirculating Linac, 2nd CERN-ECFA-NuPECC workshop on LHeC, Divonne-les-Bains, 2009.
36. I. Ginzburg, G. Kotkin, V. Serbo, and V. Telnov, Colliding ge and gg Beams Based on the Single Pass Accelerators (of VLEPP Type), Nucl.Instr.&Meth. 205 (1983) 47.
37. H. Burkhardt and V. Telnov, CLIC 3-TeV Photon Collider Options, CERN-SL-2002-013-AP, CLIC-Note-508 (2002).
38. G. Klemz, K. Mönig, and I. Will, Design Study of an Optical Cavity for a Future Photon-Collider at ILC, NIM A 564 (2006) 212.
39. F. Zimmermann et al, Positron Options for the Linac-Ring LHeC, Proc. IPAC'12 New Orleans.

4.9 Overview of Existing ERLs

Chris Tennant and David Douglas, Jefferson Lab, U.S.A.
Mail to: tennant@jlab.org

4.9.1 Introduction

An increasing number of scientific applications require intense electron beams of superior quality (extremely small 6-dimensional phase space), for the investigation of fundamental processes as well as the generation of highly coherent, high average brightness photon beams. These applications include high average power free electron lasers (FELs), synchrotron light sources, Terahertz and Compton sources as well as

electron cooling devices and electron-ion colliders for nuclear and particle physics research. Traditionally the demands for beams with these characteristics have been met by either storage rings or (energy-recovering) electrostatic accelerators. Over the years, rings have been performing at increasingly high quality; however, the ultimate performance of such systems is limited by the fact that electrons are stored for many turns in an equilibrium state. The equilibrium between radiation damping and quantum excitation sets a fundamental limit on the minimum emittance and bunch length that can be achieved. Pelletron/van der Graff based systems have been utilized with similar success but can be limited in beam quality and are generally useful only in low-energy applications.

In contrast, the RF linear accelerator (linac) – another traditional architecture – can deliver beams with very small emittance, energy spread, and very short bunch length, as these properties are established by phenomena in the low-energy electron source and can be well preserved during acceleration to high energy. However, linacs are limited to accelerating small amounts of average beam current due to the prohibitively expensive radio-frequency (RF) power required. An energy recovering linac (ERL) is a powerful alternative accelerator concept which combines the desirable characteristics of both storage rings and linacs, with the potential to accelerate hundreds of milliamperes of average current to several giga-electron volts in energy while maintaining excellent beam quality [1].

Electrons are generated in a high brightness injector, accelerated through a linac and then transported to a region where the desired interaction occurs (e.g. radiation generated in an undulator or a wiggler, interacting with an ion beam in a cooling channel, etc…). After performing their intended purpose, the electrons are returned to the linac 180° out of phase with respect to the RF accelerating field for energy recovery. At the exit of the linac, the energy of the decelerated beam is approximately equal to the injection energy and the beam is directed to a beam dump. It is in this way that the decelerated beam cancels the beam loading effects of the accelerated beam, allowing ERLs to accelerate high average currents using only modest amounts of RF power.

Furthermore, since the electron beam only exists in the accelerator for a short time (typically two passes, though more are possible), the equilibrium that is unavoidable in a storage ring does not have time to develop. Thus the beam quality in an ERL is determined, to a large extent, by the injector. Another advantage of ERLs results from the fact that the beam is dumped at low energy. The beam dump design is simplified because the energy of the beam is reduced by a factor of (E_{max}/E_{inj}) where E_{max} is the energy of the beam before energy recovery and E_{inj} is the injection energy.

4.9.2 **Challenges in ERLs**

Energy recovery linacs are not without their own set of challenges. In the following sections a brief discussion of some of the most relevant is given. These include collective effects, such as space charge, the multipass beam breakup (BBU) instability, and coherent synchrotron radiation, as well as beam dynamic and transport issues such as halo, and the interaction of the beam with the RF system and other environmental impedances.

4.9.2.1 *Space Charge*

While many ERLs achieve high beam power through modest bunch charge and high repetition rate, the role of space charge forces (both transverse and longitudinal) often dictates many operational aspects the machine. Maintaining beam brightness during the low energy injection stage is vitally important. In addition to the low energy, ERL injectors must also preserve beam quality through the merger system that directs the beam to the linac axis. Once injected into the linac, the beam energy at the front end is often still low enough that space charge forces cannot be neglected. Just as important is the longitudinal space charge (LSC) force which manifests itself by an energy spread asymmetry about the linac on-crest phase [2]. The LSC wakes acts to accelerate the head of the bunch while decelerating the tail. Operating on the rising part of the waveform leads to a decrease in the correlated energy spread, while accelerating on the falling side leads to an increase. These observations inform where acceleration, and how the longitudinal match, is performed.

4.9.2.2 *Beam Breakup Instability*

The beam breakup (BBU) instability is initiated when a beam bunch passes through an RF cavity off-axis, thereby exciting dipole higher-order modes (HOMs). The magnetic field of an excited mode deflects following bunches traveling through the cavity. Depending on the details of the machine optics, the deflection produced by the mode can translate into a transverse displacement at the cavity after recirculation. The recirculated beam induces, in turn, an HOM voltage which depends on the magnitude and direction of the beam displacement. Thus, the recirculated beam completes a feedback loop which can become unstable if the average beam current exceeds the threshold for stability.

Beam breakup is of particular concern in the design of high average current ERLs utilizing superconducting RF (SRF) technology. If not sufficiently damped by the HOM couplers, dipole modes with quality factors several orders of magnitude higher than in normal conducting cavities can exist, providing a threat for BBU to develop.

A thorough suite of measurements to characterize the BBU instability and successfully benchmark data with existing simulation codes was performed at the Jefferson Lab IR Upgrade Driver [3,4,5]. Using this information, and through clever beam optical suppression techniques, BBU is no longer an operational impediment. For high average current operations, the IR Upgrade utilizes five skew-quadrupoles to interchange the horizontal and vertical phase spaces, thereby effectively breaking the feedback loop between the beam and the offending HOM.

4.9.2.3 *Coherent Synchrotron Radiation*

Like linac-driven FELs, ERL-based light sources also suffer from the effects of CSR. This is not surprising since both system architectures require transporting a short bunch through a dipole, giving rise to coherent radiation and its attendant effects on the beam (i.e. phase space distortion, emittance growth, beam mismatch to the downstream lattice). However, while CSR is customarily associated with light sources, low energy and low energy spread beams typical of ERL-based electron cooler designs, are also susceptible [6].

Thus far CSR has not proved to be an operational impediment for ERLs. In fact it is often used as a diagnostic to tune up the longitudinal match. The bunch length is

properly compressed for the FEL when CSR begins to "turn on" [2,7]. At the Jefferson Lab FEL systems beam filamentation was, and is, evident when the bunch becomes strongly compressed. Initial beam-based measurements to characterize CSR have been taken, however due to the complexity of the longitudinal phase space it becomes difficult to distinguish the contributions from LSC, CSR and other environmental wakes.

4.9.2.4 *Halo*

Halo is defined as the relatively diffuse and potentially irregularly distributed components of beam phase that can reach large amplitudes. It is of concern because ERL beams are manifestly non-Gaussian and can have beam components of significant intensity beyond the beam core [8].

Though sampling large amplitudes, halo responds to the external focusing of the accelerator transport system in a predictable manner. It is therefore not always at large spatial amplitude, but will at some locations instead be small in size but strongly divergent. Halo can therefore present itself as "hot spots" in a beam distribution, and thus may be thought of as a lower-intensity, co-propagating beam that is mismatched to the core beam focusing, timing, and energy.

Numerous sources contribute to the halo in a high-brightness/high power accelerator. Operational experience at various laboratories suggest that the biggest culprits are: stray light striking the photocathode, photocathode emission effects, field emission/dark current from the gun, beam dynamics during beam formation/evolution, and field emission/dark current in SRF cavities.

4.9.2.5 *RF Transients*

Dynamic loading due to incomplete energy recovery is an issue for all ERLs [9]. In some machines it is due to unintentional errors imposed on the energy recovered beam; for instance, path length errors in large-scale light sources. In other machines, such as high power ERL-based FEL drivers, it is done intentionally. In cases where there is the potential for rapid changes in the relative phase of the energy recovered beam, dynamic loading would be difficult to completely control using fast tuners. In such cases adequate headroom in the RF power will have to be designed into the system.

Take as an example an ERL-driven FEL. In addition to increasing the energy spread, the FEL process leads to a decrease of the central energy of the bunch as energy is transferred from the electron beam to the optical beam. This reduction in energy couples to the nonzero momentum compaction (M_{56}) of the recirculator lattice to generate a change in the path length (or equivalently, a phase shift). Thus the RF system must deal with a phase shift of several degrees as the laser turns on and off. Because the phase shifts occur on the timescale of the laser turn on/off, even piezo-tuners cannot tune the cavities fast enough. During this time sufficient RF power must be delivered to maintain the gradient in the cavities at a level consistent with the available energy aperture of the machine. The absence of sufficient RF overhead will lead to beam loss and an eventual machine trip.

4.9.2.6 *Wakefields and Interaction of Beam With Environment*

As with other system architectures intended to handle high-brightness beams, ERLs can be performance limited by wakefield effects. Not only can beam quality be

compromised by interaction of the beam with environmental impedances, there is also significant potential for localized power deposition in beamline components. Resistive wall and RF heating have proven problematic during the operation of the Jefferson Lab IR Upgrade Driver ERL [10]; extrapolation of this experience to higher bunch charges and beam powers leads to serious concern regarding heating effects. Careful analysis and management of system component impedances is required.

4.9.2.7 *Magnet Field Quality*

In as much as they rely on the generation of specific phase-energy correlations in order to bunch and/or energy recover the beam, ERL transport systems are essentially time-of-flight spectrometers. As a consequence, they generally require magnets with spectrometer-grade field quality to avoid performance limitations during energy recovery. The underlying concern stems from the effect of a localized magnetic field error on the beam [11]. Such an error can differentially deflect a portion of a bunch relative to both its nominal trajectory and that of the rest of the charge distribution. The resulting betatron oscillation generates a path length differential – and thus a phase error – which translates into an evolving energy error during energy recovery. Potentially fatal beam loss can be a consequence if the resulting energy spread exceeds the acceptance of the linac back end.

This effect scales with the size and energy of the system; larger, higher-energy systems are more sensitive. An intuitive scale is set by the Jefferson Lab ERLs, where the FEL drivers (with ~100 MeV full energy) use a specified relative field flatness of order 10^{-4}. There is, moreover, some suspicion that system behaviour in the 1 GeV CEBAF-ER experiment (discussed below) was consistent with this concern: though successfully operated at 80 μA when recovering beam to 56 MeV, only 1 μA could be recovered to 20 MeV. The energy spread of the recovered beam could have been due in part to limited field quality in the transport system dipoles, and was relatively larger (due to additional adiabatic antidamping) at the lower final energy, thereby exceeding the dump transport line acceptance.

4.9.3 **Historical Overview of ERLs**

It is important to note that ERLs are not a mature technology in the same way as, for example, storage rings are. Rings have been successfully operated at laboratories throughout the world, reliably over the course of many decades. Conversely, the cumulative beam time of all the ERLs that have ever been in operation pales in comparison to that of rings. Therefore in order to provide proper context for the discussion of currently operating ERLs, a brief historical overview of their development is given; many of which were simply “demonstration” experiments.

The first demonstration of energy recovery occurred at Chalk River Nuclear Laboratories in 1977 using a two-pass reflexotron which passes the beam through an accelerating structure and is returned through the structure in the opposite direction by a 180° reflecting magnet [12]. By changing the distance of the reflecting magnet from the accelerating structure, the phase of the beam relative to the accelerating field can be made to generate either energy doubling or energy deceleration and recovery. Using this method, output energies between 5 MeV (with energy recovery) and 25 MeV (with energy doubling) were achieved. In 1985 a 400 MeV electron beam was energy recovered to 23 MeV at the MIT-Bates Linac as part of an experiment to operate the

recirculation system under a variety of conditions [13]. In 1986, Stanford University's Superconducting Accelerator (SCA) energy recovered 150 μA of average beam current from 55 MeV to 5 MeV [14]. This experiment was significant in that it marked the first time energy recovery had been demonstrated in a superconducting RF environment. At about the same time, the free electron laser at Los Alamos National Laboratory demonstrated energy recovery in a unique configuration where the decelerated beam deposited energy in a different cavity from which it was accelerated [15]. This scheme represents a departure from the previous examples of “same-cell" energy recovery. Using this setup, they successfully energy recovered 21 MeV to 5 MeV. Despite its success, this method of energy recovery has not been used since. More recently, in 2002 the JAERI ERL-driven FEL achieved first light [16]. This prototype machine successfully recovered 8 mA from 17 MeV to 2.5 MeV.

4.9.3.1 *Early ERLs at Jefferson Lab*

For nearly two decades, the implementation of energy recovery has been most active at Jefferson Laboratory. Over the course of 16 years, from 1993 to 2009, same-cell energy recovery was successfully demonstrated in five different accelerators. Combining the principle of energy recovery with SRF cavities leads to an accelerator capable of generating an intense beam with excellent beam qualities in an efficient and economical manner. Initial experience with SRF cavities, however, presented formidable challenges. In the early 1970s, when Stanford University began operation of the SCA, multipactoring in the SRF cavities severely limited the gradients and consequently the final beam energy. To overcome this obstacle, transport elements were installed to recirculate the beam multiple times through the linac. When the beam was recirculated, insufficiently damped HOMs caused beam breakup, thereby limiting the achievable average beam current. Thus, despite the great potential of SRF cavities, the first ERL to implement SRF technology was limited in beam energy (due to multipactoring) and average beam current (due to BBU).

When in 1985 it was proposed to build a 4 GeV electron accelerator for nuclear physics based on SRF technology at Jefferson Laboratory, a great effort was made to address the issues of implementing SRF technology on a large scale [17]. By this time Cornell University had designed a cavity using an elliptical cell shape which all but eliminated multipactoring. And while the Cornell cavity exhibited greater HOM damping than the cavities used in the SCA, much was done to address the potential problem of multipass, multibunch BBU. During the initial construction of the Continuous Electron Beam Accelerator Facility (CEBAF), the injector linac was used in conjunction with a single recirculation line to experimentally investigate the problem of BBU [18,19]. The injector was capable of providing over 200 μA of average beam current. Beam was injected into the linac at 5.5 MeV and accelerated to 43 MeV by two cryomodules. Next, the beam was recirculated and sent through the linac for a second pass where it could either be accelerated to 80 MeV or the recirculator could be configured for energy recovery in which the beam was decelerated to 5.5 MeV. In neither operating scenario were there indications of BBU developing.

Even before the construction of CEBAF was complete, a proposal was put forward to use it as a driver for an FEL [20]. In addition to the ability of an SRF linac to maintain superior beam quality, the ability for cw operation opened up the possibility of achieving high average output power while using bunches of modest charge. It had been recognized that invoking energy recovery would increase the system efficiency while at

the same time reducing the need for expensive, high power RF sources. An initial design for an ERL-based driver for an FEL at Jefferson Laboratory was developed in 1991 [21]. This design was significant in that it marked the first time energy recovery was implemented as the nominal mode of operation. By 1998 the Jefferson Laboratory IR FEL Demo successfully energy recovered 5 mA of average beam current through a single cryomodule from 48 MeV to the injection energy of 10 MeV [22]. By the end of 2001, as the IR Demo was being decommissioned to prepare for an upgrade, the machine had operated at, or exceeded, design parameters. As a result of the IR FEL Demo's demonstrated success, the attractive features of an SRF linac with energy recovery became apparent. Applications of ERLs were extended to synchrotron radiation sources, electron cooling and electron-ion colliders. Many of these applications require a significant extrapolation of the operating parameters achieved at the FEL, such as beam energy and current.

In 2001, a proposal was put forward to non-invasively test energy recovery on a large scale using CEBAF [23]. Because it is a recirculating linac, operating CEBAF with energy recovery requires only minor modifications; namely the installation of a magnetic chicane – to provide a half-RF wavelength delay – and a beam dump. In 2003, 80 μA of average beam current was successfully energy recovered from 1056 MeV to the injection energy of 56 MeV [24]. The experiment demonstrated that large scale energy recovery – through 312 SRF cavities and transported through 1.3 km of beamline – is feasible. One of the important issues that the CEBAF-ER experiment addressed is that the beam quality could be preserved in a common transport channel (in the presence of steering and focusing errors) over a large dynamic range of energy. During the experiment, maximum-to-injector energy ratios (E_{max}/E_{inj}) of 19:1 and 51:1 were demonstrated by operating with two different injector energies. For comparison, in the IR FEL Demo this ratio was 5:1. The CEBAF-ER experiment was, and is, important because it represents the first attempt to bridge the gap between the existing lower energy (order 100 MeV), compact (up to 3 cryomodules), SRF-based ERLs and the proposed large-scale ERL drivers.

Currently there are four ERLs operating in the world, all of which are used to drive an FEL. A brief summary of each, highlighting design architecture choices, is given in the sections below.

4.9.4 **Jefferson Lab IR Upgrade**

The most mature ERL, in terms of operational experience, is the Jefferson Lab IR Upgrade which began beam operations in 2003. The facility has served as an invaluable testbed to study, among other items, each of the challenges outlined previously [2,10].

The FEL Upgrade Driver is an energy recovery based linear accelerator used to condition an electron beam for high average power lasing in the IR. Electrons are generated in a DC photocathode gun, accelerated to 9 MeV and injected into the linac where they are further accelerated up to 135 MeV through three cryomodules (each containing 8 superconducting niobium cavities). The beam is transported to an undulator where in excess of 14 kW of laser power has been generated. Because the SRF linac supports cw beam, high average laser power can be achieved with a high bunch repetition rate and only modest single bunch charge. The spent electron beam is recirculated and phased in such a way that the beam is decelerated through the linac on the second pass. A schematic of the Driver is shown in Fig. 1.

Reduced to its primary objective, the ERL driver must generate a short bunch (high peak current) at the undulator and energy compress and energy recover the large longitudinal phase space of the spent electron beam following the undulator [11,25]. The injector is designed to generate a long bunch with low momentum spread. Acceleration through the linac occurs off-crest so as to impart a phase-energy correlation across the bunch. The first- and second-order momentum compactions of the first Bates-style recirculation arc are set to rotate the bunch upright at the wiggler and to eliminate phase space curvature, producing a short bunch and high peak current. Following the undulator, the longitudinal phase space must be rotated back by 90° to energy compress the beam which has acquired a large momentum spread from the FEL interaction. The energy recovery transport consists of a second Bates-style endloop. Trim quadrupoles, sextupoles, and octupoles in the arc adjust momentum compactions through third order to longitudinally rotate the short, very large momentum spread bunch and adjust its curvature and torsion in preparation for energy recovery. Because energy recovery occurs off-trough, the imposed phase-energy correlations are selected to generate energy compression during energy recovery, yielding a long (of order 30^{o} at the RF fundamental), low momentum spread bunch at the dump. All apertures in the energy recovery loop are chosen to allow very large energy spread to be transported without loss to the energy recovery dump. Operational experience with the IR Upgrade shows the Bates endloop to be a very robust design; at least 12% (full) energy spread beam has been transported cleanly to the end-of-line dump.

4.9.5 **Jefferson Lab UV Demo**

The UV driver ERL shares the linac and the recirculator endloops with the IR Upgrade driver. It is, however, a distinct system with respect to operating parameters and beam handling configuration. For UV operation, the corner dipoles of the IR transport operate at half their IR field, halving the bend angle at the end (beginning) of the IR delivery (recovery) arc. The reduction in angle directs beam toward the UV wiggler; the bend onto (off of) the axis of the optical cavity is completed achromatically through use of a FODO-focusing transport managing dispersion, controlling beam envelopes, and allowing chromatic correction with sextupoles.

As the UV system shares Bates arcs with the IR, the longitudinal match is both robust and flexible. This process has three unique features. First, compression is performed using arc momentum compactions; there is no compressor chicane. This allows, secondly, full compression with acceleration on either side of crest of the RF waveform; operation is not restricted to the rising side. Thirdly, linearization of RF curvature effects is performed with the transport system sextupoles (and, for energy compression required for lossless recovery, using octupoles as well); harmonic RF is neither used nor needed [26].

A recent experiment demonstrated that equally good lasing performance could be achieved while operating on the falling side of the RF waveform. This feat is possible only because the UV does not have a compressor chicane. Furthermore, the experiment has shown that it is not only possible, but even desirable from a beam physics standpoint, to accelerate on the falling part of the RF waveform and compress using a positive momentum compaction (M_{56}) [27].

Collective effects differ in character from those in the IR ERL. Lower bunch charge (60 pC compared to 135 pC for IR operation) alleviates space charge effects –

improving beam brightness and reduces average current – mitigating instabilities and interaction of the beam with the environment. Thus, for example, adequate control of BBU is maintained by choice of pass-to-pass phase advance, in contrast to use in the IR ERL of a horizontal/vertical phase space exchange.

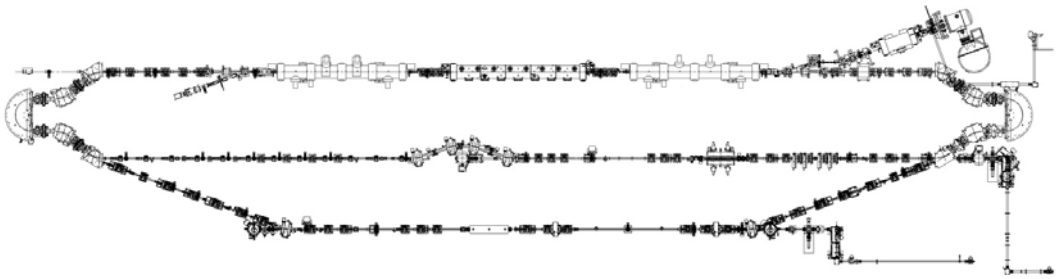

Figure 1: The Jefferson Lab IR and UV FEL. The SRF linac (top), IR FEL transport line (middle) and UV FEL transport line (bottom) are shown. Note the absence of a compressor chicane in the UV line.

4.9.6 **Daresbury ALICE**

The ALICE (Accelerators and Lasers In Combined Experiments) facility, based at Daresbury Laboratory, is the first ERL in Europe. Initially conceived as a prototype for the 4GLS project, ALICE has evolved into a robust and multifunctional facility servicing a wide range of projects. In addition to serving as a valuable testbed for accelerator physics, ALICE is an IR FEL, a THz radiation source with application to the life sciences, and is the injector for EMMA, a non-scaling FFAG (fixed-field alternating gradient) accelerator [28].

A schematic of the ALICE facility is shown in Fig. 2. Electrons are generated from a DC photocathode gun, accelerated to 6.5 MeV in a booster and injected into the SRF linac where they are further accelerated to 26 MeV. The recirculation arcs are triple bend achromats (TBA). Mounting the arcs on translation stages provides a means of path length control. Embedded sextupoles are used to linearize the bunch longitudinally and counteract the curvature imposed by the RF waveform during acceleration. Following the first arc – which is tuned to be isochronous – the beam enters a 4-dipole chicane which compresses the bunch for delivery to the undulator.

For IR FEL operation, the driver must generate a low momentum spread bunch with high peak current at the undulator. To that end, careful control and tuning of the longitudinal dynamics must be maintained. Due to site constraints, ALICE has a long injection line which exacerbates the effects of space charge and velocity bunching. These effects on the evolution of the beam dynamics have been the subject of recent studies [29]. With the recent installation of a new HV gun ceramic, the operating gun voltage has been increased from 230 kV to 325 kV. To achieve the required longitudinal manipulations, the bunch is accelerated 10° off-crest through the linac to induce a phase-energy correlation. No bunching occurs in the first arc, however the phase space is linearized using sextupoles thereby avoiding the need for a harmonic linearizer. The bunch compressor provides the required momentum compaction to rotate the longitudinal phase space upright at the undulator entrance.

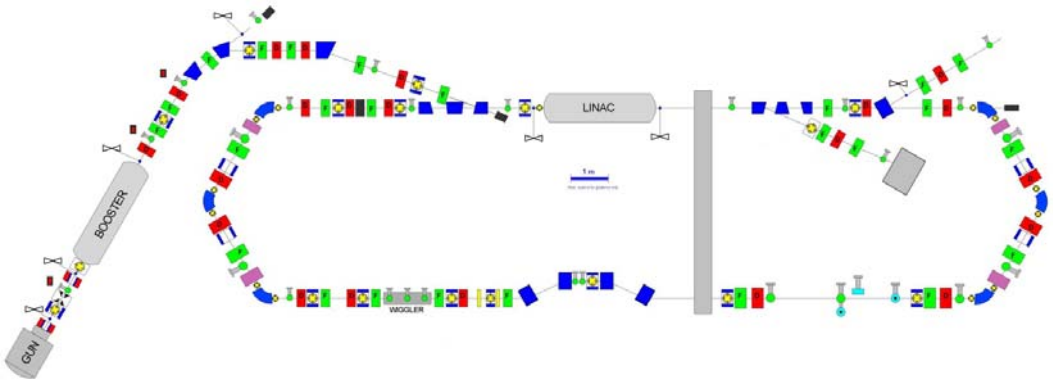

Figure 2: Schematic of the ALICE facility at Daresbury.

4.9.7 **Budker Institute FEL**

The Novosibirsk ERL driven FEL, at the Budker Institute of Nuclear Physics, represents a departure from other currently operating ERLs in many respects. Firstly, unlike the ERLs at the Jefferson and Daresbury Laboratories which are based on SRF systems that operate at 1497 MHz and 1300 MHz, respectively, the Novosibirsk machine uses low frequency (180 MHz), normal conducting RF. Secondly, rather than using a DC photocathode gun, the Novosibirsk machine uses a DC gun with a thermionic gridded cathode – ultimately giving them the distinction of generating and transporting the highest average current (30 mA) through an ERL [30]. Thirdly, limited to low repetition rates, in order to generate several tens of milliAmperes of current, Novosibirsk operates with 1.5 nC bunch charges. This is in contrast to the approach of the Jefferson Lab Driver, for instance, where high average current is obtained by using modest bunch charge (135 pC) and taking advantage of high repetition rates afforded by the use of an SRF system. Like the facility at Jefferson Lab, the Novosibirsk facility has multiple FELs which share a common linac. What makes the facility unique, however, is that in addition to one of the FELs being built out of plane of the other, it is the only operating multi-turn ERL (see Fig. 3). Recent highlights include 4-pass up (acceleration) and 4-pass down (deceleration) operation of the facility [31].

The Novosibirsk FEL is a THz radiation source with 7 user workstations. The injector provides 2 MeV electron bunches to the linac which are accelerated to 11 MeV. One might expect that with 1.5 nC bunches at 2 MeV space charge would destroy the beam quality, however, the bunch length is kept relatively long (1.1 ns from the gun, 100 ps at the FEL) which reduces the charge density thereby mitigating its effects.

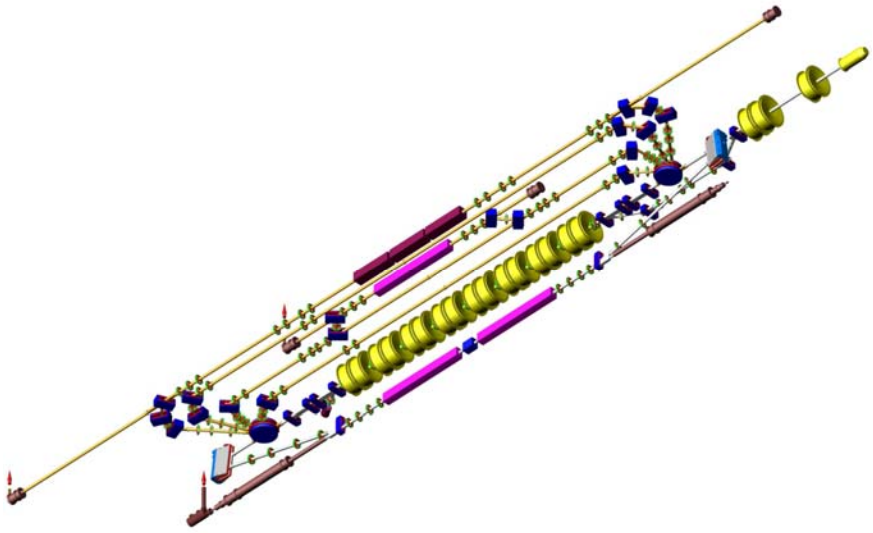

Figure 3: Layout of the Novosibirsk facility, showing the multi-orbit configuration of the machine.

4.9.8 **Summary**

Table 1 summarizes relevant beam parameters of the ERLs discussed in previous sections and represents, to the best of the authors' knowledge, a complete listing of ERL operations to date. While tremendous progress has been made in ERL development, there is still much to learn. Several ERL test facilities are expected to be operational within a few years and will be able to probe new regions of parameter space.

Table 1: Parameters of ERLs, past (italicized) and present.

	E (MeV)	I_{ave} (mA)	Q_b (pC)	ε_N (μm)	Rep. (MHz)	Duty (%)
Chalk River	*25*	*30*	*10*	*50*	*3000*	*0.1*
MIT Bates	*400*	*10*	*3.5*	*10*	*2856*	*1*
HEPL	*48*	*0.6*	*50*	*10*	*11.8*	*pulsed*
LANL	*21*	*0.2*	*8000*	*50*	*1300*	*pulsed*
CEBAF-FET	*45*	*0.3*	*0.2*	*5*	*1497*	*100*
JLab IR Demo	*20-50*	*5*	*60*	*10*	*75*	*100*
CEBAF-ER	*1050*	*0.08*	*0.2*	*1*	*500*	*100*
JAERI	*17*	*8*	*400*	*40*	*20.8*	*pulsed*
BINP	22	30	2000	30	22.5	100
JLab IR Upgrade	165	9	135	10	75	100
ALICE	27.5	8.125	100	1.2	81.25	0.1
JLab UV Demo	135	2.5	60	5	37.5	100

4.9.9 **Acknowledgements**

The authors gratefully acknowledge the help of Yuri Saveliev (Daresbury), Nikolay Vinokurov (BINP), and Bruce Carlsten (LANL) in gathering material for this paper.

4.9.10 References

1. L. Merminga, D. Douglas, G. Krafft, Annu. Rev. Nucl. Part. Sci. **53**, 387 (2003).
2. C. Tennant in *Proceedings of the Particle Accelerator Conference, Vancouver, BC, 2009* (IEEE, Piscataway, NJ, 2009), pp. 3125-3129.
3. C. Tennant, Ph.D. thesis, College of William and Mary (2006).
4. C. Tennant et al., Phys. Rev. ST Accel. Beams **8**, 074403 (2005).
5. D. Douglas et al., Phys. Rev. ST Accel. Beams **9**, 064403 (2006).
6. C. Tennant and D. Douglas, Technical Note 12-027, Jefferson Laboratory (2012).
7. F. Jackson et al., to appear in *Proceedings of the Particle Accelerator Conference, New Orleans, LA,* (2012).
8. D. Douglas et al., Technical Note 12-017, Jefferson Laboratory (2012).
9. T. Powers and C. Tennant, in *Proceedings of the 41st Advanced ICFA Beam Dynamics Workshop on ERLs, Daresbury Laboratory, UK*, pp. 75-79 (2007).
10. S. Benson et al., in *Proceedings of the Particle Accelerator Conference, Albuquerque, NM, 2007 (IEEE, Piscataway, NJ, 2007),* pp. 79-81.
11. D. Douglas, in *Proceedings of the 14th Beam Instrumentation Workshop, Santa Fe, NM,* pp. 506-515 (2010).
12. S. Schriber et al., in *Proceedings of the Particle Accelerator Conference, Chicago, IL, 1977 (IEEE, Piscataway, NJ, 1977),* pp. 1061-1063.
13. J. Flanz and C. Sargent, in *Proceedings of the Particle Accelerator Conference, Vancouver, British Columbia, 1985 (IEEE, Piscataway, NJ, 1985),* pp. 3213-3215.
14. T. Smith et al., Nucl. Instrum. Methods A **259**, 1 (1987).
15. D. Feldman et al., in *Proceedings of the Particle Accelerator Conference, Washington, DC, 1987 (IEEE, Piscataway, NJ, 1987),* pp. 221-223.
16. N. Nishimori et al., in *Proceedings of the Free Electron Laser Conference, Berlin, Germany,* pp. 265-272 (2006).
17. Report Project 87-R-203, Continuous Electron Beam Accelerator Facility (1985).
18. N. Sereno et al., in *Proceedings of the Particle Accelerator Conference, Washington, DC, 1993 (IEEE, Piscataway, NJ, 1993),* pp. 3246-3248.
19. N. Sereno, Ph.D. thesis, University of Illinois at Urbana-Champaign (1994).
20. G. Krafft and J. Bisognano, in *Proceedings of the Particle Accelerator Conference, Chicago, IL, 1989 (IEEE, Piscataway, NJ, 1989),* pp. 1256-1258.
21. D. Douglas, Technical Note 91-017, Jefferson Laboratory (1991).
22. G. Neil et al., Phys. Rev. Lett. **84** (2000).
23. D. Douglas, Technical Note 01-018, Jefferson Laboratory (2001).
24. C. Tennant et al., in *Proceedings of the 11th Workshop on RF Superconductivity, Travemunde, Germany* (2003).
25. P. Piot et al., Phys. Rev. ST Accel. Beams **6**, 030702 (2003).
26. D. Douglas et al., to appear in *Proceedings of the International Particle Accelerator Conference, New Orleans, LA* (2012).
27. D. Douglas et al., Invention Disclosure (2012).
28. F. Jackson et al., to appear in *Proceedings of the Particle Accelerator Conference, New Orleans, LA,* (2012).
29. Y. Saveliev et al., to appear in *Proceedings of the Particle Accelerator Conference, New Orleans, LA,* (2012).
30. N. Vinokurov et al., in *Proceedings of the Russian Particle Accelerator Conference, Protvino, Russia,* pp. 133-135 (2010).
31. N. Vinokurov, Private communication (2012).

4.10 Status of the Cornell ERL

Christopher Mayes for the Cornell ERL Team, CLASSE, Cornell Univ., U.S.A.
Mail to: christopher.mayes@cornell.edu

4.10.1 **Introduction**

In 1999 Cornell began exploring the possibility of building a hard x-ray ERL lightsource, and in 2001, with Thomas Jefferson National Laboratory, produced a detailed study of key research and development needed to assess practical feasibility of such a machine [1]. In 2005 the NSF began support for developing essential ERL technologies, including support for a prototype ERL injector and superconducting RF (SRF) cavity development [2, 3]. In addition, Cornell University and the State of New York have supported research towards a site-specific facility on the Ithaca NY campus.

This research has resulted in the recently completed Cornell ERL Project Definition Design Report (PDDR), which describes a full-scale hard x-ray ERL facility operating at 5 GeV, and uses the Cornell University site as an example [4]. It contains the motivation and history for such a facility, detailed simulations and designs of all major accelerator components, describes novel experiments utilizing the x-ray beamlines, and outlines the designs and studies for the supporting civil construction. It is complemented by a proposal for the construction of electron beamline components, a design for a new x-ray science building, two proposals for the cryogenic plant, a tunnel design and review, an economic impact study, and a draft environmental impact study.

This article gives a brief overview of the Cornell ERL (henceforth referred to as the ERL) layout, parameters for three planned operating modes, and a survey of beam dynamics issues. It concludes with highlights from the ERL research and development program.

4.10.2 **Layout**

The development of an ERL at Cornell presents unique opportunities, because Cornell has significant infrastructure and an existing 5 GeV particle accelerator. Therefore, the ERL makes as much use as possible of the existing facilities at the Wilson Synchrotron Laboratory, which include CESR, the CHESS G-line beamline, and the Wilson Lab building. Because the CESR components were designed to sustain 8 GeV electrons, this section can comprise part of the 5 GeV return arc of the ERL.

The location of Wilson Lab lies on a hillside between the Cornell campus and Cascadilla creek. The CESR tunnel is approximately 15 m below the athletic field to the north of this hillside. This terrain is used in the ERL design by having the accelerator housed mostly in an underground tunnel, while the x-ray beamline section is located outside the hill where a new x-ray science building is to be located.

Figure 1: Cornell ERL layout with section labels in black disks. Circled numbers indicate undulators and their corresponding x-ray beamlines. The existing Wilson Lab will house undulators 7-9, while a new x-ray science building will house the remaining eleven undulators, as well as the injector an extracted beamline (EX). The Linac sections LA and LB and turnaround arc TA and TB will occupy a single tunnel.

The ERL design on the campus map is shown in Fig. 1. The layout is divided into nine discrete sections roughly in accordance with their function: The injector (IN) delivers a 15 MeV beam into Linac A (LA), which accelerates the beam to 2.7 GeV. This beam feeds into Turnaround A (TA), which bends it around to connect to Linac B (LB). The beam is accelerated through LB to 5 GeV into the South Arc (SA) containing nine undulators, which connects to part of CESR (CE), which connects to the North Arc (NA) containing five more undulators as well as bunch compression and decompression sections. Now at about 4995 MeV (accounting for synchrotron radiation losses), the NA is merged back into LA, which decelerates the beam to 2.3 GeV, recovering 2.7 GeV. A demerging dipole separates this beam from the 2.7 GeV accelerating beam into TB. Thereafter a merging dipole combines this decelerating beam with the accelerating beam from TA and directs it into LB, where it is decelerated to 10 MeV, recovering 2.3 GeV. Finally the beam is sent to the Beam Stop (BS).

The ERL Linacs will consist of 64 identical cryomodule cells: 35 in LA and 29 in LB. Each cryomodule contains six SRF accelerating cavities and a superconducting-magnet package with a quadrupole and two steering coils, along with other elements, e.g. higher-order mode (HOM) absorbers, gate valves, and beam position monitors. Each cavity will provide an average accelerating gradient of about 16.1 MeV/m, and each cryomodule can give or take about 78 MeV from the beam. They are cooled by a new cryoplant on the surface above the tunnel.

Taking advantage of the curved hillside to the east of Wilson Lab, the SA and the NA sections are shaped to conform to the terrain. The curvature is suitable for housing 70 m long x-ray beamlines with large experimental hutches, and beamlines from both arcs are housed in a single new x-ray science building. Space has been allotted for three x-ray beamlines in Wilson lab, including the existing G-line and one from a new 25 m long undulator. The new building alone will contain up to eleven beamlines. The ERL design accommodates a total of three 25 m undulators and eleven 5 m undulators.

Table 1: Parameters for different operating modes of the Cornell ERL. SA and NA denote insertion devices in the South Arc and North Arc, respectively.

Parameter	*Mode A High Flux*	*Mode B High Coherence*	*Mode C Short Bunch*	*Unit*
Energy	5	5	5	GeV
Current	100	25	25	mA
Bunch Charge	77	19	19	pC
Repetition Rate	1.3	1.3	1.3	GHz
Horizontal Emittance (SA/NA)	31/52	13/34	21/66	pm
Vertical Emittance (SA/NA)	25/26	10/10	14/14	pm
Bunch duration (SA/NA)	2.1/2.1	1.5/1.6	1.0/0.1	ps
Relative energy spread (SA/NA)	1.9/1.9	0.9/1.0	9.1/9.3	10^{-4}

4.10.3 **Parameters**

Table 1 lists three representative operating modes for the ERL: (A) high-flux mode with full bunch charge providing 100 mA of beam current, (B) high-coherence mode with enhanced emittance at a reduced bunch charge, and (C) short-pulse mode with l00 fs duration bunches in the NA section with reduced bunch charge. All modes will operate at 5 GeV full energy and a 1.3 GHz repetition rate. Because of the flexible lattice, each insertion device can have its own customized optics.

The emittances, bunch duration, and relative energy spread numbers in Tab. 1 represent results from start-to-end simulations that incorporate space charge, incoherent and coherent synchrotron radiation (ISR and CSR), alignment and field errors, and orbit correction. A distinction is made between beam properties in the SA and NA undulators because Mode C provides 100 fs bunch durations only in the NA section, and all modes experience a relatively large amount of emittance growth due to ISR between these sections. The vertical emittance is well preserved from injection, despite the many field and alignment errors in the simulations.

Simultaneous with any of these modes, there will be a fast kicker at the beginning of the SA section that can pluck bunches with up to 1 nC of charge at a rate of $\leq$ 10 kHz to send to the EX section without energy recovery. The EX section provides a chicane bunch compressor and space for a novel insertion device, such as an XFEL-O. The geometric emittances for a 1 nC bunch in this beamline are simulated to be 2300 pm in the horizontal direction and 33 pm in the vertical direction, with a rms bunch duration of 100 fs and a relative energy spread of 0.2%.

4.10.4 **Beam Dynamics**

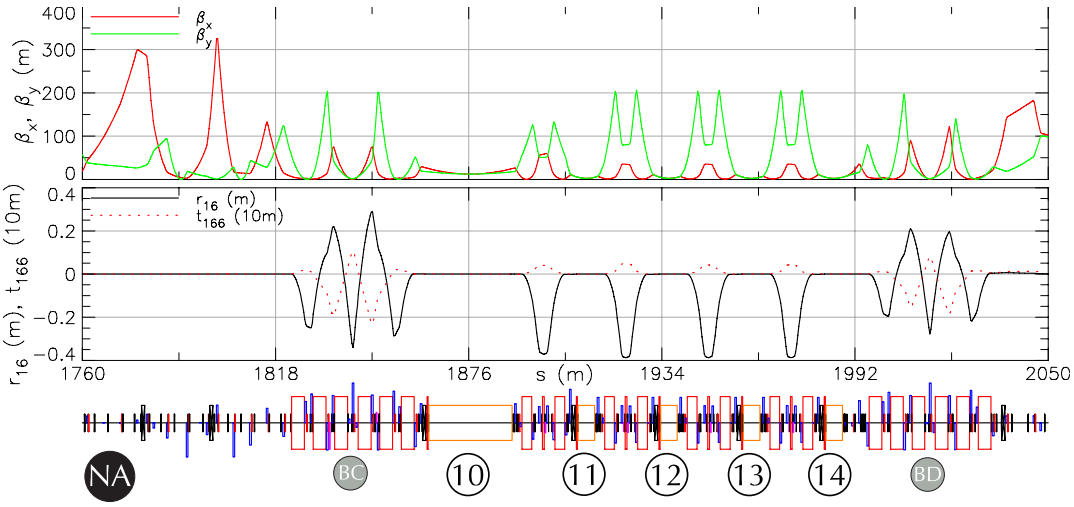

Figure 2: Beta functions and first- and second-order dispersion for the entire NA section for Mode A in Table 1. BC and BD denote bunch compression and decompression sections.

4.10.4.1 ***Lattice and Optics***

The lattice in the ERL is primarily designed and simulated using the Bmad software library and its companion optimization program Tao [5]. The first-order optics are designed to simultaneously control the accelerating and decelerating beams in the LA and LB sections, manipulate time-of-flight terms in the arc sections, and provide customized beam sizes in the insertion devices. They are additionally optimized to limit emittance growth from incoherent synchrotron radiation. Sextupole magnets are strategically placed to manipulate first and second order time-of-flight terms relevant for bunch compression and energy recovery, as well as second order geometric terms. For the bunch compression mode, the optics is tuned to limit the detrimental effects of CSR.

As an example, Fig. 2 shows the NA optics for Mode A in Tab. 1. This is a non-compression mode, so the bunch compression and decompression sections optics are tuned for zero first- and second-order time-of-flight terms in undulators 10-14. The arcs between each of the undulators are achromatic and isochronous by employing a reverse bending magnet. The vertical beta function is tuned to reduce the Touschek scattering rate described below.

4.10.4.2 ***Space Charge***

The effect of space charge on the emittances is primarily relevant in the low energy sections of the injector, and therefore the entire IN section together with its merger section and the first cryomodule of LA have been simulated using the space charge code GPT [6] and tuned via multi-objective optimization using a genetic algorithm [7]. Particles from these simulations are then tracked using Bmad.

4.10.4.3 *Orbit Correction and Tolerances*

The ERL lattice is designed assuming perfect alignment and field qualities of all components. Electron bunches injected with the design phase-space distributions will still experience some distortions due to, for example, ISR and geometric optical aberrations, but will do so in predictable ways. Unfortunately the actual machine built will not have such perfect qualities, and furthermore, many of the errors in this machine will not be known *ab initio*. Particles injected into this realistic machine should be kept near the design orbit, and to that end, a set of beam position monitors (BPMs) and orbit corrector coils are installed in the lattice. The Tao program is set up to simulate and automatically correct for particular errors, and with many simulations statistics on the resulting beam properties can be gathered [8].

4.10.4.4 *BBU*

The beam-breakup (BBU) instability can impose an upper current to any recirculative Linac [9]. We use a standalone BBU program built on Bmad libraries to calculate BBU thresholds in the ERL models, using realistic HOMs with random frequency spreads and construction errors, and gather their statistics. The most pessimistic simulations imply a 450 mA threshold current due to a realistic set of dipole HOMs, and we find that the threshold current limited by quadrupole HOMs is above 200 mA as long as the limiting quadrupole HOM Q factor is less than about half of the fundamental Q factor. These thresholds are increased when polarized cavities are employed, but these are not needed for our design 100 mA operation. Longitudinal BBU thresholds far exceed the design 100 mA of beam current [4].

4.10.4.5 *Touschek Scattering and Halo Collimation*

Even without alignment and field errors, the ERL will suffer losses from Touschek and rest-gas scattering. Touschek scattering is responsible for the vast majority of these losses. We use a standalone Touschek scattering program built on Bmad libraries that runs in parallel to scatter and track particles in the ERL model to their loss points, and we estimate their subsequent radiation using the Monte-Carlo code MCNPX [10]. To limit the losses due to these particles, the optics in the ERL are further optimized to reduce the Touschek scattering rate, and to create specified loss locations. Collimators are placed at these locations and designed to safely absorb their radiation [4].

4.10.5 **Ongoing ERL Research and Development**

The Cornell Laboratory for Accelerator-based Sciences and Education (CLASSE) continues to develop ERL technologies. Here are recent highlights from these efforts:

4.10.5.1 *Prototype Injector*

CLASSE operates a prototype ERL injector based on a DC photocathode electron gun and a 5 to 15 MeV SRF cryomodule with 500 kW installed RF power, both built in-house. It is designed to demonstrate the feasibility of the operating modes listed in Table 1.

In January 2012, the injector produced a CW current of 35 mA, beating the long-held record of 32 mA set at Boeing [11, 12]. In February 2012, 50 mA was achieved.

These new records were made possible partially by the reduction of beam halo near the gun, which causes excessive radiation and vacuum increase. The group is currently assembling a new DC gun with a segmented insulator that can operate at or above 500 kV, which should allow for lower emittances. See [13] for additional details.

4.10.5.2 *Photocathode Research and Preparation*

Cornell now has a dedicated cathode laboratory to prepare and characterize high quantum efficiency photocathodes for the prototype injector, and to understand photocathode physics. The lab recently designed and built an integrated vacuum system that reduces the need for a vacuum suitcase to one step: transportation from the chamber to the DC gun [14]. In October, Cornell will host a 3-day photocathode workshop [15].

4.10.5.3 *Superconducting RF*

The Cornell SRF group has built a prototype main linac 7-cell SRF cavity and a horizontal test cryomodule (HTC) to house it, and recently measured a fundamental Q factor of about 6×10^{10} at low voltages and 3.5×10^{10} at the operating voltage of 16 MV/m and the operating temperature of 1.8 K, significantly exceeding its design specifications. Three similar cavities will be built and tested by the fall of 2012. A prototype main linac cryomodule will be built in 2013 and RF testing is planned in 2014. See [16] for additional highlights.

4.10.5.4 *Delta Undulator*

Cornell has been developing the novel Delta undulator to take advantage of the narrow round beams of the ERL. In 2010 a 30 cm version of the Delta undulator was built at Cornell and tested with electron beam in the Accelerator Test Facility at Brookhaven National Laboratory [17]. In 2011, a 1 m long variant of the Delta undulator with only the upper and lower magnet arrays (CHESS Compact Undulator) has been built [18] and in the spring of 2012 tested for use in CHESS. At present, SLAC in collaboration with Cornell is working on 3.2 m long Delta type undulator to control the LCLS x-ray polarization state.

4.10.6 References

1. S. M. Gruner et al., “Study for a proposed Phase I Energy Recovery Linac (ERL) Synchrotron Light Source at Cornell University”, Technical report (2001).
2. Phase I Energy Recovery Linac (ERL) Synchrotron Light Source at Cornell University, NSF Award 0131508 (2005).
3. IMR: Phase Ib Energy Recovery Linac (ERL) Technology R&D, NSF Award 0807731 (2010).
4. G. S. Hoffstaetter, S. Gruner, M. Tigner, eds, “Cornell ERL Project Definition Design Report” http://erl.chess.cornell.edu/PDDR (2011).
5. D. Sagan, “Bmad Manual”, www.lns.cornell.edu/~dcs/bmad.
6. S. B. var der Greer and M. J. de Loos, GPT 2.8 www.pulsar.nl/gpt.
7. I. V. Bazarov and C. K. Sinclair, “Multivariate optimization of a high brightness dc gun photoinjector”, Phys. Rev. ST-AB **8** 034202 (2005).
8. C. E. Mayes, “Cornell ERL Tolerance Simulations”, Proceedings of PAC11, WEP067 (2011).
9. G. H. Hoffstaetter et al., “Recirculating Beam-Breakup Thresholds for Polarized

Higher-Order Modes with Optical Coupling, Phys Rev. ST-AB **10,** 044401 (2007).
10. X-5 Monte Carlo Team, "MCNP - A General N-Particle Transport Code, Version 5 - Volume I: Overview and Theory", LA-UR-03-1987, Los Alamos National Laboratory (2003).
11. G. H. Hoffstaetter, "Cornell sprints past milestones towards hard X-ray source", CERN Courier (March, 2012).
12. D. Dowell et al., "First operation of a photocathode radio frequency gun injector at high duty factor", Appl. Phys. Lett. **63**, 2035 (1993).
13. B. Dunham et al., Performance of the Cornell high-brightness, high-power electron injector, Proceedings of IPAC12, MOOAA01 (2012).
14. L. Cultrera et al., Photocathode R&D at Cornell University, Procceedings of IPAC12, WEOAB02 (2012).
15. Photocathode Physics for Photoinjectors (P3) www.lepp.cornell.edu/Events/Photocathode2012/ (October 8-10, 2012).
16. M. Liepe et al., "Progress on superconducting RF work for the Cornell ERL", IPAC12, WEPPC073 (2012).
17. A. Temnykh et al., "Delta Undulator Model: magnetic field and beam test results", Nuclear Inst. and Methods in Physics Research A **649** pp. 42-45 (2011).
18. A. Temnykh et al., "Compact PPM Undulator for Cornell High Energy Synchrotron Source", Proceedings of MT-22 (Magnetic Technology) Conference (2011).

4.11 B*ERL*inPro—addressing the challenges of modern ERLs (a status report)

J. Knobloch for the B*ERL*inPro Project Team[6], Helmholtz-Zentrum Berlin
Mail to: jens.knobloch@helmholtz-berlin.de

4.11.1 Introduction

4.11.1.1 *ERLs: Next-Generation Particle Accelerators*

Modern electron accelerators have extremely multifaceted applications, ranging from high-energy physics to synchrotron light sources for x-ray production to their use for medical treatments [1, 2]. While the beam parameters vary from application to application, it is fair to say that an increasing demand is evident for continuous-wave (CW), high-average-current, short-pulse (sub-ps) systems with beams of exceptional brilliance and low energy spread. Electron coolers for hadron colliders, electron-hadron colliders, Compton gamma-ray sources, as well as x-ray synchrotron light sources continue to push beam parameters to new limits. These are more than an order of magnitude beyond those achieved by storage-rings (SR), which already operate near their theoretical limit. Further improvements are difficult because the beam is in an equilibrium condition. This fact also restricts an SR's ability to address the demand for flexible beam manipulation.

To circumvent the limitations of SRs, one turns to linacs whose beam properties are, in theory, determined by the electron source and adiabatic damping during the

[6] M. Abo-Bakr, W. Anders, R. Barday, K. Bürkmann-Gehrlein, V. Dürr, S. Heßler, A. Jankowiak, T. Kamps, J. Knobloch, O. Kugeler, B. Kuske, P. Kuske, A. Matveenko, A. Meseck, G. Meyer, R. Müller, A. Neumann, K. Ott, Y. Petenev, D. Pflückhahn, T. Quast, J. Rahn, and S. Schubert.

acceleration. Importantly, since the beam is not in equilibrium its phase-space distribution can be rearranged by a variety of manipulation techniques. Linacs thus provide a great deal of flexibility and adjustability (and hence adaptability). But this concept places a heavy burden on the electron source, which must deliver a beam of high phase-space density and high average current at the outset.

The last requirement also points to one of the main challenges of linacs. Being single-pass devices, disposal of the beam at high energy demands a low average beam current to limit the operating power and safely dump the beam. For many applications (e.g., high-energy electron coolers, high-flux x-ray light sources) the average current is too low to merit the use of single-pass linacs.

Energy-recovery linacs (ERLs) hold the promise of circumventing this restriction. First proposed by Maury Tigner in 1965 [3], the scheme involves re-injecting the spent beam into the linac a second time, but phase shifted by 180°. The beam is now decelerated and its energy recouped by the cavities, where it remains available for acceleration of a fresh beam. The low-energy spent beam can then be dumped safely. An ERL does not store beam but it does store energy and hence it combines the efficiency (& high-current) advantage of SRs with the superb beam quality and flexibility of a linac.

While the concept of ERLs is not new, severe technological challenges have limited their construction so far. More recently, 10 to 100-MeV-class facilities (such as the Jefferson Laboratory ERL [4], JAERI ERL [5] and ALICE [6]) have demonstrated experimentally the soundness of the underlying concept. This has sparked many ideas for multi-user x-ray ERLs world-wide, including the Cornell ERL [7], KEK ERL [8], gamma-ray sources [9], as well as electron coolers [10] and electron-hadron colliders [11, 12]. All these concepts require beam parameters that are one to two orders of magnitude beyond those achieved with state-of-the-art ERLs. For these concepts to be viable, a number of technological and accelerator-physics advances are required.

4.11.1.2 *Technology and Accelerator-Physics Challenges*

Energy-efficiency considerations dictate that x-ray ERL facilities must be based on continuous-wave (CW) superconducting RF (SRF) technology. SRF systems can be designed with low higher-order mode (HOM) impedances, so that beam stability issues can also be effectively addressed. But the demands placed on the electron source, the SRF linac & beam transport, the cryogenics, and the diagnostics are severe because of the required extreme beam quality, high current and CW operation. Fortunately, much effort has been invested in developing SRF and photoinjector technology for non-ERL linacs such as CEBAF and, more recently, FLASH and the European XFEL. These projects have demonstrated the soundness of the overall technology and its *potential* for future ERL applications. What remains are the ERL-specific challenges:

- Reliable and stable generation of a low emittance, 100-mA-class CW beam.
- Preservation of the low emittance throughout the ERL.
- Stable recirculation of the beam without beam-breakup.
- Operation of SRF cavities at high average currents.
- Efficient energy recovery of the beam.
- Efficient SRF system operation to minimize refrigeration and RF power demands.
- Beam manipulation to provide flexible beam parameters.

- Reduction of electron beam loss to well below the 10^{-5} level so that radiation protection schemes commensurate with user facilities may be identified.

4.11.1.3 *Resolving the Challenges: BERLinPro*

To find solutions to these and other issues HZB has started an ERL-dedicated R&D program. Its goal is to address both the hardware and theoretical aspects of ERLs and to ready the concept for a broad range of applications. Some of the R&D areas can be treated separately. But the majority is intertwined and ultimately can only be analyzed and tested in an integrated demonstration facility. To this end, HZB is building a 50-MeV high-current ERL test facility (B*ERL*inPro = Berlin ERL Project) that can put the theory and all the subsystems relevant to large-scale ERLs to the test.

Submitted to the Helmholtz Association in 2008, the proposal was approved in Oct. 2010. B*ERL*inPro's layout as a single-pass ERL is shown in Figure 1. Its 6-MeV injection line consists of a 1.3-GHz SRF photoinjector and focusing solenoid followed by a three-cavity booster section. The beam is merged into the main linac via a dog-leg merger and accelerated by three 7-cell SRF cavities to 50 MeV. Following recirculation via a race track, the decelerated beam is dumped in a 600-kW 6-MeV beam dump. Room is provided in the return arc to install future experiments or insertion devices to demonstrate the potential of ERLs for user applications (not currently funded). Importantly, the layout of the accelerator building and shielding provides sufficient flexibility for a future upgrade to two-turn recirculation for energy doubling.

Since B*ERL*inPro's present role is a demonstration facility for accelerator R&D rather than being designed as a specific user facility, its parameter set should be considered flexible. Given HZB's background in operating synchrotron light sources, a set suitable for a future GeV-class x-ray light-source, as listed in Table 1, has been adopted as the "standard mode". However, the optics is flexible enough for exploration of a wide range of parameters, including short-pulse and low-energy-spread bunches.

Given the long-lead time in developing a high-current photoinjector, first experiments with an all-superconducting system (SRF cavity, superconducting cathode, superconducting solenoid) commenced in 2009. The focus continuous to be on the injector, and a new version that includes a normal-conducting cathode is currently being designed. In the meantime the ERL optics at the CDR-level has been developed so that building construction can begin. A staged installation of B*ERL*inPro, focused on 100-mA operation at 6 MeV will follow, before the full recirculator will be installed (2017).

4.11.2 **Beam Loss and Radiation Protection**

The minimization of beam loss will be one of the most challenging aspects of the B*ERL*inPro measurement program. This will provide invaluable insight into the feasibility of future user facilities, which must minimize the restrictions for personnel that arise from radiation protection. A storage-ring facility such as BESSY II has staggeringly low relative beam-loss rates of the order of 200 μC *per year* and is able to provide general access to the instrumentation hall. This needs to be contrasted with a *theoretically* sustainable beam loss of 600 μC *per second* in B*ERL*inPro! One goal of B*ERL*inPro will therefore be to explore means to detect lowest levels of beam loss and to develop schemes that guarantee losses of significantly less than 10^{-5}.

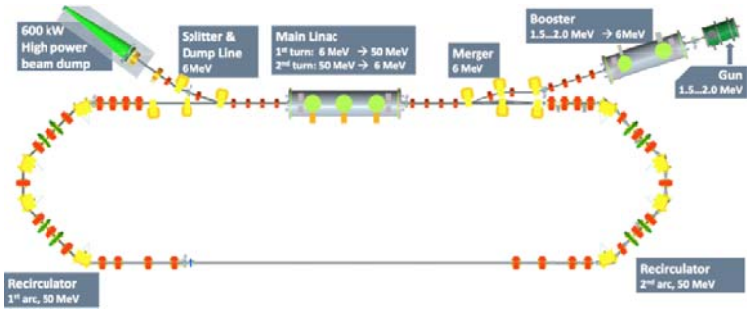

Figure 1: Schematic of B*ERL*inPro.

Table 1: Parameters adopted for the "basic mode" of BERLinPro

Parameter	***Value***	**Unit**
Beam energy	50	MeV
Beam current @ 1.3 GHz	100	mA
Bunch charge	77	pC
Bunch length	< 2	ps
Relative energy spread	0.5%	-
Transverse emittance (normalized)	< 1	mm mrad
Beam loss	$< 10^{-5}$	-

Presently, reliable beam-loss estimates are lacking. The machine protection system will be designed to trigger at losses above 5 μA (5×10^{-5} @ 100 mA). However, personnel protection requires that the shielding must be designed for a worst-case beam-loss scenario. An upper limit for sustainable continuous losses is given by the RF power installed in the main linac (30 kW), corresponding to 0.6% at 100 mA, nearly eight orders of magnitude higher than in BESSY II! This value provides the basis for the radiation-shielding layout.

Integrated dose calculations and activation estimates are based on 2000 h/a single-shift (8 h) operation with losses occurring at six equally spaced points along a stainless-steel vacuum chamber (impact angle = 1 mrad). The goal is to maintain general public access outside the radiation enclosure (dose < 1 mSv/a). In addition to bremsstrahlung, one must consider neutron production via (γ,n) reactions. Calculations have shown that at 50 MeV, fast neutrons, capable of penetrating shielding over large distances, dominate the radiation transverse to the beam direction. Unfortunately, existing extinction formulae are only valid in the GeV range, and cannot be scaled to the B*ERL*inPro energy range because the cross section increases rapidly between 50 MeV and 1 GeV. FLUKA calculations, as shown in Figure 2 were used to derive new semi-analytical formulae [13], which allowed us to calculate the required shielding. As depicted in Figure 2, the required lateral shielding is equivalent to 80 cm of concrete plus 3 m of sand. In the beamline plane, gamma radiation dominates over that of the neutrons by three orders of magnitude. A cost-effective shielding solution is thus given by an underground accelerator building (Figure 3). A slight underpressure must be maintained during operation to limit the emission of activated air. Fortunately, the ground water flow-rate is sufficiently low, that contamination of nearby waterways by activated ground water is not an issue. All auxiliary equipment (e.g., cryoplant, power

supplies, RF transmitters etc.) can be housed in a simple, above-ground building connected to the accelerator building by an access shaft.

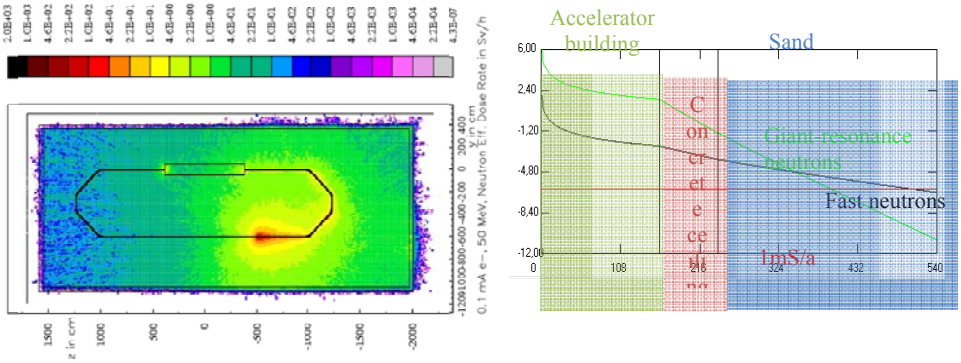

Figure 2: (left) Calculated neutron-radiation for a single source point in the recirculator generated by 0.1% beam loss at 50 MeV in a stainless-steel vacuum chamber. (right) Radiation dose (log scale) in the vertical cross section of the accelerator building (green region), the concrete ceiling (red region) and sand above (blue). The γ-radiation (not shown) is similar to that of the giant-resonance neutrons.

4.11.3 **Beam Optics**

While B*ERL*inPro's initial goal is to demonstrate the parameters in Table 1, its role as a "generic" demonstration facility requires very flexible optics to allow the exploration of other modes. Some compromises had to be made due to financial constraints. For example, the number of booster cavities was limited to three and the voltage must be constrained to avoid overfocusing by the RF field. Longitudinal cathode-laser profiling, useful to obtain a homogenous bunch profile and likely necessary for lowest emittances, will also not be implemented at this stage. Despite these trade-offs, simulations show that the parameters in Table 1 are within reach. They also demonstrated that most of the bunch properties are defined in the injector. While certainly true for the emittance, the successful compression of bunches in the recirculator also depends on maintaining a short bunch at the booster entrance to avoid subsequent accumulation of RF curvature.

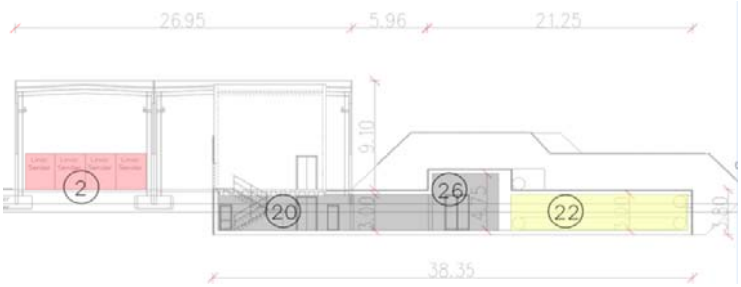

Figure 3: Cross section through the BERLinPro accelerator complex. (22) = 13×33×3 m3 underground accelerator building covered by 3 m of sand, (26) = underground anterooms housing RF klystrons, cryo-distribution box and laser, (20) = access from the above-ground part (2) that houses auxiliary equipment.

Without appropriate measures, the projected bunch emittance will increase due to space charge forces. For a 2-ps long bunch this remains an issue up to $\gamma \approx 75$. Viewing the bunch as a series of independent slices, an increase in projected emittance may be due to either a misalignment of the slices' phase-space ellipses or an increase of the individual slice emittances. The former effect can be counteracted by appropriate transverse focusing in the injector (emittance compensation). Numerous effects were considered to optimize the optics layout. These include:

- The longitudinal variation of space-charge density that results in oscillations of the transverse size of the slices around a reference value.
- The energy change due to space charge, which is comparable to the energy spread of the bunch (‰ level) and the impact of dispersion on slice angle and position.
- Emittance growth due to solenoid aberrations. This scales with higher powers of the bunch radius and solenoid field and that the bunch size must be kept small.
- Bunch over-compression due to RF non-linearity. This requires an optimization of the booster phase and the R_{56} of the merger.

The bunch length for different operating modes is determined primarily by bunch compression in the dispersive sections. It is controlled by the RF phases in combination with a fixed R_{56} of the merger and an adjustable R_{56} in the arcs (two-stage compression). For high compression, the longitudinal phase space must be very linear. Thus the bunch length delivered by the photoinjector to the booster may not exceed a 6-ps limit to minimize the sampled RF curvature. Furthermore the total RMS energy spread in the arcs must be better than 1% to limit beam losses. This constrains the bunch length in the main linac, which should operate off crest when bunch compression in the first arc is required. Hence the merger acts as a first-stage compressor to deliver < 6 ps (2 ps) bunches to the linac in the standard (short-pulse) mode.

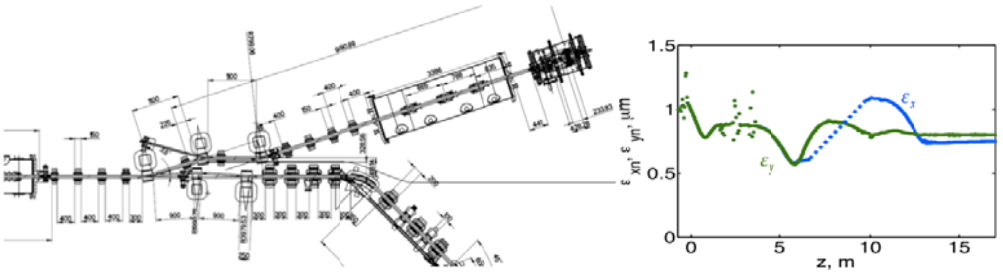

Figure 4: (left) Injection path from the superconducting RF photoinjector through the three-cavity booster and the dog-leg merger into the main linac. (right) Evolution of the transverse emittance from the cathode through the merger and main linac.

4.11.3.1 *Injection Line*

The complete injection line is shown in Figure 4. Following the 1.8-MeV SRF photoinjector, a SC solenoid refocuses the beam prior to acceleration in the 3-cavity booster. Given the previous discussion on emittance dilution, the solenoid is placed as close as possible to the photocathode (ca. 450 mm). Only minimal diagnostics are included between the injector and the booster to limit bunch lengthening in this region. To reduce the costly RF transmitters, the last two booster cavities accelerate while the first cavity operates near zero-crossing for velocity compression prior to the merger.

There the dipole spacing is kept small to limit the length of the dispersive region (R_{56} = 10 cm).

4.11.3.2 *Recirculator*

The recirculator is focused on providing beam transport without significant losses while conserving the excellent beam quality. It must also incorporate compressor capabilities for the generation of short (100 fs-range) pulses. Various beam physics aspects needed to be considered when developing its layout:

- A large acceptance is required to minimize beam loss.
- The R_{56} must be tunable over a broad range (-0.32 m $< R_{56} <$ 0.32 m).
- To control the HOM-driven BBU, the betatron phase advance must be flexible.
- Coherent-synchrotron-radiation (CSR) driven emittance dilution in the arcs. It can be reduced by tuning the bends' Twiss parameters or by a suitable phase advance between bends to cancel out the beam's energy modulation.
- Nonlinear effects like T_{566}, RF-curvature or fringe fields limit the compression. Higher-order multipoles can be used to linearize the longitudinal phase space and to optimize the transport of beam halo.
- Independent tuning of the arcs and the straight sections is required.

The resulting recirculator thus includes the 44-MeV linac with three-dipole chicanes before the merger and after the splitter to compensate their deflection of the high-energy bunches. The achromatic arcs consist of four 45° dipoles each, with a quadrupole at the center. This scheme reduces the maximum dispersion to increase the longitudinal acceptance, and the quadrupole provides flexibility for vertical matching and the choice of R_{56} (= ±0.14 m in the standard mode). Sets of four independent quadrupoles are placed up- and downstream of the arcs to match the Twiss parameters. Path-length adjustments to optimize the return-beam phase and hence energy recovery are made by shifting the two central dipoles of the second arc in beam direction by up to 2 cm with simultaneous transverse adjustment of the quadrupole to avoid steering. Several sextupoles are included in the layout for non-linear corrections. A large acceptance is provided by the use of a large vacuum chamber (minimum 40 mm diameter, in the arcs 40 × 70 mm^2) and moderate β-functions (< few 10s meters).

4.11.4 **Superconducting RF Photoinjector**

The ultimate performance of the ERL depends on the ability of the photoinjector to deliver reliably a beam of suitable brightness and current (Table 1). Furthermore, the injector should have the flexibility to generate pulses of higher charge, or shorter pulses with less charge to meet specific experimental needs. A wide spectrum of electron sources is available, including thermionic sources, DC photoinjectors, normal-conducting (NC) RF photoinjectors, SC RF photoinjectors and a combination of DC and RF injection [14, 15]. Taking the B*ERL*inPro parameter separately, these systems have demonstrated that most of them are within reach. E.g., the PITZ NC RF injector [16] has achieved the emittance requirement and both Boeing (NC RF) [17] and Cornell (DC) [18] sources have operated at high currents (20–50 mA). However, none

of these systems demonstrated the combined B*ERL*inPro parameter set and required lifetime.

For full control of the electron emission with (a) XHV vacuum conditions, (b) high accelerating gradient and (c) high-voltage operation we are convinced that laser-driven SRF photoinjectors offer the greatest potential. However, such injectors are also the least developed of the abovementioned options, the HZDR SRF injector being the only one that is routinely operated [19]. Its average current and emittance fall more than an order of magnitude short of what must be achieved for B*ERL*inPro. Hence a long-term, staged approach has been adopted to develop the SRF injector (see below).

The current (I_{ave}) of electrons charge q_{e} emitted from a photocathode with quantum efficiency Q_{e} (QE) illuminated by a laser of frequency ν and power P_{L} is given by

$$I_{\mathrm{ave}} = q_{\mathrm{e}} \cdot \frac{P_{\mathrm{L}}}{h\nu} \cdot Q_{\mathrm{e}} \,. \tag{1}$$

Metal cathodes (including SC ones) all have very low QEs and 100-mA operation is impossible. Far more promising candidates include alkali antimonides or semiconductors such as GaAs. The latter can operate in the IR but deteriorate rapidly under ion bombardment or if the vacuum exceeds 10^{-11} mbar. Also their emission is not prompt on ps time scales. CsK_2Sb is less susceptible, yields a demonstrated QE in the percent range at 532 nm [20] and emission is expected to be more prompt than from GaAs. Hence CsK_2Sb has been chosen as the baseline cathode material. For detailed studies HZB is building dedicated facilities to produce and analyze cathodes using various techniques. Dark-current emission is another important aspect, since this may dominate the B*ERL*inPro beam loss. A separate facility is being set up to study the field emission from these cathodes.

The required cavity field is governed by the minimum emittance achievable under space-charge-limited emission ($\varepsilon_{\mathrm{scl}}$). For a bunch with charge q_{b} launched at field E_{l} and a cathode work function Φ it is given by

$$\varepsilon_{sc1} = \sqrt{\frac{q_{\mathrm{b}}\left(h\nu - \Phi\right)}{12\pi\varepsilon_0 E_{\mathrm{l}} mc^2}} \,. \tag{2}$$

At this limit the bunch-induced surface field equals the launch field and severe decompression of the electron bunch results. Operation at least three times above this limit is therefore planned, which translates to a launch field of 7–20 MV/m. On the other hand, given the danger of field emission, the maximum field should not exceed 25–30 MV/m, which limits the possible launch phases. In addition, a 2-MV upper voltage limit is given by the RF power capability of the coupler system (≈ 130 kW per coupler, see below) so that a 1½-cell cavity is currently favored for the injector. Such a system provides flexibility to tune the design so that the optimum launch field is near the maximum surface field of the cavity to reduce the danger of field emission.

To preserve the emittance, the first focusing element, an SC solenoid, will be placed as close as possible to the cathode. Tests with a prototype 1½-cell SRF injector (see below) and a solenoid 45 cm from the cathode have shown no degraded cavity performance due to the solenoid field, provided the solenoid is switched off during

cavity cooldown. The resulting baseline layout of the SRF photoinjector is shown in Fig. 5.

Given the complexity of the system, tests at higher currents (> 5 mA) with the eventual goal of 100-mA operation, will not begin until 2016. A staged development, as in Table 2, is used to separate out the main challenges. The first stage (Injector 0) was designed to demonstrate operation with a fully SC injector (SRF cavity + SC cathode + SC solenoid) in HZB's HoBiCaT Test facility [21–23]. As shown in Fig. 6, the system employed a SC Pb cathode, coated directly on the cavity's back-plane by arc deposition. This removes the difficulty of incorporating an NC cathode in this early design. Given the low QE of Pb (measured QE ≈ 10^{-4}), such a system is unsuitable for ERLs but may be a viable option for <1 mA CW linacs, such as for FELs. First operation took place in 2011 and extensive beam dynamics and dark current studies were carried out. A second version of this cavity is currently being installed in HoBiCaT.

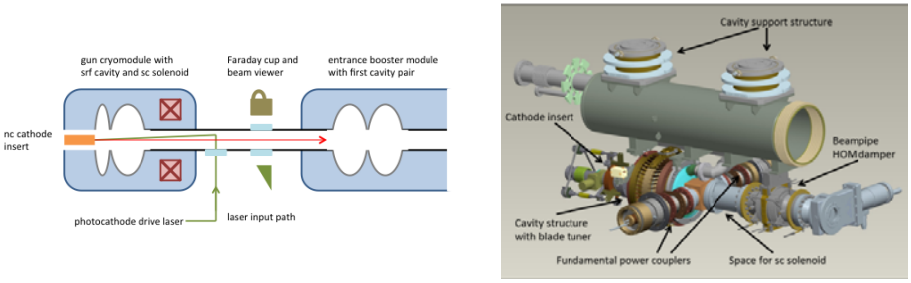

Figure 5: (left) Baseline layout of the SRF photoinjector. The distance from cathode to solenoid is approximately 45 cm and to the first booster cavity is about 250 cm. (right) First concept for the cold mass of the injector cryomodule, with cathode insert, cavity & blade tuner, dual couplers, HOM load and helium gas-return pipe.

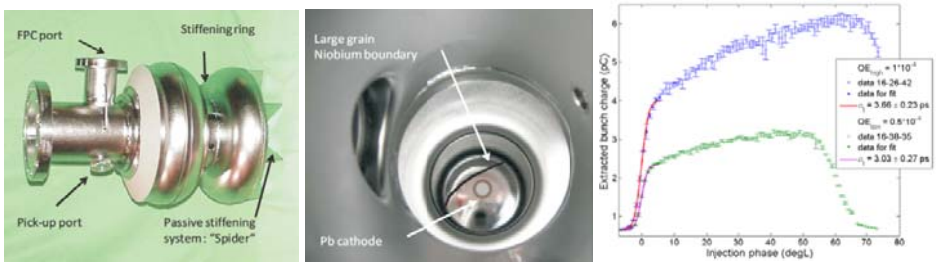

Figure 6: (left) 1½-cell SRF photoinjector designed by DESY and produced at Jefferson Lab. with (middle) Pb-coated backplane acting as a SC cathode (coating at NCBJ, Swierk). (right) Measured extracted bunch charge versus emission phase for two different regions of the photocathode, yielding bunch lengths of order 3 ps.

Insights from these first tests presently are flowing into the design of Injector 1, which will include a CsK_2Sb cathode using a HZDR-style choke filter to thermally isolate the NC cathode from the SC cavity [24]. As in Figure 5, the system uses a 1½-cell cavity that compromises between beam-dynamics requirements, and the peak surface and maximum cathode fields. Injector 1 is designed to (a) demonstrate high-brightness operation at the B*ERL*inPro bunch charge (56 MHz repetition rate) and (b) study high-QE photocathodes. It will first be tested in the HoBiCaT bunker with suitable beam diagnostics ("Gunlab"), albeit at a low repetition rate to limit the average

current to 5 μA for radiation safety. Once it is installed in the B*ERL*inPro building (2015) it can operate at up to 4 mA. Results from these measurement runs can then be used to design a follow-up, high-power system (Injector 2) that includes high-power couplers and a 1.3-GHz, 532-nm laser for 100 mA of beam loading.

Table 2: Planned parameters for the three stages of the SRF photoinjector development. Values marked by a * are measured (preliminary results).

Parameter	***Injector 0***	***Injector 1***	***Injector 2***
Goal	SRF demonstrator	High brightness (HB)	HB & high current
Cathode material	Pb (SC)	CsK_2Sb (NC)	
Drive laser wavelength	258 nm	532 nm	
Drive laser pulse	2 – 3 ps FWHM	≤ 20 ps FWHM	
Repetition rate	8 kHz	54 MHz/25 Hz	1.3 GHz
Electric peak field	20 MV/m*	10 MV/m < E_{pk} < 25 MV/m	
Electron energy	1.8 MeV*	> 1.5 MeV	
Bunch charge	6 pC *	77 pC	
Average current	50 nA*	40 μA/4 mA	100 mA
Normalized emittance	2 mm mrad*	1 mm mrad	

4.11.5 **SRF Accelerating Systems**

The remaining accelerating systems are divided into the booster and the main linac sections, which face very different challenges. The booster must provide up to 4.5 MeV acceleration without energy recovery. Very heavy beam loading dominates the design considerations, with danger of emittance dilution due to, e.g., coupler kicks. The state-of-the-art for such a system is Cornell University's booster [25], which demonstrated 50 mA average current for a short period. The design uses five 2-cell cavities, each powered by two opposing couplers while the cryostat layout follows the TELSA "philosophy". Given its success, a similar system is planned for B*ERL*inPro.

However, for budgetary reasons only three cavities will be installed of which the last two provide acceleration while the first only chirps the beam. This yields 230 kW of beam loading per cavity to be supplied by 270-kW klystrons (currently on order from CPI). The operating field can be as high as E_{acc} = 12.5 MV/m, which has already been demonstrated by the Cornell unit. Unfortunately, the input couplers are unable to handle the RF power (115 kW each). HZB is therefore in the process of modifying the module design to incorporate fixed-coupling KEK-style couplers [26], which require a vertical arrangement in their present configuration. So far, their demonstrated performance is of order 40 kW [27], limited by the warm part of the inner conductor. Modifications by KEK and HZB are under way to improve their cooling for up to 200-kW operation and to enable horizontal installation in the module. These couplers will also be used in the high-current photoinjector (Injector 2).

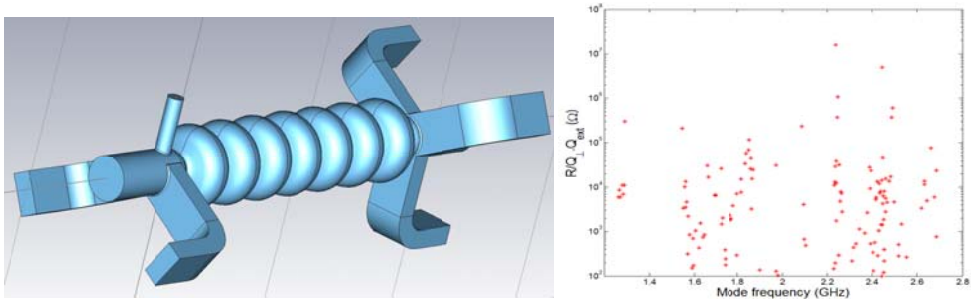

Figure 6: (left) Simulation model of a Cornell-style 7-cell cavity combined with waveguide HOM couplers and a coaxial input coupler. (right) Calculated transverse impedance. Some quadrupole modes are trapped in the center cells so that further cavity optimization is needed.

Unlike the booster, beam loading in the main linac is essentially zero due to energy recovery. Instead, HOM damping takes on a prominent role to avoid BBU issues and excessive cryogenic losses. Approximately 150 W of HOM power are expected at 100 mA. Various damping schemes can be employed, the most common being 80-K ferrite or ceramic beam-pipe absorbers between cavities. Their disadvantages include temperature dependent absorption properties, cracking and the resulting dust contamination of the cavity, as well as the additional (longitudinal) space requirements. Recent measurements also point to charging problems by stray electrons due to a low DC conductivity of some ferrites in the cold [28].

HZB is currently designing a waveguide (WG) damped system, similar to that developed by JLAB for high-current operation [29]. Its inherent advantages include the natural rejection of the fundamental mode so that WGs can be placed close to the cavity for strong damping. Also, WG dampers are broad-band (if windowless). Since the absorbers can be placed at room temperature, one can take advantage of the broad-band properties of SiC [30]. This configuration has the added benefit that the absorbers are far from the cavity, thus avoiding dust contamination and charging. The challenge with this system lies in the thermal management, requiring heat intercepts at 4.5 and 80 K.

Two cell shapes were considered: the JLAB 1.5-GHz high-current cavity scaled to 1.3 GHz [29], and the Cornell 1.3-GHz, 7-cell cavity [31]. The latter has a better ratio of peak to accelerating electric field (2 v. 2.4). In collaboration with Technische Universität Dortmund and Universität Rostock the two designs, coupled with WG dampers, are being simulated. Given that cavity operation will be at $E_{acc} \approx 18$ MV/m, a Cornell-like cell, as shown in Figure 6, is currently favored due to the lower peak electric field.

So far the HOM properties of individual cavities were analyzed, providing a basis for BBU calculations [32]. These predict that for a broad range of betatron phase advances the current limit exceeds 100 mA by a significant margin. However, given the proximity of the cavities to each other, reliable predictions require that the cavities not be treated individually but rather as a three-cavity ensemble. This increases the computational overhead significantly and the exploration of techniques that allow the efficient concatenation of cavities is currently under way.

While the negligible beam loading relaxes the coupler design, the weak coupling ($Q_{ext} \approx 5 \times 10^7$) yields a small bandwidth and microphonics dominate the RF-power requirement and achievable stability. Digital LLRF measurements at HoBiCaT demonstrated that operation at least up to $Q_{ext} \approx 2 \times 10^8$ is possible, maintaining a stability of 3×10^{-4} in amplitude and 0.02° in phase [33]. Still, electro-mechanical

modeling of the cavity design takes on an important role to shift prominent mechanical resonances to high frequencies. In principle it is also possible to design the cavity to have nearly zero helium-pressure sensitivity (the dominant source of microphonics) [34]. Such a design is being developed in collaboration with FZ-Jülich. At present, 10 kW RF power per cavity supplied by 15-kW solid-state transmitters is budgeted for field control and HZB modified the TTF-III coupler to be able to handle RF power at this level [35]. Active microphonic compensation using fast piezo-electric elements will also be incorporated in the cavities' "blade tuners" to further reduce the RF power demand and improve the stability. Past tests at HZB with TESLA cavities demonstrated for the first time that an active compensation by a factor of five is indeed possible [36].

Particular attention must be paid to the dynamic losses in the main linac cavities, since for many accelerator applications their number will be large and the cryogenics will be a significant cost driver. Tests have shown that 9-cell cavities prepared by standard BCP treatment can achieve residual resistances of less than 5 nΩ so that at 2 K BCS losses still dominate. Since BCS losses drop exponentially with temperature, B*ERL*inPro will operate at 1.8 K to realize a significant cryogenic savings. HZB has already installed a 700-l/hr 4.2-K refrigeration unit and presently is developing a concept for 1.8-K operation based on cold compressors [37]. Interestingly, recent measurements suggest that the cooldown rate through the transition temperature affects the residual resistance. Temperature cycles to < 20 K were used to improve or deteriorate the Q [38]. Changes by up to 8 nΩ were observed, which for GeV-class ERLs would have a dramatic impact on the required cryopower. This effect is not fully understood. One hypothesis is that thermo-currents generate magnetic flux, which subsequently is trapped, thereby producing additional losses. Alternatively, slow cooling may allow the cavity to expel external flux more efficiently during the SC transition [39, 40].

4.11.6 **Project Schedule**

The original plans called for first beam recirculation by the end of 2015. This schedule can no longer be maintained. For one, the initial budget (25.8 M€, year 2008) was not approved until Oct. 2010. Furthermore, detailed cost calculations yielded a total cost estimate of 36.5 M€ (year 2012) and the difference will be covered by HZB by stretching the timeline. A staged approach will focus on demonstrating the most challenging goal—100 mA in the injector—at the earliest possible date.

A Conceptual Design Report was completed in May 2012, thereby fixing the beam optics. It will now "evolve" into a technical Detailed Design Report. Since radiation considerations dictate that high-current photoinjector operation is only possible in the B*ERL*inPro building, its construction is a high-priority item. Building occupancy is expected to commence in late 2014. In parallel, the development of the SRF injector continues, and a first version with NC cathode should begin tests at HoBiCaT by 2014 at low average current.

The following year (2015) this source will be installed in the B*ERL*inPro building together with the booster, merger and beam dump for CW, 54-MHz operation (limited by the couplers and laser). This yields an average current of 4 mA, but beam properties such as emittance and bunch length at full bunch charge can be studied at 6 MeV. Cathode studies will also be an important part of the measurement program. A second

photoinjector that includes lessons learned from the first and that is upgraded with high power couplers, will be commissioned in parallel in Gunlab (@HoBiCaT). In 2016 it will be installed at B*ERL*inPro to complete the path to 100-mA operation (600 kW on the beam dump) by 2017. In a final step, the main linac module and recirculator will be installed in 2017 for energy-recovery operation in 2018.

4.11.7 **Acknowledgements**

The realization of complex accelerator projects usually relies heavily on collaborative activities. B*ERL*inPro is certainly no exception. We acknowledge and thank many colleagues from around the world for their contributions and advice both for the theoretical layout of B*ERL*inPro and for the hardware development, in particular the superconducting photoinjector! The contributing laboratories include ASTeC, BINP, BNL, Cornell University, DESY, FZJ, HZDR, Jefferson Laboratory, MBI, NCBJ (Swierk), TU-Dortmund, Universität Rostock, and UCLA. We acknowledge funding from BMBF under contract 05K10PEA.

4.11.8 **References**

1. S. Kullander, Accelerators and Nobel Laureates, *Nobelprize.org*, http://nobelprize.org/nobel_prizes/physics/articles/kullander/.
2. R.-H. Menk et al., *NIM A* **548** (1 – 2).
3. M. Tigner, *Il Nuovo Cimento* **37** (3) (1965).
4. G. Neil et al., *NIM A* **557** (1), 9.
5. R. Hajima, *NIM A* **507** (1 – 2), 115.
6. S. Smith, *Proc. ERL 2007*, 6.
7. D. Bilderback et al., *New Journal of Physics* **12** (2010) 035011.
8. S. Sakanaka et al, *Proc. IPAC 2010*, 2338.
9. R. Hajima et al., Generation and Application of Laser Compton γ-Rays at the Compact ERL, *Proc. 8th Annual Meeting of Particle Accelerator Society of Japan* (2011).
10. I. Ben-Zvi, *Proc. EPAC 2006*, 940.
11. V. Litvinenko et al., *Proc. PAC 2005*, 2768.
12. S. A. Bogacz et al., *Proc. IPAC 2011*, 1120.
13. K. Ott and M. Helmecke, *Proc. IPAC 2011*, 1503.
14. For an overview see *Beam Dynamics Newsletter* **46** (2008).
15. C. Hernandez-Garcia and T. Kamps, et al., *Proc. FLS 2012*.
16. F. Stephan, et al., *PRST-AB* **13**, 020704 (2010).
17. D. Dowell et al., *APL* **63** (15) (1993).
18. B. Dunham et al., "Performance of the Cornell High-Brightness, High-Power Electrons Injector", *Proc. IPAC 2012*.
19. R. Xiang, et al., *Proc. FEL 2009,* 488.
20. J. Smedley, et al., *Proc. IPAC 2011*, 1443.
21. T. Kamps et al., *Proc. IPAC 2011*, 3143.
22. A. Neumann et al., *Proc. IPAC 2011*, 41.
23. A. Neumann et al., *Proc. SRF 2011*, 962.
24. D. Janssen, et al., *NIM A* **526** (1 – 2) (2004).
25. M. Liepe et al*., Proc. IPAC 2010,* 3043.
26. S. Noguchi et al*., Proc. SRF 2009,* 485.
27. E. Kako, KEK (private communication).
28. E. Chojnacki et al., *Proc. SRF 2009*, 643.
29. R. Rimmer et al*., Proc. IPAC 2010,* 3052.

30. F. Marhauser et al., *Proc. IPAC 2011*, 1792.
31. N. Valles et al*., Proc. IPAC 2010,* 3048.
32. Y. Petenev et al*., Proc. IPAC 2011,* 718.
33. A. Neumann et al*., Proc. SRF 2011*, 262.
34. E. Zaplatin et al., *Proc. SRF 2009*, 560.
35. J. Knobloch et al., *Proc. PAC 2005*, 3293.
36. A. Neumann et al., *PRST-AB* **13** 082001 (2010).
37. D. Pflückhahn, et al., "Cryogenic Concept of the Berlin Energy Recovery Linac Project", *Proceedings of ICEC 24-ICMC 2012*, Fukuoka, Japan (2012) (to be published).
38. O. Kugeler et al., *Proc. SRF 11*, 724.
39. S. Aull et al., "Trapped magnetic flux in superconducting niobium samples", accepted for publication in *PRST-AB*, May 22, 2012.
40. J. Vogt et al., "Impact of Trapped Flux and Thermal Gradients on the SRF Cavtiy Quality Factor", *Proc. IPAC 2012* (to be published).

4.12 Status of the Japanese ERLs

Ryoichi Hajima, KEK Tsukuba and JAEA Tokai, Japan
Mail to: hajima.ryoichi@jaea.go.jp

4.12.1 Historical Remarks as Introduction

4.12.1.1 *Development of the ERL-FEL at JAEA*

The history of energy-recovery linac (ERL) in Japan opened with a 17-MeV ERL-FEL at Japan Atomic Energy Agency (JAEA), formerly named Japan Atomic Energy Research Institute (JAERI). The research program of JAEA FEL was established in 1987 aiming at the applications of FEL to isotope separation and other basic research of laser and accelerator science for atomic energy. In order to realize a high-power FEL at a wavelength of the infrared region, they decided to utilize a superconducting linac as a driver of the FEL. After the successful high-power FEL lasing, the accelerator was reconstructed into an ERL as shown in Fig. 1 [1]. The injector consists of a 230-kV electron gun with a gridded thermionic cathode, an 83.3-MHz subharmonic buncher (SHB), and two cryomodules, each of which contains a single-cell superconducting cavity driven at 499.8 MHz. An electron bunch of 450 pC with a length of 600 ps (FWHM) is generated by a grid pulser at a repetition rate of 20.825 MHz, that is, an average current of 9 mA. The electron bunch is accelerated to 2.5 MeV by two single cells and transported to the merger. The main linac consists of two 5-cell cavities driven at 499.8 MHz. The bunch duration and the normalized emittance at the undulator were 12 ps (FWHM) and 40 mm-mrad (rms), respectively. They employed two 50-kW inductive output tubes (IOTs) for the injector and two 50-kW solid state amplifiers for the main linac. The return loop consists of two triple-bend arcs and a small dogleg before the undulator. The arc after the undulator is equipped with two families of sextupole magnets to accept an electron beam of large energy spread due to the FEL lasing.

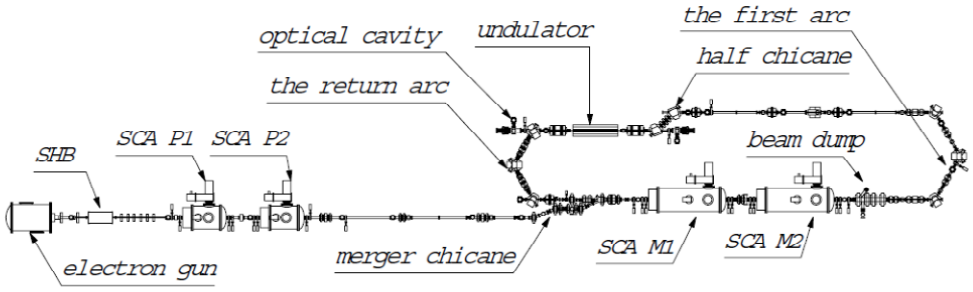

Figure 1: Layout of the 17-MeV energy-recovery linac at Japan Atomic Energy Agency [1].

They demonstrated the first energy-recovery operation on February 19, 2002, and the FEL lasing on August 14, 2002. In the lasing, the FEL power and the conversion efficiency were limited by the energy acceptance of the return loop. The maximum FEL power and conversion efficiency were 0.75 kW and 2.5%, respectively [2]. Coherent synchrotron radiation in the millimeter wavelength region was also observed from an electron bunch traveling through the middle dipole magnet in the second arc [3]. After these successful demonstrations of energy recovery and FEL lasing, the ERL FEL was shutdown in 2009.

4.12.1.2 *Launch of the R&D Program for Future ERL Light Sources*

In KEK (High Energy Accelerator Organization), they had a design study of ERL light source in 2003, in which a 2.5-5 GeV ERL was proposed as a future X-ray light source to replace the existing storage rings, 2.5 GeV PF and 6 GeV PF-AR [4].

The FEL Research Group at JAERI, who constructed the 17-MeV ERL-FEL, designed a 6-GeV ERL light source [5]. They started development of an electron gun for a future ERL light source in 2005.

Following the extensive discussion among the synchrotron light source users community in Japan, KEK and JAEA had a negotiation for possible collaboration on the development of ERL technologies, and reached to the agreement for the collaboration. They signed a memorandum of understanding at March 10, 2006. Thereafter, a joint R&D team has been organized for the development of ERL technologies, and the design study of a future ERL light source. The joint team involves members of KEK, JAEA, University of Tokyo, SPring-8, UVSOR, Hiroshima University, Nagoya University, AIST and Yamaguchi University. We see the R&D status of the collaboration team in the next section.

4.12.2 **R&D for Future ERL Light Sources**

4.12.2.1 *Overview*

The performance of ERL, electron beam current and emittance, is restricted by its electron source and accelerating structure. The Japanese collaboration team, therefore, has focused their efforts mainly on the development of electron guns and superconducting cavities. They also have decided to construct a test facility, the Compact ERL, to demonstrate all the developed accelerator components working together.

4.12.2.2 *Electron Guns*

An electron gun used for producing small emittance electron beams with a high-average current is an essential device for an ERL to exploit its full advantages—the acceleration of high-power and high-brightness electron beams. A photocathode DC gun can generate an electron beam having an ultra-small initial emittance when it is equipped with a semiconductor photocathode having a negative electron affinity (NEA) surface. In a photocathode DC gun, a high DC voltage is necessary for suppressing the emittance growth due to the space-charge force. From numerical simulations, it was found that a DC voltage higher than 500 kV is required for a future ERL X-ray light source.

In order to establish the electron gun technology satisfying the future ERL light source requirements, two electron guns are under development at JAEA and KEK, respectively.

Figure 2 shows a photocathode DC guns developed at JAEA and KEK. As seen in Fig. 2, the photocathode gun has a metallic rod to support a cathode electrode at the center of the gun vacuum chamber. This supporting rod limits the gun voltage. When a high voltage is applied to the gun, the field emission of the electrons from the supporting rod may occur. The electrons emitted from the supporting rod are intercepted by the inner surface of the ceramic and penetrate into the ceramic body. If the ceramic has a high resistivity, these electrons cause a concentration of charges in a small area and may lead to a punch-through failure of the ceramic.

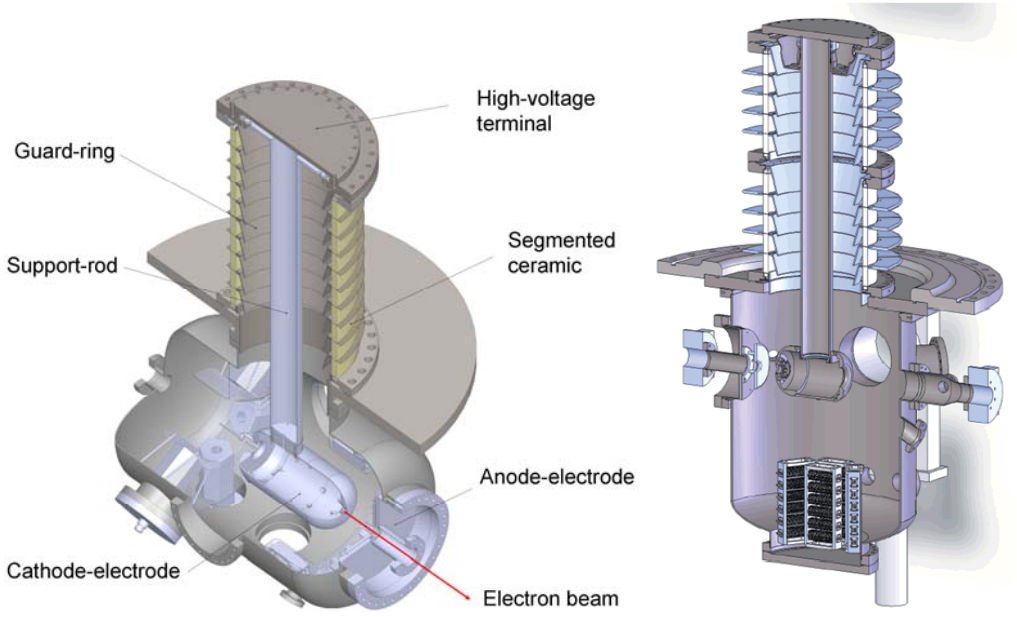

Figure 2: 500-kV photocathode DC guns at JAEA (left) and KEK (right).

In order to solve the field emission problem, a segmented ceramic insulator with guard rings was designed and fabricated for the JAEA gun. This type of ceramic insulator is expected to be tolerant to the field-emitted electrons. The insulator consists of multiple ceramics stacked in series, and a Kovar electrode is sandwiched between two ceramics and blazed. Guard rings are attached to the Kovar electrode on both the inner and the outer sides. The amount of segmentation and the shape of the guard rings

were optimized to minimize the surface electric field. The trajectories of field-emitted electrons from the rod were also taken into consideration in order to guard the ceramic surface from the field-emitted electrons from the supporting rod as shown in Fig. 3. A high-voltage test of the gun up to 550 kV was successfully achieved as shown in Fig. 4 [6]. Following this achievement, a similar type of ceramic insulator was employed at the KEK gun.

The next step is to produce an electron beam of 500 keV from the gun. The cathode electrode should be designed for its maximum surface electric field to be less than voltage breakdown criteria at 500 kV. The maximum electric field of cathode electrode and field on the cathode center are 10.3 MV/m and 6.7 MV/m, respectively, at JAEA. The gap between cathode and anode electrodes is 100 mm. High voltage processing up to 526 kV was demonstrated in 2011 at the JAEA gun but they have not reached the goal, 550 kV, yet. The applicable voltage is now limited by field emission due to small dust attached on the cathode electrode [7]. They are trying to resolve this problem by noble gas conditioning and recirculation evacuation.

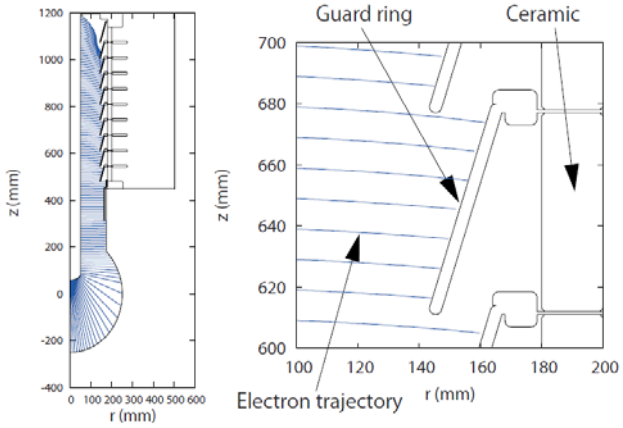

Figure 3: Results of numerical calculations on the emitted electron trajectories in the JAEA 500-kV gun [6].

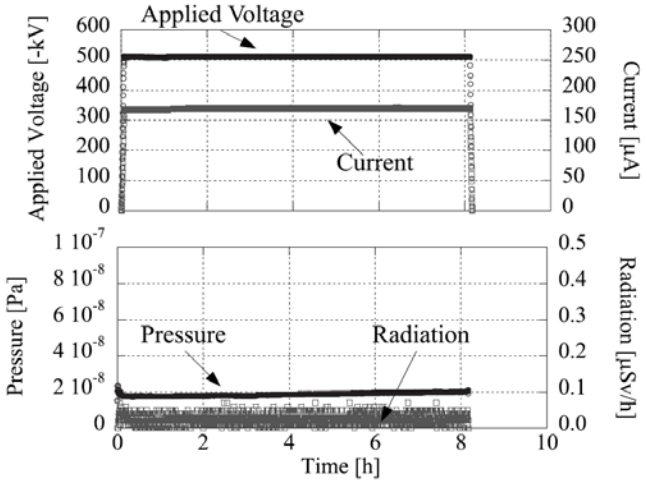

Figure 4: Results of a long-time holding test for 8 h at 510 kV [4].

For the practical operation of future ERL light sources, a photocathode must provide a sufficient electron charge, typically 10000 C (100 mA, 1 day). Thus, the life of the

NEA cathodes is a critical issue to be resolved. The surface of a negative electron affinity is created by the coadsorption of Cs and O_2 (or NF_3) on a wafer of p-doped GaAs. Since the NEA surface is easy to destroy by the collision of residual gas molecules or back-bombarding ions, the maintenance of a good vacuum is necessary to obtain long-life NEA cathodes. For the better vacuum condition, the vacuum chambers of JAEA and KEK guns are made of titanium, which has a low outgassing rate.

The outgassing rate of the KEK gun was measured by rate-of-rise method with a spinning rotor gage. The gun was equipped with a ceramic insulator and guard rings but without electrodes and NEG pumps at the measurement. Figure 5 shows the measurement result. The vacuum level was rising up at a rate of 3.04×10^{-7} Pa/h, which corresponds to the outgassing rate of 1.05×10^{-10} Pa m^3/s assuming the total contribution of H_2 gas. The outgassing rate is sufficiently low and a vacuum level better than 1×10^{-10} Pa will be achieved by installing a bakeable cryopump and NEG pumps at the gun chamber [8].

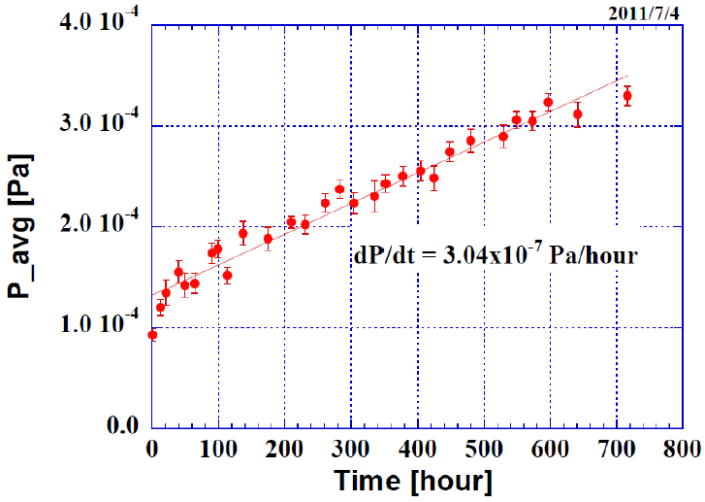

Figure 5: Raw data of the rate-of-rise measurement for outgassing rate of the assembled dc gun system at KEK [8].

A systematic study of photocathode materials for the future ERLs are conducted at KEK. They evaluated mean transverse energy (MTE) of electrons emitted from NEA photocathodes. Since the electron beam emittance is proportional to square root of MTE, the evaluation of MTE is important for designing photocathode for small emittance beams. The MTE measurements were carried out for three types of cathodes: bulk GaAs, thickness-controlled samples with active-layer thicknesses of 100 and 1000 nm, and GaAs/GaAsP superlattice samples. The dependence of the cathode quantum efficiency, the laser wavelength, and the thickness of the GaAs cathode active layer on the MTE was investigated. Figure 6 shows the measured MTEs of all the cathodes at laser wavelengths of 544 and 785 nm. No clear thickness dependence of the MTEs was seen within the error bounds [9].

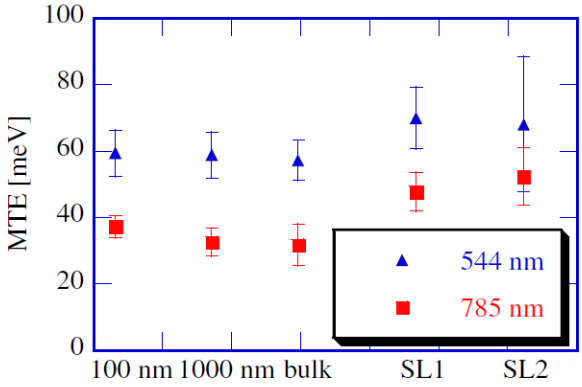

Figure 6: Measured mean transverse energy (MTE) of electrons from photocathodes at laser wavelengths of 544 nm and 785 nm. Results for thickness-controlled GaAs, 100 nm and 1000 nm, bulk GaAs and two different type of GaAs/GaAsP superlattice carthodes are plotted [9].

4.12.2.3 *Superconducting Accelerators*

The superconducting accelerator (SCA) for a high-average current electron beam is another essential component in the ERL. The research items of SCA include a high-power input coupler, an efficient damping of higher-order modes (HOM), cryomodules with small microphonics, a low-level rf controller for the precise control of rf amplitude and phase, and a superconducting cavity itself.

Superconducting cavity for the ERL is divided into two categories, one for an injector and the other for a main linac. In the injector cavity, an electron beam having a high-average current is accelerated without energy recovery, i.e., powered by external rf sources. Therefore, a high-power input coupler is a critical component to be developed.

Figure 7 shows the conceptual design of an injector cavity developed at KEK, which has a TESLA-like cell shape with two input couplers to support a higher rf power and five HOM couplers for efficient damping HOMs. An injector cryomodule for three 2-cell cavities is under assembling to be installed at the Compact ERL [10].

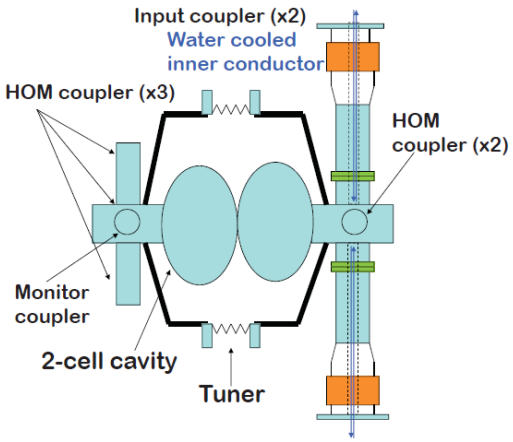

Figure 7: Conceptual design of 2-cell superconducting cavity for the ERL injector.

Fabrication of cavities and other components, high-power tests of the coupler, and vertical tests of cavities have been completed. A cryomodule for the Compact ERL

injector is under fabrication as shown in Fig. 8. The cryomodule will be soon installed at the Compact ERL and a horizontal test is scheduled this summer.

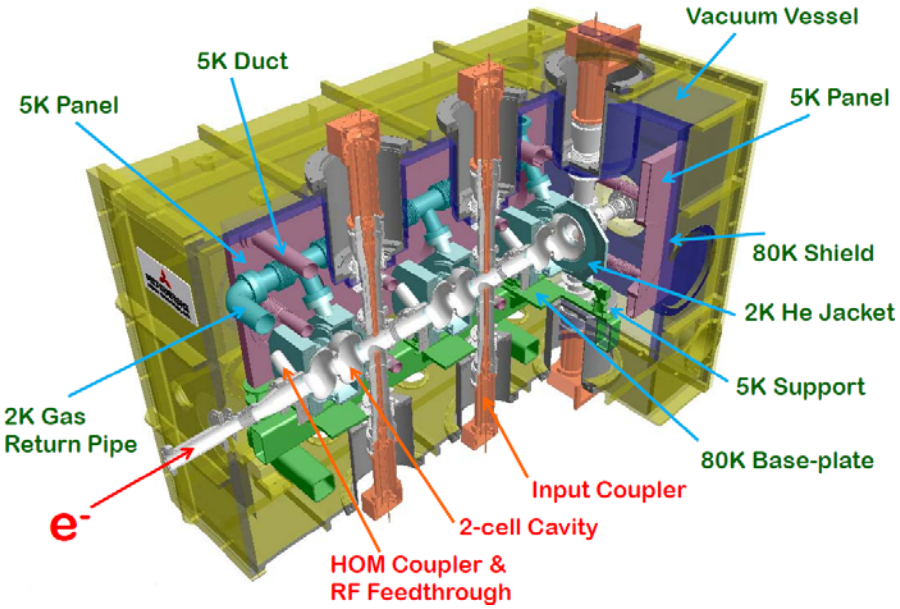

Figure 8: The cryomodule of injector SCA for the Compact ERL injector.

Superconducting cavities for ERL main linac is under development by the collaboration team (KEK / JAEA / U-Tokyo). They have chosen a 9-cell 1.3-GHz structure and obtained an optimum cavity design as shown in Fig. 9, which has an HOM-BBU threshold current large enough for practical operation of multi-GeV ERLs. The cavity has an optimized cell shape, enlarged beam pipes for efficient damping of HOMs, and eccentric-fluted beam pipe for damping the quadrupole HOMs. HOMs excited in the cavity are extracted through the beam pipes and damped by on-axis HOM absorbers installed at both ends of the cavity [9].

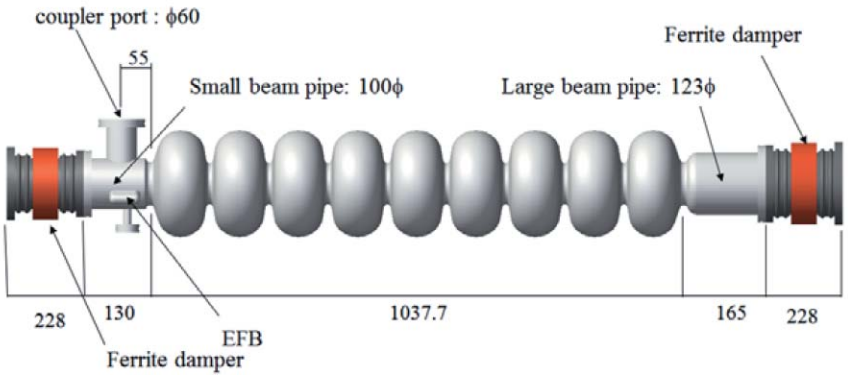

Figure 9: ERL cavity developed by KEK/JAEA/U-Tokyo. The cavity has a 9-cell shape and is operated at 1.3 GHz [11].

A couple of test cavities based on the designed shape were manufactured to confirm the characteristics of the cavity performance and also to establish the cavity fabrication

process. The results of these tests were fairly acceptable and the accelerator gradient of 25 MV/m was achieved as shown in Fig. 10.

Design and prototyping of the input coupler have been completed. The structure test of a HOM coupler model has finished. A prototype module including a pair of 9-cell cavities is being fabricated. The module will be installed at the Compact ERL [12].

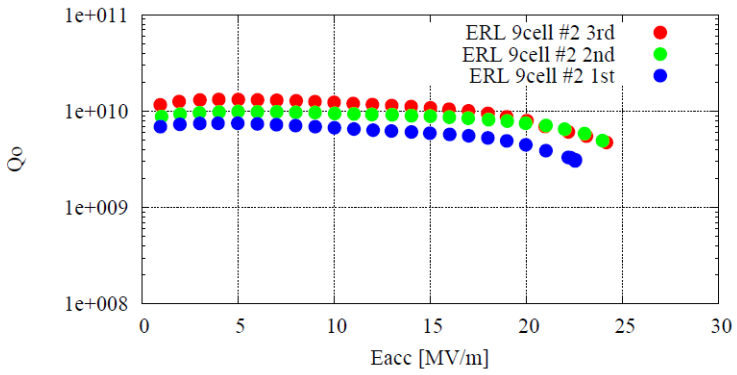

Figure 10: Results of vertical tests for the ERL 9-cell cavities

4.12.3 **Construction of a Test Facility, the Compact ERL**

The Japanese ERL team has decided to build a test facility, the Compact ERL (cERL), for the full demonstration of all the ERL technologies [13]. The construction site of cERL is an old experimental hall of 12-GeV proton synchrotron at KEK. The hall has been refurbished for the cERL.

Figures 11 and 12 show the footprint of the cERL and overall layouts in the hall. Table 1 lists parameters of the cERL. The cERL is operated with an electron beam of 35 MeV, 10 mA at the initial stage, where the main linac has two 9-cell cavities. However, we plan to increase the beam energy and current in future. The maximum energy will be 245 MeV after reinforcement of the main linac (eight 9-cell cavities) and installation of the second-loop for the double-pass acceleration.

Table 1: Parameters of the Compact ERL.

Parameter	**Value**
Beam energy (initial)	35 MeV
(maximum)	245 MeV
Injection energy	5 MeV
Beam current (initial goal)	10 mA
(future goal)	100 mA
RF frequency	1.3 GHz
Bunch length in rms (usual)	1 - 3 ps
(under compression)	< 100 fs
Accelerating gradient (main linac)	15 MV/m

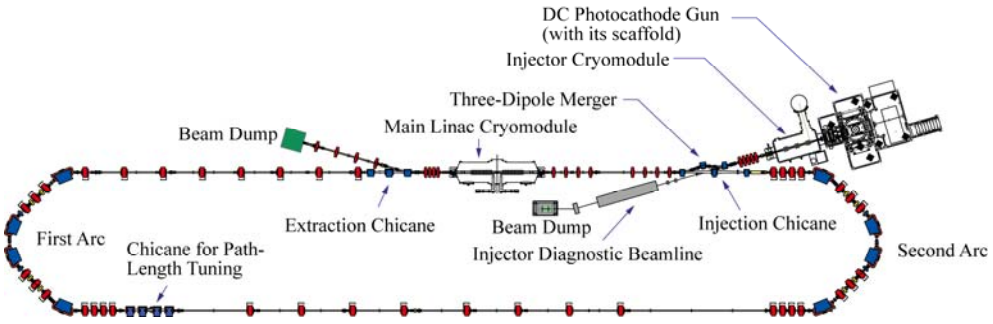

Figure 11: Layout of the Compact ERL (35-MeV version)

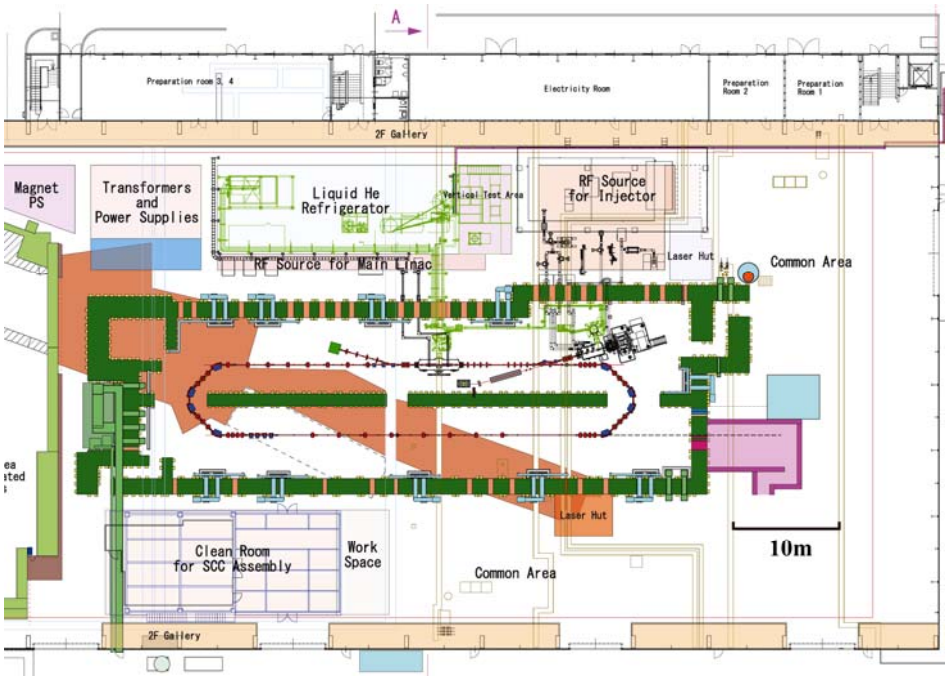

Figure 12: Overall layout of the cERL in the ERL development building at KEK (top of the figure is the north).

The cryogenic system for the cERL has already been installed. Under a test of liquefier/refrigerator, helium liquefaction rate of more than 250 L/h was successfully obtained. We are conducting cooling test down to 2K at the cold boxes. Radiation shielding for the cERL consists of concrete blocks. Installation of radiation shields started in March, 2012, and will be completed in September, 2012. Installation of the DC gun, a beamline for the injector, and the main-linac cryomodule will be started from October, 2012. Then, we will carry out cooling test of both injector and main-linac modules. We will also conduct conditioning of the DC gun, as well as rf-conditioning of both cryomodules. Commissioning of the injector is scheduled in the spring of 2013. The main part of the return loop will be installed from July to October, 2013 [14].

A research program of laser Compton scattered γ-ray generation is also carried out in the Compact ERL. Detail of the program is described later.

4.12.4 **Design of a 3-GeV ERL for a Future X-ray Source**

Energy-recovery linac with a high-average current and high-brightness electron beams can realize future synchrotron light sources, which outperform the storage-ring light sources in their X-ray spectral brightness and short-pulse availability. KEK has completed a preliminary design of 3-GeV ERL for a synchrotron radiation source as a successor of existing storage ring light sources, 2.5-GeV PF and 6-GeV PF-AR [15]. The 3-GeV ERL will be constructed within the 3-km circumference of KEK-B at KEK Tsukuba campus as shown in Fig. 13. In the return loop, about 30 undulators are installed to provide super-bright and/or ultra-short synchrotron radiation in the vacuum ultra-violet (VUV) to hard X-ray range.

They also plan to install an FEL oscillator operated in the hard X-ray region (XFEL-O) to produce X-ray pulses of excellent temporal coherence, which cannot be obtained in SASE FELs. In the current design, the XFEL-O will be driven by 6-7 GeV electron beam from double-pass acceleration without energy recovery [16].

The main parameters and the operation modes of the 3-GeV ERL and XFELO are summarized in Table 2 [17].

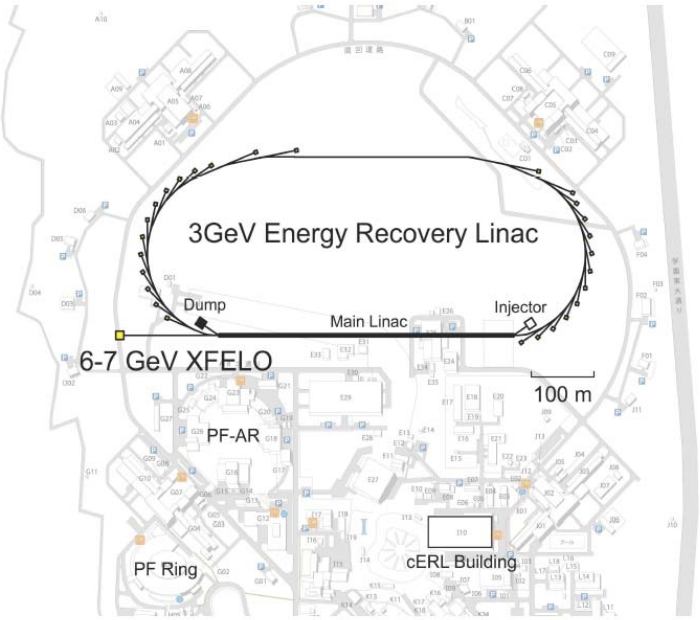

Figure 13: Layout of the 3-GeV ERL and 6-7 GeV XFEL-O at KEK

The lattice and optics design of the 3-GeV ERL was recently started [17]. The main linac consists of more than two hundred of 9-cell cavities to accelerate the electron beam up to 3 GeV with a moderate accelerating gradient of 15 MV/m or less. The return loop of the 3-GeV ERL has about 30 TBA (Triple Bend Achromat) cells with 6-m or 30-m long straight sections for insertion devices. The bending radius of the bending magnet is sufficiently long to suppress emittance growth and energy spread increase due to the incoherent synchrotron radiation effects. The optics of the main linac is designed so that the betatron function is well suppressed for achieving a high BBU

threshold current. Figure 14 shows the preliminary result of the optical functions for the main linac and the return loop of the 3-GeV ERL.

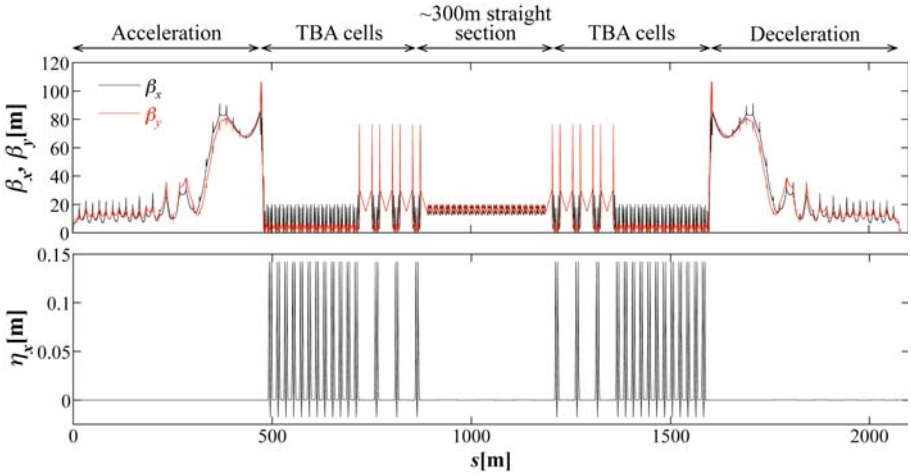

Figure 14: Betatron (upper) and dispersion (lower) functions of the main linac and the return loop for the 3-GeV ERL [17].

The 3-GeV ERL provides synchrotron radiation with the maximum brightness of 10^{22} - 10^{23} phs/s/mm^2/mrad^2/0.1%b.w. in the VUV and X-ray region as shown in Fig. 15. The 6-7 GeV XFEL-O generates fully coherent X-rays with the averaged brightness of about 10^{26} phs/s/mm^2/mrad^2/0.1%b.w. For the future development, one 300-m long straight section is reserved in the middle of the return loop. This section has large potential for (1) 300-m class undulator with the spectral brightness up to 10^{23} - 10^{24} phs/s/mm^2/mrad^2/0.1%b.w., (2) 3-GeV XFEL-O using the higher harmonics, (3) EEHG (Echo-Enabled Harmonic Generation) including attosecond pulse generation and so on.

Table 2: Beam Parameters for Typical Operational Modes for the ERL Light Source at KEK.

Parameter	*HC*	*HF*	*UL*	*US*	*XFEL-O*
Energy	3 GeV	3 GeV	3 GeV	3 GeV	6-7 GeV
Current	10 mA	100 mA	100 mA	77 μA	10 μA
Charge	7.7 pC	77 pC	77 pC	77 pC	10 pC
Repetition	1.3 GHz	1.3 GHz	1.3 GHz	1 MHz	1 MHz
Norm. emittance	0.1 mm-mrad	1.0 mm-mrad	0.1 mm-mrad	-	0.2 mm-mrad
Energy spread	2×10^{-4}	2×10^{-4}	2×10^{-4}	-	5×10^{-5}
Bunch length	2 ps	2 ps	2 ps	< 100 fs	1 ps

HC: High Coherence mode, HF: High Flux mode, UL: Ultimate mode, US: Ultra-Short Pulse mode.

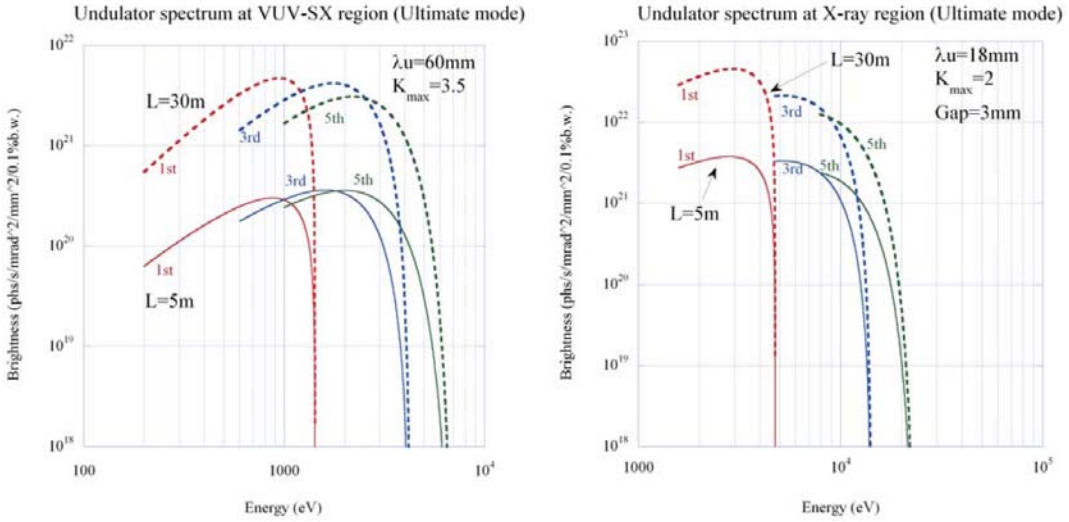

Figure 15: Calculated undulator spectrum for the VUV-SX source (left) and the X-ray source (right) for the 3-GeV ERL at KEK [15].

4.12.5 **Proposal of a LCS Gamma-Ray Source**

High-energy γ-ray photons can be generated from laser Compton scattering (LCS). The energy of the scattered γ-ray photon is a function of the incident photon energy, electron energy, and scattering geometry. Owing to the energy tunable monochromatic γ-ray generation, LCS γ-ray sources have been developed by using storage rings and linacs. The on-axis brightness of the generated γ-ray increases, when the electron beam has a large current, a small emittance and a small energy spread [18]. The ERL is, thus, a promising source of high-flux γ-rays [19,20].

Figure 16 shows a schematic view of an ERL γ-ray source. At the collision point, electron bunches circulating the ERL loop collide with laser pulses stored in an enhancement cavity, which is a high-finesse Fabry-Perot optical resonator to stack a train of laser pulses from a mode-locked laser [21].

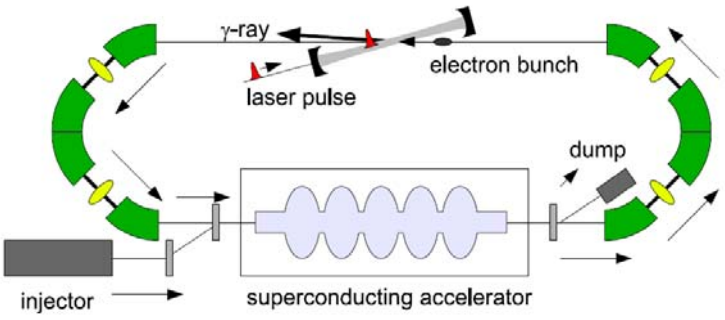

Figure 16: LCS γ-ray source based on an ERL and a laser enhancement cavity.

The effect of electron beam emittance on the dilution of γ-ray brightness becomes as small as the effect of laser diffraction, when we have a normalized emittance: $\varepsilon_n = \lambda/4\pi$ [18]. According to this criterion, we can define the "diffraction limited" electron beam. For a typical laser wavelength, 1μm, the diffraction limited electron

beam for LCS γ-ray sources has a normalized emittance of 0.08 mm-mrad, which is a similar value to the required emittance for ERL-based synchrotron radiation sources to obtain coherent hard X-rays. Consequently, we can share accelerator components such as electron injector and accelerator for both ERL-based X-ray sources and ERL-based γ-ray sources.

Table 3: Parameters for a 2-MeV **γ**-ray source. Two operation modes are considered: high-flux mode (100 pC, 1 mm-mrad) and narrow-bandwidth mode (10 pC, 0.1 mm-mrad).

ERL electron beam		**Laser**	
Energy (MeV)	350	Wavelength (nm)	1064
Bunch charge (pC)	10 / 100	Pulse energy (μJ)	1.5
Repetition (MHz)	130	Repetition (MHz)	130
Bunch length (rms, ps)	3	Pulse length (rms, ps)	3
Norm. emittance (mm-mrad)	0.1 / 1.0	Enhancement	2000
Energy spread (rms)	0.03%	Intracavity power (kW)	400
Collision spot (rms, μm)	10	rms Collision spot (rms, μm)	10
Collision angle (degree)	3.5		

Table 3 shows an example set of parameters for 2-MeV γ-ray source designed for nuclear material measurements, where γ-ray with a total flux of 1.0×10^{13} ph/s is generated.

ERL is an ideal electron accelerator for laser Compton scattering light source to produce γ-rays of high flux and narrow bandwidth. Electron beams of small emittance and high-average current available from ERLs realize unprecedented light sources in photon energies of MeV, γ-rays, as well as X-rays. The improvement of γ-ray performance from the existing LCS γ-ray sources includes the enhancement of flux by 5-8 orders and the bandwidth narrowing by 1-2 orders in comparison with existing LCS γ-ray sources based on storage rings. Such ERL γ-ray sources are of great use in many scientific and industrial applications: nuclear physics [22], nuclear astrophysics [23], hadron physics [24], management of nuclear waste [25], nuclear security and safeguards [26].

In order to demonstrate the performance of ERL γ-ray source and explore applications of ERL γ-ray sources to nuclear security and safeguards purposes, JAEA has launched a 3-year program (2011-2013) supported by Ministry of Education, Culture, Sports, Science and Technology (MEXT) in Japan [27]. The program aims at generation of a high-flux and narrow-bandwidth γ-ray beam at the Compact ERL in collaboration with KEK. Application of the γ-ray to non-destructive measurement of isotopes is also planned. Figure 6 shows a schematic view of the proposed experiment at the Compact ERL.

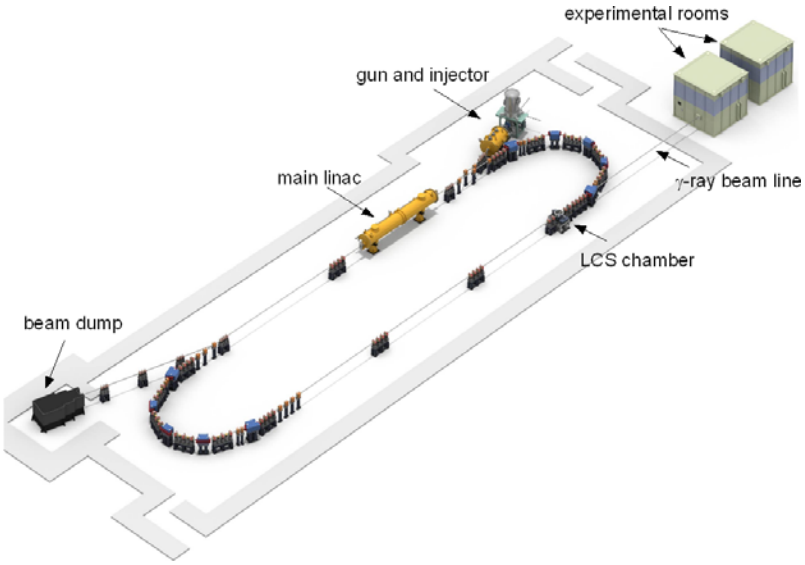

Figure 17: A schematic view of the LCS γ-ray experiment at the Compact ERL.

4.12.6 **Summary**

Research and development of ERLs have been conducted continuously in Japan since the construction of JAEA ERL FEL. As future ERL light sources, a 3-GeV ERL synchrotron light source is proposed by KEK and a 350-MeV ERL γ-ray source is proposed by JAEA, respectively. The major components of these ERLs, 500-kV DC guns and superconducting cavities, have been developed by collaborative efforts in Japan. A test facility, the Compact ERL, is under construction and will be completed in 2013 for the full demonstration of these developed components with an electron beam operation.

4.12.7 **References**

1. R. Hajima et al., Nucl. Instr. Meth. A507, 115 (2003).
2. N. Nishimori et al., Proc. FEL-2006, 265 (2006).
3. R. Hajima et al., Proc. FEL-2005, 301 (2005).
4. T. Suwada and A. Iida, “Study Report on the Future Light Source at the Photon Factory –Energy Recovery Linacs and Science Case–, KEK (2003) (in Japanese).
5. R. Nagai et al., Proc. PAC-2003, 3443 (2003).
6. R. Nagai et al., Rev. Sic. Instr. 81, 033304 (2010).
7. N. Nishimori, Proc. FLS-2012 (2012).
8. M. Yamamoto, Proc. IPAC-2011, 979 (2011).
9. S. Matsuba et al., Jpn. J. Appl. Phys. 51, 046402 (2012).
10. K. Watanabe et al., Proc. Linac-2010, TUP005 (2010); E. Kako et al., Proc. IPAC-2012, WEPPC015 (2012).
11. K. Umemori et al., Proc. SRF-2009, 355 (2009).
12. K. Umemori et al., Proc. IPAC-2012, MOOBC02 (2012).
13. R. Hajima et al., “Design Study of the Compact ERL”, KEK Report 2007-07 / JAEA-Research 2008-032 (2008) (in Japanese).
14. S. Sakanaka et al., Proc. IPAC-2012, MOPPP018 (2012).
15. H. Abe et al., “Energy Recovery Linac Preliminary Design Report”, KEK (2012).

16. R. Hajima et al., Nucl. Instr. Meth A637, S37 (2011).
17. N. Nakamura, Proc. IPAC-2012, TUXB02 (2012).
18. W.J. Brown and F.V. Hartemann, Phys. Rev. ST-AB 7, 060703 (2004).
19. R. Hajima et al., Proc. AccApp07, 182–188 (2007). ISBN: 0-89448-054-5.
20. V.N. Litvinenko et al., IEEE Trans. Plasma Sci. **36**, 1799–1807 (2008).
21. K. Sakaue et al., Nucl. Instr. Meth. **A637**, S107–S111 (2011).
22. T. Shizuma et al., Phys. Rev. C **78**, 061303(R) (2008).
23. T. Hayakawa et al., Phys. Rev. C **74**, 065802(R) (2006).
24. A.I. Titov, M. Fujiwara and K. Kawase, J. Phys. G **32**, 1097–1103 (2006).
25. R. Hajima et al., J. Nucl. Sci. and Tech. **45**, 441–451 (2008).
26. T. Hayakawa et al., Nucl. Instr. Meth. **A621**, 695–700 (2010).
27. R. Hajima et al., Proc. 52nd INMM Annual Meeting (2011).

4.13 Status of the Mainz ERL-facility MESA

Kurt Aulenbacher, Marco Dehn, Hans-Joachim Kreidel, Robert Heine
Institut für Kernphysik der Johannes Gutenberg-Universität Mainz,
J. J. Becherweg 45 D-55118 Mainz, Germany

Ralf Eichhorm, Cornell Univ., U.S.A.

Mail to: aulenbac@kph.uni-mainz.de

4.13.1 **Introduction**

University of Mainz has long standing experience in designing, commissioning and operating multi-turn c.w. accelerators. Given the restrictions in budget and building size in Mainz, the 1.6 GeV MAMI-C machine [1] will probably represent the final word in such normal conducting recirculators on our site at the Institut für Kernphysik (cf. Fig. 1). In order to maintain our capabilities for designing complete accelerator systems we tried to identify a follow up project. We suggest to build a small multi-turn superconducting accelerator, offering 100 MeV in energy recovery operation (ERL-mode) and 150-200 MeV for conventional (non-energy recovering) external beam mode (EB-mode). The ERL option, as a new feature in Mainz, gives the projects its name: "Mainz Energy-recovering Superconducting Accelerator" (MESA).

It is evident that obtaining a compelling reason for such a machine is related to the potential of realizing specific advantages, such as hitherto unachievable experimental conditions and extraordinary possibilities for efficient project realization. Several advantages of the latter type are available in our case, since for instance a suitable heavily shielded underground experimental area (cf. Fig. 1) is available. Concerning the former prerequisite, we decided NOT to direct the punch line of MESA towards radiation generation, but to look towards particle physics experiments. A first such application has been identified as a "Pseudo internal target" experiment using ERL-mode [2] in order to do explorative searches for hitherto unknown gauge bosons [3]. The second experiment is a parity violating electron scattering experiment with spin-polarized beam using EB-mode [4]. A third unique feature of MESA would be to investigate beam dynamics in a superconducting multi-turn ERL environment, which should provide valuable input for large-scale projects such as eRHIC or LHeC. Last, but

probably not least, MESA as a small, but ambitious, project creates an ideal environment to attract and to educate young students in accelerator physics.

On June 15, 2012 the Deutsche Forschungsgemeinschaft (DFG) decided to give financial support for the MESA project within a "cluster of excellence" named "Precision physics, fundamental interactions and structure of matter (PRISMA)". This means that detailed design work with a scope to realize the project within the next 5-6 years can now begin. The conceptual work done so far is presented in the following sections.

4.13.2 **General Layout**

MESA will be located in the areas which are presently in use for the PVA4 experiment, being finalized in 2012. We will have 3 halls available: 2 experimental halls and a stretch of the MAMI beam line tunnel. The 600 m^2 floor-space, albeit very small, is sufficient for installation of MESA while still leaving one hall for experimentation. The low beam energy allows significant space reduction with respect to experiments at MAMI energies, which may very well compensate for the loss of about half the space in comparison to the existing experiments. All halls are heavily shielded towards the other areas and against each other by concrete walls of 2.5 - 3 meter thickness. This allows independent accessibility of accelerators and experiments. We therefore envisage independent and parallel operation of MESA and MAMI –a highly desirable feature since the research program of the latter is presently foreseen to continue for more than ten years. Furthermore, a separate room with a high power beam dump is available and will be used for the EB-mode experiments. The 12 meter below surface areas can be accessed by a 7×5 meter wide shaft, so that transportation of heavy and/or bulky loads for experiments or accelerator can be considered as feasible. A 140 l/hour Helium liquefier which can expanded towards 280 l/h with modest investment is already installed near the site.

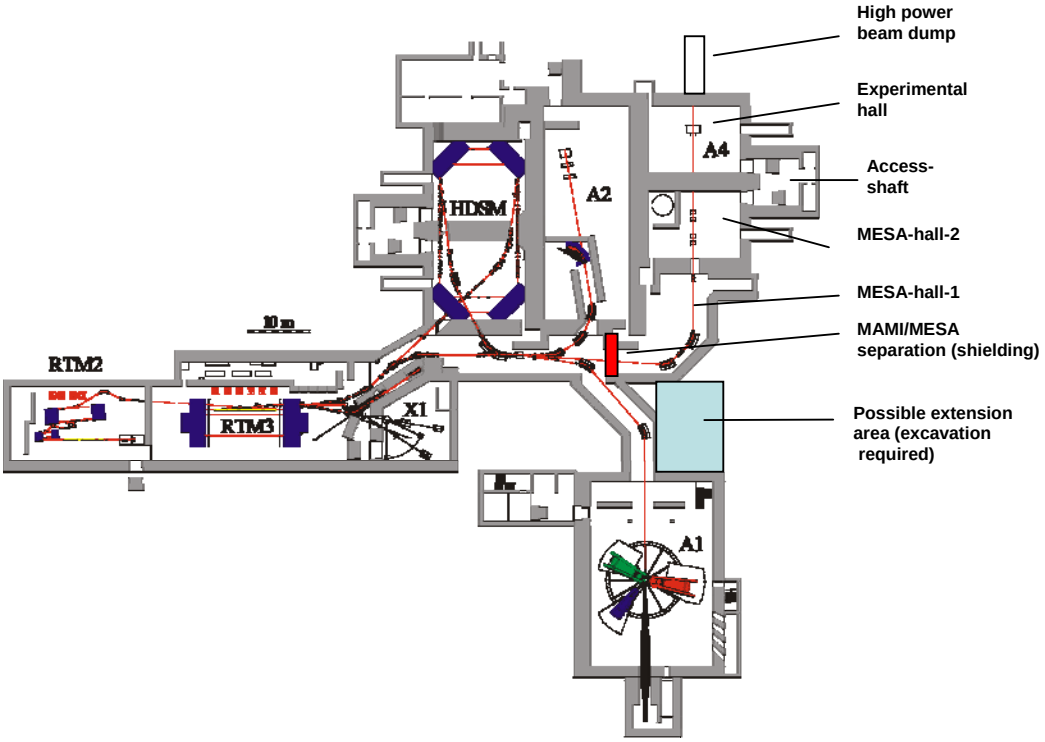

Figure 1: Floorplan of underground areas at Mainz indicating the existing MAMI machine and the place foreseen for MESA.

In order to pursue a timely start of the particle physics experiments, MESA is foreseen to be erected in two stages, whose parameters can be found in Table 1. In stage-1, the superconducting main Linac is supposed to give 50 MeV energy gain from 2 Rossendorf-like cryomodules [5]. Since such modules do not allow for very high average current we foresee to change towards more heavily HOM-damped structures in stage-2.

Table 1: MESA parameter set for stage-1 (stage-2)

Beam Energy ERL/EB [MeV]	105/155 (105/205)
Operating mode	1300 MHz, c.w.
Source type	Photosource d.c. 100keV, polarized (Photosource 200keV, non-polarized)
Bunch charge EB/ERL [pC]	0.15/0.77 (0.15/7.7)
Norm. Emittance EB/ERL [μm]	0.2/<1 (0.2/<1)
Beam polarization (EB-mode only)	> 0.85
Beam recirculations	2 (3)
Beam power at exp. ERL/EB [kW]	100/22.5 (1000/30)
Total R.f.-power installed [kW]	120 (160)

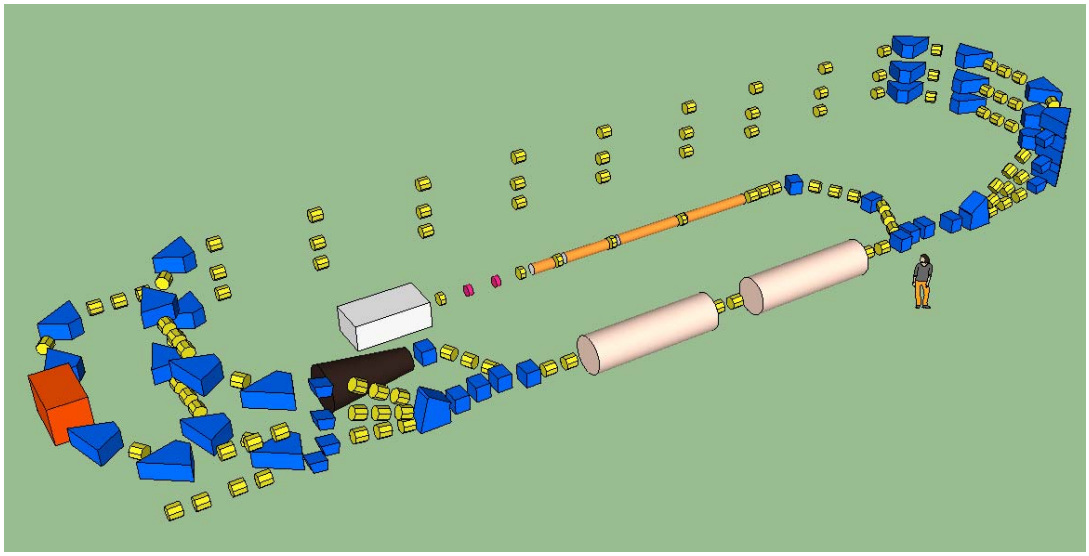

Figure 2: MESA with three-fold recirculation (stage-2, 200MeV in EB mode). The red cube indicates the position of the PIT in the second recirculation at 100 MeV in ERL-mode. The beamline elements (quadrupoles) in the lower left corner point towards the position of the EB parity-violation experiment.

4.13.3 **Subsystems**

4.13.3.1 ***Sources***

The polarized beam will be produced by an available copy of the photosource installed at MAMI [6]. It will deliver a beam current of 150 μA from a superlattice photocathode with a beam polarization > 0.85. For this very small bunch charge (~0.15 pC), the photocathode gradient and potential (0.9 MV/m and 100 kV) is sufficient to achieve a normalized emittance of about 200 nm for the EB experiment. This source will also be used for the stage-1 ERL mode experiments with currents of up to 1 mA (bunch charge 0.8 pC) where we still expect an emittance below 1 μm. Specific spin rotation systems will be installed in order to provide systematic variation of the spin direction at the place of the experiment [7]. The technical risks of operating the polarized source and the spin rotation systems at voltages greatly exceeding 100 kV have lead to the choice of this injection energy. In order to match the beam to the acceptance, a collimation system and a chopper will be installed for the 100 keV beam. After longitudinal focusing with a harmonic buncher system [8] the beam is accelerated by a normal conducting graded-beta structure to 550 keV. These components will be very similar to the ones used at MAMI, though they will be scaled to the operation frequency of 1.3 GHz.

In stage-2 we will increase the bunch charge to 7.7 pC. This will require a dedicated source. Since experiments with high bunch charge do not require polarized beam, a photosource based on more robust photoemitters such as KCsSb can be employed. First estimations indicate that 3 MV/m gradient and 200 kV potential are sufficient to achieve an emittance < 1 μm. Such a source would probably be based on the recent success of “inverted” designs [9] which are reasonably compact to be stacked onto a

350 kV acceleration column – a similar system was used for a very long time at the MIT/Bates LINAC [10]. The emerging 550 keV beam would be injected behind the graded-β used for the polarized beam, hence allowing to maintain the polarized beam option.

4.13.3.2 *Injector*

We will use a normal conducting injector based on the on-axis coupled biperiodic structure developed for MAMI [11]. These structures are designed to run with high average current, since HOM excitation is suppressed. Stable operation has already been demonstrated with > 9 mA average current in the linac of the RTM-3 recirculator of MAMI-B. We will scale the structures to 1.3 GHz operation. Following the design of the MAMI-injector, the graded-β structure will be followed by a structure with two half structures with individual β-values. Two β=1 structures will boost the injector energy to 5 MeV. The total r.f. power needed is ~ 130 kW resulting from 80 kW for the ohmic losses and 45 kW beam loading.

In our baseline design we favor the n.c. solution over an SRF-booster for two reasons. Firstly the reliable and proven technology combined with the in-house knowledge reduces technical risks and complexity. This may allow for considerable shortening of the project timeline. Second, application of a graded-β structure allows for minimum longitudinal phase space distortion. Since the real estate gradient of the normal conducting device is only about a factor 2 lower than present SRF-boosters, we expect also to be able to handle space charge effects for the 8 pC bunch charge in stage-2 operation.

4.13.3.3 *Main Linac*

The cryomodules will operate at ~ 1.8 K, for stage-1 we will use 9-cell TESLA cavities, corresponding to the ones produced for the ELBE accelerator [5]. Compared to the modules presently installed at ELBE the quality factor may be increased by a factor 2-3 to $Q_0=10^{10}$ by applying state of the art preparation techniques developed since then. The sum of dynamic and static losses could allow for, even with our present liquefaction capacity, a gradient of 13 MV/m which yields an energy gain of 50 MeV. Due to their limited HOM damping we expect this set-up to be useful only for currents of up to 1 mA which would nevertheless allow for attractive conditions to start ERL experiments. The EB performance would already be sufficient for the experiments presently envisaged. In stage-2 of the project we may change to modules suitable for higher average currents, which are currently being developed for various accelerator projects, such as the Cornell recirculator, Berlin Pro or for the ERL projects in Japan.

4.13.3.4 *Mergers and Spreaders*

The merger/spreader systems have been designed as a 4 magnet chicanes/dispersion free dogbones, which give sufficient flexibility to merge the four beams at (5, 50, 100 MeV (+150 MeV in EB stage-2)) mode. Another, almost identical merger serves to separate the recovered beam from the recirculated beams. It should be noted that in contrast to light source applications the energy spread of the recovered beam is minimal ($\sim 10^{-3}$), which will make dealing with the recovered beam comparatively easy. The 4 magnet chicane separates the low energy beam horizontally while the dispersion free

dogbones provide different vertical deflection angles to separate the energies into the different recirculation paths.

4.13.3.5 *Recirculations*

The recirculations are stacked vertically above each other. Several deflections systems have been compared with respect to first order beam optics. Presently a system based on 45 degree deflection magnets results in the most attractive parameters. The single sided design allows for separate recirculation straights, which may offer better flexibility concerning investigation of beam dynamics (e.g. BBU) in this multi –turn environment. Concerning flexibility we will also try to work with non-isochronous settings of the recirculations, since this may allow for superior inherent energy stability of this small scale recirculator, if a fractional longitudinal tune is applied [12,13].

4.13.3.6 *SRF Infrastructure*

We will have to design a 2 K cryosystem with the goal to make most efficient use of our existing liquefaction capacity. Concerning installation, maintenance and testing of SRF components we will be able to profit from an investment in university infrastructure by the state of Rhineland palatinate, called the Helmholtz Institute Mainz (HIM). This institute will house clean room facilities with the milder options for surface treatment, such as HPR. Furthermore a bunkered horizontal test stand for SRF cavities will allow for testing of modules independently of activities at the accelerator site.

4.13.4 **Conclusion**

With a considerable initial project funding now available, the MESA project will now be able to gain momentum. This especially means that the project team of presently 4 scientists can be multiplied in order to achieve a CDR until the end of 2013. Especially the beam dynamics concept requires a thorough examination. We expect that final refinement of the individual subsystems will require another year, so that the majority of components can be ordered during 2015. This would allow us to provide first beam for the experiments by the end of 2017.

4.13.5 **Acknowledgements**

This work was supported by the state of Rhineland-Palatinate through the center of excellence “Elementarkräfte und mathematische Grundlagen (EMG)”.

4.13.6 **References**

1. M. Dehn, K. Aulenbacher, R. Heine, H.-J. Kreidel, U. Ludwig-Mertin, and A. Jankowiak, “The MAMI-C accelerator” Eur. Phys. J. Special Topics **198**, 19 (2011).
2. K. Aulenbacher, “Opportunities for parity violating electron scattering experiments at the planned MESA facility” Hyperfine Interactions, **200** 3-7 (2011).
3. H. Merkel, P. Achenbach, C. Ayerbe Gayoso, J.C. Bernauer, J. C. and R. Böhm, R. D. Bosnar, L Debenjak, A. Denig, M.O. Distler, A. Esser, H. Fonvieille, I. Friscic, D.G. Middleton, U. Müller, L. Nungesser, J. Pochodzalla, M. Rohrbeck, S. S\'anchez Majos, B.S. Schlimme, M. Schoth, S. Sirca, M. Weinriefer, “Search for Light Gauge Bosons of the Dark Sector at the Mainz Microtron”, Phys.Rev.Lett **106**, 251802, (2011).

4. F. Maas, "The new Mainz parity violation experiment to measure the weak charge of the proton", Proceedings PAVI 2011 From Parity Violation to Hadronic Structure and more.Rome,September, 5-9 2011 http:// www.roma1.infn.it/pavi11/.
5. J. Teichert, A. Büchner, H. Büttig, F. Gabriel, P. Michel, K. Möller, U. Lehnert, Ch. Schneider, J. Stephan, A. Winte, "RF status of superconducting module development suitable for CW operation: ELBE cryostats" NIM A **557** 239.242 (2006).
6. K. Aulenbacher "Polarized Beams for electron accelerators" Eur. Phys. J. Special Topics **198**, 361-380 (2011).
7. K. Aulenbacher "The polarimeter chain for the PV-experiment at MESA" Proceedings PAVI 2011 From Parity Violation to Hadronic Structure and more, Rome, September 5-9, 2011, http://www.roma1.infn.it/pavi11/.
8. V. I. Shvedunov, M. O. Ihm, .H. Euteneuer, K.-H. Kaiser, Th. Weis, "Design of a prebuncher for increased longitudinal capture efficiency of MAMI" Proceedings of the fifth European Particle Accelerator Conference (EPAC96), Barcelona 1996 1556-1558 (1996).
9. P.A. Adderley, J. Clark, J. Grames, J. Hansknecht, K. Surles-Law, D. Machie, M. Poelker, M.L. Stutzman, R. Suleiman. Load-locked dc high voltage GaAs photogun with an inverted-geometry ceramic insulator. Phys. Rev. ST Accel. Beams **13** 010101 (2010).
10. G. D. Cates, V. W. Hughes, R. Michaels, H. R. Schaefer, T. J. Gay, M. S. Lubell, R. Wilson, G. W. Dodson, K. A. Dow, S. B. Kowalski, K. Isakovich K. S. Kumar, M. E. Schulze, P. A. Souder and D. H. Kim, "The BATES polarized electron source", Nucl. Instrum. Methods A **278** 293-317 (1989).
11. H. Euteneuer, H. Braun, H. Herminghaus, R. Klein, H. Schoeler and T. Weis. "The Injector Linac for the Mainz Microtron" Proceedings of the first European accelerator conference EPAC1988 550-552 (1988).
12. H. Herminghaus, "On the inherent stability of non-isochronous recirculating accelerators" NIM A **314** 209-211 (1992).
13. R. Eichhorn, A. Araz, U. Bonnes, M. Brunken, M. Gopych, H.-D. Gräf, W. F.O. Müller, S. Paret, M. Platz, A. Richter, B. Steiner, S. Watzlawik, and T. Weiland, "Methods to Reduce the Electron Beam Energy Spread at the S-DALINAC" Proceedings Linac 2006, Knoxville, USA 73-76 (2006).

4.14 The Status of the BNL R&D ERL

Ilan Ben-Zvi, Zeynep Altinbas, Dana Beavis, Sergey Belomestnykh, Jin Dai, Leonard DeSanto, David Gassner, Lee Hammons, Harald Hahn, Ady Hershcovitch, Animesh Jain, Puneet Jain, James Jamilkowski, Dmitry Kayran, Nikolaos Laloudakis, Robert Lambiase, Dewey Lederle, Eduard Lessard, Xue Liang, Vladimir Litvinenko, Chuyu Liu, George Mahler, Michael Mapes, Gary McIntyre, Robert Michnoff, Wuzheng Meng, Toby Miller, David Pate, Phillip Pile, David Phillips, Stephen Pontieri, Jonathan Reich, Thomas Roser, Miguel Ruiz Osés, Carl Schultheiss, Thomas Seda, Brian Sheehy, John Smedley, Triveni Rao, Kevin Smith, Roberto Than, Robert Todd, Joseph Tuozzolo, Erdong Wang, Daniel Weiss, Michelle Wilinski, Wencan Xu, Alexander Zaltsman
Collider-Accelerator Department, Brookhaven National Laboratory, U.S.A.
Mail to: mailto: benzvi@bnl.gov

4.14.1 **Introduction**

The Collider-Accelerator Department at Brookhaven National Laboratory is building a high-brightness 500 mA capable Energy Recovery Linac (ERL) (see Fig. 1) as one of its main R&D thrusts towards eRHIC, the polarized electron – hadron collider as an upgrade of the operating RHIC facility. The ERL is in final assembly stages, with injection commisioning starting in October 2012. The objective of this ERL is to serve as a platform for R&D into high current ERL, in particular issues of halo generation and control, Higher-Order Mode (HOM) issues, coherent emissions for the beam and high-brightness, high-power beam generation and preservation. The R&D ERL features a superconducting laser-photocathode RF gun with a high quantum efficiency photocathode served with a load-lock cathode delivery system, a strongly HOM-damped 5-cell accelerating cavity, a highly flexible single-pass loop and a comprehensive system of beam instrumentation. In this ICFA Beam Dynamics Newsletter article we will describe the ERL in a degree of detail that is not usually found in regular publications. We will discuss the various systems of the ERL, following the electrons from the photocathode to the beam dump, cover the control system, machine protection etc and summarize with the status of the ERL systems.

4.14.2 **Photocathode**

It is natural to start the description of the ERL from the photocathode, where the electron beam is born, and where its initial emittance is constrained.

The design of photocathodes for ERLs is one of the key challenges for these machines. In particular, various applications, like X-ray sources and hadron cooling require very low transverse emittance electron beams from the cathode as well as high Quantum Efficiency (QE) at visible wavelengths. This latter requirement is driven by the need to have efficient transverse and longitudinal pulse shaping and by the desirability of using compact and efficient laser sources, such as fiber lasers as the excitation source. To meet these requirements, we have been working on green sensitive, low emittance and highly efficient photocathodes based on K_2CsSb in collaboration with Stony Brook University and Lawrence Berkeley Laboratory. Some of the results were reported [1] on their fabrication, QE, transverse emittance and robustness under laser illumination and exposure to contamination that might be expected in a photo-gun. To briefly summarize our results, the maximum QE reached was typically 6% at 532 nm. We find a 50% decay time for QE at 532 nm to be around 17 hours for water partial pressure of $2x10^{-9}$ mBar. As the partial pressure of water in the superconducting RF gun is vanishingly small, the cathode lifetime given by residual vacuum is quite acceptable. In addition, when illuminated with a laser focused to a spot diameter of 100 μm, a current density of 100 mA/cm^2 could be maintained without deterioration over the course of a measurement lasting several days. Finally, we measured a thermal emittance of 0.37 microns / mm-rms at 532 nm laser wavelength.

In addition to the multi alkali photocathode, the collaboration also carries out R&D on Diamond Amplified Photocathodes (DAP). We will not elaborate here on this subject but provide references for the interested reader [2].

Insertion of photocathodes in the ERL superconducting RF electron gun presents special challenges. The cathode system includes a preparation chamber and two cathode transporters making up a “load-lock” system.

The purpose of the photocathode deposition and transport system is to produce a robust, high yield multialkali photocathode away from the injector complex and have a method of transporting the multialkali photocathode for insertion into a super conducting RF electron gun. This process is only successful if the high quantum efficiency is maintained during the transport and insertion in the SRF electron gun,. One important element in producing and maintaining a high QE multialkali photocathode is maintaining the strict vacuum requirements of 10^{-11} torr. We have developed several multi-alkali deposition systems for a number of years. Our third generation system is a load-lock system, comprising a preparation chamber and transport carts, designed and produced by Advanced Energy Systems Inc. of Medford NY (AES), modified and adapted by BNL.

There are certain design criteria and principles required. One must be able to install, remove, rejuvenate and replace a cathode without exposing the source or cathode to atmosphere. The system must allow one to deposit Cs, K, and Sb on a cathode tip surface at pressures in the 10^{-10} torr range. The cathode needs to be heated to as high as 850 degrees C for cleaning and maintained at 130 degrees C to 150 degrees C during deposition. There should also be the capability for in-situ quantum efficiency (QE) measurements. Finally the transport cart must be mobile and be able to negotiate the ERL facility labyrinth, couple to the SRF gun and insert the cathode into the gun.

4.14.3 **Laser System**

The laser systems of the ERL comprise of two lasers, one for a high bunch-charge, low repetition rate of 9.38 MHz and the other for low bunch charge of 0.7 nC but a high rate of 703.5 MHz, designed to reach 500 mA in the ERL. The high repetition rate optical fiber 35-watt laser designed and built by Aculight needs some repair and is not yet commissioned, so the following detailed description is for the first laser.

Operation of the photocathode gun in the ERL requires that a tightly controlled optical pulse train, consisting of temporally and spatially shaped pulses, be delivered at the photocathode in synchrony with the RF field in the gun cavity. The pulse train must also be dynamically variable, in order to tune or ramp up the current in the ERL. A laser was developed especially for this task by Lumera Laser GmbH, of Kaiserslautern Germany, under design supervision and review of the ERL project. Following the final design review, the laser was delivered in August 2009. Tests certifying its compliance with design specifications have been performed. The development of the necessary spatial and temporal shaping techniques is an ongoing project: proof-of-principle experiments have been successfully carried out with a laser of similar pulse width, operating at 532 nm and 81.5 MHz. A transport line has been designed and built and the propagation of a shaped pulse through it to the photocathode simulated and tested experimentally [3]. As the performance of the complete photocathode drive system is critical for ERL operation, an extensive set of diagnostics will be in place to monitor and maintain its performance. The repetition rate of 9.38 MHz is the 75th subharmonic of the RF frequency of the gun and accelerating cavity, 703.5 MHz. Synchronization with the RF field in the gun is extremely important; asynchrony impacts beam energy fluctuations, emittance, energy recovery, and ultimately overall stability. The total jitter must be less than 1 psec rms. Timing requirements also include the ability to ramp up the repetition rate of the laser while maintaining synchronization, in order to run the ERL at low repetition rate while tuning up, and ramp up its current in operation.

The optimal width of the optical pulse at the photocathode is much longer than the 10-12 picoseconds specified for the laser. The pulse shape of the drive pulse is optimally flat-topped, and the specified width for the nominally $sech^2$-shaped pulse from the laser was chosen to obtain, within the constraints imposed by this type of mode-locked laser, an adequately short rise and fall time in the photocathode drive pulse produced by the shaping methods described below. Similarly, the mode quality specification is driven by the mode requirements of the spatial shaping techniques. The total power requirement of 10 W at 532 nm fits a maximum ERL current of 50 mA. This current would require ~6 W of 532 nm light delivered at the photocathode, at the conservative quantum efficiency of 2%, leaving over a four-watt margin to cover losses in shaping, transport, and diagnostics, and to compensate for less than optimal quantum efficiency.

The Seeder is a mode-locked Nd:YVO4 oscillator, end-pumped with 25 W of 808 nm light, which is fiber-coupled in from diodes located in an off-board power supply. A semiconductor saturable absorber mirror (SESAM) is used for mode-locking. A White-cell multipass configuration is used to achieve the long path length required for the low, 9.38 MHz repetition rate. This is a cavity folding technique which uses a cell comprised of three mirrors of identical curvature that repeatedly image the spot to the mirror surface, each time with a small displacement, so that the beam ultimately exits the cell after a large number of traversals.

An isolation stage and a Nd:YVO4 power amplifier follow the oscillator. The 100 watts of pump light is brought in by fiber. The 2.2W, 1064 nm output of the oscillator is amplified to 20 W in the amplifier. A pulse picker follows, enabling us to select single pulses or groups of pulses at burst rates up to 1 kHz, with up to 90% duty cycle. Continuous operation at the full 9.38 MHz is also possible. The selected optical pulses are then passed sequentially through the second harmonic generation (SHG). The conversion efficiency is ~ 50% for the SHG.

The laser output will be shaped transversally by a π−shaper and longitudinally by pulse stacking. Space is too constrained to allow more detail here. We have simulated and tested both methods on another laser and plan to implement it in the ERL laser.

4.14.4 **SRF Electron Gun**

4.14.4.1 ***Introduction to the SRF Gun***

The SRF gun is a half-cell cavity that is designed to deliver 0.5 A at 2 MeV with 1 MW of CW RF power. It incorporates a double quarter-wave (QW) choke joint cathode insert, a pair of opposing fundamental power couplers (FPC), a high-temperature superconducting (HTSC) emittance compensation solenoid and damper of Higher Order Modes (HOMs) [4].

The design of the gun must balance good beam dynamics for high charge bunches with damping of HOMs and a good geometry for the peak surface fields.

Among the challenges for this device are achieving the high RF coupling (external Q of 40,000) without excessive FPC probe penetration, while engineering a compact cavity configuration that addresses the high-power thermal issues. The coupler port and entire liquid helium vessel underwent significant adjustment to increase the coupling. Another challenge, possibly the largest, is the introduction of a removable cathode and choke joint that yields adequate cathode lifetime, avoids cavity contamination when using the baseline multialkali cathodes and avoid multipacting that cannot be

conditioned. Yet another challenge - an emittance compensation solenoid has to be inserted close to the gun in the cryostat, but one that keeps the field on the superconductor low enough. Finally, the HOM power has to be drained from the gun cavity to avoid cryogenic losses or emittance dilution.

4.14.4.2 *The Cavity Design*

The cavity iris had to be made small for beam dynamics reasons (reduction of effective length of the cavity).

At a beam pipe diameter of 10 cm, the same as the iris of the cavity, most of the HOMs propagate adequately to the load. Analysis shows that the three remaining modes do not affect the gun performance [4]. The reduced beam pipe size simplifies the strong coupling of the 1 MW RF power to the beam and reduces the size of the exit vacuum valve.

The cavity was fabricated utilizing both RRR-300 Nb sheet and ingot material. This was necessary as the back surface of the cavity and the base of the choke joint region needed to be machined from one piece to ease the welding and fabrication processes, as well as to produce a cavity that could be built and inspected as required by the ASME code. The helium vessel for the cavity is titanium, which is then surrounded by multi-layer super-insulation and then two layers of mu-metal magnetic shielding with a liquid nitrogen shield in between them and then the space frame, which supports all of the aforementioned structures. The ballast tank is then be installed over the cavity, insulated and lowered into the rectangular vacuum vessel.

4.14.4.3 *The Cathode Insertion System*

The cathodes are deposited on the tip of an insert. The insert can be moved from the cathode preparation system to the gun. The insert has a triple choke-joint design to allow thermal isolation of the cathode insert from the gun body while sealing the RF currents. The choke joint innermost conductors are grooved. This grooved design reduces significantly the strength of multipacting in the choke joint. The cathode insert is introduced into the gun beam-line vacuum through a pair of gate-valves, one on the transport cart and one on the gun cathode-side line. Once the insert is near its correct position, a special fork is motor-driven to grab the insert and press it with a pre-determined load to its exact final position, making the RF seal between the insert's choke joint and the gun body. The fork motor and gear is located in the insulating vacuum, to avoid the introduction of particulate matter into the gun.

4.14.4.4 *The Fundamental Power Couplers*

One of the key features that required extensive analysis was the FPC and the shape of the tip of the antenna. After several iterations it was decided to use an antenna tip that matched the radius of the beampipe of the injector. This "pringle" tip provides a very nice way to achieve the desired Q external of the FPC ($4x10^4$) while not penetrating the beampipe more than 2 mm.

The FPCs were conditioned before installation in the gun on a special stand, which allowed us to expose them to 125 kW CW and 250 kW pulsed power in standing wave with a variable reflection phase. Various multipacting regions were encountered and processed completely [5].

4.14.4.5 *High Temperature Superconducting Emittance Compensation Solenoid*

The final key item is the high temperature superconducting solenoid that is being placed at the end of the cavity to help focus the electron beam on its way to the accelerating cavity. This solenoid has been designed and built by Ramesh Gupta and the Superconducting Magnet Division at BNL and has already undergone its acceptance testing. The solenoid is designed to provide a field of 0.014 Tesla (integral of field squared 0.001 meter Tesla squared) while keeping the stray fields that reach the cavity to below 10 mGauss. This has been accomplished by using a bucking coil adjacent to the primary coil, and by moving the magnetic shielding in between the solenoid and the cavity. The coils are made with a tape of the HTS material Bi2223 with spiral wrapped Kapton insulation. A detailed description of both the solenoid design and the simulation data can be found in the reference [6].

4.14.4.6 *The Higher Order Mode Damping*

The gun propagates all but 3 of the HOMs down the beam pipe to a room temperature ferrite HOM absorber. The three trapped modes can be easily missed by harmonics of the beam repetition frequency and detailed calculations [4] have shown that the effect of long range wake fields can be neglected if the beam amplitude and phase noise are under a reasonable limit. In addition, it has been shown that the strong coupling of the fundamental power couplers damps these modes [7].

The HOM analysis for this cavity was carried out using ABCI and later by CST Microwave Studio. The total HOM power dissipated by a 500 mA, 1.4 nC beam was calculated to be ~ 0.5 kW [4]. Due to the frequency of the injector the harmonics spectrum is fairly sparse and spreads out and avoids overlapping with any HOMs.

4.14.5 **SRF Accelerating Cavity and HOM Damping**

The BNL 5-cell ampere-class cavity was constructed in collaboration with AES and BCP processed at JLab. The BNL design aims to address the most extreme HOM conditions by virtue of its low frequency (703.75 MHz), small number of cells (5) and very good damping of HOMs.

The loss factor of SRF cavities varies considerably from under 1 V/pC up to 10 V/pC, depending on the structure's frequency (the lower the frequency the better), the degree to which the cavity aperture has been maximized (possibly sacrificing some other parameter) and the number of cells (the fewer the better). Beam properties enter in three places: the HOM power is proportional to the average current to the bunch charge, and (through the loss factor, approximately) to the square root of the bunch length. Good damping of the HOM power is important for a number of reasons. First, one has to remove this power from being intercepted at cryogenic temperatures. Second, it will increase the threshold for beam-breakup (BBU) and help to avoid beam quality degradation.

The cavity has very large cavity irises (17 cm diameter) and extremely large beam pipe, 24 cm in diameter. The beam pipe is large enough to propagate all the HOMs to the ferrite HOM loads, which are at room temperature on either side of the cavity. The HOM dampers are commercially available, derived from the Cornell 500 MHz storage ring cavity design. As a result of these design features the cavity is a "single mode"

cavity, all HOMs are strongly coupled to the HOM damper, and the loss factor is very low [8]. The cell shape also enhances mechanical stability.

4.14.6 **Radio Frequency Power**

The Energy Recovery Linac requires two high power RF systems. The first RF system is for the 703.75 MHz superconducting electron gun. The RF power from this system is used to drive nearly half an Ampere of beam current to 2 MeV. There is no provision to recover any of this energy so the minimum amplifier power is 1 MW. It consists of 1 MW CW klystron, transmitter and power supplies, 1 MW circulator, 1 MW dummy load and a two-way power splitter to distribute RF power between two FPCs. The second RF system is for the 703.75 MHz superconducting cavity. As the cavity accelerates the beam to 20 MeV and then recovers this energy, the beam power is nearly zero and the RF system has to provide only power necessary to maintain stable cavity field under various disturbances. It consists of 50 kW CW transmitter, circulator, and dummy load.

4.14.6.1 ***High Power RF***

4.14.6.1.1 The 1 MW System

There are several main equipment groups in this system. The Klystron_tube, manufactured by CPI, is rated to produce 1.0 MW CW at 703.75 MHz. This tube is similar to one produced by CPI for LANL, but the BNL tube does not have a modulating anode. The output of the tube is WR1500.

The klystron characteristics are as following. The collector is grounded, and -92 kV at -17.1 A will produce 1 MW in our tube. While the maximum drive specified for 1 MW is 100 W (40 dB gain), this tube only requires 15.2 W to get full power. The driver amplifier provided has 200 W max output and 52 dB gain. Other tube electrical requirements include the cathode heater, two solenoid circuits, and two 8 l/s vac-ion pumps. These are all controlled and monitored by the transmitter. There are three water cooling loops. The collector requires 380 gpm, and is not temperature controlled. The two body loops are each about 7 gpm, and are temperature controlled. There are two inlets for forced air-cooling of the output window, fed from one 100 CFM blower in the transmitter. The exhaust heat in this air plus the heat put into the air by the air-cooled solenoids and other heat sources must be removed from the radiation enclosure.

The transmitter for the klystron is manufactured by Continental Electronics Corporation. The high voltage power supply (HVPS) is a stack of 96 isolated IGBT gated power supplies in series. Because the IGBTs permit a fast shut down mode, a crow bar is not required to limit the energy in an arc to 40 Joules. The transmitter also contains the support equipment for the klystron, including the filament power supply, two solenoid power supplies, two vac-ion pump controllers, several cooling water monitoring circuits, two air blowers (one for the klystron window and one for a window in the ring), a drive RF amplifier, and a PLC to keep track of everything, including interlocks and monitoring of directional couplers in the system. Electrical characteristics are AC input: 4160 VAC (chosen to match the previous design); DC output: -100 kV at -21 A; filaments: 30 Vrms at 30 Arms, isolated to operate at -100 kV; solenoid power supplies: 30 A at 30 V and 30 A at 300 V. Water circuits include

three at 400 gpm max (collector, RF load, beam dump), and four at 35 gpm max (body, output cavity, circulator, spare).

The HVPS unit is very efficient, as the IGBTs are switched at maximum rate of about 400 Hz. This low frequency is consistent with a high ripple frequency as timing techniques result in a fundamental ripple frequency of almost 40 kHz. The unit is entirely air-cooled.

The klystron is protected by a circulator with a water-cooled termination. This water-cooled dummy load, manufactured by CML Corp, is rated for 1.3 MW of continuous power. It has a WR1500 waveguide input, a ceramic window, and a stand with six-point leveling.

The water-cooled circulator is manufactured by AFT Microwave. It is rated at 1 MW into any port. The center frequency is 703.75 MHz, bandwidth: ±17 MHz. Over this bandwidth the insertion loss is < 0.1 dB, isolation > 20 dB and VSWR < 1.2.

4.14.6.1.2 The 50 kW System

The Thomson ***SIIA*** Scientific and Industrial IOT Amplifier family is adapted from the highly successful, field-proven IOX and DCX family of high power IOT UHF television broadcast transmitter line. This line of equipment has been a world standard in the television broadcast industry. Inductive Output Tube (IOT) utilized in the amplifier is the industry standard for its high efficiency (over 50%). It also provides a gain of 22 to 23 dB with remarkably low phase shift at wide range of output power.

To isolate and protect transmitter from very high VSWR we have installed a 50 kW circulator manufactured by AFT Corporation.

4.14.6.2 ***Low Level RF***

The low level RF system for the R&D ERL (5-cell cavity and RF gun) is a variant of a newly designed digital LLRF controller platform, recently commissioned at RHIC and the Electron Beam Ion Source (EBIS). The central component of the LLRF hardware is a chassis referred to as a "controller". Essentially the controller is a powerful, flexible, software/firmware configurable digital signal-processing platform, adaptable to many tasks. The controller consists of a "carrier" board together with up to six associated "daughter" mezzanine modules, which attach to the carrier via an IEEE standard XMC interface. The carrier serves as a stand-alone network attached control system interface, host platform for the daughter mezzanine modules, communication hub and diagnostic data acquisition engine. Daughter modules provide system specific functionality and signal processing horsepower – an example being a four channel ADC board used to digitize RF signals from a cavity. All boards are custom designed at BNL, based on a common powerful Field Programmable Gate Array (FPGA) family, the Xilinx Virtex-5 FX devices. The Virtex-5 FX FPGA family provides a number of very powerful resources. Depending on the specific version used, there are either one or two hard-core PPC processors available. 16 multi-gigabit serial transceivers provide very high bandwidth communication, and even deterministic data links as needed. Hardware "DSP Slices" provide very high-speed signal processing functionality. Large arrays of programmable logic and static RAM, high speed low jitter clock generation and distribution, very large IO pin count, support for numerous single ended and differential IO standards, and relatively low power dissipation complete a feature list which we exploit to the fullest.

For the R&D ERL, two of these controllers will be integrated into a LLRF control system. To provide ultra low noise LLRF signal processing with absolute synchronism (phase lock) across multiple controllers and daughter modules, the system relies on two key components. First, an ultra low noise 100MHz master clock is distributed to both chassis, and within, to the carriers and daughter modules. This clock has a typical integrated phase noise of < 100 fs rms in a 1 Hz to 100 kHz bandwidth (BW 1-100k). This clock is distributed within the controllers via high-speed differential PECL fan-outs, and on each daughter board is used as a reference clock for a 1600 MHz PLL. This PLL provides a variety of divided output clocks for on board DACs, ADCs, FPGAs, etc., with a typical integrated phase noise of about 140 fs rms (BW 1-100k). The RF DACs used to provide RF drive signals produce carrier signals with phase noise of 170 fs to 200 fs rms (BW 1-100k), when clocked at 400 MSPS.

Second, a multi-gigabit serial link referred to as the "Update Link" and employing the same 100 MHz master clock as a reference, provides a deterministic timing in the form of an encoded "Update Pulse" event occurring every 1000 clock cycles, or at a 100 kHz "Update Rate". This Update Pulse is decoded locally at every carrier and daughter module providing deterministic timing across the system. The Update Link also broadcasts global event and data packets, which if desired can maintain a fixed timing relationship to the Update Pulse via pre-assigned "slotting" within an Update Period. An example of this would be a "Master Reset" event, used to deterministically reset all RF synthesizers to known reference phases.

The combination of these permits a complete LLRF system to be built up from the requisite number of chassis and daughter modules, while ensuring that all sub-components can maintain the desired RF phase relationships.

4.14.7 **Cryogenic System**

The ERL cryogenic system will supply cooling to a super-conducting RF gun and the 5-cell super-conducting RF cavity system that need to be held cold at 2K. The engineering of the cavity cryomodules were carried out by AES in collaboration with BNL. The 2K superfluid bath is produced by pumping on the bath using a sub-atmospheric warm compression system.

The cryogenic system makes use of mainly existing equipment relocated from other facilities: a 300 W 4.5 K coldbox, an 45 g/s screw compressor, a 3800 liter liquid helium storage dewar, a 170 m^3 warm gas storage tank, and a 40,000 liter vertical low pressure liquid nitrogen storage dewar. An existing wet expander obtained from another facility has been added to increase the plant capacity. In order to deliver the required 3 to 4 bar helium to the cryomodules while using up stored liquid capacity at low pressure, a new subcooler has been installed to function as the capacity transfer device.

A 2 K to 4 K recovery heat exchanger is also implemented for each cryomodule to recover refrigeration below 4 K, thus maximizing 2 K cooling capacity with the given sub-atmospheric pump. No 4 K to 300 K refrigeration recovery is implemented at this time of the returning sub-atmospheric cold vapor, hence the 2 K load appears as a liquefaction load on the cryogenic plant. A separate LN2 cooling loop supplies liquid nitrogen to the superconducting gun's cathode tip. The following details the components of the system.

Sub-atmospheric pumping System: An oil injection cooled Roots blower backed by 2 liquid rings pumps is used to pump on the liquid helium bath to produce the 2 K cooling. The system is capable of pumping 5.5 g/s with the bath held at 2 K. The Roots blower is a Tuthill MB5400 belt geared down to 1900 rpm from the 2400 rpm max using a 40 HP motor. The blower is backed by two (2) Kinney KLRC-525 2- stage liquid ring pumps with 50 HP motors. A high to low by-pass valve controls the suction pressure at the pump from dropping below its setpoint. Coalescing element at the discharge of the each liquid ring pump prevents carry over of oil to the discharge line. The vacuum pump discharge will go to the low pressure (suction side) of the main helium plant.

4.5 K Coldbox: The Process Systems International 300 W @ 4.5 K model 1660S built in 1993, has 2 pairs of 3 inch (76 mm) diameter piston expanders, configured as a Collins cycle with liquid nitrogen precooling. The first expansion stage operates at an inlet of 50K, and the second expansion stage at an inlet of ~ 19 K in liquefaction mode.

Wet expander: A 1985 Koch Process System wet expander consisting of a pair of 2 inch (50 mm) diameter piston has been added to the system, providing an additional 0.7 g/s liquefaction capacity to the plant.

Main compressor: The main helium compressor is a 1975 Sullair C20LA4.8-400HP screw compressor, complete with bulk oil separator. The oil demisting system consists of 2 parallel banks of 4 Balston coalescing elements in series: DX, BX, BX, BX. A 18 inch diameter charcoal bed is used for oil vapor removal. Flow throughput of the compressor is 45 g/s @ 1.05 atm.

Liquid helium inventory: Liquid helium inventory will be stored in an existing 3800 liters liquid helium storage dewar manufactured in 1992 by Cryofab. The dewar has 3 liquid fill and one vapor line as interface.

Gas Storage Tank: An existing 170 m^3 warm gas storage tank is used for inventory storage when the system is warm.

Subcooler: Because helium at 3 to 4 bar is required for the intercept flows in the cryomodules, the plant's high pressure flow is used to supply the cryomodules, instead of low pressure liquid from the storage dewar. The subcooler serves to condition the plant's warmer liquid helium to 4.5 K and simultaneously serves to use-up liquid inventory from the main low-pressure storage dewar.

5-cell valvebox: A valvebox containing the 2 K to 4 K recovery heat exchanger, top fill valve, cooldown/fill valve, vapor return control valve and equalization valve between the cooldown line and vaporspace provides helium to the 550 liters reservoir above the cavity cryostat.

5-Cell Cryostat and Reservoir: A 550 liter reservoir, above the 5-cell cavity allows the system to operate for a while without filling with liquid helium from the cryogenic system. This will allow the subatmospheric pump to handle the maximum heat load when required. 4 intercept circuits using 3 bar liquid helium to intercept the 2 beam tube

cold to warm transitions, and fundamental power coupler outer conductor, and tuner mass cooling are returned after warming to room temperature using electric heaters, to each thermal mass flow controller located outside the radiation blockhouse. The cryostat also has a liquid nitrogen cooled shield that surrounds the cavity.

SRF Gun valvebox: This valvebox contain the helium vapor return control valve, liquid nitrogen cooling loop for the cold cathode head. The liquid nitrogen cooling loop consists of a phase separator to provide liquid to the cathode head, and the returning 2 phase flow is returned, except for the flex line section, in a coaxial arrangement to intercept the heat leak and keep the supply line liquid nitrogen from generating vapor. The returning flow is vaporized with a heater, followed by a flowmeter to monitor flow through the cathode. A machine protection interlock is provided by this flowmeter when the flow stops through the cathode head.

SRF Gun Cryostat: A 150 liter reservoir, located above the gun cavity, allows the system to operate for a while without filling with liquid helium from the cryogenic system. This will allow the subatmospheric pump to handle the maximum heat load when required. 5 intercept circuits flows, using 3 bar liquid helium to intercept the two beam tube flanges, the two fundamental power coupler outer conductors, and the HTS solenoid are returned after warming to room temperature using electric heaters, to each thermal mass flow controller located outside the radiation blockhouse. The cryostat also has a liquid nitrogen cooled shield thst surround the cavity and helium reservoir.

The expected loads and consumption of the system follows below.

Liquid nitrogen consumption: 5-cell Cavity/Ballast Tank, 14 l/hr; SCRF Gun, 6 l/hr; Gun Cathode, 20 l/hr when powered; 1660S Coldbox, 70 l/hr.

2 K liquid helium heat load: 5-cell cavity, 6 W static, 40 W dynamic; 5-cell LHe reservoir, 2 W; 5-cell J-T valve, 6 W; Gun cavity, static 8 W, dynamic 7 W; Gun LHe reservoir, 3 W; Gun J-T valve, 3 W.

5 K, 3 Bar LHe flow: 5-cell cavity FPC, 0.075 g/s; 5-cell beamtube transitions, 2 x 0.075 g/s; Gun end flanges 2x 0.075 g/s and solenoid, 0.075 g/s; Gun FPC 2 x 0.075 g/s.

With a 2 K load of at least 75 W, the vacuum pump flow will be 4.3 g/s, and with approximately 0.8 g/s liquefaction load from the intercepts, the total liquefaction demand load is 5.1 g/s, which is higher than the net 3.0 g/s liquefaction capacity of the plant. The additional 2.1 g/s capacity will come from the low pressure storage dewar, using the subcooler as the transfer device.

With 2000 liters reserve, the system can operate 24 hours, before stopping. If the cavities operate at the full capacity of the vacuum pump, 5.5 g/s, then the total demand is 6.3 g/s. The run time becomes 16 hours.

Reliquefaction of the equivalent of 2000 liquid liters from warm storage while keeping the cavities cold at 4.5K requires 50 hours.

4.14.8 **Magnets and Optics**

One of the critical parts of the ERL is the merger of the low-energy and high-energy beams. The injection energy is not recovered. A low injection energy requires less RF power and lowers dumped beam energy. The original emittance compensation scheme does not include any dipoles between RF gun and linac (or booster cavity). In the R&D ERL the novel emittance preserved merger system will be tested for the first time. As a result of beam dynamics simulation the R&D ERL injector is expected to provide electron beam 0.7 nC of charge and equal normalized emittances in vertical and horizontal planes 1.4 mm-mrad [9].

The lattice of the ERL loop controls the parameters of a symplectic transport matrix, which affect the stability and operation conditions of the ERL. The lattice of the loop is intentionally chosen to be very flexible for the R&D ERL to be a test-bed of new ampere-range of beam currents in ERL technology. The adjustable part of the lattice has two arcs and a straight section. Each arc is an achromatic with adjustable longitudinal dispersion value from + 1 m to - 1 m. Quadrupoles in the dispersion-free straight section provides for matching of the end quadrupoles. These quadrupoles will be used for conducting the transverse beam break up studies. The simulation for normal operation of R&D ERL shown that BBU threshold current is in the level of 20 A.

In order to change the returning path length one of the 180 degrees arc is movable to/from the main Linac by 1/8 of RF wavelength (6 cm). By changing the path length ERL can operate in normal CW energy recovery mode as well as more exotic modes: double acceleration and three passes through the Linac. More details about R&D ERL optics can be found [10].

The return loop magnets are of traditional design with the following exceptions:

a) The bending radius of the 60^o dipole magnets is 20 cm, which is rather small. We use 15^o edges on both sides of the dipoles to split the very strong focusing evenly between the horizontal and vertical planes (so-called chevron-magnet).

b) The requirements on field quality of the loop's quadrupoles had been determined by the requirement to preserve a very low normalized transverse slice emittance of electron beam ($\varepsilon_n \sim 1$ mm-mrad). We used direct tracking of a sample electron beam to verify a high degree of the emittance preservation.

c) Each quadrupole is equipped with a dipole trim coil, which can be also used to excite a sextupole component, if required, for emittance preservation of e-beam with a large energy spread.

One of the unique features of all ERLs is the necessity for merging low and high-energy electron beams. In the R&D ERL, 2 MeV from the SRF gun merges with the 20 MeV electron beam coming around the return loop into the same trajectory at a position within the SRF linac. In the linac, injected bunch is accelerated to 20 MeV, while the returned or "used" bunch is decelerated to 2 MeV. The challenge for a merger design is to provide conditions for emittance compensation and also for achromatic conditions of a low energy, space-charge dominated electron beam. The scheme that satisfies these requirements (called Z-bend) is used on the R&D ERL [9]. The Z-bend is approximately 4-meter long. It bends the beam trajectory in the vertical plane. It is comprised of four dipole magnets designed to be equally focusing in both planes, with bending radius ~ 60 cm, and bending angles of $+ 15^o$, $- 30^o$, $+ 30^o$ and $- 15^o$. The beam dynamics in the Z-bend results in a large-size (centimeters) near-laminar electron beam. The large beam size and very low slice emittance of the e-beam dictates the tolerances

on the magnetic field to be very tight. The integrated nonlinear kicks should not exceed ~ 20 micro-radian per magnet at a typical radius ~ 1 cm. The magnets in the Z-bend are rather short (15 cm effective length for the 15^o magnet) and have a rather large aperture of 6 cm. Analysis predicts that the influence of various field components on the emittance growth are complicated by the fact that the beam trajectory bends significantly in the fringe fields. Hence, we decided to use direct tracking in the calculated fields extracted from Opera3d of test beam to evaluate and to minimize influence of magnetic field on the beam emittance.

All R&D ERL magnets were designed using Opera3d for 3D magnetic field calculations as well as the influence of geometric tolerances on the field quality [11].

All four dipole magnets (15 and 30 degree) used at the merger have a rather complex window-frame design with parallel edges, constructed with four coil sets (vertical dipole, main quadrupole, small sextupole coils in the corner, and horizontal correction dipole, wound with the quadrupole coils). The quadrupole coil is used to split the focusing strength equally between the planes, while the main dipole coil is designed to create both dipole and sextupole components of the field which is necessary for emittance preservation. The amount of the sextupole component is controlled by the gap between the yoke and the main dipole coil. A small additional coil in the corners is a sextupole trim coil. Magnetic measurements of the ERL magnets employed both rotating coil and Hall probe array mapping.

The Hall probe array comprises of four Group3 Hall probes spaced by 10 mm. The relative centers of the probes are measured in a quadrupole with accuracy of a few micrometers. The hall probe array is calibrated against an NMR probe in a test dipole. Overall accuracy of the magnetic field measurements is ~ 0.03 %, while relative accuracy of the rotating coil measurements is better than 50 ppm.

We used direct tracking of 2,000 particles in the 3D magnetic field, which calculated by Opera3d/Tosca. For the Z-chicane dipoles we used initial distribution of electron with kinetic energy of 2.77 MeV and transverse radius of 1 cm. These particles were tracked from the center of the magnet to far (0.5 m to be exact) outside the magnet using Opera-3d Post-processor with the step of 1 mm. The output file contains all 3D position and velocity components at each step. Another program was used to translate these components to a local coordinate system, which was defined by the final position and momentum of the central ray. These results led to the extraction of the final phase space distribution (x, x', y, y'). This data was then analyzed using various programs and the next iteration of the magnet design was processed.

One of the tools used was the expansion of angles of the trajectory (x',y')out far from the magnet exit as function of initial coordinates (x,y)in. Since the trajectories are strongly curved, these expansions do not have clear harmonic content (for example x2 and y2 terms have different coefficients). Therefore we had used the increase of the beam emittance as a figure of merit, while using coefficients in second and third order expansions as guidance.

All the ERL magnets are accurately CNC machined and installed on similarly machined bases. Within each base there is no provision for alignment, the CNC machining achieves tolerances better than a survey procedure.

A portion of the ring is mounted on a movable gantry with a total stroke of 10 cm, to allow phasing of the return beam to various values.

The Ring Arc Dipoles gap is 3 cm with a central field of 3.3 kGauss. The magnetic length is around 19 cm with a field quality of sextupole b3 to dipole integral ratio

approximately equal to $1.2x10^{-4}$ at a radius equal to 1 cm and the quadrupole ratio required is about 2.1 %.

The Ring Quadrupoles have a required gradient of 0.3 kGauss/cm. Pole diameter aperture is 6 cm, with a tip field of approximately 900 G and magnetic length of about 16 cm. The field quality 12-pole integral ratio is $1.6x10^{-4}$ at a radius of 2.5 cm.

The injection 30-degree z-bend Dipole/Quad combined magnet has a half-gap of 3.644 cm and is designed to minimize the b3 sextupole component. The central field is 191.3 G with a magnetic length of approximately 29.6 cm. The field quality has an integrated sextupole ratio of $4x10^{-4}$ and octupole ratio of $3x10^{-4}$ at a radius of 1.5 cm.

The injection 15-degree z-bend Dipole/Quad combined magnet has a half-gap of 3.544 cm and is designed to minimize the b3 sextupole component. The central field is 145.1 G with a magnetic length of approximately 19.2 cm. The field quality has an integrated sextupole ratio of $2.3x10^{-4}$ and an octupole ratio of $1.3x10^{-4}$ at a radius of R=1.5 cm.

The solenoid pair is designed with a peak field of 984 G, assuming a separation of 5 inches steel to steel or 9.5 inches center to center. Maximum coil current is 8.4 amps at a maximum voltage of 13.4 volts.

The Quadrupole Doublet used in the arc has a required field gradient of 58 Gauss/cm. The field quality, assuming all coils are powered, has an integrated octupole ratio of $5.3x10^{-4}$ and a 12-pole ratio of $4.1x10^{-4}$.

4.14.9 **Power Supplies**

The magnet assemblies used in the ERL consist of one or more windings on a common core. Each of the windings represents a separate magnet load for the power supply. As the ERL is operated in a DC fashion, interaction between the windings is not a concern. Some of the coils are connected in series. The connection scheme, plus cabling provides the electrical load characteristics. The load information, plus the operating current, and the stability define the power supply requirements.

Five different models can satisfy all of the magnet power supplies requirements for the ERL. The capsule specifications and quantities are listed below:

- One IE Power model UD320A35V, 35V, 320A, 100 ppm,
- Thirty four Danfysik Shim Amplifier 892, 15V,10A, 100 ppm,
- Five Kepco model BOP 50-20GL, 50V, 20A, 100ppm,
- Thirty two BiRa model MCOR12 / 2A, 25V, 2A, 100 ppm,
- Six BiRa model MCOR12 / 6A, 25V, 6A, 1000 ppm.

With the exception of the UD320A35V unit, all models are bipolar, even though not all loads require bipolar operation. But, by using standard off-the-shelf units, development costs were minimized.

4.14.10**Vacuum**

The ERL has a number of vacuum volumes with various sets of requirements. These are the superconducting RF Cavity, superconducting electron-gun, injection region, ERL loop, beam dump and laser transport line.

The beamline vacuum regions are separated by electro-pneumatic gate valves. The beam dump is common with loop beamline but is considered a separate volume due to geometry and requirements. Vacuum in the 5-cell SRF cavity is maintained in the ~ 10^{-9} torr range at room temperature by two 20 l/s ion pumps and in the electron-gun SRF cavity by one 60 l/s ion pump. Vacuum in the SRF cavities operated at 2ºK is reduced to low 10^{-11} torr via cryopumping of the cavity walls. The cathode of the electron-gun must be protected from poisoning, which can occur if vacuum adjacent to the electron-gun in the injection line exceeds 10^{-11} torr range in the injection warm beamline near the electron-gun exit. The vacuum requirements for beam operation in the loop and beam dump are 10^{-9} torr range. The beamlines are evacuated from atmospheric pressure to high vacuum level with a particulate free, oil free turbo-molecular pumping cart. 25 l/s shielded ion pumps distributed throughout the beamlines maintain the vacuum requirement. Due to the more demanding vacuum requirement of the injection beamline proximity to the electron-gun, a vacuum bakeout of the injection beamline is required. In addition, two 200 l/s diode ion pumps and supplemental pumping provided by titanium sublimation pumps are installed in the injection line just beyond the exit of the electron-gun. Due to expected gas load a similar pumping arrangement is applied at the beam dump. The cryostat vacuum thermally insulating the SRF cavities need only reduce the convective heat load such that heat loss is primarily radiation through several layers of multi-layer insulation and conductive end-losses which are contained by 5ºK thermal transitions. Prior to cool down rough vacuum ~ 10^{-5} torr range is established and maintained by a dedicated turbomolecular pump station. Cryopumping by the cold mass and heat shields reduces the insulating vacuum to 10^{-7} torr range after cool down.

The superconducting cavities are processed in particulate free environments to achieve the highest gradient possible. Particulates must also be eliminated from adjacent components of the injection and loop beamlines to avoid particulate migration into the SRF cavities. The particulate free requirement of beamline components represents the most challenging aspect to meeting the beamline vacuum requirements. A significant effort is focused on developing particulate free capability. Procedures and an on-site clean room processing facility at BNL were developed for processing new beamline components and QA of particulate processed components supplied by outside sources.
The laser beam travels from the laser room to the photocathode through a transport line consisting of evacuated tube sections and a series of mirrors and lenses prior to entering the ERL injection beamline. Laser transport vacuum is established with a mechanical pump, maintained with a small ion pump and monitored with a vacuum gauge.

Pressure relief to protect both personnel and equipment has been incorporated into the warm and superconducting beamlines to meet the requirements of Section VIII of the Pressure Vessel and Boiler Code. Relief devices include spring-loaded plates for cryostats and burst diaphragms for the beamlines. The SRF pressure relief devices are installed on the warm ends of the SRF strings. Cryostat and SRF beamlines relief devices are plumbed into vent headers to prevent an Oxygen Deficiency Hazard (ODH) condition in the ERL experimental area. Burst diaphragms installed on warm beamlines are vented directly into the experimental area because failure modes and conditions indicate an ODH 0 level can be maintained and the complexity of routing extra vent headers can be avoided.

The electron loop environment is entirely room temperature. The beamline is composed of dipole and quadrupole magnet chambers, drift chambers and various beamline components. Vacuum components include ion pumps, gauges and valves. All

magnet chambers are made from non-magnetic materials to adhere to the strict magnetic field requirements. Dipole magnet chambers are made from aluminum. Ease of machining and low outgassing rates when processed properly are added benefits of using aluminum. Results of outgassing measurements performed with a baked first article aluminum dipole chamber reveal rates of low 10^{-12} torr·liter/sec·cm^2. This result compares favorably with clean, baked stainless steel material. The dipole chambers were built by Atlas Technologies.

Dipole chambers are machined as half cores and externally welded together. The weld is not full penetration to keep the chamber inner surface smooth. The proprietary weld prep maintains a smooth chamber ID profile without trapping volume. Atlas explosion bonded bimetal Conflat type flanges are welded to the chamber assembly allowing standard Conflat gasket and hardware to interconnect mating beamline components.

Chambers passing through quadrupoles are made from inconel tube. The magnetic permeability of the quad chamber inconel beam tubes is less than 1.01. The remainder of the quadrupole chamber is made from 304L stainless steel. Hydroformed bellows that form part of each quadrupole chamber are made from inconel. The quadrupole chambers were built by MDC.

Vacuum gauging and pumps are all mounted on crosses at the end of quadrupole beampipes. In addition button beam position monitor (BPM) cubes are integrated with the quadrupole chambers. BPM buttons are installed in the cubes. The BPM cube incorporates the primary chamber mount. The cube dimensions are controlled to very tight tolerances for positioning the BPM buttons such that beam based alignment techniques are not required. The dipoles quadrupoles and associated beam pipe supports are pinned to a tight-tolerance strong back to insure the precision of the BPM buttons to the magnets and beam centerline.

A basic assembly of magnets and chambers installed on a strong back otherwise known as a triplet assembly (3 quads and a single dipole) is used as a unit in the ERL loop. A few other basic units are also used. All the components are fabricated to a high tolerance and mounted to precision milled positions on a single support plate. The chambers are interconnected with 4-1/2 inch Conflat type flanges. The cross ports for gauging and beam components are either 2-3/4 inch or 4-1/2 inch Conflat flanges.

The BPM buttons are sealed to the BPM cube with Helicoflex delta seals. The seal groove is machined into a mini-Conflat (1.33 inch) bolt circle. The sealing force, less than a comparable Conflat seal, insures an even metal-to-metal interface between button and cube. This lower compressive force seal helps maintain the precision placement of the button relative to the beam centerline with more uniform contact between the machined face of the BPM cube and that of the BPM button flange. The seal has an aluminum jacket that limits bakeout temperature to 150ºC.

Components destined for the ERL beamline are either delivered to BNL or processed at BNL for suitability of service in an ISO 14644 Class 5 clean room. This processing includes vacuum flange seals and hardware. Components delivered Class 5 ready are double bagged and are only opened in a Class 5 environment. All QA is performed in the class 5 environment. If QA outside the Class 5 environment is needed, then re-processing for particulate free service is needed. So, careful attention and coordination is needed to avoid costly re-work if at all possible.

In case helium processing of the SRF cavities is desired, a helium introduction system was installed on the beam line. Research grade 99.9999% helium is passed

through a purifier and 0.003 micron filter before being introduced to the cavity through a all metal variable leak. This system requires local access to the cavity for adjustments in pressure. The helium system is remote operational by controlling the variable leak with Selsyn (self synchronous) motors.

4.14.11 **Beam Instrumentation**

A variety of beam instrumentation systems will be provided for the purpose of commissioning, tuning, and protecting the ERL facility. Measurements that include beam position, profiles, current, emittance, and losses will be available for the planned modes of operation [12].

4.14.11.1 ***Beam Position Monitors***

There are 16 dual plane 10 mm diameter button style Beam Position Monitors (BPMs), 4 in the injection transport, 11 in the recirculation loop, and 1 in the dump line. The buttons are Times Microwave Systems model SK-59044; they are mounted on stainless cubes that are welded to the adjacent 6 cm diameter beam pipes. The orientation of the cubes are installed either at 45^0 or 90^0 depending on their location. A 45^0 orientation is used if there are space limitations, and to avoid beam related energy deposition on a button downstream of bending magnets. The BPMs will be baked to 150 C.

Libera Brilliance Single Pass electronics from Instrumentation Technologies will process signals from the BPMs. These modules have been customized with a 700 MHz SAW band pass filter that matches the fundamental frequency of the SCRF gun and Linac accelerating cavities. A few fundamental characteristics of the Libera system are that it employs a digitizer with a 117MHz-sampling rate, a variable buffer length of 1 k–8 kB, a maximum trigger rate of 200Hz, and position threshold comparison beam inhibit output for machine protection. BPM signals will be transported to the signal processing electronics using Andrew LDF1-50 1/4" heliax cable to preserve the signal power at the 700 MHz Libera pass band. When operating with typical ERL bunch trains of 9.3 MHz, 351 MHz, or 703 MHz, performance parameters should be compatible according to simulations. Since the spacing between bunches in a bunch train will be ~ 100 ns or less, and the 700 MHz filter will ring for > 100 ns, the individual bunch position will be difficult to distinguish within bunch trains. The configurable beam position range interlock feature offered by the Libera electronics will be employed as the first line of defense for machine protection and to avoid beam losses.

The Libera BPM electronic units will be integrated into the standard RHIC control system. ADO (accelerator device object) software has been written and will execute directly on the Linux kernel that is resident in the Libera hardware. The ADO provides on-board communication to the Libera hardware through the CSPI (control system programming interface) library provided by I-Tech, and communicates to higher level workstations via Ethernet using standard RHIC control system utilities.

4.14.11.2 ***Beam Profile Monitors***

Transverse beam profiles will be measured by two methods, depending on the amount of beam charge in the bunch train. When in low charge operating mode with 1-100 pC bunch charge trains, we will use 0.1 X 50 mm YAG:Ce (yttrium aluminum

garnet doped with Cerium) screens from Crytur (40 mm clear aperture). For higher charge modes we will use OTR (optical transition radiation) screens that are comprised of a 250 micron thick silicon wafer coated with ~ 1000 angstroms of aluminum. The profile monitor stations were specified by BNL and designed and fabricated by Radiabeam Technologies. Images from the YAG and OTR screens are transported through a mirror labyrinth to a 3-motor lens and CCD camera in a local enclosed optics box. We plan using our ERL Linux Red Hat Controls [C] interface to a Grasshopper2 GigE camera.

A more simplified YAG profile monitor has been designed to plunge into the beam path of the injection 30^0 dipole chambers through an auxiliary port.

Synchrotron light monitors will be used to measure transverse beam profiles while running with high power beams. Due to the long wavelength of synchrotron radiation at 20 MeV, and low sensitivity of CCD cameras at these wavelengths, using these monitors could be challenging. We plan to install optical transports and CCD cameras at a number of the ERL loop 60^0 dipole locations. The dipole chambers have dedicated synchrotron light output viewing ports.

Halo scrapers will be installed in the injection transport to measure the amount of beam in the halo. Horizontal and vertical pairs of stepper motor controlled 2 mm thick copper jaws will be located at several locations in the injection transport. After the halo characteristics are measured, a collimator will be designed to scrape off the undesired halo at low energy to reduce higher power beam losses downstream.

4.14.11.3 ***Beam Emittance***

There are two techniques planned to measure beam emittance. The expected normalized emittance range is 2-10 um.

In the first method, a pepper pot station will be used to measure 2 MeV beam emittance in the injection transport. The pepper pot will be comprised of two plunging tungsten masks upstream of a YAG:Ce profile monitor, one located at 0.25 m, and the other 0.5m. The dynamic range of the emittance measurement will be limited by the space charge effect. The space charge effect can be characterized by the ratio of the space charge and emittance contribution in the beam envelope equation.

The second method will measure the 20MeV Beam emittance will be measured using the traditional quad scan technique, and image data from downstream YAG & OTR profile monitors.

4.14.11.4 ***Beam Current Monitors***

High precision DC current measurements will be made using a matched set of Bergoz NPCT-S-115 DC current transformers (DCCT) and standard NPCT electronics.

There will be one each installed in the injection and extraction transport beam lines. These DCCTs are configured in a nulling mode where their calibration windings are joined in a single loop, and driven opposite the beam by a low-noise Khronhite model 523 current source. The output level of the dump DCCT is fed back as a reference to the current source to drive the dump DCCT output to zero. The output of the gun DCCT is then a differential current measurement [13].

We are presently considering several signal processing and data analysis hardware solutions from National Instruments for handling DCCT system tasks that include

absolute and differential measurements. Drift (magnetic field, thermal, and gain) compensation will be automatically removed by periodic nulling without beam.

The anticipated sub-microamp resolution may permit using this diagnostic as a second layer of the machine protection system in the case the beam loss monitors fail to detect beam losses.

Bunch-by-bunch & bunch train charge will be measured by a Bergoz in-flange Integrating Current Transformer (ICT) part number ICT-CF6-60.4-070-05:1-H-UHVTHERMOE, located in the upstream injection line. This ICT assembly has internal type E thermocouple for bake out (to 150 C) temperature monitoring.

Beam charge signals will be processed by standard Bergoz BCM-IHR Integrate-Hold-Reset electronics feeding a beam synched triggered digitizer. The nominal integrating window is 4 us, but can be adjusted shorter or longer based on the temporal limits of the electronics. We have ordered the BCM-IHR module with the option to trigger at a maximum frequency of 10 kHz.

4.14.11.5 ***Beam Loss Monitors***

Photomultiplier tube (PMT) based loss detectors will be installed at locations where beam loss is most likely. The design of this detector is based on ones developed at Jefferson Lab, using the Burle 931B PMT; a more modern tube was chosen for ERL. The Hamamatsu R11558 side-on tube is very similar to the 931B and has lower dark current, higher gain, and improved anode and cathode responsivity. The PMT was installed in light tight PVC housing containing a 10 mA green LED for testing with 1 μS light pulses. In an effort to extend the use of the existing RHIC BLM System [14] processing electronics to the ERL, a preprocessing VME module had to be designed. As the RHIC BLM front-end V119 typically takes loss signals from positively biased ion chambers, the characteristically negative signal from the PMTs had to be inverted. Thus a custom interface for the VME chassis was developed containing eight independent channels of inverting amplifiers with integration matching that of the V119 card, and having an output stage for driving the capacitive input of the V119 card. A maximum gain of 200 was demonstrated with good signal to noise ratio. The interlock response time to a loss signal that exceeds a programmable threshold is ~ 10 μs. The actual PMT gain at each location will be field adjusted by setting the high voltage bias during beam commissioning. A CAEN HV multi-channel chassis with full remote control will bias the PMTs.

Eight Ion Chamber (IC) loss detectors, as currently used in RHIC, will be employed at select locations in ERL. These are 113cc glass bottles with BNC & SHV connectors for signal and bias. These will be collectively biased to 1400 V in two groups by two Bertan 205B-03R 3 kV 10 mA rack mount power supplies. The signals from each IC are transported on 75 ohm cables to the V119 modules. All V119 modules (PMT and IC connected) are supervised by a V118 module that monitors integrated signal level data compared to thresholds. The V118 module has a discrete loss output signal that will signal the machine protection system in the event of detected loss from any of the PMTs or ICs.

Ion chamber type loss monitors based on gas filled heliax cable, as used in the AGS ring, will be employed at ERL. The cable is 7/8 inch heliax, Andrews type RG318, filled with Argon to 10 psig. Four long loss monitor cables will run along the inside of the loop while 12 short loss monitor cables will hug the outer casing of the final beam dump. The cable loss monitors are biased to ~ 150V by custom floating bias supplies

mounted in NIM modules. The loss signal returns on the bias cable and is integrated by a custom integrating amplifier modules whose analog outputs are digitized by standard VME DAC modules.

In addition to amplitude proportional beam loss detection as provided from the PMT, IC, & heliax detectors, event count based detectors are employed. PIN Diode loss detector modules, Bergoz model BLM, will be installed at eight select locations in ERL. These modules are built around two PIN photodiodes mounted face-to-face making use of coincidence counting to be insensitive to synchrotron radiation photons. With extremely low spurious count rate of < 1 in 10 sec, up to 10 MHz counting, dynamic range of 10^8, and 100 nS recovery time, these detectors are of the lowest costs and highest dynamic ranges available. The TTL data output of each detector is counted by a Struck model SIS3808 scalar VME module.

Thermal imagers will be used at several locations to measure beam pipe temperature gradients to ensure beam losses not seen by other loss detectors are monitored. We chose the FLIR A310 camera. It offers image transfer and control via Ethernet, and configurable location specific temperature thresholds on the image can be programmed and used to provide a machine protection alarm or interlock signal from a digital output port on the camera assembly.

4.14.12 **Beam Dump**

We use a commercially available beam dump modified to the ERL special needs. The beam dump design is based on a similar 1 MW ERL klystron electron gun beam dump from CPI, which was purchased a few years ago. However, that and other similar commercially available MW beam dumps were designed to remove 10's of Ampere beams with energies of 10's of KeV. Therefore, upon entry into the beam dump, the electron beams spread out due to their high space charge and relatively low energies.

However for the ERL parameters, the beam dump has to address the issues of cascade showers, forced magnetic beam spreading due to low space charge at high energy, and issues associated with extremely high radiation doses. Therefore, a modified beam dump was designed and a purchased order was sent to CPI. Beam spreading is to be done magnetically to address the first two issues. All elastomer seals are to be replaced by metallic seals, or flanges are to be welded. Dimensions of this beam dump are roughly 62" in length and 19" in diameter. Spreading the beam over this large area is to ensure that local boiling of the cooling water does not occur. The beam will be spread over this large surface area by magnetic field coils. Elastomer seals, which are replaced by welding flanges, have a 1" lip in order to facilitate easy opening, even though it is very unlikely that such a need will arise. To mitigate debris and outgassing streaming back into the rest of the ERL system, the inner copper walls of the beam dump are to be conditioned at low power without cooling; backscattering, secondary electrons etc. are not an issue due to the fact that the electron beams striking the inner copper walls have multi-MeV, and thus penetrate deeply into the walls.

The beam dump is designed to have the capability for removing 1 MW of unrecovered electron beam power with beam energy of 5 MeV. Similar design with identical heat removing capability was successfully tested at 1.6 MW.

4.14.13 Control System

4.14.13.1 *Machine Protection System*

The Machine Protection System (MPS) is a device-safety system that is designed to prevent damage to hardware by generating interlocks, based upon the state of input signals generated by selected sub-system. It exists to protect key machinery such as the 50 kW and 1 MW RF Systems. When a fault state occurs, the MPS is capable of responding with an interlock signal within several microseconds. The Machine Protection System inputs are designed to be fail-safe. In addition, all fault conditions are latched and time-stamped.

The ERL MPS is based on a National Instruments hardware platform, and is programmed by utilizing National Instruments' development environment for a visual programming language. The MPS runs on a programmable automation controller called CompactRIO (Compact Reconfigurable Input Output). The National Instruments CompactRIO is an advanced embedded control and data acquisition system designed for applications that require high performance and reliability. This small sized, rugged system has an open, embedded architecture, which allows developers to build custom embedded systems in a short time frame. The National Instruments CompactRIO device that is used for the MPS is an NI cRIO 9074. The cRIO 9074 is an 8-slot chassis with an integrated real-time processor and an FPGA. The embedded real-time processor is a 400 MHz Freescale MPC5200 that runs the WindRiver VxWorks real-time operating system. The FPGA is a Xilinx Spartan 3 with 2 million gates (46,080 logic cells) and 720 KB embedded RAM. The cRIO 9074 also features a 256 MB nonvolatile memory. CompactRIO combines an embedded real-time processor, a high-performance FPGA and hot-swappable I/O modules to form a complete control system. Each module is connected directly to the FPGA and the FPGA is connected to the real-time processor via a high-speed PCI bus.

ERL critical sub-systems such as the RF system require the MPS to respond on a microsecond scale. High-speed I/O modules were chosen to meet the necessary timing requirements. The MPS currently uses three of these I/O modules: a 32-channel 24 V input module, an 8-channel TTL input-output module, and a 4-channel SPST relay output module. The 24V module has sinking digital inputs with 7 μs response time, and the TTL module has digital inputs and outputs with 100 ns response time.

The MPS interface is written in LabVIEW (Laboratory Virtual Instrumentation Engineering Workbench). LabVIEW is a graphical programming environment used to develop measurement, test, and control systems utilizing graphical icons and wires that resemble a flowchart. The National Instruments CompactRIO platform requires two different LabVIEW software modules corresponding to the System's interface, one for the Real-Time processor and one for the FPGA. These modules contain custom functions specific to the Real-Time processor or the FPGA in addition to all the functionalities of the standard LabVIEW module.

The code for both the Real-Time processor and the FPGA is developed on a host computer. The program for the FPGA is developed by using a standard LabVIEW software module. The LabVIEW FPGA code is then converted to VHDL code and compiled using the Xilinx tool chain. The program for the Real-Time processor is also developed by using a standard LabVIEW software module. When ready, the code for

the Real-Time processor and the FPGA is downloaded to the CompactRIO device via Ethernet. Once the code is downloaded, the CompactRIO can run in a stand-alone mode, or communicate directly with a host via Ethernet.

Running directly on the cRIO platform, the MPS interface accepts the various input signals and generates any necessary interlocks. An interlock is generated when a logic high (fault) at the input is seen (if a cable is disconnected or broken, an internal pull-up ensures the System will generate an interlock. Exception is given to the RF sub-system which provides high-level inputs due to equipment constraints. These inputs are inverted within the LabVIEW FPGA). If one of the continuously polled input levels change to high (indicating a fault), the fault is latched, and the time of the event is recorded using a 32-bit LabVIEW tick counter function. This provides a microsecond time stamp. The MPS interface also provides the capability to enable and disable inputs. Enabled and latched inputs are then combined and passed to other critical systems as interlocks. The input latches are cleared only after a software reset has been issued.

Operators communicate to the MPS interface using the main ERL server. Operators have the ability to enable/disable individual system inputs, clear latches via a reset button, and check the overall system status. The Real-Time processor code performs a handshake with the main server to ensure connectivity. National Instruments also provides web server capability, which allows the developer to monitor and control the system remotely, avoiding interaction with the ERL main server.

4.14.13.2 *Infrastructure for the Control System*

The control system runs on server PC's running Red Hat LINUX, with one being dedicated to laser-related activities. End-user access to the ERL controls system is handled by three Wyse thin-client terminals located in the Control Room. Each terminal has the capability of connecting via Ethernet to three different remote hosts that are running as No Machine servers, and can drive up to two separate video displays. Three VME chassis running VxWorks on multiple processor platforms are used to support remote device integration with the controls system. Remote diagnostics are also available for each unit via RS-232 connections. Continuous time synchronization between all chassis and a networked timeserver is achieved using Extended Network Time Protocol (XNTP). RS-232 and 485 serial connections are integrated with the controls system Ethernet network using several different types of Digi Terminal Server modules. All GPIB interface devices are integrated with the controls system Ethernet network using National Instruments GPIB/ENET-100 modules. Commonly used application software within the Collider-Accelerator Complex for device interaction (PET), live-information plotting (GPM), logged-information plotting (LogView), and video image display/analysis (FlagProfileMonitor) will continue to serve has the primary controls system tools for the ERL project. Motif Editor and Display Manager (MEDM) will be used to create synoptic displays that will eventually provide the primary user interface to the ERL. A 100 Megabit Ethernet network serves as the backbone of the controls system. Dedicated Gigabit Ethernet links will likely be needed in support of selected high-frame rate video connections between video servers and the ERL Control Room. Data logging services are provided by a set of networked servers shared by other projects at the Collider-Accelerator Complex. Each machine utilizes RAID storage in order to maintain a high level of reliability.

4.14.14 Summary, Status and Plans

We provided a detailed description of the design of the various subsystems of the R&D ERL which is in advanced construction and commissioning at the Collider-Accelerator Department at Brookhaven National Laboratory. At the time of writing of this manuscript, all elements of the ERL are in house and most are installed and surveyed to their exact positions. The first beam from the SRF gun is expected in October 2012, beam through the 5-cell cavity is anticipated in December 2012 and beam through the ERL loop in March 2013. We plan to study the performance of this unique machine: The high QE photocathodes and their load-lock delivery system, the SRF gun capable of 500mA current at 2MeV beam kinetic energy, the zig-zag beam merger, the highly damped 5-cell SRF accelerating cavity, and various advanced instrumentation elements. Of particular interest are the high-current, low-emittance properties of the system, like coherent emissions, beam halo evolution and mitigation and emittance preservation. We plan to increase the current gradually from sub-mA to ampere-class in stages.

4.14.15 References

1. T. Vecchione, I. Ben-Zvi, D. H. Dowell, J. Feng, T. Rao, J. Smedley, W. Wan, and H. A. Padmore, A Low Emittance and High Efficiency Visible Light Photocathode for High Brightness Accelerator-Based X-ray Light Sources, Appl. Phys. Lett. **99**, 034103 (2011).
2. Diamond amplified photocathode references:
    a. BNL Collider-Accelerator Department note C-A/AP/149 04/04 Secondary Emission Enhanced Photoinjector, I. Ben-Zvi, X. Chang, P. D. Johnson, J. Kewisch, T. S. Rao, 2004.
    b. Xiangyun Chang, Ilan Ben-Zvi, Triveni Rao, John Smedley, Erdong Wang, Qiong Wu, Tianmu Xin, Neutralizing trapped electrons on the hydrogenated surface of a diamond amplifier, Phys. Rev. ST Accel. Beams 15, 013501 (2012).
    c. Erdong Wang, Ilan Ben-Zvi, Triveni Rao, D.A.Dimitrov, Xiangyun Chang, Qiong Wu, Tianmu Xin, Secondary-electron emission from hydrogen-terminated diamond: Experiments and model, Phys. Rev. ST Accel. Beams 14, 111301 (2011).
    d. Erdong Wang, Ilan Ben-Zvi, Xiangyun Chang, Qiong Wu, Triveni Rao, John Smedley, Jorg Kewisch, and Tianmu Xin, Systematic study of hydrogenation in a diamond amplifier, Phys. Rev. ST Accel. Beams **14**, 061302 (2011).
    e. D. A. Dimitrov, R. Busby, J. R. Cary, I. Ben-Zvi, T. Rao, J. Smedley, X. Chang, J. W. Keister, Q. Wu, and E. Muller, Multiscale three-dimensional simulations of charge gain and transport in diamond, Journal of Applied Physics **108**, 073712 (2010).
    f. X. Chang, Q. Wu, I. Ben-Zvi, A. Burril, J. Kewisch, T. Rao, J. Smedley, E. Wang, E. M. Muller, R. Busby, and D. A. Dimitrov, Electron Beam Emission from a Diamond-Amplified Cathodes, Physical Review Letters **105**, 164801 (2010).
3. A.K. Sharma, T. Tsang, and T. Rao; Theoretical and Experimental Study of Passive Spatio-Temporal Shaping of Picosecond Laser Pulses; BNL 81555-2008JA; Phys. Rev. Special Topics 12, 033501 (2009).
4. R. Calaga, I. Ben-Zvi, M. Blaskiewicz, X. Chang, D. Kayran and V. Litvinenko, High current superconducting gun at 703.75 MHz , Physica C: Superconductivity, **441**, 159,

(2006).
5. Wencan Xu, et al, Design, Simulation and Conditioning of 500 kW Fundamental Power Couplers for a SRF Gun, accepted for publication in Phys. Rev. ST Accel. Beams.
6. R. Gupta, et al, Design Construction and Test Results of a HTS Solenoid for Energy Recovery Linac, Proceedings of 2011 Particle Accelerator Conference, New York, NY, USA, TUP163.
7. L. Hammons and H. Hahn, HOM Damping Properties of Fundamental Power Couplers in the Superconducting Electron Gun of the ERL at BNL, Proceedings of 2011 Particle Accelerator Conference, New York, NY, USA page 901.
8. H. Hahn, I. Ben-Zvi, R. Calaga, L. Hammons, E. C. Johnson, J. Kewisch, V. N. Litvinenko, and Wencan Xu, Higher-order-mode absorbers for energy recovery linac cryomodules at Brookhaven National Laboratory, Phys. Rev. ST Accel. Beams **13**, 121002 (2010).
9. D. Kayran, V.N. Litvinenko, Merger system optimization in BNL's high current R&D ERL. Proceedings of PAC'07, pp. 3711-3713.
10. D. Kayran et al, Optics for High Brightness and High Current ERL Project at BNL, in Proceedings of PAC 2005, pp. 1775-1777.
11. W. Meng, A. Jain, G. Ganetis, D. Kayran, V.N. Litvinenko, C. Longo, G. Mahler, E. Pozdeyev, and J. Tuozzolo, *Unique Features in Magnet Designs for R&D Energy Recovery LINAC at BNL*, Proceedings of PAC07, Albuquerque, New Mexico, USA, p. 655-7.
12. David Gassner, Dmitry Kayran, Leonard DeSanto, Chuyu Liu, George Mahler, Rob Michnoff, Toby Miller, Michelle Wilinski, BNL Energy Recovery Linac Instrumentation, Proceedings of the 2011 ERL Workshop, WG4-003.
13. P. Cameron, et al., "Differential Current Measurements in the BNL ERL Facility", ERL2005 Workshop, Newport News, Virginia, OSTI ID: 15020019. (2010).
14. R. L. Witkover, et al., "RHIC Beam Loss Monitor System Initial Operation", PAC99, p. 2247.

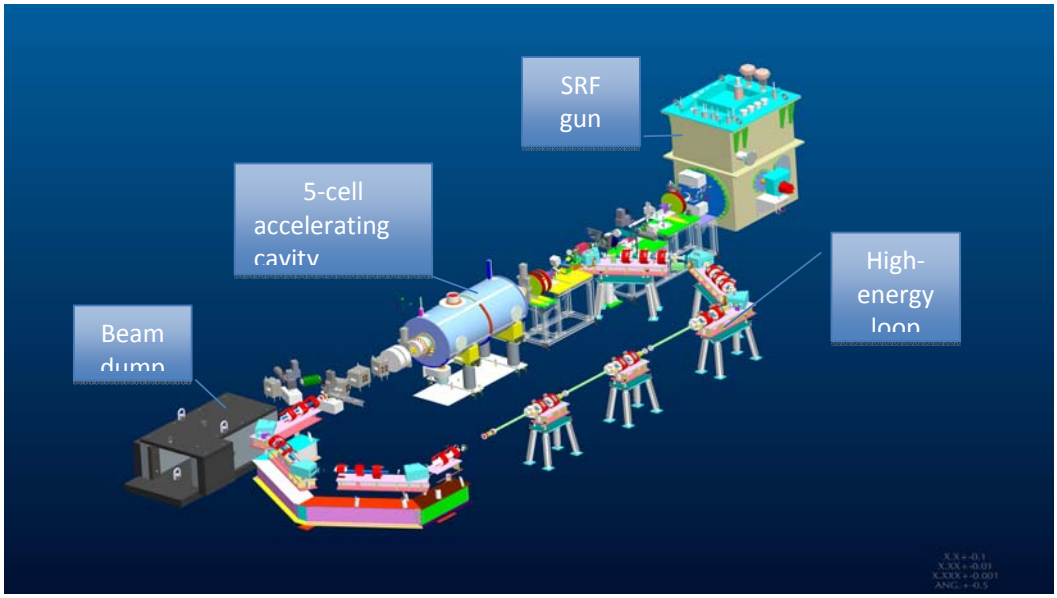

Figure 1: Schematic layout of the R&D Energy Recovery Linac at BNL.

4.15 Status of the Electron Guns

Triveni Rao[1], Bruce Dunham[2], Carlos Hernandez-Garcia[3], Thorsten Kamps[4], Boris Militsyn[5], Fernando Sannibale[6]
[1]Brookhaven National Laboratory, Upton, NY 11973, USA
[2] Department of Physics and CLASSE, Cornell University, Ithaca, NY 14850, USA
[3]Thomas Jefferson National Laboratory, Newport News, VA23606, USA
[4]Institute of Accelerator Physics, Helmholtz-Zentrum Berlin, Germany
[5]STFC Daresbury Laboratory, Warrington, WA4 4AD, UK
[6]Lawrence Berkeley National Laboratory, Berkeley, CA 94720, USA
Mail to: triveni@bnl.gov

4.15.1 **Introduction**

The electron gun for future electron-hadron collider should be able to produce high average current beams with low emittance. For a given current, the initial brightness in the gun, and hence the maximum final brightness for a given current, is determined by the choices of the gun design, cathode and the laser system. Currently, there are three prevalent gun designs in operation to produce such beams: DC, normal conducting RF (NCRF) and superconducting RF (SRF) guns. The most popular cathode materials at present are cesiated GaAs and multi alkali such as K_2CsSb. In order to obtain the high electron yield and low thermal emittance from the cathode simultaneously, the preferred laser wavelength is in ~ 530 nm regime for unpolarized electrons and ~ 780-800 nm regime for polarized electrons from GaAs:Cs. In the following sections, we will discuss the merits and draw backs of each of these options. We will also present the state of the art performance and research under way to improve it. Discussions in this section are limited to performance achievable at the exit of the gun but do not include the injector, which should be designed with equal care to preserve the quality of the beam.

4.15.2 **Photocathode**

The photocathode performance is characterized by its quantum efficiency (QE), response time, intrinsic emittance of the electrons beam at the cathode and the cathode life time. The high average current required for colliders dictates that the cathode should have quantum efficiency at visible wavelength to simplify the laser system. In typical hadron colliders, the hadron bunch length and hence the electron bunch length are in hundreds of ps range. Hence the prompt emission is not a critical requirement unless beam shaping is required to minimize the emittance growth in the space charge limited region. Table 1 lists [1] a number of possible cathode materials for this application and some of their properties. The QE value of the cathodes in the Table is based on measurements by a number of researchers. The theoretical value of the intrinsic emittance is calculated using the formula

$$\varepsilon_{nx,th}\,[mm\ mrad] = 1.40\,\sigma_x\,[mm]\sqrt{MTE\,[eV]}\,, \qquad (1)$$

where σ_x is the transverse rms spot size of the electron-beam (same as the laser spot with a uniform QE distribution), MTE is the mean transverse energy, defined as MTE = $\langle \tfrac{1}{2}\, m_0\, v_x^2 \rangle + \langle \tfrac{1}{2}\, m_0\, v_y^2 \rangle$, with x and y denoting the directions perpendicular to the

cathode's emission normal, and, $m_0 c^2$ = 0.511 MeV is the electron's rest energy. The MTE can also be defined as the difference between the photon energy and the threshold energy needed by the cathode to excite the electron from the top of the valence band to the vacuum level near the conduction band (= band gap energy + electron affinity).

As can be seen from the Table 1, three cathodes GaAs:Cs, K_2CsSb and Cs_3Sb have relatively high quantum efficiency at 532 nm and low intrinsic emittance. Currently, two types of cathode material, GaAs:Cs and multi alkali, are being investigated for high average current applications. These cathodes are highly sensitive to contamination and need to be fabricated and used in vacuum levels of 10^{-11} to 10^{-12} Torr. This is achieved routinely in DC guns and it is not expected to be a problem in SRF guns due to the cryo pumping inherent in these guns. Special consideration should be given in designing NCRF guns.

Table 1: Cathode materials and their relevant properties suitable for collider application

Cathode	***Wavelength, λ(nm), E_{ph}(eV)***	***QE (%)***	***E_a + E_g (eV)***	***Thermal emittance (mm mrad)/ mm rms***	
				Theory	***Experimental***
Cs_2Te	262, 4.73	~10	3.5	0.9	12±0.1
Cs_3Sb	262, 2.33 473, 2.62 405, 3.06	~4 ~7 ~9	1.6+0.45	0.42 0.62 0.82	0.56±0.03 0.66±0.03 0.80±0.04
Na_2KSb	330, 3.76	~10	1+1	1.07	NA
Na_2KSb:Cs	390, 3.18	~20	1+0.55	1.03	NA
K_2 CsSb	532, 2.33 473, 2.62 405, 3.06	~4 ~11 ~25	1+1.1	0.38 0.58 0.80	0.56±0.03 0.69±0.03 0.87±0.04
GaAs(Cs,F)	532, 2.33	~10	1.4±0.1	0.77	0.47±0.03
GaN(Cs)	260, 4.77	~15	3.4±0.1	0.94	1.35±0.11

Measurements and calculations [2] have shown that the roughness of the cathode surface results in non-uniform emission and increased emittance. In applications where very low emittance is a necessity, cathodes/substrates of atomic smoothness should be used.

4.15.2.1 *GaAs:Cs*

Cesiated GaAs has been used extensively in high average DC electron guns. The major advantages of this cathode are the high QE at visible wavelength and the ability to deliver polarized electrons. The latter property is important for collider applications. Since GaAs is a bulk emitter, the response time of the cathode depends on the absorption depth of the photon i.e. the higher the photon energy, the shorter the absorption length and the response time [3]. However, since the intrinsic emittance increases with the photon energy, the operating regime of the cathode and the laser are application specific. Typically, GaAs is activated to produce a negative electron affinity surface and increase the QE by applying fractional monolayer of Cs to the surface. This activation places a stringent vacuum requirement (< 10^{-11} Torr) in the vicinity of the cathode for acceptable life time of the cathode. Another major disadvantage is the limit on the total charge deliverable from the cathode before it needs to be rejuvenated or replaced. Recently, using a GaAs photocathode we reached a maximum current of 52

mA at 5 MeV [4], a record setting current. The lifetime was not long, as the beam halo degraded the vacuum in the vicinity of the gun. In routine operation, operational 1/e life time of 100-250 hours, dark life of 900 hours, maximum QE of 3.7% and maximum charge of 150 pC/bunch has been demonstrated at ALICE in the Accelerator Science and Technology Centre, Daresbury. Average current of up to 9 mA at 74.85 MHz and ~ 1-2 kC/cm^2 has been extracted at JLab [5].

4.15.2.2 ***K_2CsSb***

Development of multi alkali cathodes were originally prompted by the need for high QE material for photon detection applications. Boeing [6] was the first to produce 32 mA current at 27 MHz repetition rate and 25% duty factor, cathode QE of up to 14% and operating life time of ~ 1 hour from K2CsSb cathode for high current applications. The authors of this work postulate the short cathode life time was due to the presence of water vapor in the gun. Later experiments have shown a 50% decay time for QE at 532 nm to be of around 17 hours for water partial pressure of $2x10^{-9}$ mBar [7]. This cathode has been used in the DC gun at Cornell to deliver 20 mA at 1.3 GHz for more than 8 hours without observable decay. Similar results have been obtained with JLab test gun as well [8]. Alkali-based photocathodes in the form of thin films are used in modern streak camera devices, demonstrating a very fast response time (a time resolution of 200 fs is commercially available). Recent measurements carried out in photoinjectors by using an RF deflecting cavity confirmed that the response time from Cs_2Te and Cs_3Sb is on the picoseconds scale, or shorter [1].

4.15.3 **Laser System**

For a given cathode, the current, bunch length and the transverse dimensions of the electron beam determine the laser power, pulse duration and spot size. Since the intrinsic emittance of the electron beam is determined by the kinetic energy of the electron at birth, in order to minimize the emittance, the photon energy of the laser should be closely matched to the threshold energy of the cathode. Two of the most common laser platforms to drive high current, GaAs:Cs and K_2CsSb cathodes are yttrium based diode pumped solid state (DPSS) laser and fiber laser.

In DPSS, a train of infrared (IR) output pulses from a mode-locked laser oscillator are amplified through a series of power amplifiers. The IR radiation is then converted to green using a second harmonic crystal. The macropulses can be picked from the train using either an acousto-optic or an electro-optic pulse picker. Power level in the range of 10 W, pulse duration of a few ps, power stability of a few %, pointing stability of ~ 3 μradian, s/n of 10^6, jitter of < 1 ps and repetition rate up to 750 MHz are possible with such a system. The DPSS technology is a mature one and is being used in a number of installations including FEL facility at JLab, ALICE at Daresbury, and ERL at BNL. The major disadvantage of DPSS is its size, especially for repetition rates << 100 MHz. Since the cavity round trip time is matched to the inverse of the repetition rate, the cavities tend to be very long for low frequency systems. This increases the sensitivity of the system to thermal and mechanical fluctuations resulting in larger jitter that needs to be compensated by active feedback/feed forward. However, careful design and engineering can overcome this problem, as shown by the BNL ERL laser. This sensitivity is not an issue either for frequencies > 100 MHz or electron bunches longer than 100 ps.

Recent developments in large area, single mode fibers and high power diode pump lasers have made fiber laser an attractive alternative. In this platform, the output from the oscillator is modulated either directly by modulating the voltage/current of the diode or modulating the CW output of the laser with e-o modulators to generate a train of pulses. Since the modulation is done electronically, the jitter can be reduced substantially. In addition, the pulse duration, pulse profile and the repetition rate of the laser can be changed by changing the modulating voltage accordingly. Amplified beam with up to 90 W at 1.06 μm and 40 W at 0.532 μm, with ~ 50 ps pulse duration and 700 MHz repetition rate has been generated by researchers at Aculight [9]. By modulating both the amplitude and phase, pulse duration tunable from 10 to 50 ps has also been produced by this group. Fiber laser systems with up to 65 W at 532 nm, ~ 1 ps pulse duration operating at 1.3 GHz has been developed at Cornell [10].

The fiber lasers are still in the developmental stage and commercial products that meet the requirements for the electron gun are not readily available. The tolerances and reliability of these lasers are yet to be well documented.

In order to reduce the emittance growth due to space charge effects in the low energy regime, some applications require shaping both the longitudinal and transverse shape of the laser beam from a Gaussian to flat top. There are a number of commercial devices that can be used to convert the Gaussian transverse profile of the laser to one of uniform distribution. Approaches for shaping the longitudinal profile vary depending on the initial pulse duration of the laser. For initial pulse durations longer than 100 ps, direct modulation using e-o crystal is the preferred method. For pulse durations in the fs regime where the bandwidth of the laser pulse is large, modulating the pulse in the frequency domain has shown to be successful [11]. Flat top pulses in the ps regime have been obtained by pulse stacking [12, 13].

4.15.4 **Gun Designs**

4.15.4.1 ***DC Gun***

In DC guns, the electrons from the cathode are accelerated by the field established by hundreds of kV applied between the cathode and the annular anode. In order to minimize emittance degradation near the cathode due to space charge forces, high accelerating fields and hence applied voltages are preferred. The maximum applied voltage is limited by the voltage breakdown threshold of the system and is in the range of 350 kV with a gap spacing of ~ 50 mm. Typical accelerating gradients are thus in the 5-10 MV/m range, making this gun more suitable for low charge/bunch, high repetition rate, high average current applications. A number of institutions have operational DC guns delivering average currents in excess of 1 mA.

In recent years, significant effort has been expended in redesigning the insulating ceramic to increase the maximum hold off voltage. One approach is to bulk dope the ceramic to control its resistivity. An alternate design with segmented insulator, where the line of sight between the electrodes and the insulator is completely blocked, has been successfully tested to 550 kV [14]. An inverted gun design, being tested at JLab [15] also shows considerable promise.

Another cause for the electrical breakdown is the cesium contamination of the electrodes when GaAs:Cs cathodes are activated in the gun's vacuum chamber. Cesium evaporated inadvertently on the electrodes lowers the work-function of the high voltage electrodes and increase their propensity for breakdown. Modern guns use a load-lock

system where the cathodes are activated in a separate vacuum chamber and the prepared cathode is inserted into the gun. The design of this load-lock system has undergone many iterations and the most successful ones have the load-lock system at the ground potential [16].

State-of-the-Art The DC gun at Cornell, operating with an applied voltage of 350 kV, with GaAs cathode has delivered ~ 5 ps long, 80 pC charge with a normalized emittance of 0.8 μm and 20 pC with a normalized emittance of 0.4 μm at 5 MeV. Although a maximum current of 52 mA was obtained in this gun with GaAs:Cs cathode [17], life time was not long, due to vacuum degradation in the vicinity of the cathode, caused by the beam halo. Using K_2CsSb cathode, 20 mA current at 1.3 GHz and 5 MeV energy and 16 mA DC current with negligible cathode degradation have been produced with DC guns at Cornell [18] and JLab [8] respectively.

4.15.4.2 *Superconducting RF Gun*

The superconducting RF gun can support larger (up to 45 MV/m) [19] peak fields compared to DC guns, and hence can handle higher peak currents without degrading the emittance. Another major advantage of these guns is the low resistive power loss. Furthermore, with multiple cells forming the cavity, the electrons can reach relativistic velocity at the exit of the gun.

The RF gun provides a number of design choices such as the shape of the cells, number of cells forming the cavity. The cells can be either quarter wave or elliptical with pill box shape or re-entrant shape. The number of cells can be a simple half-cell or multiple cells. Number of SRF guns with single or multicell elliptical cavities and single cell quarter wave cavities are currently under construction and testing. In addition to the shape and number of cells, two other key factors to consider in the design of the gun are i) incorporation of the photocathode into the cell and ii) fundamental power couplers.

Incorporation of the photocathode into the RF gun, especially when a normal conducting cathode is used in a SRF injector, is nontrivial and different designs are under development and testing. For average currents of < 1 mA, metal photocathodes are still a viable option. In such a case, a cathode (for example, a superconducting cathode such as lead) can be deposited onto the back wall of the cavity [20]. For higher average currents, high QE cathodes need to be used. If the cathode life time is not long enough, care must be taken in the engineering of the insertion device so that the cavity stays superconducting while the spent cathode is being exchanged for a fresh one. One approach is to have the cathode in a separate stalk that is not in electrical contact with the SRF cavity walls. In ELBE SRF gun, the stalk is designed to be a RF choke and is described in detail in [21]. Another option is to incorporate the cathode on a plug that is inserted into the cavity and is in contact with the cavity walls [22]. In this design, care must be taken to sufficiently cool the plug to preserve the high Q of the cavity.

The high RF power needed to accelerate high average current electron beams imposes special requirements on RF coupling. SRF electron guns based on elliptical cavities use traditional coupling of RF power to SRF cavities via coaxial antennae connected to beam pipe ports. At lower RF power a single fundamental power coupler (FPC) is used [23, 24], while at high power two FPCs, symmetrically placed, are used to lower power load per coupler and eliminate transverse kick for beam on axis [25]. The latter FPCs were successfully tested in standing wave regime with full reflection up to 250 kW in pulsed mode and 125 kW in CW mode [26]. The FPC design of choice for

the coaxial quarter wave gun is based on a coaxial beam tube at the beam exit [26-28]. These couplers are axially symmetric and, if properly designed, should cause even less beam disturbance than two antenna-type couplers.

Another design consideration is the sensitivity of the cavity to microphonics and fluctuations in He pressure. Changes in the cavity shape due to this sensitivity lead to instability in the cavity field. Careful design and stiffening has been shown to reduce such deformation from > 8 μm to < 2 μm [29].

State-of-the-Art At Elbe, niobium cavity with 3 ½ cells, has been operated 1.3 GHz, with an accelerating gradient of 6.5 MV/m and peak gradient of 17.6 MV/m. Using Cs_2Te cathode located in the choke cell, 3 MeV electron beams with a maximum bunch charge of ~ 300 pC at a repetition rate of up to 125 kHz, peak current of 20 A and average current up to 18 μA has been produced. The Q_0 of the cavity showed no degradation even after 500 hours of operation with Cs_2Te cathode [30]. A number of other SRF guns are being built and tested as seen in this Newsletter and more results are expected within a short time.

4.15.4.3 *Normal Conducting Gun*

The normal conducting guns can achieve very high peak gradients (> 100 MV/m) and have been used traditionally for high charge, low average current applications. With higher average current, the thermal management becomes a critical design factor, even at reduced accelerating gradients. In one design, the thermal loading is addressed by integrating cooling channels into the cell walls of the RF cavity. This 700 MHz, 2 ½ cell cavity has undergone RF testing to validate thermal and RF integrity. Electron production is expected soon.

Another issue to be addressed is meeting the vacuum requirements associated with high QE photocathode. At LBNL, a 186 MHz cavity with sufficient pumping has been designed and built to maintain UHV in the gun. This gun has undergone RF testing and generated the first photo-emitted beam at the design energy of 750 keV [31].

4.15.5 **Issues to be Addressed**

The control and diagnostic system for the high current gun poses unique challenges. Since the average current is ramped from a small value needed for ensuring correct beam trajectory to the high value needed for collider, agility in changing the properties of micro- and macro- pulse structure of the electron beam is highly desirable. This implies a large dynamic range of more than 10^6 on the diagnostic elements for measuring beam current, noise and halo and the cameras for measuring emittance. Fast monitoring to look for signal between laser and electron pulses need to be developed for determining the origin of unwanted electron beam.

With high average current beams, the halo associated with the principal beam poses a significant problem. This halo can hit the wall of the beam pipe, causing i) degradation of the vacuum and associated degradation of the cathode, ii) damaging the beam pipe, if the current density is high enough, iii) production of ion clouds that impacts the beam trajectory. Identification, characterization and elimination of the halo have been a topic of discussion in a number of recent workshops.

This work was supported by U.S. Department of Energy under Contract No. DE-AC02-98CH10886.

4.15.6 References

1. I. Bazarov, L. Cultera, T. Rao, " Semiconductor photocathodes for unpolarized electron Beams" in Photoinjectors-An Engineering Guide, Ed.: T. Rao, D. Dowell, to be published by Bentham Scientific Publishers.
2. D. Dowell," Photoinjector Theory" in Photoinjectors-An Engineering Guide, Ed.: T. Rao, D. Dowell, to be published by Bentham Scientific Publishers.
3. I. V. Bazarov, B. M. Dunham, Y. Li, X. Liu, D. G. Ouzounov, C. K. Sinclair, F. Hannon and T. Miyajima, "Thermal emittance and response time measurements of negative electron affinity photocathodes", J. Appl. Phys., vol. 103, (2008) pp. 054901(1).
4. B. Dunham, A. Bartnik, I. Bazarov, J. Dobbins, C. Gulliford, S. Karkare, V. Kostroun, Y. Li, X. Liu, F. Loehl, J. Maxson, D. Rice, K. Smolenski and Z. Zhao, "Performance of the Cornell High-Brightness, High-Power Electron Injector", Presented at Int'l Particle Accelerator Conference, May, 21-25, 2012 New Orleans USA.
5. C. K. Sinclair, "DC photoemission electron guns as ERL sources", Nuclear Instruments and Methods in Physics Research A 557 (2006) 69–74.
6. D.H. Dowel1 , S.Z. Bethel, K.D. Friddell, "Results from the average power laser experiment photocathode injector test", Nuclear Instruments and Methods in Physics Research A 356 (1995) 167.
7. T. Vecchione, I. Ben-Zvi, D. H. Dowell, J. Feng, T. Rao, J. Smedley, W. Wan, and H. A. Padmore, "A Low Emittance and High Efficiency Visible Light Photocathode for High Brightness Accelerator-Based X-ray Light Sources", Appl. Phys. Lett. 99, (2011), 034103.
8. J. McCarter, "Charge Life time, emittance and surface analysis studies of K2CsSb photocathode in a JLab DC High Voltage gun", ERL 2011 workshop, 16-21 Oct 2011, KEK Japan. http://kds.kek.jp/conferenceDisplay.py?confId=7855&view=nicecompact.
9. P.Madasamy, L. Coressel, D. R. Jander, and E. C. Honea, "Tunable pulse width, short pulse high power green laser", presented at Conf. Lasers and Electro-Optics, 2010. http://ieeexplore.ieee.org/stamp/stamp.jsp?tp=&arnumber=5500976.
10. Z. Zhao, B. Dunham, I. Bazarov and F. Wise, Generation of 110 W infrared and 65 W green power from a 1.3-GHz sub-picosecond fiber amplifier, Optics Express 20, (2012), 4850.
11. H. Tomizawa, H. Dewa, T. Taniuchi et al., "Adaptive shaping system for both spatial and temporal profiles of a highly stabilized UV laser light source for a photocathode RF gun", Nucl. Instr. Meth A, vol. 557, (2006), 117.
12. I. V. Bazarov, D. G. Ouzounov, B. M. Dunham et al., "Efficient temporal shaping of electron distributions for high-brightness photoemission electron guns", Phys. Rev. ST Accel. Beams, vol. 11, (2008), 40702-1.
13. A. K. Sharma, T. Tsang, and T. Rao, "Theoretical and experimental study of passive spatiotemporal shaping of picosecond laser pulses", Phys. Rev. ST Accel. Beams, vol. 12, (2009), 33501-1.
14. R. Nagai, R. Hajima, N. Nishimori et al., Rev. Sci. Instr. 81, (2010), 033304.
15. R. Suleiman, "The Jefferson Lab 200 KV inverted gun, Life time measurements using strained superlattice GaAs and K2CsSb", ERL 2011 workshop, 16-21 Oct 2011, KEK Japan. http://kds.kek.jp/conferenceDisplay.py?confId=7855&view=nicecompact.
16. B. M. Dunham, "DC/RF injectors" in Photoinjectors-An Engineering Guide, Ed.: T. Rao, D. Dowell, to be published by Bentham Scientific Publishers.
17. B. Dunham, A. Bartnik, I. Bazarov, J. Dobbins, C. Gulliford, S. Karkare, V. Kostroun, Y. Li, X. Liu, F. Loehl, J. Maxson, D. Rice, K. Smolenski and Z. Zhao, "Performance of the Cornell High-Brightness, High-Power Electron Injector", Int'l Particle Accelerator Conference, May, 2012 (to be published).
18. L. Cultrera, J. Maxson, I. Bazarov et al., Photocathode behavior during high current

running in the Cornell energy recovery linac photoinjector, PRST-AB 14, (2011), 120101.
19. T. Rao, I. Ben-Zvi, A. Burrill, H. Hahn, D. Kayran, Y. Zhao, P. Kneisel, H. Bluem, M. Cole, A. Favale, E. Peterson, T. Schultheiss, and J. Rathke; Design, Construction and Performance of all Niobium Superconducting Radio Frequency Electron Injector, NIM A 562 (2006), 22.
20. J. Smedley, T. Rao, P. Kneisel et al. "Photoemission Tests of a Pb/Nb Superconducting Photoinjector" Proc. Of PAC 07 (2007) 1365.
21. T. Kamps, et al., "Electron beam diagnostics for a superconducting radio frequency photoelectron injector," Rev. Sci. Instrum. 79, (2008), 093301.
22. J. S. Sekutowicz, J. Iverson et al. "Status of Nb-Pb Superconducting RF-Gun Cavities",Proc. Of PAC 07, (2007), 962.
23. A. Arnold, "Rossendorf SRF Gun Operational Experience", http://kds.kek.jp/conferenceDisplay.py?confId=7855&view=nicecompact.
24. K. Liu, et al., "DC-SRF photocathode injector for ERL at Peking University", ERL 2011 workshop, 16-21 Oct 2011, KEK Japan. http://kds.kek.jp/conferenceDisplay.py?confId=7855&view=nicecompact.
25. S. Belomestnykh, "Status of BNL SRF guns", ERL 2011 workshop, 16-21 Oct 2011, KEK Japan. http://kds.kek.jp/conferenceDisplay.py?confId=7855&view=nicecompact.
26. S. Belomestnykh and W. Xu, "Fundamental power couplers for the ERL prototype SRF gun at BNL", ERL 2011 workshop, 16-21 Oct 2011, KEK Japan. http://kds.kek.jp/conferenceDisplay.py?confId=7855&view=nicecompact.
27. J. Harris, K. L. Fergusson, J. W. Lewellen et al., "Design and operation of a superconducting quarter-wave electron gun," Phys. Rev. ST Accel. Beams 14 (2011) 053501.
28. R. Legg, J. J. Bisagnano, M. Bissen et al., "Development of a Frequency Map for the WiFEL SRF Gun," Proc. SRF'11, 2011, Chicago, IL, to be published, MOPO032. http://199.190.250.75/prepress/MOPPP045.PDF.
29. T. Rao A. Arnold, S. Belomestnykh, D. Nguyen, T. Quast, "ERL2011 Summary of Working Group 1: Progress with RF injectors", to be published in Proc. Of ERL 2011 workshop, 16-21 Oct 2011, KEK Japan.
30. R. Xiang, A. Arnold, H. Buettig, et al. "The ELBE Accelerator Facility Starts Operation With The Superconducting RF Gun", Proceedings of IPAC'10, Kyoto, Japan, 1710.
31. F. Sannibale, et al., "Status of the APEX project at LBL", To be published in Proc. of IPAC12, New Orleans, LA, May 20-25, 2012.

5 Workshop and Conference Reports

5.1 Report from the ICFA Mini-Workshop on Higher Order Mode Diagnostics & Suppression in SC Cavities (HOMSC12)

Roger M. Jones, Cockcroft Institute/Univ. of Machester, U.K.
Mail to: roger.jones@stfc.ac.uk

From the 25th of June through Wednesday lunchtime of the 27th of June the Cockcroft Institute and ASTeC hosted an ICFA supported mini workshop on Higher-Order-Mode Diagnostics and Suppression in Superconducting Cavities (HOMSC12). The local organizing committee for this international workshop was chaired by S. Buckley (ASTeC/STFC) and the scientific programme committee by R.M. Jones (Cockcroft Institute/University of Manchester).

Issues related to beam-excited wakefields in superconducting cavities were focused on. These wakefields can be decomposed into a series of higher order modes (HOMs), lower order modes, and same order modes. If left unchecked these HOMs in particular can appreciably dilute the beam quality, and in the worst case scenario can give rise to a beam break up instability. This workshop brought together approximately 60 delegates participated from Europe, Asia, and Northern America -all with a common purpose to study HOM suppression in superconducting cavities in fields ranging from energy recovery linacs, light sources and linear collider applications. Delegates with a vast experience in this area were present, along with those new to this area of study. Both invited plenary and contributed sessions were part of the 2.5 day meeting. This workshop encompassed issues in both electron and proton linacs, TESLA style cavities, third harmonic cavities, and TEM crabbing and other cavity designs.

The morning sessions were focused on plenary presentations whilst the afternoon sessions were devoted to five working groups:

A. HOM Damping Requirements on a Project Basis (chaired by: J. Sekutowicz, and V.P. Yakovlev)

B. HOM-based Diagnostics (chaired by: N. Baboi, C. Welsch and R.M. Jones)
C. RF Simulations and Beam Dynamics (chaired by: M. Liepe and S. Molloy)
D. HOM Damping Couplers and Loads (chaired by: J. Delayen and G. Burt)
E. Low-level RF, Controls and System Integration (chaired by: T. Power)

Lively discussions ensued in several of these working groups, and it is clear that delegates profited from participating in working groups with a diversity of participants. Provision was made in the penultimate day to allow for a tour of the world class facilities of the Daresbury laboratory, which included the non-scaling FFAG EMMA and the energy recovery accelerator ALICE. Working group summaries concluded the event. In addition, tutorials were presented each day by I. Nesmiyan, J. Smith and I.R.R. Shinton.

Bursaries were provided, on a competitive basis, to support the attendance of two students. During the conference banquet at a nearby 700 year old Welsh castle, a prize was presented to the best student poster and a certificate to the runner up. Selected papers from this workshop will be published in a HOMSC12 special issue of Nuclear Instruments and Methods in Physics Research Section A. Sponsors of the event included: ICFA, IOP, RF Tech, ASTeC and the Cockcroft Institute. Details of the workshop, including a complete timetable and talks for download are available here: http://www.cockcroft.ac.uk/events/HOMSC12/. Further information regarding the workshop and submission to the NIMA special issue is also available on request from the chair of the scientific programme committee, Prof. Roger M. Jones (roger.jones@manchester.ac.uk).

6 Recent Doctorial Theses

6.1 The LHC Transverse Coupled-Bunch Instability

Nicolas Mounet
Mail to: Nicolas.Mounet@cern.ch

Graduation date: March 16th, 2012
University: EPFL (École Politechnique Fédérale de Lausanne), Switzerland
Supervisors: Prof. L. Rivkin and Dr. E. Métral

Abstract:

In this thesis, the problem of the transverse coupled-bunch instabilities created by the Large Hadron Collider (LHC) beam-coupling impedance, that can possibly limit the machine operation, is addressed thanks to several new theories and tools. A rather complete vision of the problem is proposed here, going from the calculation of the impedances and wake functions of individual machine elements, to the beam dynamics study. Firstly, new results are obtained in the theory of the beam-coupling impedance for an axisymmetric two-dimensional structure, generalizing Zotter's theories, and a new general theory is derived for the impedance of an infinite flat two-dimensional structure. Then, a new approach has been found to compute the wake functions from such analytically obtained beam-coupling impedances, overcoming limitations that

could be met with standard discrete Fourier transform procedures. Those results are then used to obtain an impedance and wake function model of the LHC, based on the (resistive-) wall impedances of various contributors (collimators, beam screens and vacuum pipe) and additional estimations of the geometrical impedance contributions. Finally, the existing code HEADTAIL, which is a macroparticle simulation code for beam dynamics studies with wake fields, is improved to make possible the simulation of multibunch trains, and a spectral analysis technique is found to facilitate the analysis of the output given by this code, giving the complex tune shifts of the unstable modes present in a simulation. All those theories and tools are used to obtain new results concerning the LHC transverse coupled-bunch instabilities, demonstrating the rather small impact on coupled-bunch instabilities of the number of bunches in a train when the bunch spacing is fixed, and the existence of coupled-bunch modes with intrabunch motion which are more critical than their single-bunch counterparts. A full verification of the complete procedure (impedance theories, impedance model and simulation code) is also performed by comparing the simulation results with actual measurements in the LHC, giving a very good agreement at injection energy and a correct order of magnitude at 3.5 TeV/c. In the end, several predictions concerning the beam stability at the future 7 TeV/c operation of the machine are performed in the case of 50 ns spacing (1404 bunches), revealing that the coupled-bunch transverse mode coupling instability threshold is far above the ultimate bunch intensity but about 20% smaller than its single-bunch counterpart. Stability studies with Landau octupoles at their maximum currents reveal that the beam remains stable at nominal intensity with Q' = 2 in both planes, provided the particle transverse distributions are Gaussian. At ultimate intensity with either Q' = 0 or Q' = 2, or at nominal intensity when the chromaticity is zero, the beam happens to be unstable, even with the octupoles at their maximum currents.

6.2 Characterization and Control of Femtosecond Electron and X-Ray Beams at Free-Electron Lasers

Christopher Behrens
Mail to: cbehrens@slac.stanford.edu

Graduation date: July 6th, 2012
University: University of Hamburg
Supervisors: Prof. Dr. J. Rossbach and Dr. Ch. Gerth

Abstract:

X-ray free-electron lasers (FELs) open up new frontiers in photon science, and in order to take full advantage of these unique accelerator-based light sources, the characterization and control of the femtosecond electron and X-ray beams is essential. Within this cumulative thesis, recent results achieved within the active research field of femtosecond electron and X-ray beams at FELs are reported. The basic principles of X-ray FELs are described, and concepts of longitudinal electron beam diagnostics with femtosecond accuracy are covered. Experimental results obtained with a transverse deflecting structure (TDS) and spectroscopy of coherent terahertz radiation are presented, and the suppression of coherent optical radiation effects, required for diagnostics utilizing a TDS, is demonstrated. Control of the longitudinal phase space by using multiple radio frequencies for longitudinal electron beam tailoring is presented,

and a new technique of reversible electron beam heating with two TDSs is described. For the characterization of femtosecond X-ray pulses, a novel method based on dedicated longitudinal phase space diagnostics for electron beams is introduced, and recent measurements with a streaking technique using external terahertz fields are presented.

7 Forthcoming Beam Dynamics Events

7.1 ICFA Mini-Workshop on Beam-Beam Effects in Hadron Colliders (BB2013)

This workshop, which will be held at CERN in Geneva, Switzerland from March 18th to 22nd, 2013, is a successor and follow up to similar workshops held at CERN in April 1999 and at Fermilab in June 2001. It is motivated by the successful start of the LHC and the emergence of a vast amount of beam-beam observations. We feel the need to review the progress made since the last workshop on beam-beam effects.

The purpose of this workshop is to review the present knowledge and compare with the observations, and to discuss and plan future research work, with special emphasis on the performance of the LHC after the first long shutdown as well as on studies needed for the planned LHC upgrade projects such as HL-LHC and LHeC.

The workshop web site is:

https://indico.cern.ch/conferenceDisplay.py?ovw=True&confId=189544.

Workshop chair: Werner Herr (CERN), Werner.Herr@cern.ch.

7.2 1st International Beam Instrumentation Conference (IBIC 2012)

We are delighted to announce the first International Beam Instrumentation Conference, IBIC2012 (http://ibic12.kek.jp/), to take place at the Tsukuba International Congress Center, Tsukuba, Japan, from 1 to 4 October 2012.

The conference will be hosted by the High Energy Accelerator Research Organization (KEK).

In 2010, representatives from the Americas, Europe, and Asia agreed to merge the two regional workshops, BIW in North America and DIPAC in Europe, and combine with a newly-established Asian regional committee to create a new International Beam Instrumentation Conference, IBIC, from 2012. This is a great milestone for the world beam instrumentation community, and it reflects the maturity of international collaboration in the field of beam instrumentation for accelerators.

IBIC will be dedicated to exploring the physics and engineering challenges of beam diagnostic and measurement techniques for charged particle accelerators worldwide. The conference program will include tutorials on selected topics and invited and contributed talks, as well as poster presentations. An industrial exhibition and a tour of the accelerator facilities at KEK and J-PARC will also be included.

The venue of IBIC 2012 is the Tsukuba International Congress Center, a modern, dedicated conference venue, located in the heart of the city. Tsukuba is located 60 km east of Tokyo, and is Japan's largest research city with more than 300 research institutes. Tsukuba is also one of the world's key sites for basic research in science and technology.

Workshop chair: Toshiyuki Mitsuhashi (KEK), hayashiy@post.kek.jp.

7.3 ICFA Beam Dynamics Workshop on Accelerators for a Higgs Factory: Linear vs. Circular (HF2012)

Dates: November 14-16, 2012.
Place: Fermilab, U.S.A.
Website: http://conferences.fnal.gov/hf2012.

With the discovery of a Higgs boson at ~125 GeV, the world high-energy physics community is investigating the feasibility of a Higgs Factory, a complement to the LHC for studying the Higgs. This 3-day workshop aims to bring the community together for a discussion on a future Higgs Factory, in particular for a comparison between a linear 125 × 125 GeV e^+e^- collider and a circular 125 GeV e^+e^- collider. It will also discuss physics requirements for a Higgs Factory and other options for a Higgs Factory, including a muon collider and a γγ collider. All sessions will be plenary. The outcome of this workshop will be used as input to the U.S. Snowmass 2013, European Strategy Upgrade and HEP roadmap in Japan. The topics include:

- Higgs physics beyond the LHC
- Merits and requirements of each type of Higgs factory
- Linear Higgs factories – ILC, CLIC, SLC
- Circular Higgs factories – LEP3, TLEP, SuperTristan, Fermilab site-filler
- Limits of circular e^+e^- colliders
- Muon collider as a Higgs Factory
- γγ collider as a Higgs Factory

Organizing Committee:

Alain Blondel (CERN)
Alex Chao (SLAC)
Weiren Chou (Fermilab, Chair)
Jie Gao (IHEP)
Daniel Schulte (CERN)
Kaoru Yokoya (KEK)

Local Committee:

Elliott McCrory (Fermilab)
Cynthia Sazama (Fermilab)
Tanja Waltrip (Fermilab)
Suzanne Weber (Fermilab)

Contact:

Cynthia M. Sazama
Conference Office
Fermi National Accelerator Laboratory
M.S. 113, P.O. Box 500
Batavia, IL 60510, U.S.A.
Fax: +1-630-840-8589
E-mail: sazama@fnal.gov

7.4 Photocathode Physics for Photoinjectors (P3)

Following the first highly successful P3 Workshop held in 2010 at Brookhaven National Laboratory, we are pleased to announce the second in the series Physics of Photocathodes for Photoinjectors Workshop to be held at Cornell University in October 8-10, 2012. See the following website for details:

http://www.lepp.cornell.edu/Events/Photocathode2012/WebHome.html.

7.5 ICUIL Conference 2012

Dates: September 16-21, 2012.
Place: Mamaia, Romania.
Website: http://icuil2012.inflpr.ro/Index.html.

This biennial meeting emphasizes on the generation, amplification, compression, and measurement of high-intensity pulses as well as applications. The scope of ICUIL 2012 includes, but is not limited to:

- Ultrahigh-intensity-laser design and performance
- Novel Technologies for Ultra-Intense Lasers
- Laser Acceleration
- Applications with extreme light
- Short-wavelength sources
- Attosecond science
- Plasma optics

This conference will also feature a special workshop on high-damage threshold laser components and a student poster competition.

Abstract submission deadline: June 30, 2012.
Early registration: May 4, 2012.
Hotel reservation deadline: June 22, 2012.

8 Obituaries

8.1 In Memoriam of Andrey N. Lebedev (1933-2011)

Igor Meshkov, JINR, Russia
Mail to: meshkov@jinr.ru

Andrey Lebedev, a distinguished accelerator physicist, passed away on December 29, 2011. Lebedev had an important influence on several generations of accelerator physicists who learned the field of accelerator physics from the advanced textbook by A. A. Kolomensky and A. N. Lebedev, "*Theory of Cyclic Accelerators*," translated from the Russian into several languages.

After graduation in 1955 from Moscow University Andrey Lebedev joined the Lebedev Physics Institute (LPI) of the Academy of Sciences in Moscow where he worked for the rest of his life. Shortly after arriving there, he published, together with Kolomensky, his scientific supervisor, the first scientific article predicting the effect of radiation damping of electron beam emittance in synchrotrons. This paper formulated the criterion of beam radiation instability development. In 1958 Lebedev elaborated the theory of the phase stability principle in the presence of particle radiation for general conditions of acceleration field geometry. One year later, he formulated the theory of resonance acceleration, taking into account the influence of beam space charge. Simultaneously with that important work, he discovered the "negative mass effect."

During the period 1959–1963, Andrey Lebedev worked with his colleagues on the construction, commissioning and beam studies of a cyclic accelerator with an original focusing system – the so called "Ring Phasotron". Then he focused his interest on new methods of particle acceleration. He discovered the effect of the autoresonant interaction of electrons with a plane electromagnetic wave. This allowed him to formulate the principles of the maser on cyclotron autoresonance and reversed free electron laser (published together with Kolomensky in 1961). At the beginning of the 1970s, the era of "collective acceleration methods" reached its apogee. Andrey contributed several fruitful ideas to this field, particularly wake field particle acceleration with high intense electron beams (1972). At the same time he created the kinetic theory of magnetic isolation and proved it experimentally (1973). He developed the single particle theory of the free electron laser and explained the physics of induced radiation in classic particle beam systems (together with Kolomensky, 1971–1974).

Later his research interests switched to kiloampere beams of negative ions. He proposed and demonstrated, with his group, an original method for generating such beams. During his last years, Andrey Lebedev led a research group at the LPI in developing coherent infrared radiation sources for spectroscopy.

Andrey Lebedev was a remarkable teacher who educated many talented accelerator physicists. Fifteen of them earned PhD degrees and five became professors. He has written several textbooks on accelerators and related topics.

Lebedev was an exceptional man. Friends admired him; his colleagues deeply respected him. He was a man of fine humor, of encyclopedic knowledge and strong moral principles.

Figure 1: Andrey Lebedev (third from the right) during the "Cooling and Damping Conference" held on board the ship "Alexander Suvorov" cruising along the Volga River in June 1996 (picture from the photographer Yuri Tumanov, JINR). From left to the right: Igor Ivanov (JINR), Flemming Pedersen (CERN), Igor Meshkov (JINR), unidentified, Andrey Lebedev (LPI RAS), Alexander Skrinsky (Budker INP), Simon Van der Meer (CERN). Andrey liked this photo very much and told a related story: "One evening on board a friendly group of us was sitting on the upper deck, chatting and, of course drinking. Soon a couple bottles of vodka became empty and I tried to run down to the bar to get more. 'No!' Simon Van der Meer stopped me, 'I will do it!' " At this point in the story Andrey usually makes a short pause, and then says: "It was an historic event: the first time in Russian history that a Nobel Prize Winner was running to bring vodka!"

8.2 In Memoriam of Dieter Möhl (1936-2012)

Stephan Maury, CERN, Switzerland
(Reprinted from CERN Weekly Bulletin with permission)
Mail to: Stephan.Maury@cern.ch

It is with great emotion and deep sadness to learn of the loss of our colleague and friend Dieter Möhl on the 24th of May. An accelerator physicist of world reputation he made essential contributions to a lot of projects at CERN and around the world. Here at CERN his name will remain tied forever to the success of the antiproton programme since its beginnings but he also made substantial contributions to the FAIR project in Germany and to many other storage rings where beam cooling was an essential ingredient. His theoretical work was unique for the understanding, improvement and extension of the beam cooling techniques to many accelerators and storage rings.

He was one of the pioneers who demonstrated by the Initial Cooling Experiment (ICE) that stochastic cooling was a viable proposition. This was essential for the

approval of the CERN antiproton programme and its success. Then, he was a leading member of the team initiating and designing the Low Energy Antiproton Ring (LEAR) where the first ultra-slow beam extraction extending over hours to the experiments was performed. After the decision to stop LEAR he actively participated in the study and design of a simplified antiproton source which became later the Antiproton Decelerator ring (AD) after the project SUPERLEAR of which he was one of the prominent promoters was not approved. He also initiated the Extra- Low ENergy Antiproton ring (ELENA) at AD already in 1982 and he was very happy to see that in 2011 this project providing antiprotons with a kinetic energy as low as 100 keV was finally approved. Dieter has made important contributions also to electron cooling, a token of this is found in AD and in the modified of LEAR machine to become the Low Energy Ion Ring (LEIR) acting as buffer and accumulation ring between the fast-cycling ion Linac 3 and the slow-cycling PS, an essential element in the LHC ion injector chain.

Dieter was not only a famous Accelerator Physicist but played also an important role in Human Rights issues, in particular in the framework of the Orlov Committee created at CERN with him as one of the founding fathers to provide efficient help to Soviet dissidents in the 1970/80s.

Retired since 2001, Dieter was nearly every day at work to help us in our projects and to give us advice. Even the day before his untimely death, he was still at CERN to discuss with us the ELENA project. He certainly was one of the kindest, gentlest persons with an infinite patience and a proverbial generosity we have ever known. We gratefully remember Dieter's human quality and we miss his wise counsel.

9 Announcements of the Beam Dynamics Panel

9.1 ICFA Beam Dynamics Newsletter

9.1.1 **Aim of the Newsletter**

The ICFA Beam Dynamics Newsletter is intended as a channel for describing unsolved problems and highlighting important ongoing works, and not as a substitute for journal articles and conference proceedings that usually describe completed work. It is published by the ICFA Beam Dynamics Panel, one of whose missions is to encourage international collaboration in beam dynamics.

Normally it is published every April, August and December. The deadlines are 15 March, 15 July and 15 November, respectively.

9.1.2 **Categories of Articles**

The categories of articles in the newsletter are the following:

1. Announcements from the panel.
2. Reports of beam dynamics activity of a group.
3. Reports on workshops, meetings and other events related to beam dynamics.
4. Announcements of future beam dynamics-related international workshops and

meetings.

5. Those who want to use newsletter to announce their workshops are welcome to do so. Articles should typically fit within half a page and include descriptions of the subject, date, place, Web site and other contact information.
6. Review of beam dynamics problems: This is a place to bring attention to unsolved problems and should not be used to report completed work. Clear and short highlights on the problem are encouraged.
7. Letters to the editor: a forum open to everyone. Anybody can express his/her opinion on the beam dynamics and related activities, by sending it to one of the editors. The editors reserve the right to reject contributions they judge to be inappropriate, although they have rarely had cause to do so.

The editors may request an article following a recommendation by panel members. However anyone who wishes to submit an article is strongly encouraged to contact any Beam Dynamics Panel member before starting to write.

9.1.3 **How to Prepare a Manuscript**

Before starting to write, authors should download the template in Microsoft Word format from the Beam Dynamics Panel web site:

http://www-bd.fnal.gov/icfabd/news.html

It will be much easier to guarantee acceptance of the article if the template is used and the instructions included in it are respected. The template and instructions are expected to evolve with time so please make sure always to use the latest versions.

The final Microsoft Word file should be sent to one of the editors, preferably the issue editor, by email.

The editors regret that LaTeX files can no longer be accepted: a majority of contributors now prefer Word and we simply do not have the resources to make the conversions that would be needed. Contributions received in LaTeX will now be returned to the authors for re-formatting.

In cases where an article is composed entirely of straightforward prose (no equations, figures, tables, special symbols, etc.) contributions received in the form of plain text files may be accepted at the discretion of the issue editor.

Each article should include the title, authors' names, affiliations and e-mail addresses.

9.1.4 **Distribution**

A complete archive of issues of this newsletter from 1995 to the latest issue is available at

http://icfa-usa.jlab.org/archive/newsletter.shtml.

This is now intended as the primary method of distribution of the newsletter.

Readers are encouraged to sign-up for electronic mailing list to ensure that they will hear immediately when a new issue is published.

The Panel's Web site provides access to the Newsletters, information about future and past workshops, and other information useful to accelerator physicists. There are links to pages of information of local interest for each of the three ICFA areas.

Printed copies of the ICFA Beam Dynamics Newsletters are also distributed (generally some time after the Web edition appears) through the following distributors:

Weiren Chou	chou@fnal.gov	North and South Americas
Rainer Wanzenberg	rainer.wanzenberg@desy.de	Europe[++] and Africa
Toshiyuki Okugi	toshiyuki.okugi@kek.jp	Asia[**] and Pacific

++ Including former Soviet Union.

** For Mainland China, Jiu-Qing Wang (wangjq@mail.ihep.ac.cn) takes care of the distribution with Ms. Su Ping, Secretariat of PASC, P.O. Box 918, Beijing 100039, China.

To keep costs down (remember that the Panel has no budget of its own) readers are encouraged to use the Web as much as possible. In particular, if you receive a paper copy that you no longer require, please inform the appropriate distributor.

9.1.5 **Regular Correspondents**

The Beam Dynamics Newsletter particularly encourages contributions from smaller institutions and countries where the accelerator physics community is small. Since it is impossible for the editors and panel members to survey all beam dynamics activity worldwide, we have some Regular Correspondents. They are expected to find interesting activities and appropriate persons to report them and/or report them by themselves. We hope that we will have a "compact and complete" list covering all over the world eventually. The present Regular Correspondents are as follows:

Liu Lin	Liu@ns.lnls.br	LNLS Brazil
Sameen Ahmed Khan	Rohelakan@yahoo.com	SCOT, Oman
Jacob Rodnizki	Jacob.Rodnizki@gmail.com	Soreq NRC, Israel
Rohan Dowd	Rohan.Dowd@synchrotron.org.au	Australian Synchrotron

We are calling for more volunteers as Regular Correspondents.

9.2 ICFA Beam Dynamics Panel Members

Name	eMail	Institution
Rick Baartman	baartman@lin12.triumf.ca	TRIUMF, 4004 Wesbrook Mall, Vancouver, BC, V6T 2A3, Canada
Marica Biagini	marica.biagini@lnf.infn.it	LNF-INFN, Via E. Fermi 40, C.P. 13, Frascati, Italy
John Byrd	jmbyrd@lbl.gov	Center for Beam Physics, LBL, 1 Cyclotron Road, Berkeley, CA 94720-8211, U.S.A.
Yunhai Cai	yunhai@slac.stanford.edu	SLAC, 2575 Sand Hill Road, MS 26 Menlo Park, CA 94025, U.S.A.
Swapan Chattopadhyay	swapan@cockroft.ac.uk	The Cockcroft Institute, Daresbury, Warrington WA4 4AD, U.K.
Weiren Chou (Chair)	chou@fnal.gov	Fermilab, MS 220, P.O. Box 500, Batavia, IL 60510, U.S.A.
Wolfram Fischer	wfischer@bnl.gov	Brookhaven National Laboratory, Bldg. 911B, Upton, NY 11973, U.S.A.
Yoshihiro Funakoshi	yoshihiro.funakoshi@kek.jp	KEK, 1-1 Oho, Tsukuba-shi, Ibaraki-ken, 305-0801, Japan
Jie Gao	gaoj@ihep.ac.cn	Institute for High Energy Physics, P.O. Box 918, Beijing 100039, China
Ajay Ghodke	ghodke@cat.ernet.in	RRCAT, ADL Bldg. Indore, Madhya Pradesh, 452 013, India
Ingo Hofmann	i.hofmann@gsi.de	High Current Beam Physics, GSI Darmstadt, Planckstr. 1, 64291 Darmstadt, Germany
Sergei Ivanov	sergey.ivanov@ihep.ru	Institute for High Energy Physics, Protvino, Moscow Region, 142281 Russia
In Soo Ko	isko@postech.ac.kr	Pohang Accelerator Lab, San 31, Hyoja-Dong, Pohang 790-784, South Korea
Elias Metral	elias.metral@cern.ch	CERN, CH-1211, Geneva 23, Switzerland
Yoshiharu Mori	mori@rri.kyoto-u.ac.jp	Research Reactor Inst., Kyoto Univ. Kumatori, Osaka, 590-0494, Japan
George Neil	neil@jlab.org	TJNAF, 12000 Jefferson Ave., Suite 21, Newport News, VA 23606, U.S.A.
Toshiyuki Okugi	toshiyuki.okugi@kek.jp	KEK, 1-1 Oho, Tsukuba-shi, Ibaraki-ken, 305-0801, Japan
Mark Palmer	mark.palmer@cornell.edu	Wilson Laboratory, Cornell University, Ithaca, NY 14853-8001, USA
Chris Prior	chris.prior@stfc.ac.uk	ASTeC Intense Beams Group, STFC RAL, Chilton, Didcot, Oxon OX11 0QX, U.K.
Yuri Shatunov	Yu.M.Shatunov@inp.nsk.su	Acad. Lavrentiev, Prospect 11, 630090 Novosibirsk, Russia
Jiu-Qing Wang	wangjq@ihep.ac.cn	Institute for High Energy Physics, P.O. Box 918, 9-1, Beijing 100039, China
Rainer Wanzenberg	rainer.wanzenberg@desy.de	DESY, Notkestrasse 85, 22603 Hamburg, Germany